

**NONLINEAR OPTICAL PROPERTIES OF POLYMERS
CONTAINING AZOMESOGENS AND CHIRAL
MOLECULES: THEORETICAL AND EXPERIMENTAL
EVALUATIONS**

*Thesis submitted to
Cochin University of Science and Technology
in partial fulfilment of the requirements
for the Degree of*

Doctor of Philosophy

in

Chemistry

Under the faculty of science

by

Dafy Davis

**DEPARTMENT OF APPLIED CHEMISTRY
COCHIN UNIVERSITY OF SCIENCE AND TECHNOLOGY
KOCHI-22, India**

September 2005

എന്റെ അമ്മിച്ചിയ്ക്ക്.....
(To my Mother)

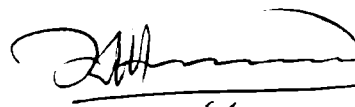
COCHIN UNIVERSITY OF SCIENCE AND TECHNOLOGY
DEPARTMENT OF APPLIED CHEMISTRY

Dr. K. SREEKUMAR
Reader

CUSAT Campus
Kochi - 682 022
Kerala, India.
Tel: 0484-2575804
0484 -2421530 (Res)
E-mail: ksk@cusat.ac.in

CERTIFICATE

This is to certify that the thesis entitled "**Nonlinear optical properties of polymers containing azomesogens and chiral molecules: theoretical and experimental evaluations.**" submitted for the award of the Degree of Doctor of Philosophy of the Cochin University of Science and Technology, is a record of original research work carried out by Ms. Daly Davis under my supervision and guidance in the Department of Applied Chemistry.



Kochi-22
Date 12.09.05

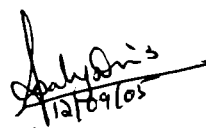
Dr. K. Sreekumar
(Supervising Teacher)

DECLARATION

I hereby declare that the thesis entitled "**Nonlinear optical properties of polymers containing azomesogens and chiral molecules: theoretical and experimental evaluations**" submitted for the award of Ph.D. Degree, is based on the original work done by me under the guidance of Dr. K. Sreekumar, Reader, Department of Applied Chemistry, Cochin University of Science and Technology and further that it has not previously formed the basis for the award of any other degree.

Kochi-22

Date 12.09.05



Daly Davis

Acknowledgment

Dr. K. Sreekumar- My Supervising Guide – For being most generous supervisor, suggesting a novel problem and the barrierless freedom offered during my research period.

Prof. M. R. Prathapachandra Kurup -Head of the Department for providing necessary facilities for carrying out this research.

Dr. K. K. Mohammed Yusuff - former Head of the Department - For the guidance and financial support during the early stage of my research.

Dr. S. Sugunan - former Head of the Department.

Dr. N. Sridevi - For the support given to me during the beginning of my research period.

All other faculty members and non-teaching staff of the department - For generating a research culture and ambience.

Dr. Swapan K. Pati, JNCASR, Bangalore - Our collaborator.

Prof. Sourav Pal, NCL, Pune –For offering me a summer research studentship.

Dr. Reji Philip, RRI, Bangalore - For NLO measurements.

Sandeep C. S – For his help in NLO measurement.

Ayan Datta - For helping me to do the ZINDO calculations.

Dr. Anas K – Great supporter- For taking NMR and IR spectra

Dr. Suja Haridas - My ever green friend-for a real support through my research period

Suni V- My roommate – For her support and encouragement.

Mini, Bessy and Roshini – My hostel mates-for making a friendly atmosphere during my dry hostel days.

All other friends - For their love, support and help.

Rajesh, Kannan, Suresh, Mangala and other lab mates- for their tolerance and support.

CDRI-Lucknow, SIF- IISc, Bangalore- For Spectral analysis

DRDO- For the financial support

My father, brother and family – For their love, patience, support and interest.

Neena Susan John- My great friend- For her pure love.

Sajeev- My husband- For being mine.

My mother- For being my mother. She is my real strength. She taught me how elaborate the definition of a mother is!

Daly

If everything were linear, nothing influences nothing.
Albert Einstein

PREFACE

Current research in nonlinear optics is focused on the design and synthesis of nonlinear optics active materials in view of their tremendous potential for application in telecommunication, optical computing and data storage. The *state of the art* in the field of NLO has been to construct smart polymeric materials with large second order optical response functions. Hence present-day polymer synthesis has the challenge of constructing smart polymeric materials with second-order nonlinear optical (NLO) properties. One can design macroscopic nonlinear materials by knowing their microscopic nonlinear coefficients (molecular hyperpolarizabilities) that are the molecular equivalents of bulk nonlinear optical susceptibilities.

The necessary and essential condition for the existence of second order hyperpolarizability is the attainment of charge and spatial asymmetry. The requirement for second-order (and other even-order) nonlinear materials is particularly stringent, because such processes are forbidden in centrosymmetric materials in the electric-dipole approximation of the matter-field interaction. The most common way to break centrosymmetry in polymers is through electrical poling. Alternatively, second-order NLO devices can be constructed by synthesizing nonlinear molecules as chromophores into a noncentrosymmetric supramolecular structure. When such structures extend to macroscopic dimensions, the poling of chromophores can be achieved through chemical synthesis, and there is no need for external poling. The permanent dipole moment of such structures can be very large because of the coherent addition of dipole moments achieved by a high degree of polar order.

A facile way to synthesize chiral main-chain NLO polymers involves the polycondensation of chiral units and donor-acceptor-conjugated chromophores. The use of chiral building blocks tends to crystallize the polymer into a chiral supramolecular organization. Additionally, cooperative chiral order plays a vital role in the self-

assembly of ordered supramolecular structures. Chiral order in a polymer material always exists in parallel with its optical activity.

The present work emphasizes the use of chirality as an efficient tool to synthesize new types of second order nonlinear materials. Second harmonic generation efficiency (SHG) is used as a measure of second order nonlinear response. Nonlinear optical properties of polymers have been studied theoretically and experimentally. Polymers were designed theoretically by *ab initio* and semiempirical calculations. All the polymeric systems have been synthesized by condensation polymerization. Second harmonic generation efficiency of the synthesized systems has been measured experimentally by Kurtz and Perry powder method.

Objective of the present study

- Theoretical optimization of linear and nonlinear coefficients in terms of substituent, spacer and chiral effects
- Design of polymeric structures with high second order NLO activity, based on the theoretical results.
- Theoretical evaluation of NLO activity of designed polymer systems
- Synthesis and experimental evaluation of the NLO efficiency of the polymers.

This thesis comprises of six chapters,

Chapter 1 - Nonlinear Optical Properties of Polymers: a Review

This chapter presents an introduction about the nonlinear optical properties of polymeric systems, especially based on the chiral aspects. This chapter will also give a general introduction on the different types of theoretical calculations used in the present work.

Chapter 2 - Optimization of Nonlinear Optical Properties by Substituent Position, Geometry and Symmetry of the Molecule: An *Ab Initio* Study

Static polarizability and first and second order hyperpolarizability tensors are computed at the correlated level (MP2, using GAMESS-US, Quantum chemical code) for

a series of *para*-nitroaniline derivatives. The importance of including electron correlation effects in the determination of equilibrium structure and the molecular properties are investigated. Qualitative description of the substitution effects, planarity and symmetry effects of the molecule on the molecular susceptibility are studied. Effect of methyl/ethyl substitution on amino nitrogen and ring carbons of *para*-nitroaniline on the electric properties is investigated.

Chapter 3 - Effect of Spacer Groups on the Non Linear Optical Properties

The odd-even oscillations of the effect of spacer methylene groups on the electric properties of organic molecules (of the type $O_2N-Ph-N=N-Ph-(CH_2)_n-Ph-N=N-Ph-NO_2$) are calculated using sum-over states (SOS) method. The calculations are performed using a ZINDO code which uses CI and correction vector method. The molecules exhibited a very strong odd-even oscillation behavior for the first Hyperpolarizability. The effect of spacer methylene groups on *para*-nitroaniline (PNA) derivatives by varying the number of CH_2 groups is also studied. The polymeric systems incorporating PNA derivatives were synthesized by the condensation polymerization of PNA derivatives with azo chromophores. The SHG efficiency was calculated experimentally by Kurtz and Perry powder method. While substituting both the hydrogens of $-NH_2$ in *para*-nitroaniline, instead of showing odd even oscillation, the SHG efficiency increased with increase in the number of CH_2 groups. The calculations at the Hartree-Fock level (6-31++G** basis set, available in the Gaussian 03 quantum chemical package is used for the calculation.) and the ZINDO-SOS method have shown agreement with the experimental observations.

Chapter 4 - Chiral Polyesters Containing Azomesogens for Nonlinear Optics: Role of Stereochemistry of Chiral Molecules

A series of polymers are synthesized by incorporating the chiral monomers and azomesogens. The monomers and polymers are designed using tools of computational chemistry at the Hartree-Fock level and ZINDO calculations. The polymers were designed as condensation polymers of three repeating units (each repeating unit contains of *one* chiral molecule, *one* azo chromophore and *one* acid chloride). Since the chiral molecules are incorporated in the polymer chain, noncentrosymmetric

supramolecular structures are obtained. In the polymer, such structures extend to macroscopic dimensions and the poling of chromophores can be achieved through chemical synthesis (chemical poling). Hence there is no need of external poling. The permanent dipole moment of the polymeric systems is large because of the coherent addition of dipole moments achieved by a high degree of polar order. The chirality of the material is associated with the helical supramolecular configuration of the backbone, and strong coupling exists between the backbone and the chromophore. Thus the polymeric systems with chiral molecules showed enhanced SHG efficiency which was double as that of the reference molecule, 2-Methyl, 4-nitroaniline.

Chapter 5 - L-Tyrosine Based Chiral Poly (ester-amide) s Containing Main Chain and Side Chain Azo Group

This chapter includes the design of L-tyrosine based chromophore with high β values. It also includes the design of chiral and achiral diols for polycondensation with the designed chromophore for the purpose of studying the effect of incorporation of additional chiral molecules into an already chiral medium. The poly (ester-amide) s are synthesized using high temperature polycondensation method and SHG efficiencies are measured using Kurtz and Perry powder method. Thus, the concept of design and synthesis of highly active NLO materials is attempted in this work.

Chapter 6 - L-Tyrosine Based Chiral Poly (ester-amide) s Containing Azo Group in the Side Chain

This chapter discusses the effect of side chain azo group in the chiral framework of L-tyrosine. The comparison is made with the polymers containing both the main chain and side chain azo group incorporated with in the same L-tyrosine chiral framework. Poly (ester-amide) s with only side chain azo group have been designed and the properties are studied using *ab initio* and semiempirical methods. All the systems are synthesized in the laboratory and SHG efficiency is measured experimentally using Kurtz and Perry powder method.

References are given to the end of each chapter. A summary of the work done and conclusions drawn out of the study are given towards the end of the thesis.

CONTENTS

Chapter 1	NONLINEAR OPTICAL PROPERTIES OF POLYMERS: A REVIEW	1
Chapter 2	OPTIMIZATION OF NONLINEAR OPTICAL PROPERTIES BY SUBSTITUENT POSITION, GEOMETRY AND SYMMETRY OF THE MOLECULE: AN AB INITIO STUDY	45
Chapter 3	EFFECT OF SPACER GROUPS ON THE NON LINEAR OPTICAL PROPERTIES	67
Chapter 4	CHIRAL POLYESTERS CONTAINING AZOMESOGENS FOR NONLINEAR OPTICS: ROLE OF STEREOCHEMISTRY OF CHIRAL MOLECULES	113
Chapter 5	L-TYROSINE BASED CHIRAL POLY (ESTER-AMIDE) S CONTAINING MAIN CHAIN AND SIDE CHAIN AZO GROUP	169
Chapter 6	L-TYROSINE BASED CHIRAL POLY (ESTER-AMIDE) S CONTAINING AZO GROUP IN THE SIDE CHAIN	210
	SUMMARY AND CONCLUSIONS	241

NONLINEAR OPTICAL PROPERTIES OF POLYMERS: A REVIEW

1.1. Introduction

Nonlinear optics (NLO) refers to any light-induced change in the electrical properties of a material. The impact of nonlinear optics on science and technology has been two fold. First, it has enhanced our understanding of the fundamentals of light-matter interactions. Second, it has been a driving force in the rejuvenation of optical technology for several areas of science and engineering. Nonlinear optics has matured in the sense of being a well-developed and systematic theory as well as providing applications for a variety of engineering tasks. Second and third order phenomena and devices are now at a stage of understanding and development such that a coherent description and summary of these areas forming the core of the subject are now possible and desirable.

The field of research and development of nonlinear optical materials has progressed impressively since the invention of the laser in 1960. NLO materials, defined as materials in which light waves can interact with each other¹, are the key materials for the fast processing of information and for dynamic or permanent optical storage applications. In addition to a large and fast response, a material useful for applications must have low loss at the operating wavelength, should show high thermal, mechanical and chemical stability, and be easily processable to various device configurations. Hence present-day polymer synthesis has the challenge of constructing smart polymeric materials with second-order nonlinear optical (NLO) properties. Polymers with such tailor made properties have replaced the traditional materials in opto-electronics and photonics.

The field of nonlinear optics had its birth in 1875 with the publication by J.Kerr of his observations of a quadratic electric field induced change in the refractive index of

CS_2 , now known as Kerr effect. This discovery was followed shortly in 1883 by the observation of a similar but linear electric field effect in quartz. This latter process is known as the Pockels effect. (Figure 1.1)

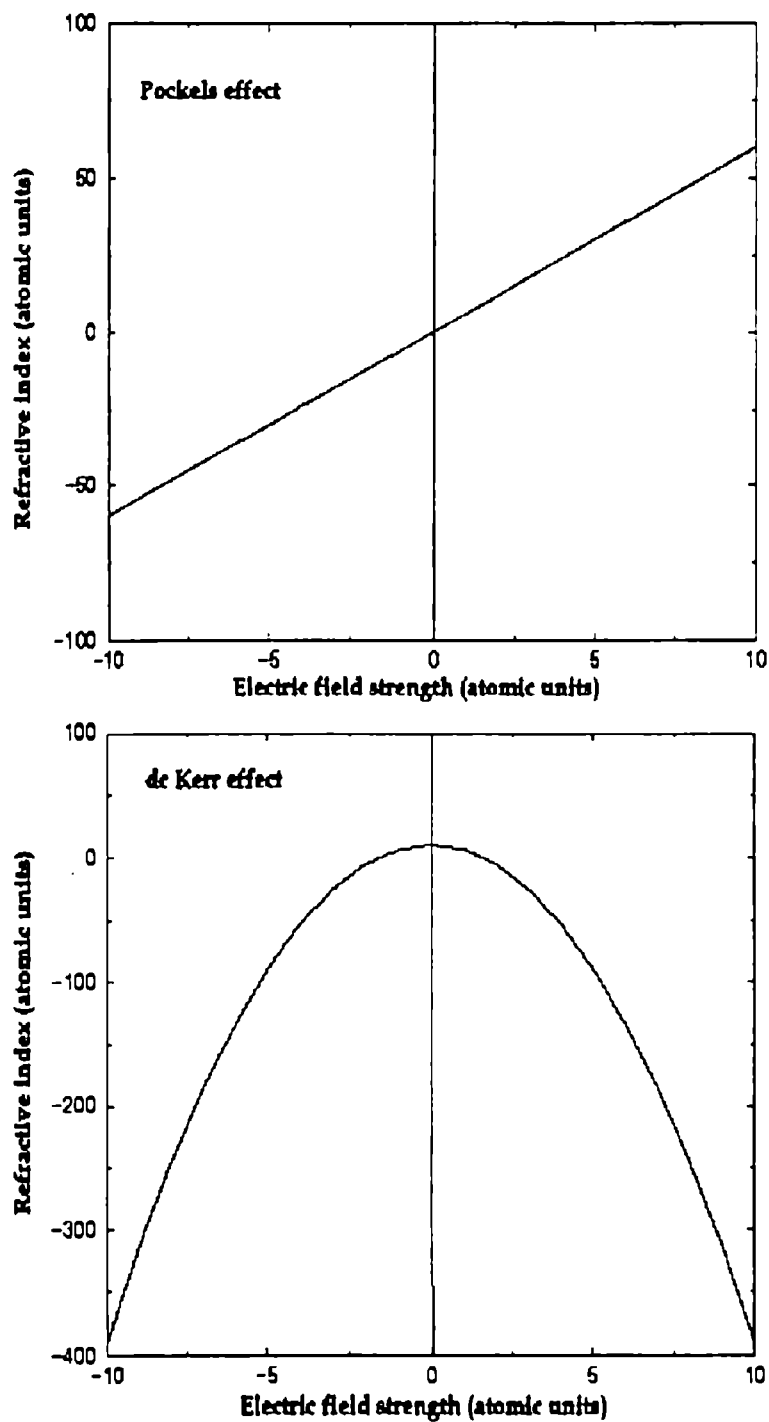


Figure 1.1 Pockels and dc Kerr effects

These nonlinear effects had limited use until the invention of the laser in 1960, followed the next year by the observation by P. Franken et al ^{2a}. of second harmonic generation (SHG) in quartz. Following these events, the field of nonlinear optics has developed explosively throughout the 1960s, highlighted by the work of N. Bloembergen ^{2b} and co-workers in exploring the full range of nonlinear optical responses of material systems and that of A.D Buckingham and colleagues in exploring nonlinear process in atoms and molecules of interest to chemist.

1.2. Theory of nonlinear optics

In pre-laser era, under the ordinary experience of every day life, the optical properties and parameters of a medium was independent of the intensity of light that permitted observation of the optical phenomena such as reflection, refraction, diffraction, absorption, and scattering. This is the realm of what is called linear optics. The invention of laser gave rise to the study of optics at high intensities, leading to new phenomena not seen with ordinary light such as the generation of new colors from monochromatic light in a transparent crystal, or self-focusing of an optical beam in a homogeneous liquid. At the intensities used to generate these types of effects, the usual optical parameters of materials cannot be considered constant but become functions of light intensity. The science of optics in this regime is called nonlinear optics. This is because of the reason that the field strength of the conventional light source used before the advent of lasers, were much smaller than the field strength of atomic and inter-atomic fields. The electric charges in matter are held in equilibrium by atomic fields of the order 10^8 - 10^9 V/cm, and anharmonicity in their motion can only be observed by using perturbing fields that are not negligible compared to these values. Due to coherence, the laser beam can be focused to an area $A \approx \lambda^2$. If the laser wavelength is assumed to be 1μ , then $A = 10^{12}$ m² and hence $J_E \approx 10^{16}$ MW/m² giving $E \approx 3 \times 10^{10}$ V/m which is with in the range of atomic field. At such high fields, the relationship between the electric polarization P and the field strength E ceases to be linear and some interesting nonlinear effects come to the fore.

The first nonlinear optical phenomena observed were electro-optic effects (Kerr, 1875; Pockels, 1886). But with conventional energy source, usually the nonlinear

phenomena are practically undetectable. Shortly after the demonstration of first laser in 1960, Peter Franken and coworkers (1961) ushered in nonlinear optics with the observation of second harmonic generation in a quartz crystal.^{2,3} They observed the second harmonic (at $\approx 3473 \text{ \AA}$) produced upon projection of an intense beam of 6943 \AA light through crystalline quartz. This experiment attracted widespread attention and marked the beginning of the experimental and theoretical investigation of nonlinear optical properties.

When a ray of light of frequency ν strikes a material system, the elementary particles of which it is made of are influenced in their relative motion and begin to oscillate with the frequency ν . By this induced polarization, the material system is transformed into a secondary emitter like an antenna. The simple assumption concerning such a scattering process is that electric field component of the electromagnetic radiation induces an oscillating dipole in the molecule, the magnitude of which is proportional to the electric field. If an elastic or linear scattering occurs, no net energy is transferred from the radiation to the molecule, i.e., the molecule will be in the same energy state before and after the scattering. However, during the time of scattering, the molecule is not in a pure stationary state. But it is in a time dependent, non-stationary state, which may be described as a superposition of many stationary states. The duration of such a scattering process may be estimated from the angular frequency of the interacting radiation. If it is ω , the time for such an interaction lasts is $\tau=1/\omega$. In spite of this very short time, the molecule can interact several times with the radiation. As a direct consequence, the radiation-induced polarization consists of a major part, which depends on the first power of field strength, but may also contain nonlinear contributions, which are proportional to the radiation field to second, third or even higher order. Thus the induced polarization consists of a variety of contributions giving rise to very fast secondary re-emission, i.e., scattering at different frequencies.³⁻⁶

Nonlinear interaction between electromagnetic radiation and matter can be described in quantum mechanical terms as multi photon process. In multi photon process an interaction between radiation and matter accompanied by absorption or emission or both, of not less than two photons per elementary act is observed. Second

harmonic generation is a three-photon process as shown in Figure 1.2. Two photons, each with energy $\hbar\omega$, are absorbed and one photon with energy $2\hbar\omega$ is emitted. The state of the quantum system remains unaltered. This gives an impression that two colliding photons merge “directly” into a single one. The levels shown in the figure by dotted lines are the “virtual levels”.

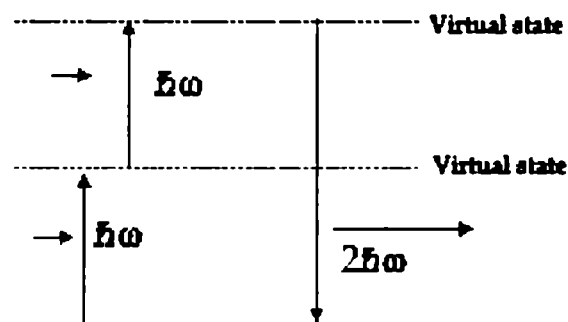


Figure 1.2 Schematic representation of second harmonic generation

1.2.1. Electromagnetic basis of nonlinear optics ⁷

Ordinary matter consists of a collection of positively charged cores (of atoms or molecules) and surrounded by negatively charged electrons. Light interacts primarily with matter via the valence electrons in the outer shells of electron orbitals. The fundamental parameter in this light-matter interaction theory is the electronic polarization of the material induced by light. When an electric field is applied to a dielectric medium (of neutral electric charge), a separation of bound charges is induced as illustrated in Figure 1.3. Within the electric-dipole approximation, this separation of charge results in a collection of induced dipole moments μ , which, as designated, may be rapidly oscillating if induced by a rapidly varying applied field.

$$\mu = -er \quad 1.1$$

where e the electric charge, r the displacement induced by the electric field.

The electric polarization P is defined as the net average dipole moment per unit volume and is given by

$$P = N \langle \mu \rangle \quad 1.2$$

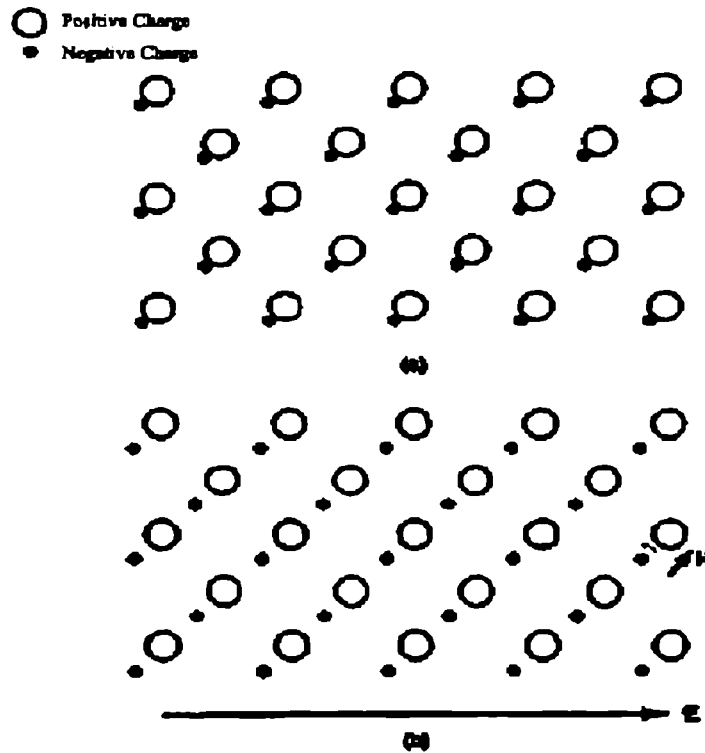


Figure 1.3. Illustration of response of a dielectric medium to an applied electric field.(a) Without field applied (b) field applied

Where N is the number of microscopic dipoles per unit volume, and the angular brackets indicates an ensemble average over all the dipoles in the medium. In what follows, any permanent dipoles within the medium will be ignored since they will not be oscillating at optical frequencies and hence will not radiate electromagnetic waves.

By the principle of causality, P must be a function of the applied field E . To an excellent

approximation, at the low intensity levels of natural light sources, the relation of the applied field is linear i.e. proportional to the applied field. As shown in **Figure 1.5** (part a) This is the regime of linear optics. The most general form of the electric polarization for a homogeneous medium is given by

$$P_L(r,t) = \int_{-\infty}^{\infty} \int_{-\infty}^{\infty} \chi^{(1)}(r-r',t-t') \cdot E(r',t') dr' dt' \quad 1.3$$

The equation is in cgs system. In SI system the equation should be multiplied with $\epsilon_0=8.85 \times 10^{-12}$ farad/meter, the electric permittivity of free space. Where the subscript L signifies a linear polarization. $\chi^{(1)}(r-r', t-t')$ is the linear dielectric response tensor. The functional form of $\chi^{(1)}$ reflects the principles of space and time invariance.⁸ In other words, the polarization response of the medium does not depend on whether (in an

absolute sense) the driving field is applied, or not, but only on the time, since it was applied. Consequently, $\chi^{(1)}(r-r', t-t')$ must be defined in such a way that it vanishes when $t-t' < 0$ to preserve causality. Similarly, the polarization response in a homogeneous medium does not depend on the absolute position in space of the applied field, but only on the distance away from this position. A non zero value of $\chi^{(1)}(r-r', t-t')$ for $r \neq r'$ is called a non local response. If there is no response except within a small neighborhood where $r \approx r'$, then the response is called local. This is equivalent to saying that the linear dielectric response tensor has a δ -function dependence. For the vast majority of problems in nonlinear optics, the media of interest produces approximately a local response. Consequently we shall ignore the spatial dependence of $\chi^{(1)}$ in what follows.

The form of the linear dielectric response tensor allows a simpler relation to be made between the Fourier transforms of the polarization and the applied field,

$$P_L(\omega) = \chi^{(1)}(\omega).E(\omega) \quad 1.4$$

where $\chi^{(1)}(\omega)$, the linear susceptibility tensor, is the Fourier transform of the linear dielectric response tensor. The tensor relation in equation (1.4) can also be written as

$$P_{L,i}(\omega) = \sum_J \chi_{ij}^{(1)}(\omega)E_j(\omega) \quad 1.5$$

Where the subscript i signifies the i^{th} Cartesian coordinate ($i = x, y, z$) and the sum is over $J=x, y, z$. The tensor $\chi^{(1)}(\omega)$ thus has nine components. In an isotropic medium, there is only one independent, non-zero component, and the susceptibility is written as a scalar quantity, $\chi^{(1)}(\omega)$. This can be represented in the molecular (microscopic) level as

$$\langle \mu(\omega) \rangle = \alpha^{(1)}(\omega).E_{local}(\omega), \quad 1.6$$

where $\alpha^{(1)}$ is the molecular polarizability, E_{local} is the local electric field (at the molecule), which is a superposition of the applied field E and the net field due to the surrounding dipoles. An analytical expression for the local field can be obtained for isotropic and cubic medium. The relationship between the susceptibility and the polarizability for this media is given by

$$\chi^{(1)} = \left(\frac{n^2 + 2}{3} \right) N \alpha^{(1)} \quad 1.7$$

The quantity $f(\omega) = [n^2(\omega) + 2]/3$ is called the local field factor.

The nonlinear optical phenomena arise from the break down of equation 1.4 at sufficiently intense fields. As the applied field strength increases, the polarization of the medium is no longer linear as showed in Figure 1.5 parts b and c. Only after the advent of the laser could optical fields of sufficient intensity be produced to observe this effect.² To account for the “nonlinearity” of the medium response, the induced polarization is given as a power series expansion in the applied electric field.

It is assumed that the nonlinear polarization can be written as

$$P = P_L + P_{NL} \quad 1.8$$

$$P_{NL} = P^{(2)} + P^{(3)} \quad 1.9$$

$$P^{(2)}(r, t) = \int_{-\infty}^{\infty} \int_{-\infty}^{\infty} \chi^{(2)}(t-t', t-t'') : E(r, t') E(r, t'') dt' dt'' \quad 1.10$$

$$P^{(3)}(r, t) = \int_{-\infty}^{\infty} \int_{-\infty}^{\infty} \int_{-\infty}^{\infty} \chi^{(3)}(t-t', t-t'', t-t''') : E(r, t') E(r, t'') E(r, t''') dt' dt'' dt''' \quad 1.11$$

It is important that the field in the equations above is the *total* applied, which can be a superposition of many fields of different frequencies. $\chi^{(n)}$ is called nth order dielectric response, and is a tensor of rank n+1. As for the linear dielectric response, it is assumed that the response is local and hence the spatial dependence of $\chi^{(n)}$ is suppressed.

If the applied field is a superposition of monochromatic or quasi monochromatic waves, then it is possible to write expressions analogous to equations 1.10 and 1.11 in terms of Fourier transforms of the nonlinear polarization, fields, and the dielectric response tensor, provided the frequency dependence of the Fourier transform of $\chi^{(n)}$ is slowly varying in the region of each Fourier components (e.g., its various laser

frequencies), then, the nonlinear polarization will consist of several terms oscillating at various combination frequencies. For example, if the total field consists of two waves oscillating at frequencies ω_1 and ω_2 , the second-order nonlinear polarization will have components oscillating at $2\omega_1$, $2\omega_2$, $\omega_1+\omega_2$, and $\omega_1-\omega_2$ and dc terms at zero frequency. Similarly, with three fields oscillating at frequencies ω_1 , ω_2 , ω_3 , the third-order polarization will oscillate at $3\omega_1$, $3\omega_2$, $3\omega_3$, $\omega_1+\omega_2+\omega_3$, $\omega_1+\omega_2-\omega_3$, etc.

Thus, applying Fourier transform the equation 1.10 can be written as follows. Consider a second-order polarization oscillating at ω_3 due to the presence of fields oscillating at frequencies ω_1 and ω_2 with $\omega_3 = \omega_1 + \omega_2$. Then the i^{th} Cartesian component of the complex polarization amplitude is expressed as

$$P_i^{(2)}(\omega_3) = D^{(2)} \sum_{JK} \chi_{iJK}^{(2)}(-\omega_1; \omega_2, \omega_3) E_J(\omega_2) E_K(\omega_3) \quad 1.12$$

$$D^{(2)} = \begin{cases} 1 & \text{for indistinguishable fields} \\ 2 & \text{for distinguishable fields.} \end{cases}$$

where $\chi^{(2)}(-\omega_3; \omega_1, \omega_2)$ is the second order susceptibility and Fourier transform of $\chi^{(2)}(t)$. The form of equation 1.12 allows for the possibility that the frequencies ω_1 and ω_2 are equal or equal in magnitude and opposite in sign. In this case, there may actually be only one field present, and the degeneracy factor $D^{(2)}$ takes this into account.

This notation is easily extended to higher orders. When three frequencies ω_1 , ω_2 , ω_3 are present, the third-order polarization at $\omega_4 = \omega_1 + \omega_2 + \omega_3$ is given by

$$P_i^{(3)}(\omega_4) = D^{(3)} \sum_{JKL} \chi_{iJKL}^{(3)}(-\omega_1; \omega_2, \omega_3, \omega_4) E_J(\omega_2) E_K(\omega_3) E_L(\omega_4) \quad 1.13$$

Where degeneracy factors, in this case, becomes

$$D^{(3)} = \begin{cases} 1 & \text{all fields indistinguishable} \\ 3 & \text{two fields indistinguishable} \\ 6 & \text{all fields distinguishable} \end{cases}$$

This form of third-order polarization allows for various combination frequencies, even when only two fields are present, such as $\omega_1+2\omega_2$, or $2\omega_1-\omega_2$, etc. the degeneracy factor is just due to the number of different ways in which the products of the Fourier components appear in the expansion of the *total* field to some power.

Hence the total polarization can be represented as

$$P_i(\omega_1) = \sum_j \chi_{ij}^{(1)}(-\omega_1; \omega_2) E_j(\omega_2) + \frac{1}{2} \sum_{JK} \chi_{iJK}^{(2)}(-\omega_1; \omega_2, \omega_3) E_j(\omega_2) E_k(\omega_3) + \frac{1}{6} \sum_{JKL} \chi_{iJKL}^{(3)}(-\omega_1; \omega_2, \omega_3, \omega_4) E_j(\omega_2) E_k(\omega_3) E_L(\omega_4) + \dots \quad 1.14$$

The macroscopic susceptibilities are related to the corresponding molecular susceptibilities by local field corrections (f)⁹ and the molecular number density (N)⁶

$$\chi_{ij}^{(1)} = N \sum_{ij} f_i \langle \cos \theta_{ii} \rangle f_j \langle \cos \theta_{jj} \rangle \alpha_{ij} \quad 1.15$$

$$\chi_{iJK}^{(2)} = N \sum_{ijk} f_i \langle \cos \theta_{ii} \rangle f_j \langle \cos \theta_{jj} \rangle f_k \langle \cos \theta_{kk} \rangle \beta_{ijk} \quad 1.16$$

$$\chi_{iJKL}^{(3)} = N \sum_{ijkl} f_i \langle \cos \theta_{ii} \rangle f_j \langle \cos \theta_{jj} \rangle f_k \langle \cos \theta_{kk} \rangle f_l \langle \cos \theta_{ll} \rangle \gamma_{ijkl} \quad 1.17$$

Where the variables, i, j, k and l now span the molecular axes, and the angle between the macroscopic axis I and microscopic i is denoted as θ_{ii} . The local field factors essentially correct for the difference between an applied field that would be felt by the molecule in free space and the local field detected in a material. These factors usually take the form of the well known Onsager¹⁰ or Lorentz¹¹ correction fields. The microscopic polarization (p_i) can then be expressed as

$$p_i(\omega_1) = \sum_j \alpha_{ij}(-\omega_1; \omega_2) E_j(\omega_2) + \frac{1}{2} \sum_{jk} \beta_{ijk}(-\omega_1; \omega_2, \omega_3) E_j(\omega_2) E_k(\omega_3) + \frac{1}{6} \sum_{jkl} \gamma_{ijkl}(-\omega_1; \omega_2, \omega_3, \omega_4) E_j(\omega_2) E_k(\omega_3) E_l(\omega_4) + \dots \quad 1.18$$

The manifestation of nonlinear optical behavior can be clearly seen by substituting a sinusoidal field $E = E_0 + E_1 \cos \omega t$ in to the polarization. Substitution this in equation 1.14 gives:

$$P = (E_0 + E \cos \omega t) \chi^{(1)} + (E_0 + E \cos \omega t)^2 \chi^{(2)} + (E_0 + E \cos \omega t)^3 \chi^{(3)} + \dots \quad 1.19$$

Rearranging the equation,

$$\begin{aligned} P = & (\chi^{(1)} E_0 + \chi^{(2)} E_0^2 + \chi^{(3)} E_0^3) + \\ & (\chi^{(1)} E_1 + 2\chi^{(2)} E_0 E_1 + 3\chi^{(3)} E_0^2 E_1) \cos \omega t \\ & + (\chi^{(2)} E_1^2 + 3\chi^{(3)} E_0 E_1^2) \cos^2 \omega t \\ & + (\chi^{(3)} E_1^3) \cos^3 \omega t + \dots \end{aligned} \quad 1.20$$

Using Trigonometric relations, $\cos^2 \omega t = (1 + \cos 2\omega t)/2$ and $\cos^3 \omega t = (\cos 3\omega t + 3\cos \omega t)/4$, equation 1.20 becomes

$$\begin{aligned} P = & \chi^{(1)} [E_0 + E_1 \cos \omega t] \\ & + \chi^{(2)} [E_0^2 + (1/2)E_1^2 + 2E_0 E_1 \cos \omega t] + (1/2)E_1^2 \cos 2\omega t \\ & + \chi^{(3)} [E_0^3 + (3/2)E_0 E_1^2 + 3E_0^2 E_1 \cos \omega t] + (3/4)E_1^3 \cos 2\omega t \\ & + 3/2 E_0 E_1^2 \cos 2\omega t + (3/4)E_1^3 \cos 3\omega t + \dots \end{aligned} \quad 1.21$$

The 1st terms in the brackets for all $\chi^{(n)}$ are constant factors. They give rise to a dc field across the medium

1.3. Second order nonlinear optical processes

This section explains the processes associated with the $\chi^{(2)}$ in detail. From equation 1.21,

$$P^{(2)} = \chi^{(2)} [E_0^2 + (1/2)E_1^2 + 2E_0 E_1 \cos \omega t] + (1/2)E_1^2 \cos 2\omega t \quad 1.22$$

The coefficients E_0 , E_1 corresponds to the linear electro-optic effect and is represented as $\chi^{(2)}(-\omega; \omega, 0)$. The sign attached to a frequency is negative if the photon is emitted and positive, if it is absorbed. The last term, which is square in the ac electric field and has a frequency of 2ω is known as second harmonic generation (SHG) process.

Consider that two coherent light waves of unequal frequencies ω_1 and ω_2 are traveling in the material, then the 2nd and 4th terms in the previous equation 1.22 becomes

$$\chi^{(2)}(1/2)E_1^2[\cos(\omega_1 - \omega_2) + \cos(\omega_1 + \omega_2)] \quad 1.23$$

Thus it contains two frequencies, $(\omega_1 + \omega_2)$ and $(\omega_1 - \omega_2)$. This phenomenon is known as *optical mixing*. While $(\omega_1 + \omega_2)$ is called sum frequency generation (SFG), $(\omega_1 - \omega_2)$ is called the difference-frequency generation (DFG). The second harmonic generation (SHG) process, actually, is a special case of SFG, where the frequencies of the photons from the incident beams are equal ($\omega_1 = \omega_2$). Similarly, *optical rectification (OR)* is a special case of DFG for $(\omega_1 = \omega_2)$. Thus OR susceptibility, is represented as $\chi^{(2)}(0; \omega, -\omega)$.

Three-wave mixing (two inputs and one output) is known as a parametric process, if the initial state and the final state of the system remains unchanged after interaction with light. This is because in an emission process the system comes back to the same state after emission. The same is not true for an absorption process where the initial and final states differ. The most prominent example of a non-parametric process is two-photon absorption. Various processing nonlinear optical spectroscopy are listed in **Table 1.1**

Parametric processes can be used to make various devices (**Figure 1.4**). For example, *Optical Generators* can produce a wave of higher (up-conversion) or lower frequency (down-conversion) than the initial frequency. In *Parametric Amplifiers* three waves interact at frequency ω_1 , ω_2 and ω_3 , so that one wave at frequency ω grows at the expense of the input frequency called the pump frequency. A very important device using parametric amplification is the *Optical Parametric Oscillator*. In this device, one uses a single pump source as an input and the output intensity can be controlled by changing the positions of the two mirrors surrounding the material.

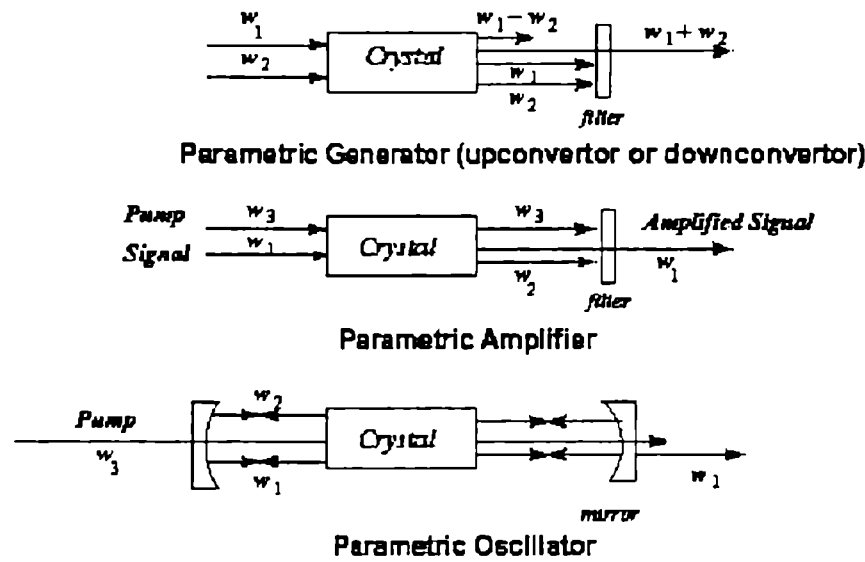


Figure 1.4. Some important *Parametric* processes

Table1.1: Some important processes involving Nonlinear Optical Spectroscopy

Process	Order	Frequency relation
Linear Response	1	$-\omega; \omega$
Pockels Effect (EO effect)	2	$-\omega; \omega, 0$
Sum Mixing	2	$-\omega_3; \omega_1, \omega_2$
Second Harmonic Generation (SHG)	2	$2\omega; \omega, \omega$
Optical Rectification (OR)	2	$0; \omega, -\omega$
Intensity- dependent refractive index	3	$-\omega; \omega, -\omega, \omega$
Optical Kerr Effect	3	$-\omega_1; \omega_2, -\omega_2, \omega_1$
Dc Kerr Effect	3	$-\omega; 0, 0, \omega$
Two-photon Absorption (TPA)	3	$-\omega_1; \omega_2, \omega_2, \omega_1$
Third Harmonic Generation (THG)	3	$3\omega; \omega, \omega, \omega$
Coherent anti-stokes Raman scattering	3	$-(2\omega_1, -\omega_2); \omega_1, \omega_1, -\omega_2$
General four Wave mixing (FWM)	3	$-\omega_4; \omega_1, \omega_2, \omega_3$
Three-Photon Absorption (TPA)	5	$-\omega_1; \omega_2, -\omega_3, \omega_3, \omega_2, \omega_1$
n^{th} Harmonic Generation	n	$n\omega; \omega, \omega, \dots, \omega$
Multi-photon Absorption	$2n-1$	$-\omega; \dots, -\omega, \omega, \dots, \omega$

1.4. Symmetry requirements for second-order process

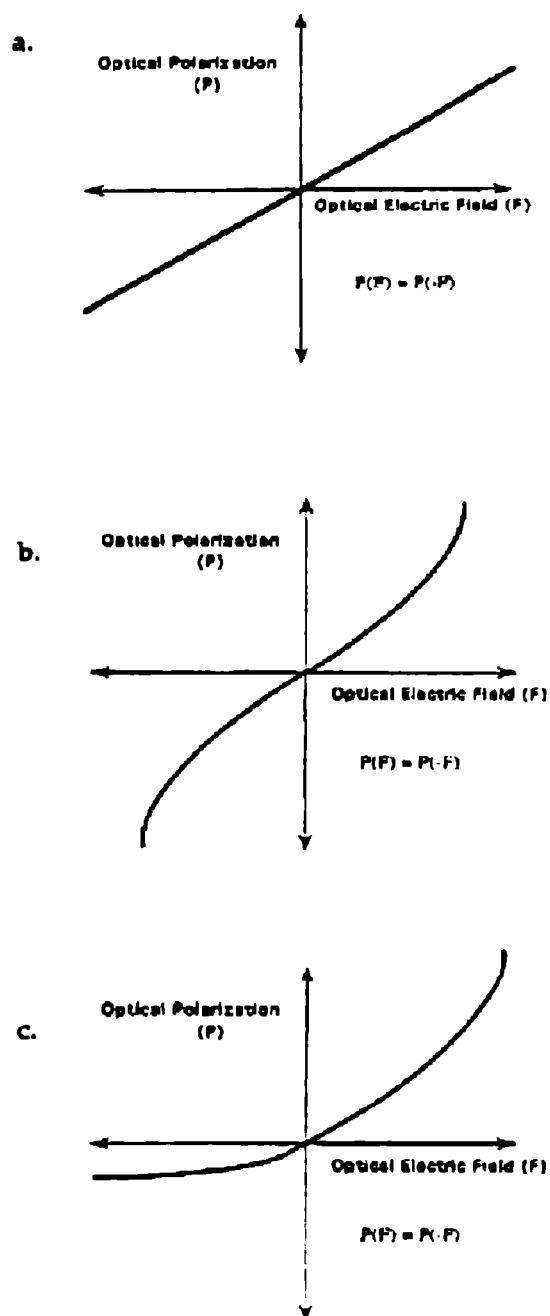


Figure 1.5 Scheme showing the dissipation of the optical polarization.(a) Linear (b)centrosymmetric nonlinear (c) non-centrosymmetric nonlinear

Owing to the spherical nature of nearly all molecular structures, and the differing atomic charges, δ^+ and δ^- , that each element possesses relative to each other in a given molecule, the overall polarization inevitably has a net direction, i.e. it is anisotropic. The relative orientation of a molecule with respect to others within the repeating (unit cell) crystal-lattice motif is also important, since the SHG effect is a supramolecular rather than a molecular one. This polarization anisotropy is therefore three dimensional and thus (beyond the molecule) dependent upon supramolecular symmetry. The associated mathematics of the symmetry considerations is therefore very much involved, since the SHG effect is a third rank tensor. But it is only the results that are important

here: in total the symmetry conditions dictate that SHG active compounds can only occur in 18 out of the 32 crystallographic point groups.⁵

In 1962 Kleinman found that in many nonlinear processes where all the interacting frequencies are far away from resonance, energy is simply exchanged between the fields and not dissipated in the medium.¹² Thus, the dispersion of the $\chi^{(n)}$ is negligible and therefore the susceptibility tensors are invariant under any permutation of their Cartesian indices. For instance, in the $\chi^{(2)}$, the symmetry relations give rise to

$$\chi_{ijk}^{(2)} = \chi_{ikj}^{(2)} = \chi_{jik}^{(2)} = \chi_{jki}^{(2)} = \chi_{kij}^{(2)} = \chi_{kji}^{(2)} \quad 1.24$$

Thus due to Kleinman symmetry relations, the number of independent components of $\chi^{(2)}$ reduces from 7 to 10 and that of $\chi^{(3)}$ from 81 to 15.

Thus for a medium to exhibit frequency conversion process mediated by $\chi^{(2)}$, the medium must have $\chi^{(2)} \neq 0$. This condition requires that at a molecular level the nonlinear coefficient β must be nonzero. Furthermore, the orientationally averaged sum of β at all sites that gives rise to the macroscopic $\chi^{(2)}$ should not be zero. These two conditions lead to the following symmetry requirements for the realization of $\chi^{(2)} \neq 0$:

1. The molecules are non-centrosymmetric (do not possess an inversion symmetry). For such a structure, β -being an odd rank (3rd rank) tensor-is not zero (**Figure 1.5**)
2. The molecules in the bulk form are arranged in a noncentrosymmetric structure. Only then the overall $\chi^{(2)}$ is not zero

A molecular design often used to make molecules with large β values is

D- π -conjugation-A

A molecular unit involving π -conjugation is connected to an electron donor, D (such as $-NH_2$), at one end and to an electron acceptor group, A (such as $-NO_2$), at the other end. A classic example is *para*-nitroaniline (PNA) molecule.

1.5. Nonlinear optical properties of organic molecules

First observed in quartz in 1961² the SHG effect was achieved using materials like inorganic-crystals of KDP and lithium niobate, $LiNbO_3$. In inorganic materials, the process relies on suitable perturbation of key ions within the solid-state crystalline (periodic) structural framework of a compound.

A lot of effort in the last two decades has been put in towards the understanding and the controlling factors that may lead to an acentric crystal that shows large NLO response functions. It is quite a non-trivial task to arrange molecules in a noncentrosymmetric fashion in the crystal. One requires a combination of chemical intuition; theoretical understandings of intermolecular forces as well as very sound knowledge of crystal engineering to tailor the molecules for such applications.⁵

The symmetry of the molecular structure is crucial:¹³ SHG can only be observed in non-centrosymmetric compounds, i.e. materials whose three dimensional (3D) structures lack a centre or inversion symmetry. This is because the SHG effect is proportional to the polarization in the molecule. This understanding has led, not only to the discovery of other inorganic materials for SHG applications, e.g. $KTiO_3$ (KTP), but also to the investigations of organic compounds as optical materials. These studies were catalyzed by the realization that organic materials which exhibit the SHG effect do so by the transfer of electronic charge across the molecule. Their optical response is therefore much faster than that in inorganic materials, where ionic perturbations cause the effect. This has evident consequences for speeding-up optical processes in, for example, telecommunication and optoelectronics industries. Moreover, the SHG output in many organic materials has already been shown to exceed those of their inorganic counterparts.

Second harmonic generation in organic molecule was first reported by Pao¹⁴ in 1964. It was observed that, when crystals of 3,4 benzpyrene and 1,2 benzanthracene were irradiated with intense ruby laser light, they emit narrow line radiation at about 3470 Å, corresponding to the second harmonic of the incident ruby laser radiation. In the same year Heilmeyer and coworkers also reported the SHG in the crystal hexamine.¹⁵ They found a relationship between optical second harmonic generation and molecular electro-optic effect.

An important development in nonlinear optical materials occurred in 1970, when Davydov *et al* reported a strong second harmonic generation (SHG) in organic materials having electron donor and acceptor groups connected by a benzene ring, due to charge transfer.¹⁶ Basic analysis of molecular structures of organic SHG-active materials allowed a series of axioms to be established that described the components of a molecule that will optimize the nature of these electronic charge-transfer processes. Planar molecules, with a strongly electron-donating (highly δ^+) group on one end an electron-withdrawing (highly δ^-) group at the other (i.e a "push-pull" system), joined together with an extended π -conjugated "electronic bridge" to facilitate the charge transfer across the molecule, were found to be the best basic structural form.¹⁷⁻²⁰ The presence of aromatic ring within this electronic bridge was generally found to ameliorate the effect further.

These favorable structural components can be thought of as a kind core 'Molecular Lego' with additional bridges and extra side groups subtly changing their molecular shape and electronic form.²¹ This paradigm continues to be the basis of most of the work in this area world wide.

The π conjugated system could be azobenzene, stilbene, biphenyl, heterocycles, polyenes etc. The electron acceptors and donors that can be attached to a π -conjugated system are as follows:

Acceptor Groups: NO₂, COOH, CN, CHO, CONH₂, CONHR, CONR, CONR₂, SO₂R, CF₃, COCH₃, C₂(CN)₃, CH=C(CN)₂ etc

Donor Groups: NH₂, NHR, NR₂, F, Cl, Br, OR, OH, C(CH₃), COOR etc.

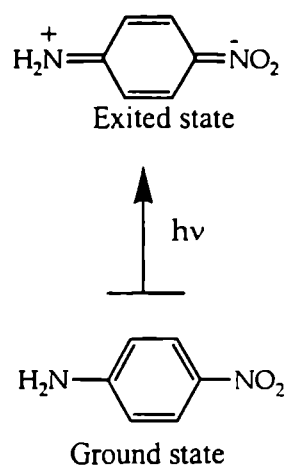


Figure 1.6 Molecular structure of ground-state and lowest energy excited state for PNA

Much interest in second-order NLO properties of substituted benzene derivatives stems from the basic studies of the chemistry and physics of *para*-nitroaniline (PNA) molecule. PNA molecule consists of a benzene ring in which an electron donor amino (NH₂) group and an electron acceptor nitro (NO₂) group in the *para* position. These opposite ends of the conjugated system lead to maximum acentricity in the molecule. The π -electron donor and acceptor configuration composed of NH₂ and NO₂ group, respectively, in PNA results in intramolecular charge transfer interactions. Therefore, PNA exhibits extremely large first hyperpolarizability (β) compared to nitrobenzene and aniline due to highly asymmetric charge distribution arising from the π -electronic structure of the molecule. The origin of first hyperpolarizability in PNA can be explained as follows. In benzene molecule, β disappears due to the symmetry with the centre of inversion. The electron donor or electron acceptor substitution in benzene ring removes such a restriction and thus generates β . β value of PNA (21.1×10^{-30} esu) is about 11 times larger than nitrobenzene (1.97×10^{-30} esu) and 26 times larger than aniline (0.79×10^{-30} esu)²². The β values of *ortho* (6.4×10^{-30} esu) and *meta*-nitroaniline (4.21×10^{-30} esu) are also much lower than PNA. It is because, in PNA molecule, strong donor-acceptor charge transfer interactions are prominent by attaining the most desirable resonance structure having alternating single and double bonds. Even though *ortho*-nitroaniline also has the same type of resonance structure, the donor-acceptor interaction in *ortho* isomer (in *meta* also) are negligible because, β predominates in a mesomeric manner. PNA exhibits very large first hyperpolarizability due to its highly asymmetric charge-correlated excited states of the π -electronic structure.¹⁹ (Figure 1.6). Hence PNA represents a model for one-dimensional donor-acceptor charge-transfer interactions.

D- π -conjugation-A molecular systems have large NLO response because of the delocalized nature of the π -electrons resulting in low-energy excitonic levels in an anti-parallel arrangement in the crystal PNA crystallizes in a centrosymmetric space group,

thereby making the NLO response for the whole crystal almost zero, which restricts the observation of any macroscopic second-order optical effects. This drawback has led to the search for other molecular materials. The most important of such molecules has been 3-methyl-4-nitropyridine-1-oxide (POM) shown in Figure 1.7. For this molecule, there is a cancellation of the ground state dipole moment as the dipole moments for the pyridine-1-oxide and the nitrobenzene fragments are equal and opposite. So, the molecules have no urge to crystallize in an anti-parallel arrangement. Thus, for such a system, even though the ground state dipole moment is zero, the excited states have finite dipole moments. Such molecules thus exhibit large β values. The crystals of POM thus have a substantial $\chi^{(2)}$ (about two times that of LiNbO₃).

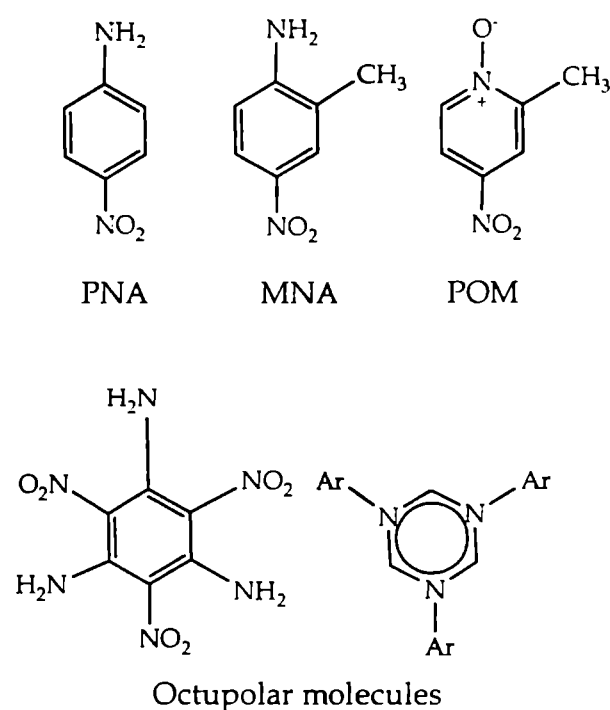


Figure 1.7 Molecules which exhibit significant $\chi^{(2)}$ in bulk crystals

Also, closely related derivatives of PNA, which do not have a center of symmetry in the crystalline state, have been found to display interesting NLO properties and are gaining considerable attention. The most important derivative and the commonly used reference for measuring the second harmonic generation efficiency is 2-methyl-4-nitroaniline molecule (MNA). This consists of a donor amino (NH₂) group located at the first carbon atom of the benzene ring, a methyl (CH₃) group at the second carbon atom, and an acceptor nitro group at the fourth carbon atom. This chemical substitution provides the maximum acentricity to the molecule and gives rise to a noncentrosymmetric crystal structure with substantially large value of $\chi^{(2)}$. In MNA, the simple substitution of a methyl group at second carbon atom of a PNA molecule changes the whole physical

aspects of the optical nonlinearity. Using the same concept of donor-acceptor intermolecular interactions as in PNA and substituting a methyl group to PNA provides a novel chemical species, MNA molecule that exhibits exceptionally large SHG activity because of being non-centrosymmetric. The nonlinear optical coefficient (which represents the measured induced polarization), d_{11} of MNA in solution was determined by an electric-field induced second harmonic generation (EFISH) technique to be $500 \pm 25\%$ over that of d_{11} of quartz, which is 2000 times larger than d_{11} coefficient of LiNbO_3 . MNA has been taken as the reference material through out this work.³ Therefore the molecular engineering approach offers an avenue to design and tailor second-order NLO materials of interest.

In 1993, Zyss had shown that molecules with octupolar moments are very promising candidates for NLO applications in crystals.²³⁻²⁵ For these molecules even though the ground state dipole moment is zero, the higher order multipoles like the octupolar moments are non-zero. Very similar to that for POM, these molecules also have non-centrosymmetric arrangements in the crystal structure. Some such molecules exhibiting octupolar moments are shown in **Figure 1.7**.

Another way of ensuring spatial acentricity in a crystal is the incorporation of chiral substituents in the molecular structure. Optically pure materials, which have only left handed/right handed symmetry, are inherently non-centrosymmetric. Such compounds are, in fact, readily available in nature (amino acids, sugars and alkaloids are well known examples existing only in single enantiomer). Thus crystals of these materials are expected to be NLO active. Some of the best known examples are 2-methyl-2-(2, 4-dinitroaniline)-propionic acid (MAP), (+)-camphor-10-sulphonic acid and N-(4-nitrophenyl)-L-prolinol (NPP). They are shown in **Figure 1.8**

For biological systems, important second-order effects are associated with the interface and with electric field poling. Surface second harmonic generation from biological membrane provides a powerful method for second-harmonic imaging to selectively probe interactions and dynamics involving membranes. The electric-field-

induced second harmonic generation provides an excellent probe for membrane potential. This has a very promising use in bio-imaging.²⁶⁻²⁸

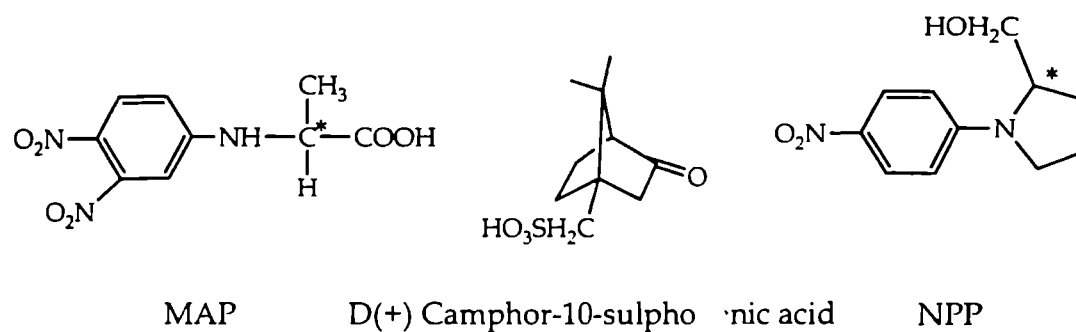


Figure 1.8. Chiral molecules forming non-centrosymmetric crystals

Factors such as increased spacer length, increased planarity, and overall increased conjugation (i.e. Hammett reaction -constant parameters) and the strength of donor and acceptors (Hammett substituent-constant parameters) all play significant roles and are amenable to design.

1.6. Polymers for nonlinear optics

Organic polymers are considered as the most valuable specialty materials for the next generation photonic materials because,²⁹

1. They provide tremendous architectural flexibility to tailor the desired photonic function and material performance
2. They can be economically produced on a large scale.
3. Their chemical modification facility and the generation of new properties.
4. They provide ease of processing and fabrication. They are compatible to metals, glasses and ceramics.
5. They are environmentally stable and robust materials
6. They are light and tough materials.

The topic of nonlinear organic polymers have been reviewed by Chemla and Zyss,³⁰ Burland³¹ and Nalwa et al¹. The recent developments in the field of polymer based nonlinear materials reflect continued growth of interest.

Several design strategies have been developed for the synthesis of NLO active polymers, such as guest-host systems (NLO chromophores doped in a host polymer matrix), side chain systems (NLO chromophores incorporated as side chain) and main chain systems (NLO chromophores incorporated in the main chain⁵). NLO chromophores are molecules having electron donor and acceptor groups separated by a conjugated π -system.

1.6.1 Guest-host systems

A guest-host system is generally prepared by mixing a NLO dye possessing a large β value with an amorphous polymer matrix of high optical transparency. A NLO dye is dissolved in the polymer host using a common solvent and spin coated as a film on a substrate. The films are dried under an electric field. The advantages and disadvantages of the systems can be summarized as follows,

Advantages:

1. There is an unlimited selection of NLO chromophore guests and host polymer matrices.
2. Relatively inexpensive and ease of processing into thin films.
3. High mechanical strength and low dielectric constant.
4. Wide range of operating frequencies.

Disadvantages:

1. Large decay of NLO activity due to orientational relaxation.
2. Low NLO activity due to limited solubility of chromophore in polymer matrix.
3. Inhomogeneity leads to scattering losses.
4. Sublimation of NLO dye at elevated temperatures.
5. Thermal instability

1.6.2 NLO chromophore functionalized polymers

Several chemical strategies have been used to attach NLO chromophores into a polymeric backbone. The most important of these belongs to two classes

- a) NLO chromophore functionalized side chain polymers: This class presents linear polymers with covalently attached NLO active side groups. A NLO chromophore is covalently bound as a pendent group to the polymer backbone. **(Figure 1.9)**
- b) NLO chromophore functionalized main chain polymers: In this class, the polymer main chain comprises of NLO chromophore. **(Figure 1.10)**

The main chain systems are found to be more effective because, they offer several advantages over guest-host systems. The advantages of polymers containing NLO chromophores are

1. A high concentration of NLO chromophore can be introduced by covalently functionalized polymers. Tailoring of NLO property and better material performance is possible via chemical modification.
2. Show increased stability towards relaxation after poling.
3. High film homogeneity can be achieved which reduces scattering.
4. Ease of processing.

The main-chain polymers can be divided in to head to tail random and accordion. For the head to tail and random type, the dipole moments of rigid chromophore units are arranged parallel to the polymer backbone; however, the dipole moments of chromophores in the accordion polymer are essentially perpendicular to the main chain.³⁶

It is important that the medium for second harmonic generation is non-centrosymmetric. The second order NLO response of the polymeric systems can be achieved after the alignment of dipoles by applying an electric field at a temperature above T_g , which induces non-centrosymmetry in the material. This method is called

poling. Once the dipoles are aligned, relaxation may take place, which destroys non-centrosymmetry and hence the second order NLO response reduces.³⁷

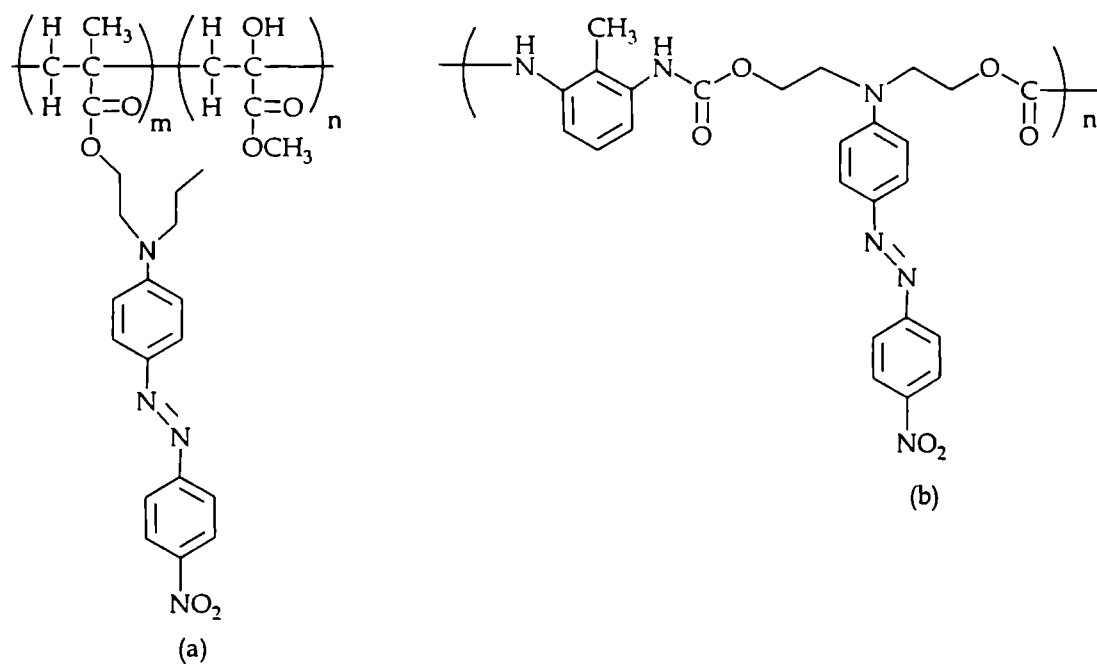


Figure 1.9 NLO active side chain polymers^{32,33}

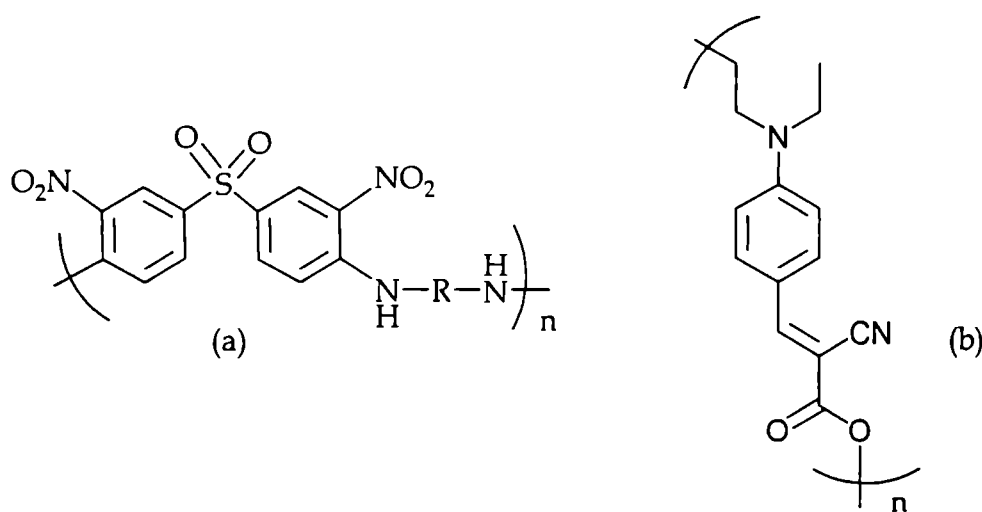


Figure 1.10. Main chain NLO polymers^{34,35}

1.7. Chiral polymers

Cooperative chiral order plays a vital role in the self-assembly of supramolecular structures in liquid crystals, organic thin films and lipid membranes. One adopted

strategy to introduce non-centrosymmetry in simple organic crystals is to incorporate an optically active substituent, which force the molecule to crystallize into a noncentrosymmetric arrangement. Many organic molecules reported on the basis of this idea have high second harmonic generation ability.^{30, 38-41}

A recent development in the field of polymer chemistry is the precise control of higher-order structures of macromolecules. Especially, much attention has been paid to chiral polymers in which the chirality is mainly based on helical backbones with an excess of one-handed screw sense. One goal in the study of helical polymers is to understand nature that elegantly utilizes self-organization process to construct helical and multiple helical architectures such as helical polypeptides and nucleic acids. In addition to this, the excellent ability of helical polymers to recognize chiral molecules has led not only to the discovery of a variety of helical polymers, but also to the development of new functions based main-chain chirality and chiral chain framework. Among the helical polymers, conjugated helical polymers are very interesting since they are potentially useful as polarization-sensitive electro-optical materials, asymmetric electrodes, and so forth.^{42, 43}

The simplest method of synthesizing optically active polymers involves the polymerization of optically active monomers. However, this is often less attractive from the view point of the polymerization reaction. Asymmetric polymerization which produces configurationally or conformationally specific optically active polymers starting from optically inactive monomers is much more attractive and challenging, and remarkable advances, particularly on helical polymers, have been made over the past two decades. Optically active polymers may be obtained in several ways including (a) polymerization with a chiral catalyst or initiator,^{44, 45} (b) chiral doping of achiral (racemic) polymers with enantiopure chiral ions,⁴⁶ (c) separation of racemic mixture of enantiomeric helices using chiral stationary phase (CSP) chromatography (for nondynamic systems,⁴⁷ (d) chiral complexation of achiral or racemic polymers with enantiopure chiral ligands/guests,⁴⁸ (e) post-polymerization functionalization with chiral moieties,⁴⁹ (f) polymerization of enantiopure chiral monomers,⁵⁰ (g) incorporation of enantiopure chiral end groups⁵¹ and (h) copolymerization of enantiopure chiral

monomers with achiral monomers or with an enantiomeric excess (ee) of one enantiomer over the other.⁵² In the last two cases, it is the presence of enantiopure chiral “seeds” which results in the adoption of a preferential helical screw sense; in even non-enantiopure-substituted backbone regions by the preferential stereo relationship between enantiopure chiral side chains and their nearest neighbours.

The chiro-optical properties exhibited by optically active polymers are very useful for understanding their configurational and conformational characteristics. Optical activity is a physical spectral property of a chiral material caused by asymmetric configurations and conformations, which have no plane or centre of symmetry. Chirality (optical activity) can be introduced in a macromolecule by attaching chiral centers in the lateral chains or in the main chain.⁵³ The attachment of chiral groups in the polymer chain is observed to twist the main chain in predominantly one screw sense to generate helical structures.^{54,55} Polymers with chirality in the main chain were also reported to have twisted helical crystal shape.⁵⁶ Polymers without any asymmetric center (carbon or hetero atom) can have chiral conformation links or steric hindrance, which direct such molecules into helical conformation and their mirror planes pass through bonds and not through atoms.⁵³

Only non-centrosymmetric molecules or aggregates can possess a second order nonlinear response, that is, a nonvanishing molecular hyperpolarizability. The most common way to break centrosymmetry in polymers is through electrical poling with an applied electric field. Alternatively, second order nonlinear devices can be constructed by synthesizing non-linear molecules or chromophores into a noncentrosymmetric supramolecular structure. When such structures extend to macroscopic dimensions, the poling of the chromophore can be achieved through chemical synthesis and there is no need of external poling. The permanent dipole moments of such structures can be very large because of the coherent addition of dipole moments achieved by high degree of polar order.⁵⁷ Persoons et al.⁵⁸ showed that nonlinear optical chromophores could be organized in a fixed non-centrosymmetric arrangement as side groups of polymers with a rigid backbone. They investigated the second order response of chiral polyisocyanides⁵⁸ (**Figure 1.11**) that contain nonlinear chromophore as side groups. The

chirality of the material is associated with the helical supramolecular configuration of the backbone. This results in a strong orientational correlation of side groups.

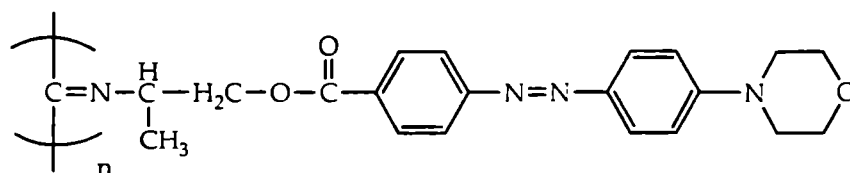
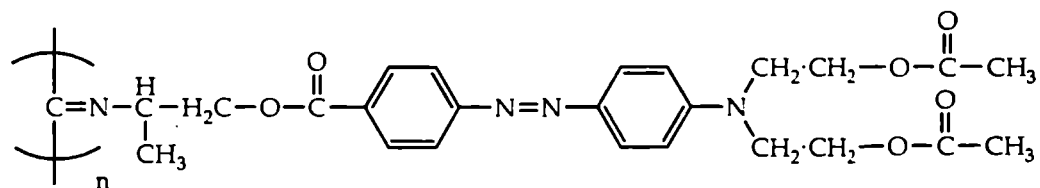


Figure 1.11 Structures of chiral polyisocyanides

Chiral polythiophenes (Figure 1.12) with helical backbone having second order nonlinear response suggests that a strong coupling exists between backbone and chromophore.⁵⁹ The nonlinear response arises from properties of the $\pi \rightarrow \pi^*$ transition, which corresponds to displacement of electrons along the helical conjugate backbone.

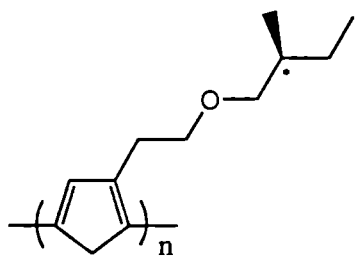


Figure 1.12 Structure of chiral polythiophenes

The incorporation of chiral binaphthyl units into polymer chains by *Pu et al* led to a class of conjugated polymers with inherently chiral main chains. These polymers possess a very stable main chain chiral helical configuration. This made them potentially useful for nonlinear optics. NLO chromophores can be organized in chiral binaphthyl polymer chains to construct non-centrosymmetric and multipolar

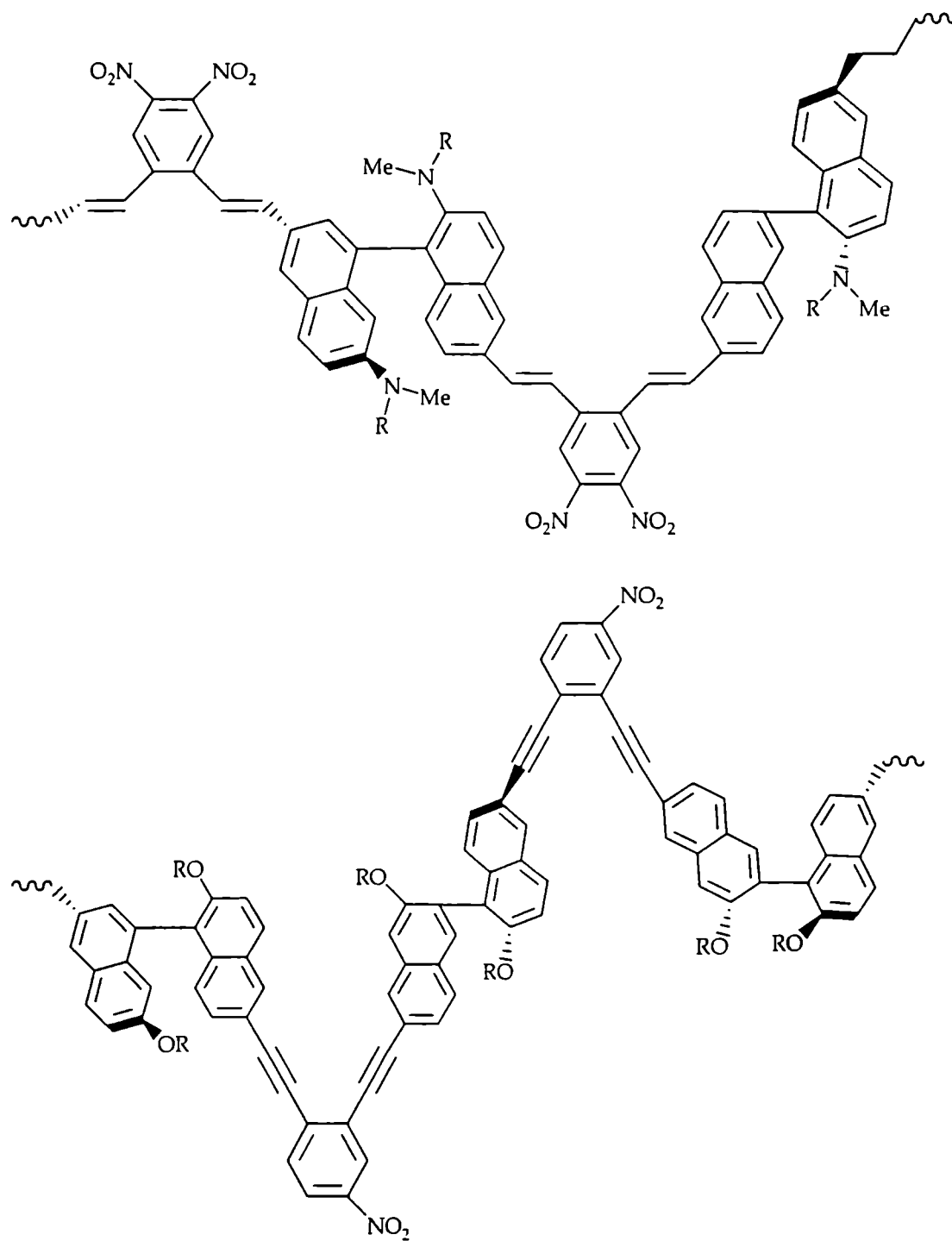


Figure 1.13 Structures of chiral polymers based on binaphthyl unit

materials⁶⁰⁻⁶³ Chiral polymers containing different electron acceptors and conjugated dipole units were reported. Pu *et al* prepared a dipole oriented chiral binaphthyl based polymers (Figure 1.13), which have a large dipole moments since the dipole units are

tilted in one direction along the polymer axis.⁶⁰ Polymers of such organized geometry are very interesting since, orientation correlated NLO chromophore on a helical polymer have been observed to generate an enhanced second order NLO response.^{60, 64}

There are mainly two theories proposed to explain the large SHG efficiency of chiral films and materials.

1. Electric-dipole approximation: By this method, there are different number of chiral and achiral tensors of β and $\chi^{(2)}$. Chiral tensor components arise due to the chirality of the medium and the contribution of these components will be higher in chiral media while it is negligible in achiral media.
2. Magnetic-dipole approximation: Chiral molecule may possess strong magnetic-dipole transitions, in addition to the electric-dipole transitions, which allow second order nonlinearities in macroscopically centrosymmetric materials.

The strongest experimental evidence supporting the significance of magnetic - dipole contributions to chiro-optical effects in SHG was presented by Persoons *et al.*^{63,65} Despite the wide spread use of magnetic-dipole contributions in interpreting chiral SHG measurements, there is a significant body of evidence suggesting that magnetic dipole contributions may be of only minor importance in oriented systems.²⁸

1.8. Calculation of nonlinear optical polarizabilities

To begin to understand how to optimize the second order NLO property that can be exploited in chiral media, the molecular hyperpolarizability is expressed in terms of β . Based on quantum mechanics, there are two types of molecular property (e.g. polarizability) calculations, such as *static property* and *dynamic property*. In *static* method, time independent Hamiltonian is solved (coupled treatment) to compute the polarizabilities; while in *dynamic* method, time dependent Hamiltonian is used (uncoupled treatment). This time dependence can be converted in to frequency dependence by Fourier Transformation. In the experiment to find second order NLO properties periodically oscillating (*dynamic*) electric field (laser) is used. Thus frequency independent hyperpolarizability is named as *static* hyperpolarizability [$\beta(0; 0, 0)$], while

frequency dependent one is the *dynamic* hyperpolarizability. E.g. Second harmonic generation [$\beta(-2\omega, \omega, \omega)$], Pockels effect [$\beta(-\omega, \omega, 0)$] etc⁶⁶

There are many approaches to calculate static molecular properties. Only two of them will be outlined here, which are used extensively in the subsequent chapters.

1) Numerical method, e.g. finite field method. 2) Analytical method e.g. CPHF (coupled perturbed Hartree-Fock) method.

1.8.1 Molecular properties (static) through Finite-Field and Analytical methods.⁶⁶

The quantum mechanical electronic Hamiltonian operator for an isolated molecule in a uniform static electric Field ε is

$$\hat{H}(\varepsilon) = \hat{H}^0 + \sum_{\sigma} \varepsilon \cdot r_{\sigma} - \sum_I Z_I \varepsilon \cdot R_I \quad 1.25$$

where σ and I label electrons and nuclei, respectively, Z_I is the atomic number of I^{th} nuclei, and H^0 is the "field-free" Hamiltonian. The field perturbed molecular energy is the appropriate expectation value for the many electron wave function, $\Psi(\varepsilon)$, determined in the presence of the applied field.

$$E(\varepsilon) = \langle \Psi(\varepsilon) | \hat{H}(\varepsilon) | \Psi(\varepsilon) \rangle \quad 1.26$$

If we treat the field as a weak perturbation, a Taylor expansion around the 'field-free' energy $E(\varepsilon)$ is a good description and yields for field perturbed energy $E(\varepsilon)$

$$E(\varepsilon) = E + \left. \frac{dE}{d\varepsilon} \right|_{\varepsilon=0} \varepsilon + \frac{1}{2} \left. \frac{d^2E}{d\varepsilon^2} \right|_{\varepsilon=0} \varepsilon^2 + \dots \quad 1.27$$

The first-order term in equation 1.27, i.e., the term linear in ε , involves the first derivative (gradient) of the energy with respect to ε , the second-order term, i.e., the term quadratic in ε , the corresponding second derivative, etc.

From equation 1.27, it is clear that, derivatives of the energy play a key role in describing the response of a molecule to an external perturbation. However, to identify

these derivatives with the molecular properties of interest, it is essential to consider also the physical aspect of the interaction with the external field. Doing that, it becomes clear that the first-order interaction with an external electric field involves the molecular dipole moment, the second-order interaction, the molecular polarizability etc. We can therefore make the following identifications,

$$\begin{aligned}
 \text{Dipole moment} \quad \mu &= -\left. \frac{dE}{d\varepsilon} \right|_{\varepsilon=0} && \text{(first derivative)} \\
 \text{Polarizability} \quad \alpha &= -\left. \frac{d^2 E}{d\varepsilon^2} \right|_{\varepsilon=0} && \text{(second derivative)} \\
 \text{First hyperpolarizability} \quad \beta &= -\left. \frac{d^3 E}{d\varepsilon^3} \right|_{\varepsilon=0} && \text{(third derivative)} \quad 1.28
 \end{aligned}$$

In principle, derivatives of the energy can be computed in a rather straight forward manner using finite-differentiation techniques, e.g., the gradient can be obtained via

$$\begin{aligned}
 \left. \frac{dE(\varepsilon_i)}{d\varepsilon_i} \right|_{\varepsilon=0} &= \frac{\langle \Psi(+n\varepsilon_i) | \hat{H} | \Psi(+n\varepsilon_i) \rangle - \langle \Psi(-n\varepsilon_i) | \hat{H} | \Psi(-n\varepsilon_i) \rangle}{2n\varepsilon_i} \\
 &= \frac{E(+n\varepsilon_i) - E(-n\varepsilon_i)}{2n\varepsilon_i}
 \end{aligned} \quad 1.29$$

with $n\varepsilon_i$ as an appropriate chosen step size of an electric field applied in the i direction. The main advantage of such a numerical differentiation scheme is that, it just requires the calculation of energies (though in the presence of the perturbation) and, thus, is rather easily implemented. As a consequence, finite-differentiation techniques have been and are still often used for the calculation of electric properties (so-called "finite-field" calculations). The disadvantages of the numerical differentiation scheme, however, are the limited accuracy (a problem in particular for the computation of higher derivatives), the high computational cost, as numerical differentiation requires for each derivative two additional energy calculations.

An approximate solution to the Finite Field energy derivative can be obtained perturbing the one electron Hartree-Fock operator.

$$\mathbf{H}^{HF} = -\frac{1}{2}\nabla^2 - \sum_i \frac{Z_i}{|\mathbf{r} - \mathbf{Z}_i|} + \sum_j^{occ} \{2J_j(\mathbf{r}) - K_j(\mathbf{r})\} \quad 1.30$$

where J and K are Coulomb repulsion and exchange interaction operators. The resulting Finite-Field version of the Coupled Perturbed Hartree-Fock,

$$\mathbf{H}^{FF-HF} = -\frac{1}{2}\nabla^2 - \sum_i \frac{Z_i}{|\mathbf{r} - \mathbf{Z}_i|} + \sum_j^{occ} \{2J_j(\mathbf{r}) - K_j(\mathbf{r})\} - r \cdot \boldsymbol{\varepsilon} \quad 1.31$$

provides acceptable and useful estimates of the polarizability components. This is, because, the HF-FF approach takes into account, directly and in a self-consistent way, the orbital relaxations in the presence of the perturbing external electric field. The components of the (hyper) polarizability tensors are obtained by the derivatives of the field dependent gradient (first derivative) with respect to the external field in the limit of zero field.

$$\alpha_i = \left. \frac{d \frac{dE(\varepsilon_i)}{d\varepsilon_i}}{d\varepsilon} \right|_{\varepsilon=0} = \frac{1}{2n\varepsilon_i} [\mu_i(n\varepsilon_i) - \mu_i(-n\varepsilon_i)] \quad 1.32$$

At higher values of ε , the self-consistency is not reached, and generally the best value for ε will be that just below numerical divergence threshold. It should be noted that in these equations, the perturbation of electric field on the nucleus (the last term in equation 1.25) is neglected.

Further disadvantages of the numerical differentiation scheme are;

- a) that there is no straight forward extension to the computation of frequency dependent properties and
- a) that handling of magnetic properties is less straight forward, as the computation of the latter requires the capability of dealing with complex wave function parameters. This capability in most cases is not available.

The alternative to numerical differentiation is analytic differentiation. This means that first an analytic expression for the corresponding derivative is deduced and then implemented within a computer code for the actual computation of the corresponding property. One might ask why a property such as the dipole moment is not just calculated as a simple expectation value, as it should be possible according to the postulates of quantum mechanics. Indeed, the Hellmann-Feynman theorem states the identity of the derivative and expectation value expression for first-order properties.

Differentiating equation 1.26 gives

$$\begin{aligned} \frac{dE(\varepsilon_i)}{d\varepsilon_i} &= \left\langle \frac{d}{d\varepsilon_i} \Psi(\varepsilon_i) \left| \hat{H}(\varepsilon_i) \right| \Psi(\varepsilon_i) \right\rangle + \left\langle \Psi(\varepsilon_i) \left| \frac{d}{d\varepsilon_i} \hat{H}(\varepsilon_i) \right| \Psi(\varepsilon_i) \right\rangle + \\ &\left\langle \Psi(\varepsilon_i) \left| \hat{H}(\varepsilon_i) \right| \frac{d}{d\varepsilon_i} \Psi(\varepsilon_i) \right\rangle \end{aligned} \quad 1.33$$

According to Hellmann-Feynman theorem, the first and third terms on the right hand side of the above equation are zero if the true wave function.

ie.,

$$\begin{aligned} \frac{dE(\varepsilon_i)}{d\varepsilon_i} &= \mu(\varepsilon_i) = \left\langle \Psi(\varepsilon_i) \left| \frac{d}{d\varepsilon_i} \hat{H}(\varepsilon_i) \right| \Psi(\varepsilon_i) \right\rangle = \left\langle \Psi(\varepsilon_i) \left| -\sum_{\sigma} r_{\sigma} \right| \Psi(\varepsilon_i) \right\rangle \\ \frac{dE(\varepsilon_i)}{d\varepsilon_i} \Big|_{\varepsilon_i=0} &= \mu_i = \left\langle \Psi \left| -\sum_{\sigma} r_{\sigma} \right| \Psi \right\rangle \end{aligned} \quad 1.34$$

It should be noted that, application of analytic derivative techniques is not that straight forward and often requires a complicated computer implementation. It often requires substantial programming efforts as well as theoretical work for the derivation of the appropriate derivative expressions. Nevertheless, as the implementation needs, in principle, to be carried out only once, this cannot be considered a major disadvantage. Analytic derivatives have been implemented for most of the standard quantum chemical approaches. Analytic derivatives are the preferred choice (if available for a quantum chemical approach) for the following reasons:

- a) First of all, analytic derivatives generally provide higher accuracy for the calculated derivatives, as they are not affected by rounding errors (too small step sizes in the numerical differentiation) or problems due to contamination by higher derivatives (too large step size in the numerical differentiation)
- b) the cost of analytic gradients is independent of the number of perturbations
- c) extension to frequency-dependent properties is possible in the framework of response theory.

In coupled treatment (*static*), the basic equation to find β is

$$\mu_i(F) = \mu_i^0 + \sum_j \alpha_{ij} F_j + \frac{1}{2} \sum_{jk} \beta_{ijk} F_j F_k + \frac{1}{6} \sum_{jkl} \gamma_{ijkl} F_j F_k F_l \dots \quad 1.35$$

where $i, j, k,$ and l label the $x, y,$ and z components with respect to the reference frame in which the molecular system is described. In this contribution only the time-independent (*static* or frequency-independent) molecular responses will be considered. They can be calculated by taking the derivatives of the induced dipole moment of the system:

$$\alpha_{ij} = \left. \frac{\delta \mu_i}{\delta F_j} \right|_{F=0} \quad 1.36$$

$$\beta_{ijk} = \left. \frac{\delta^2 \mu_i}{\delta F_j \delta F_k} \right|_{F=0} \quad 1.37$$

$$\gamma_{ijkl} = \left. \frac{\delta^3 \mu_i}{\delta F_j \delta F_k \delta F_l} \right|_{F=0} \quad 1.38$$

An analogous formulation for α, β, γ coefficients can be obtained by examining the molecular energy expansion,

$$E(F) = E^0 - \sum_i \mu_i^0 F_i - \sum_{ij} \alpha_{ij} F_i F_j - \frac{1}{2} \sum_{ijk} \beta_{ijk} F_i F_j F_k - \frac{1}{6} \sum_{ijkl} \gamma_{ijkl} F_i F_j F_k F_l \dots \quad 1.39$$

rather than the dipole expansion, with respect to the field.⁶

The resultant dipole moment and total polarizability given here are obtained from the equations given below⁶⁷⁻⁶⁹

$$\mu = \sqrt{\mu_x^2 + \mu_y^2 + \mu_z^2} \quad 1.40$$

$$\alpha = \frac{1}{3}(\alpha_{xx} + \alpha_{yy} + \alpha_{zz}) \quad 1.41$$

By taking the tensor product of the 10 tensor components, orientationally averaged hyperpolarizability can be calculated from the equations given below⁶⁹

$$\beta_{vec}(-2\omega; \omega, \omega) = \sqrt{\beta_x^2 + \beta_y^2 + \beta_z^2} \quad 1.42$$

with

$$\beta_i = \sum_{j=x,y,z} \frac{\beta_{ij} + \beta_{ji} + \beta_{jii}}{3}, \quad i = x, y, z \quad 1.43$$

1.8.2. Frequency-dependent (*Dynamic*) properties through Sum Over States method⁶⁶

While analytic derivative theory is sufficient for the theoretical treatment of time independent (*static*) properties, the underlying theory needs to be extended for the calculation of time dependent (*dynamic*) properties. In particular, the fact that, there is (unlike for the static case) in the time-dependent case, no well-defined energy explains why the simple derivative theory discussed so far is not applicable. Nevertheless, there is large interest in the calculation of *dynamic* properties. Major examples are frequency-dependent polarizabilities and hyperpolarizabilities, which are the key quantities in the area of nonlinear optics.

The starting point for the discussion of *dynamic* properties is the time dependent Schrödinger equation

$$H(t)|\Psi\rangle = i \frac{\partial}{\partial t} |\Psi\rangle \quad 1.44$$

with the Hamiltonian $H(t)$ consisting of the usual time-independent molecular part H^0 and a time-dependent perturbation $V(t)$

$$H(t) = H^0 + V(t) \quad 1.45$$

For $V(t)$ one generally assumes that it can be written as a sum of periodic perturbations

$$V(t) = \sum_{k=-N}^N \exp(-i\omega_k t) \sum_X \varepsilon_X(\omega_k) X \quad 1.46$$

with ω_k as the frequency and $\varepsilon_X(\omega_k)$ and X denoting the corresponding perturbation strengths and operators. For a periodically oscillating electric field (the most common example), X the dipole operator μ and the $\varepsilon_X(\omega_k)$ corresponding electric field strength.

The expectation value of an operator $X = \mu$ can now be expanded in the form

$$\begin{aligned} \langle \mu_i \rangle(t) = & \langle \mu_i \rangle_0 + \sum_{k_1} \exp(-i\omega_{k_1} t) \sum_j \alpha_{i,j}(-\omega_{k_1}; \omega_{k_1}) \varepsilon_j(\omega_{k_1}) + \\ & \frac{1}{2} \sum_{k_1, k_2} \exp(-i(\omega_{k_1} + \omega_{k_2}) t) \sum_{jk} \beta_{ijk}(-\omega_{k_1} - \omega_{k_2}; \omega_{k_1}, \omega_{k_2}) \varepsilon_j(\omega_{k_1}) \varepsilon_k(\omega_{k_2}) + \dots \end{aligned} \quad 1.47$$

with $\alpha_{i,j}(-\omega_{k_1}; \omega_{k_1})$ as the tensor elements of the frequency-dependent polarizability, $\beta_{ijk}(-\omega_{k_1} - \omega_{k_2}; \omega_{k_1}, \omega_{k_2})$ as the tensor elements of the frequency-dependent first hyperpolarizability, etc. Table 1.1 gives an overview about the various types of polarizabilities and hyperpolarizabilities as well as their relationship to physical effects. It is important to note in this context that the sum of the frequencies (with explicit consideration of signs) determines the frequency of the corresponding contribution in the expectation value expression. For example, in the case of the SHG, the resulting contribution to the dipole moment has twice the frequency of the original perturbing field.

Dynamic property can be calculated through Sum Over States method (SOS) eg ZINDO SOS method.

The basic equation for frequency dependent NLO response is

$$\begin{aligned} \mu_i(F) = & \mu_i^0 + \sum_j \alpha_{ij}(-\omega_1; \omega_2) F_j(\omega_2) + \frac{1}{2} \sum_{jk} \beta_{ijk}(-\omega_1; \omega_2, \omega_3) F_j(\omega_2) F_k(\omega_3) + \\ & \frac{1}{6} \sum_{jkl} \gamma_{ijkl}(-\omega_1; \omega_2, \omega_3, \omega_4) F_j(\omega_2) F_k(\omega_3) F_l(\omega_4) + \dots \end{aligned} \quad 1.48$$

Based on this equation, the Sum Over States time dependent, second order perturbation theory, gives the following expression for the second order molecular polarizability for SHG (neglecting a damping term which becomes important only when ω is close to a resonant frequency of the molecule)

$$\beta_{ijk}(2\omega; \omega, \omega) = \frac{1}{2\hbar^2} \sum_{n=0}^{\infty} \sum_{l=0}^{\infty} \left[\begin{array}{l} \mu_{on}^i (\mu_{nl}^j \mu_{lo}^k + \mu_{nl}^k \mu_{lo}^j) \frac{\omega_{no} \omega_{lo} + 2\omega^2}{(\omega_{no}^2 - 4\omega^2)(\omega_{lo}^2 - \omega^2)} + \\ \mu_{on}^k \mu_{nl}^i \mu_{lo}^j \frac{\omega_{no} \omega_{lo} - \omega^2}{(\omega_{no}^2 - \omega^2)(\omega_{lo}^2 - \omega^2)} \end{array} \right] \quad 1.49$$

Where $\mu_{pq}^l \equiv \int \psi_p^* \hat{\mu}^l \psi_q dV$ and $\hat{\mu}^l$ is the component of dipole moment operator along axis l , ψ_p and ψ_q are the stationary state wave functions of the molecule in states p and q , \hbar is planks constant divided by 2π and ω_{pq} is the frequency of transitions from state q to state p .

Even though, *ab initio*-CPHF computations are numerically more accurate and precise, the results are not easily amenable to chemical interpretation. Since they are based on derivative rather than SOS formalism, the interpretation of computed response is difficult, albeit of their accuracy in predicting trends. Also, in experimental measurements, electrons will go to the higher excited states and the higher level contribution may not be too small to neglect. Almost all the semiempirical -SOS procedures provide second order responses in reasonable agreement with experiments. Moreover, they permit a basic understanding of the origin of the NLO response in a chemical sense, by identifying the molecular excited states primarily responsible for an NLO response within the SOS formalism.⁶

Oudar and Chemla established a link between β and the details of a low-lying charge-transfer transition through the two-level model. NLO properties of organic charge transfer complexes like D- π -A can be captured very nicely by this model.⁷⁰ This model assumes that the electronic properties of the molecules are determined by the ground state and a low energy charge transfer excited state. Polarization results primarily from the mixing of charge transfer state with the ground state through the interaction of the molecule with the electric field. The Sum Over States (SOS) formalism lies within the limit of two level model, when the contribution from higher excited states are negligible compared to the first excited state.⁶ So the complicated expression of equation-1.49 reduces to the simplified form. From the two-level model, using electric

dipole approximation, the second harmonic generation response (SHG) can be written as

$$\beta_{\text{two-level}} = \frac{3e^2}{2\hbar} \frac{\omega_{12} f \Delta\mu}{(\omega_{12}^2 - \omega^2)(\omega_{12}^2 - 4\omega^2)} \quad 1.50$$

Where ω_{12} is the frequency of the optical transition between state 1 and 2, f the oscillator strength and is the square of the transition moment between the ground state and the charge transfer excited state $\langle 1|er|2\rangle$, $\Delta\mu$ the difference between the dipole moments of the ground and the excited state, are the crucial two-level parameters in chromophore design. The most important factor in the above expression is that the SHG coefficient is directly proportional to the oscillator strength f and dipole moment difference, $\Delta\mu$ and is inversely proportional to the optical gap, δE (defined as the energy difference between the ground state and the lowest energy dipole allowed state.) Thus, any phenomenon that decreases the optical gap, δE and increases the dipole moment difference between the ground and the excited state, $\Delta\mu$ will enhance β .

1.9. Objectives of the present work

- Theoretical evaluation of the parameters which affect the second order NLO response of molecules based on PNA and its derivative . Study of the influence of varying number of spacer methylene groups.
- To design different series of monomers and polymers with high SHG response based on the optimized parameters
- Design of main chain and side chain azo polymers with chiral framework having high SHG response.
- Design of polymers with spacers
- Synthesis of polymers with spacers and with main chain and side chain azo mesogenic groups and having chiral framework.
- Measurement of SHG efficiency experimentally
- Correlation of experimental and theoretical results

1.10 Methodology adapted

Throughout the thesis it is assumed that the molecular plane coincides with the YZ plane, the Y axis being along the direction of maximal extension of the molecule and the X axis perpendicular to the molecular plane. An important aspect of *ab initio* calculation is the choice of the basis set which describe reorganization the electronic distribution resulting from the external perturbation. It determines both the quality and the cost of the results. Various extended basis sets, including polarization functions and diffuse functions, are generally required for computation of hyperpolarizability. Since polarizability is quite sensitive to geometry, it is preferable that all geometries be optimized at the common level of theory to avoid geometry effects in the predictions. Static polarizability has been calculated using CPHF algorithm available with Gaussian 03 code,⁷¹ to follow the trend of the molecules towards NLO activity. Using ZINDO SOS method *dynamic* hyperpolarizability has been calculated to get the results that can be correlated with experimental results. In the thesis, all the calculations have been performed at 1064 nm (1.67 eV) corresponding to the Nd:YAG laser. The correlation has been done using the two level parameters. The levels of CI calculations have been varied with singles (SCI) to obtain a reliable estimate of the second order optical response functions. The CI approach adopted here has been extensively used in earlier works and was found to provide excitation energies and dipole matrix elements in good agreement with experiment.⁷²⁻⁷⁴ For the Hartree-Fock determinant, varying number of occupied and unoccupied molecular orbitals are used to construct the CI space. To calculate second-order NLO properties, correction vector method has been used, which implicitly assumes all the excitations to be approximated by a correction vector (CV). The polarizabilities were also computed using the sum-over-states (SOS) formalism, and values similar to those provided by the CV method were obtained.⁷⁵⁻⁸⁰

Since the value of β obtained from the theoretical calculations is very much sensitive to the input geometry, the choice of geometry of the molecule is one of the important factors in the molecular design.⁸¹ Three different strategies for defining geometric parameters can be found in the NLO literature: (1) employing experimental structures, (2) using geometries obtained through molecular energy minimization algorithms, or (3) using idealized molecular geometries constructed from experimental

geometric parameters of related architectures. Usually, the studies examining large numbers of complicated structural motifs tend to either optimize the structure via quantum mechanical routines or use molecular templates to build idealized structures. Here the first method has been used throughout. All the designed geometries are optimized via quantum mechanical methods.⁶

1.11. Instrumentation used in this work

Optical rotations were measured using an Atago AP100 automatic digital polarimeter. CHN analysis was performed using a Elementar Vario EL III Carlo Erba 1108 instrument. ¹H-NMR and ¹³C-NMR spectra were recorded on a Varian Gemini 300 (300MHz) spectrometer with TMS as internal standard. Infrared (IR) spectra were recorded on a Shimadzu IR Prestige -21 Spectrophotometer with 32 scan per experiment at a resolution of 1 cm⁻¹. UV-Vis spectra were recorded on an Ocean Optics SD 2000 UV-Vis spectrophotometer. The electrospray mass (ESI) spectra were recorded on Micromass Quattro II triple quadrupole mass spectrometer. The MALDI TOF Mass spectra were run a Micromass ToFSpec 2E instrument using a nitrogen 337 nm laser (4ns pulse). TG /DTA were recorded on a Perkin Elmer Pyres Diamond 6 TG/DTA instrument at a heating rate of 5^o C per minute in nitrogen atmosphere using platinum crucible. Purification of the chromophores was done by gravity column chromatography using 100-200-mesh silica gel using appropriate solvents. Commercial grade solvents were used for column chromatography and were distilled and dried before use. Analytical thin layer chromatography was performed on Merck aluminum sheets coated with silica gel 60 F254 (0.25mm thickness) containing 13% calcium sulphate as binder. The purity of the crude and recrystallized products was monitored by TLC employing appropriate solvent systems for development and the developed plates were visualized by exposure to iodine.

¹H NMR and ¹³C-NMR (solution state) and IR spectra were taken from the Department of Polymer Science & Engineering., Pusan National University, Busan, S. Korea , Organic Chemistry Department, IISc, Bangalore and JNCASR, Bangalore. Solid state ¹³C-NMR spectra were taken from SIF IISc, Bangalore. CHN analysis and mass

spectra were recorded from RSIC, CDRI, Lucknow. SHG measurements were done from RRI, Bangalore.

References

- (1) Gunter, P. *Nonlinear Optical Effects and Materials, Springer Series in Optical Sciences*, Vol, 72; Springer-Verlag: Berlin, 1965.
- (2) (a) Franken, P.A.; Hill, A.E.; Peters, C.W.; Weinreich, G. *Phy.Rev.Lett.* **1961**, *7*, 118. (b) Bloembergen, N. *Nonlinear Optics*; W. A. Benjamin: New York, 1965
- (3) Nalwa, H. S.; Miyata S. *Nonlinear Optics of Organic Molecules and Polymers*; CRC Press: New York, 1997.
- (4) Prasad, P. N.; Williams, D. J. *Introduction to Nonlinear Optical Effects in Molecules and Polymers*; Wiley: New York, 1991.
- (5) Chemla, D. S.; Zyss, J. *Nonlinear Optical Properties of Organic Molecules and Crystals*; Academic Press, Inc: New York, 1987.
- (6) Kanis, D. R.; Ratner, M. A.; Marks, T. J. *Chem. Rev.* **1994**, *94*,195.
- (7) Richard L. Sutherland, *Handbook of nonlinear Optics*; Marcel Dekker, Inc: New York, 2003.
- (8) Louisell, W.H.; Yariv, A.; Siegman, A.E. *Phys.Rev.* **1961**, *124*, 1646.
- (9) Munn,R.W. *J. Mol.Electron.***1988**,*4*,31.
- (10) Onsager, L. *J. Am. Chem.Soc.* **1936**, *58*, 1486.
- (11) Lorentz, H.A. *The Theory of Electric Polarization*; Elsevier: Amsterdam., **1952**.
- (12) (a) Kleinman, D. A.; *Phy. Rev.* **1962**, *125*, 87,(b) Kleinman, D. A.; *Phy. Rev.* **1962**, *128*, 1761.
- (13) Nye, J. F. *Physical Properties of Crystals*; Oxford University Press: London, **1960**.
- (14) Rentzepis, P. M.; Yoh-Han Pao *Appl. Phys. Letters* **1964**, *5*, 156.
- (15) Heilmeyer, G. H.; Ockman, N.; Braunstein, R. ;. Kramer D.A, *Appl. Phys.Letters*, **1964**, *5*, 229.
- (16) Davydov, B. L.; Derkacheva, L .D.; Dunina,V. V.; Zhabotinski, M. K.; Zolin, V. K.; Kreneva, L.G.; Samokhina, M. A. *JEPT lett.*, **1970**, *12*, 16.
- (17) Oudar, J. L. *J.Chem.Phys.* **1977**, *67*, 446.
- (18) Oudar, J. L.; Zyss, J. *Phys.Rev. A.* **1982**, *26*, 2016.
- (19) Lalama, S. J.; Garito, A. F. *Phys.Rev. A.* **1979**, *20*, 1179.

- (20) Morell, J. A.; Albrecht, A. C. *Chem. Phys. Lett.* **1979**, *64*, 46.
- (21) Cole, J. M. *Phil. Trans Royal. Soc. Lond. A* **2003**, *361*, 2751.
- (22) Levine, B. F. *Chem. Phys. Lett.*, **1976**, *37*, 516.
- (23) Zyss, J.; *J. Chem. Phys.* **1993**, *98*, 6583.
- (24) Alcaraz, G.; Euzenat, L.; Mongin, O.; Katan, C.; Ledoux, I.; Zyss, J.; Desce, D.; Vaultier *Chem. Commun.* **2003**, *22*, 2766.
- (25) Fave, C.; Hissler, M.; Senechal, K.; Ledoux, I.; Zyss, J.; Reau, R.; *Chem. Commun.* **2002**, *16*, 1674.
- (26) Fine, S.; Hansen, W. P.; *Appl. Opt.* **1971**, *10*, 2350.
- (27) Bouevitch, O.; Lewis, A.; Pinevsky, L.; Wuskell, J.P.; Loew, L.M.; *Biophys. J.* **1993**, *65*, 672.
- (28) Simpson, G. J.; *ChemPhysChem*, **2004**, *5*, 1301.
- (29) Nalwa, H. S. *Nonlinear Optical Properties of π - Conjugated Materials*, in *Hand Book of Organic Conducting Molecules and Polymers*, Vol. 4. Nalwa, H. S. Ed.; John Wiley and Sons, Inc.: England, 1997.
- (30) Zyss, J.; Oudar, J. L. *Phys. Rev. Lett.*, **1982**, *A26*, 2028.
- (31) Burland, D. M., Ed.; *Chem. Rev.* **1994**, *94*, 31.
- (32) Amano, M.; Kaino, T. *J. Appl. Phys.*, **1990**, *68*, 6024.
- (33) Kitipichai, P.; Laperuta, L.; Korenowski, G. M. Wneck, G. E. *J. Polym. Sci. Polym. Chem.*, **1993**, *31*, 1365.
- (34) Tao, X. T.; Watanabe, T.; Shimoda, S.; Zou, D. C.; Sato, H.; Miyata, S. *Chem. Mater.*, **1994**, *6*, 1961.
- (35) Smith, S. J. *Polym. Sci. A Polym. Chem.* **1991**, *29*, 1623.
- (36) Mengaa, F.; Renb, Q.; Xua, D.; Yuaba, D.; Lua, M.; Zhanga, G.; Guoa, S.; Zhaoa, X.; Wanga, X.; Fanga, C.; Xuc, G.; Liuc, X.; Yec, P. *React. Funct. Polym.* **2000**, *46*, 59.
- (37) Kauranen, M.; Verbiest, T.; Persoons, A. *J. Nonlinear Opt. Phys. Mater.*, **1999**, *8*, 171.
- (38) Zyss, J.; Nicoud, J. F.; Coquullay, M. *J. Chem. Phys.*, **1984**, *81*, 4160.
- (39) Kitazawa, M.; Higucgi, R.; Takahashi, M.; Wada, T.; Sasabe, H. *Appl. Phys. Lett.*, **1994**, *64*, 2477.
- (40) Sutter, K.; Knopfle, G.; Saupper, N.; Hulliger, J.; Gunter, P.; Petter, J.W. *J. Opt.*

Soc. Am., **1991**, *8*, 1483.

- (41) Das, S.; George, M.; Mathew, T.; Asokan, C. V. *J. Chem. Soc. Perkin Trans. 2*, **1996**, 731.
- (42) Okamoto, Y. *Prog. Polym. Sci.*, **2000**, *25*, 159.
- (43) Nakako, H.; Mayahara, Y.; Nomura, R.; Tabata, M.; Masuda, T. *Macromolecules*, **2000**, *33*, 3978.
- (44) Deming, T. J.; Novak, B. J. *J. Am. Chem. Soc.*, **1992**, *114*, 7926.
- (45) Takei, F.; Koichi, Y.; Onitsuka, K.; Takahashi, S.; *Angew. Chem. Int. Ed. Engl.* **1996**, *35*, 1554.
- (46) Majidi, M. R.; Kane-Maguire, A.P.; Wallace, G. G. *Polymer* **1996**, *37*, 359.
- (47) Nolte, R. J. M.; van Beijnen, A. J. M.; Drenth, W. *J. Am. Chem. Soc.* **1974**, *96*, 5932.
- (48) Yashima, E.; Maeda, Y.; Okamoto, Y. *Nature* **1999**, *399*, 449.
- (49) Terunuma, D.; Nagumo, K.; Kamata, N.; Matsuoka, K.; Kuzuhara, H. *Chem. Lett.* **1998**, *31*, 4666.
- (50) Shinihara, K.; Aoki, T.; Kaneko, T.; Oikawa, E. *Chem. Lett.* **1997**, *6*, 361.
- (51) Obata, K.; Kira, M. *Macromolecules* **1998**, *31*, 4666.
- (52) Jha, S. K.; Cheon, K. S.; Green, M. M.; Selinger, J. V. *J. Am. Chem. Soc.* **1991**, *121*, 1665.
- (53) Selegny, E.; *Optically Active Polymers*; D. Reidel Publishing Company: Holland, **1979**.
- (54) Green, M. M.; Park, J. W.; Sato, T.; Teramoto, A.; Lifson, S.; Selinger, R. L. B.; Selinger, J. V. *Angew. Chem. Int. Ed. Engl.* **1999**, *38*, 3138.
- (55) Koe, J. R.; Fujiki, M.; Motonaga, M.; Najashima, H.; *Macromolecules*, **2001**, *34*, 1082.
- (56) Li, C. Y.; Yan, D.; Cheng, S. Z. D.; Bai, F.; He, T.; Chein, L.; Harris, F. W.; Lotz, B. *Macromolecules* **1999**, *32*, 524.
- (57) (a) Lehn, M. *Supramolecular Chemistry*; VCH: Weinheim **1995** (b) Clays, K. *Science*, **1993**, *26*, 1419.
- (58) (a) Kauranen, M.; Verbiest, T.; Boutton, C.; Teerenstra, M. N.; Clays, K.; Schouten, A. J.; Nolte, R. J. M. Persoons, A. *Science*, **1995**, *270*, 966. (b) Kauranen, M.; Verbiest, T.; Meijer, E. W.; Havinga, E. E.; Teernstra, M. N.; Schouten, A. J.; Nolte, R. J. M.; Persoons, A. *Adv. Mater.* **1995**, *7*, 641

- (59) Bouman, M. M.; Haviga, E. E.; Hanseen, R.A.J Meijer, E. W. *Mol. Cryst. Liq. Cryst.* **1994**, *256*, 439.
- (60) Pu, L. *Chem. Rev.* **1998**, *98*, 2405.
- (61) Pu, L. *Macromolecular Rapid Communications*, **2000** *21*, 795.
- (62) Koeckelberghs, G.; Verbiest, T.; Vangheluwe, M.; Groof, L. D., Asselberghs, I.; Picard, I.; Clays, K.; Persoons, A.; Samyn, C. *Chem. Mater.*, **2005**, *17*, 118.
- (63) Kauranen, M.; Verbiest, T; Maki, J. J.; Persoons, A. *J. Chem. Phys.* **1994**, *101*, 8193.
- (64) Wang, L.; Warburton, P. L.; Szekeres, Z.; Surjan, P.; Mezey, G. P. *J. Chem. Inf. Model.* **2005**, *45*, 850.
- (65) Elshocht, S. V.; Vebiest, T.; Kauranen, M.; Persoons, A. LAngeveld-Voss, B. M. W. Meijer, E. W.; *J. Chem. Phys.* **1997**, *107*, 8201.
- (66) Guass, J. *Modern Methods and Algorithms of Quantum Chemistry, Proceedings, Second Edn..* **2000**, *3*, 541.
- (67) Daniel, C.; Dupuis, M. *Chem Phys Lett.* **1990**, *171*, 209.
- (68) Sim, F.; Chin, S.; Dupuis, M.; Rice, J. E. *J. Phys. Chem.* **1993**, *97*, 1158.
- (69) Bishop, D. M. *Adv. Chem. Phys.* **1998**, *104*,1.
- (70) Oudar, J. L.; Chemla, D. S. *J. Chem. Phys.* **1977**, *66*, 2664.
- (71) Gerratt, J.; Mills, I. M.; *J. Chem. Phys.* **1968** *49*, 1719.
- (72) Buenker, R. J.; Peyerimhoff, S. D. *Theor. Chim. Acta* **1974**, *35*, 21.
- (73) Shuai; Z.; Beljonne, D.; Bredas, J. L. *J. Chem. Phys.* **1992**, *97*,1132.
- (74) Beljonne, D.; Shuai, Z.; Cornil, J.; dos Santos, D.; Bredas, J. L. *J.Chem. Phys.* **1999**, *111*, 2829.
- (75) (a) Ramasesha, S.; Soos, Z. G. *Chem. Phys. Lett.* **1988**, *153*, 171. Soos,G.; (b) Ramasesha, S. *J. Chem. Phys.* **1989**, *90*, 1067.
- (76) Ramasesha, S.; Shuai, Z.; Bredas, J. L. *Chem. Phys. Lett.* **1995**,*245*, 224.
- (77) Albert, I. D. L.; Ramasesha, S. *J. Phys. Chem.* **1990**, *94*, 6540.
- (78) Ramasesha, S.; Albert, I. D. L. *Phys. Rev. B* **1990**, *42*, 8587.
- (79) Pati, S. K.; Ramasesha, S.; Shuai, Z.; Bredas, J. L. *Phys. Rev. B* **1999**, *59*, 14827.
- (80) Pati, S. K.; Marks, T. J.; Ratner, M. A. *J. Am. Chem. Soc.* **2001**,*123*, 7287.
- (81) Kanis, D. R.; Marks, T. J.; Ratner, M. A. *Int.J. Quantum Chem.* **1992**, *43*, 61.

OPTIMIZATION OF NONLINEAR OPTICAL PROPERTIES BY SUBSTITUENT POSITION, GEOMETRY AND SYMMETRY OF THE MOLECULE: AN *AB INITIO* STUDY

2.1. Introduction

The nonlinear optical susceptibilities of a material provide a quantitative measure of the ability of a bulk material to modulate light and are the parameters that researchers in NLO material seek to optimize. One can define microscopic nonlinear optical coefficients (molecular hyperpolarizabilities) that are the molecular equivalents of bulk nonlinear optical susceptibilities. In fact, the bulk susceptibilities can be readily related to the susceptibilities of the constituent molecules. Hyperpolarizabilities may be deduced experimentally from the direct observations of harmonic generations^{1,2} and from the measurements of Kerr effect.³ However, the experiments are difficult and the range of uncertainty is often large. Since the hyperpolarizability is a property of a single atom or a molecule, it may be predicted from quantum mechanical calculations.⁴

The general theory underlying the calculation of nonlinear electric properties is already well developed.⁵ However, most research in this area is still being focused on the study of relatively small molecules for which the corresponding calculations can be made both accurate and conclusive.⁶⁻¹⁰ The optically induced polarization in organic donor-acceptor dyes generates large value of nonresonant (nonabsorptive) optical nonlinearities over a wide frequency range. Certain dye chromophoric systems restrict their applications to NLO devices, although they have parallel potentials in applications associated with light absorption, light emission, photoelectrical, and photochemical activities.¹¹ Since the field of nonlinear optics is uniquely concerned with the molecular design of fundamental dyes in which NLO response is governed largely by the chromophores involving interactions with light, the optical nonlinearity is primarily

derived from molecular structure. The primary step in optimizing optical nonlinearities in this class of materials is at the molecular structural level, which then requires a detailed understanding of the relationship between molecular electronic structure and nonlinear polarization that can be induced in the molecule.¹² An understanding of the structure-property relations for the NLO responses provides guidelines for the design of novel molecular and polymeric NLO materials. Quantum chemistry can help to rationalize the experimental results and rank the existing molecular structures according to their linear and nonlinear susceptibilities prior to experiment and thus to propose new promising compounds to chemists. At the molecular level, the NLO properties are determined by first and second hyperpolarizabilities. One of the main issues in the calculation of nonlinear electric properties is the role of the electron correlation effects,¹³ which need to be carefully studied.

Nonlinear optical properties of a variety of linear push-pull phenylenes have been extensively studied over the last two decades.^{14,15} It was known that the NLO properties of these molecules are sensitive to many factors such as the conjugation length, strength of the donor and acceptor substituents and symmetry effects.¹⁶ *Para*-nitroaniline (PNA) derivatives are the favorite test systems for investigation of different aspects of the accuracy and computational methodology used in calculations of nonlinear electric properties.^{6,8} Frequency dependent polarizabilities and hyperpolarizabilities of PNA were calculated by Ågren et al. using multiconfiguration SCF based response approach.¹⁷ The solvent effect on the hyperpolarizability and their frequency dispersion has been studied by Mikkelsen et al.¹⁸ Champagne et al. applied a DFT based approach for the calculation of nonlinear optical properties of PNA.¹⁹ Using a double harmonic oscillator approximation, the vibrational contributions to the polarizability and first and second hyperpolarizability tensors of PNA for different optical processes by adopting the infinite frequency or enhanced approximation have been calculated by Champagne.²⁰ The first-order zero-point vibrational averaging correction for second harmonic generation in PNA have been determined analytically at the time-dependent Hartree-Fock level of approximation.²¹

Both the structure-property relationships and the effect of electron correlation on NLO properties will be considered in this chapter and exemplified by the calculations (second order Møller-Plesset (MP) perturbation calculation) of electric properties of PNA derivatives.

2.2. Computational methods

The concepts about optical nonlinearities and the quantum chemical methods applied for the calculations have been given in chapter 1. The molecules considered in this work are shown in Figure 2.1- 2.5. The calculations have been performed at MP2 level using the 6-31++G** basis set and all the geometric parameters of the parent molecules (PNA, N-methyl-4-nitroaniline (MPNA), N-ethyl-4-nitroaniline (EPNA), N,N-dimethyl-4-nitroaniline (DPNA)) have been optimized at that level of theory using the same basis set. The other geometric parameters of the molecules in Figure 2.1 have been obtained from the parent molecules by substituting the hydrogen of benzene with a fixed geometry methyl group. Finite-Field perturbation approach is used for the NLO property calculations using the GAMESS-US quantum chemical program. In this work, the derivatives based on energy have been chosen for the MP2 polarizabilities. An electric field of minimum strength 0.0010 au was applied for the finite-field calculation of electric field susceptibilities.

2.3. Results and discussion

The electric field susceptibilities of PNA and its two methyl substituted derivatives at the ring positions are compared in Table 2.1. Similarly, Table 2.2 -2.4 list the axial components of the susceptibility tensors of other parent molecules and their methyl substituted derivatives as shown in Figures 2.2-2.5. While optimizing geometry, all the atoms except the methyl hydrogens, were restricted to be in the molecular plane. This model planar structure simplifies the computation. A similar strategic approach for the PNA molecule using a [3s2p2d/2s1p] basis set can be found elsewhere.⁸ For EPNA, a structure with out of plane ethyl group is very low in energy compared with the in plane ethyl group. For comparison, the NLO property calculation for the planar EPNA

Table 2.1: Dipole moment (μ), polarizability (α), hyperpolarizabilities (β and γ) and the HOMO-LUMO energy gap (ΔE) of PNA and its two methyl substituted derivatives, PNA-2 and PNA-3. The reported values are in atomic units.

Method of property evaluation	HF	HF	MP2	MP2	MP2	MP2
Coefficients	PNA ^a	PNA ^b	PNA ^a	PNA ^b	PNA-2	PNA-3
μ_x	2.969	3.082	2.697	2.754	2.771	2.63
μ_y					-0.176	-0.139
μ_z						
μ	2.969	3.082	2.697	2.754	2.776	2.633
α_{xx}	125.46	131.95	140.36	148.4	156.44	159.71
α_{yy}	92.55	95.82	97.23	101.01	116.89	116.8
α_{zz}	48.51	49.17	50.26	50.95	59.31	59.27
α	88.84	92.31	95.95	100.12	110.88	111.92
β_{xxx}	529.06	647.58	837.55	1064.6	1051.4	1007.27
β_{xyy}	-93.28	-106.55	-31.71	-34.1	-28.64	-64.56
β_{xzz}	-19.98	-21.38	-26.21	-28.47	-27.18	-27.77
β_x	415.79	519.66	779.62	1002.02	995.58	914.94
β_{yxx}			-0.16	0.03	-20.96	-4.15
β_{yyy}			0.03	0.06	-5.14	-17.84
β_{yzz}			-0.1	0.03	-7.64	-15.49
β_y		0.01	-0.23	0.12	-33.74	-37.48
β_{zxx}			-0.24	-0.02	0.14	-0.88
β_{zyy}		0.01	0.14	-0.2	0.31	-0.18
β_{zzz}			0.02	-0.04	0.05	-0.02
β_z		0.01	-0.08	-0.26	0.51	-1.08
β	415.80	519.66	779.61	1002.03	996.15	915.72
γ_{xxxx}	10862	13951	21641	30368	30351	25490
γ_{xyy}	-242	-375	351	-1480	-203	1341
γ_{zzxx}	459	449	3893	5108	4072	2886
γ_{yyy}	1461	713	2406	-4252	4101	6702
γ_{zyy}	700	1507	2671	-490	4859	3836
γ_{zzzz}	1662	1680	7284	10589	8978	9125
γ	2637	3251	7527	7164	10148	9574
ΔE				0.3717	0.3657	0.3760

^a HF optimized geometry

^b MP2 optimized geometry

and its substituted derivatives with non-planar geometry were also carried out. The results are given in **Table 2.5**.

In the model calculations, the attention was restricted mainly to linear response coefficients α_{ij} , and the main tensor elements of the nonlinear response coefficients that arise due to the polarization in the molecular plane. **Table 2.1** reports the nonlinear optical coefficients of PNA for two different geometries, the SCF optimized geometry and the MP2 optimized geometry. At this point, it is worthwhile to remark on the comparison between the calculations performed for PNA molecule using MP2 optimized geometry and HF optimized geometry. For the same level of property evaluation, the MP2 optimized geometry gives a higher dipole moment value and higher linear and nonlinear optical coefficients. When comparing the property evaluation at the MP2 level for both the SCF (column 3) and MP2 geometry (column 4), it has been observed that, although the hyperpolarizabilities along the molecular axis follow the trend observed for the polarizabilities along the same axis, the average value of γ is lesser for a MP2 geometry than that of SCF geometry. Since both the geometries are very similar, there are no dramatic changes in the coefficients obtained from the same level of theory. However, this conclusion might not be valid for systems in which the HF-SCF method yields a poor geometry. It is interesting to note that for a fixed geometry, the SCF and MP2 methods yield entirely different susceptibility values.

The percentage of change becomes larger and larger as the order of the susceptibility increases. For example, in the case of a MP2 optimized geometry, the γ obtained by MP2 calculation is twice as that of the γ obtained by HF calculation. The same is true for the β value also and the percentage of increment is around 80. Except for a couple of terms, the MP2 values for dipole moment, axial components of polarizability and the tensor components of hyperpolarizability are quite clearly higher than those of the corresponding SCF results. This is not surprising, since the higher order susceptibilities demand more electron correlation as the contribution of higher energy states in these susceptibilities is larger. Thus, the predictions based on the Hartree-Fock

level are not very rigorous. In order to obtain reasonable values for the various individual contributions to the hyperpolarizability, it is necessary to include electron correlation. Qualitative results for the relative importance of these contributions can often be obtained at the HF level, but beyond that, correlation must be included for this purpose as well. A comparison for PNA molecule between MP2 and HF-SCF property evaluation from Table 2.1 indicates that the MP2 method adequately reproduces the effect of correlation on the relative magnitude of the various contributions to each property and gives a reasonable prediction for the individual values. These observations about the PNA also agree with the other theoretical calculations available in the literature.^{6,8}

From a chemical perspective, the most important feature of the NLO response calculation is the insight they provide into the effects of subtle variations in the molecular architecture on the NLO responses. While analyzing the relationship between the chemical structure and second-order nonlinear optical properties, the observation is that second-order NLO effects in organic molecules originate from a strong-donor-acceptor intramolecular interaction. Davydov et al.¹⁰ showed that dipolar aromatic molecules possessing an electron donor group and an acceptor group contribute to large second-order optical nonlinearity arising from the intramolecular charge transfer between two groups of opposite nature. Therefore, a typical SHG-active molecule can be presented as a donor- π -conjugate bridge-acceptor system, if it lacks a center of symmetry. On the other hand, π -conjugate molecule with a donor and an acceptor will not display SHG-activity if it possesses a center of symmetry. Hence, while designing the NLO material, more attention has been focused on the donor-acceptor tailoring, symmetry, and geometry requirements.¹² Much interest in second-order NLO properties of substituted benzene derivatives stems from the basic studies of the chemistry and physics of PNA. Here, variation in NLO response with tailored architecture in PNA is studied using PNA derivatives obtained by substituting the hydrogen in NH_2 group and benzene ring with methyl group. In a covalent single bond between unlike molecular fragments, the electron pair forming σ bond is never shared

absolutely equally between the two fragments: it tends to be attracted more towards the electron deficient fragment of the two. This influence of electron distribution in σ bond is known as inductive effect²² and the methyl group attached to C or N of the PNA molecule exerts such an electron-donating inductive effect in the direction of the other fragment. Though the effect is quantitatively rather small, it is responsible for the increase in basicity that results when one of the H atom of ammonia is replaced by a CH₃ group, and, in part at any rate, for the readier substitution of the aromatic nucleus in methyl benzene than in benzene itself. All inductive effects are permanent polarizations in the ground state of a molecule, and are therefore manifested in its physical properties, for example, its dipole moment.

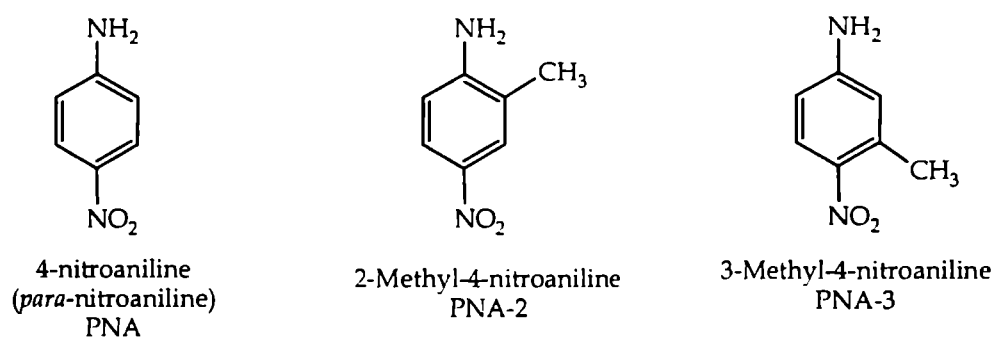


Figure 2.1 PNA and its methyl derivatives

The substitution of methyl group at 2nd carbon of benzene ring (PNA-2) does not change the dipole moment and the average value of β much compared to the parent PNA molecule, whereas the substitution of methyl group at 3rd C (PNA-3) decreases both the values (all the values are given in Table 2.1). In both the substituents, the average values of α and γ are larger than that of parent molecule and the increment in γ is about 90% compared to that of PNA. Although the Y component of the β vector for the PNA-3 is larger in magnitude, the β_{xxx} value is less in magnitude compared to the PNA-2 and PNA molecules. The molecular orbital picture can be used to predict the trend in β with varying substitution patterns. Because of charge transfer, the absorption band of an organic dye with π -conjugated donor-acceptor system can be tailored by either increasing the π conjugation length by substituting donor-acceptor groups to a

conjugated system. As a result, the absorption band of the UV-Vis spectrum can be shifted and will have either bathochromic or hypsochromic features. Electron-donor-acceptor groups cause bathochromic shifts which also increase the intensity of the absorption bands.²³ A donor group can increase the electron density in the π conjugated system leading to a strong interaction from the donor-acceptor combination. The donor-acceptor interaction is also affected by the relative position of the π conjugated system. This changes the charge transfer and electronic distribution.

The PNA, which is the basic molecule for organic NLO, consists of a benzene ring in which an electron donor amino (NH_2) group is substituted in the *para* position with an electron acceptor nitro (NO_2) group. These opposite ends of the conjugated system lead to maximum acentricity in the molecule. The π electron donor and acceptor configuration composed of NH_2 and NO_2 respectively in PNA results in intramolecular charge-transfer interactions. The PNA molecule exhibits extremely large first hyperpolarizability (β) due to the highly asymmetric charge distribution arising from the π electronic structure of the molecule. Moreover, in PNA molecule, intramolecular charge transfer interaction is prominent because of desirable resonance structure leading to large β . Its highly asymmetric charge-correlated excited states of the π electron structure also contribute to the large β value. But in practice, the PNA molecule crystallizes in a centrosymmetric space group, which restricts the observation of any macroscopic second-order nonlinear optical effect. Therefore, closely related PNA derivatives, which do not have center of symmetry in the crystalline state, have been considered here. When the benzene ring of PNA is substituted with a CH_3 group, the resulting chemical substitution provides the maximum acentricity to the molecule and gives rise to a non-centrosymmetric crystal structure. In PNA-2 and PNA-3, the asymmetric derivatives of PNA, the first one gives a higher β , which can be explained as follows. Since the major contribution to β is due to charge transfer, one will get higher β with the factors, which enhance the charge transfer. The highest occupied molecular orbital (HOMO)-lowest unoccupied molecular orbital (LUMO) gap in the molecular orbital picture plays a vital role in the charge transfer.¹² If the gap is small, it is very easy

Table 2.2: Calculated dipole moment (μ), polarizability (α), hyperpolarizabilities (β and γ) and the HOMO-LUMO energy gap (ΔE) of DPNA and its two methyl substituted derivatives, DPNA-2 and DPNA-3. The reported values are in atomic units.

Coefficients	DPNA	DPNA-2	DPNA-3
μ_x	3.1	3.258	2.971
μ_y	-0.004	-0.1	-0.13
μ_z			
μ	3.1	3.259	2.974
α_{xx}	193.2	198.89	204.75
α_{yy}	123.57	75.89	138.95
α_{zz}	69.43	138.86	77.51
α	128.73	137.88	140.4
β_{xxx}	1587.41	1471.63	1496.38
β_{xyy}	-72.82	-56.86	-98.73
β_{xzz}	-28.41	-19.15	-24.65
β_x	1486.19	1395.62	1373
β_{yxx}	-3.5	-17.04	-0.24
β_{yyy}	-0.02	-21.07	-16.6
β_{yzz}	0.59	-27.09	-13.67
β_y	-2.92	-65.2	-30.5
β_{zxx}	0.46	0.95	0.9
β_{zyy}	0.03	0.94	0.92
β_{zzz}	-0.14	0.79	0.49
β_z	0.35	2.67	2.32
β	1486.20	1397.16	1373.34
γ_{xxxx}	47895	51223	37287
γ_{xxyy}	1523	3078	-1975
γ_{zzxx}	5807	6642	3695
γ_{yyyy}	6822	5367	2029
γ_{zzyy}	2190	7314	4371
γ_{zzzz}	12056	13510	9577
γ	17162	20834	12215
ΔE	0.3598	0.3534	0.3644

for the charge transfer to occur. Thus the HOMO largely dictates the source of charge transfer and the details of the molecular LUMO govern the acceptor portion of the excitation. One can tailor the asymmetry of the electron density by tuning the energetics (HF-SCF) of the appended substituents. The HOMO-LUMO gap (ΔE) of the molecules is given in Table 2.1 to Table 2.7. In the case of methyl substitution at 2nd carbon, one more donor group is added near to the parent donor group, while in the substitution at 3rd carbon, the added donor group is nearer to acceptor group. This provides higher HOMO energy and a lower LUMO energy for PNA-2 than that of PNA-3. This leads to a smaller HOMO-LUMO energy gap for the former, and clearly the former one has more β value than that of the latter. This shows that substitution of H with a methyl group (electron donating group) at the second C of benzene ring increases the HOMO energy. The electron density of the HOMO orbital, which is confined more to electron donating group (-NH₂), will favor the charge transfer to the LUMO orbital, confined towards the electron acceptor part (-NO₂) of the molecule. On the other hand, substituting at 3rd C with methyl group increases the LUMO energy and a higher LUMO would not favor a charge transfer from a HOMO. Furthermore, based on the orientation of ring substitution by different groups, substitution in the position 2 is more favorable. Position 2 is *ortho* to the NH₂ group (*ortho* and *para* directing) and *meta* to the NO₂ group (*meta* directing) of PNA.

From the two-level model, using electric dipole approximation, the second harmonic generation response (SHG) can be written as ²⁴

$$\beta_{\text{two-level}} = \frac{3e^2}{2\hbar} \frac{\omega_{12} f \Delta\mu}{(\omega_{12}^2 - \omega^2)(\omega_{12}^2 - 4\omega^2)} \quad (2.1)$$

Where $\hbar\omega_{12}$ is the excitation energy, f the oscillator strength, $\Delta\mu$ the difference between the dipole moments of the ground and the excited states and ω specifies the excitation frequency of the oscillating electric field. The most important factor in the above expression is that the SHG coefficient is directly proportional to the oscillator strength f , and dipole moment difference, $\Delta\mu$ and is inversely proportional to the optical

gap. Thus, any phenomenon that decreases the gap and increases the dipole moment difference between the ground and the excited states will enhance β . So it is very much clear from the Table 2.1 that methyl substitution at 2nd carbon will lead to higher β value. The α and γ can also be greatly enhanced by the donor-acceptor push pull phenylenes in which the donor-acceptor substituted benzene show large optical nonlinearity than the unsubstituted ones.²³

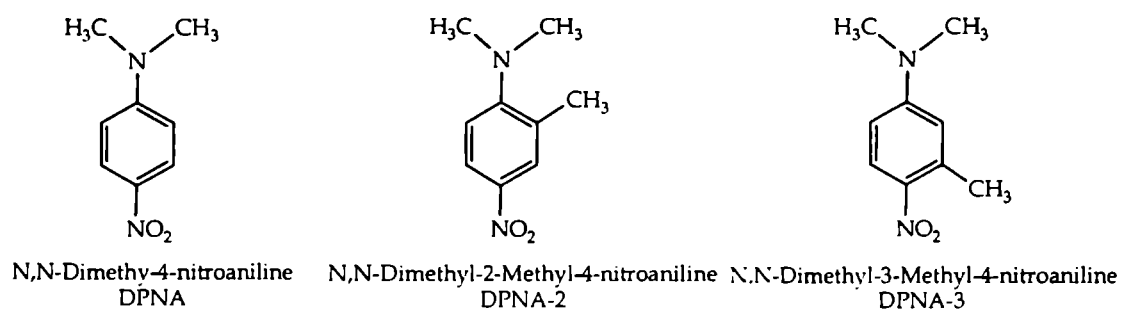


Figure.2.2. N,N-Dimethyl-4-nitroaniline and its methyl derivatives

DPNA also has the same symmetry point group as that of PNA. The DPNA and its two derivatives (Figure 2.2 and Table 2.2) also show a similar trend observed in Table 2.1 for the average value of the susceptibilities except for the γ values. The molecular orbital picture is also similar. The γ value of DPNA-2 molecule is 20% higher than that of parent molecule. The γ value for DPNA-3 is lower than that of parent molecule. In both the PNA and DPNA parent molecules, the 2-substituted derivative has a higher β value than that of 3-substituted derivative whereas the average value of α is higher for a 3-substituted derivative. α values increase in the order DPNS < DPNA-2 < DPNA-3

For an unsymmetrical MPNA (Figure 2.3 and Table 2.3) and EPNA (Figure 2.4 and Table 2.4), the 2, and 6 substituted derivatives show a higher α value than that of the parent and other substituted molecules. In these cases, the 2 and 6 substituted derivatives have larger γ value than that of parent and other substituted derivatives. The β values for 2 and 6 substituted derivatives are larger than those of 3 and 5 substituted derivatives.

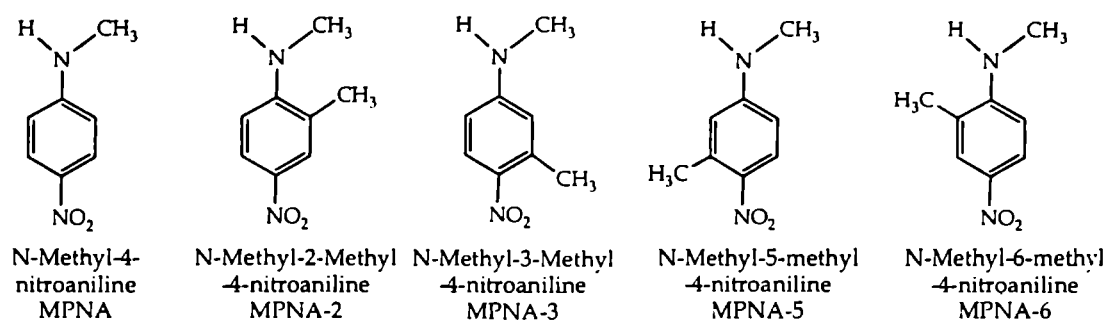


Figure 2.3 N-Methyl-4-nitroaniline and its methyl derivative

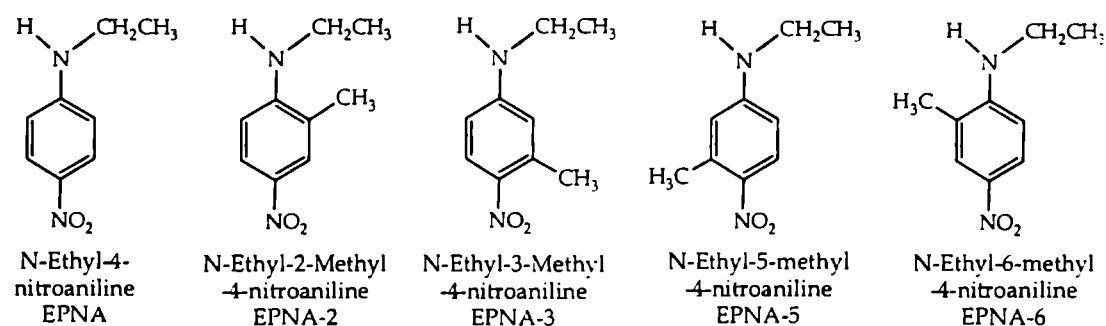


Figure 2.4 N-Ethyl-2-nitroaniline and its methyl derivatives

For EPNA, the 6 substituted derivatives have larger β and γ value than that of 2 substituted derivative. The observed trend in β can be interpreted in terms of SCF energy. The substitution of H with methyl group at the 2nd and the 6th positions increases the HOMO energy and the substitution at the 3rd and 5th position increases the LUMO energy. The HOMO-LUMO energy gap is minimum for the molecules derived from the substitutions at the 2nd and 6th position of the benzene ring. Here also, the positions 2 and 6 are nearer to the parent donor group, thus giving an additive effect to the donor contribution compared to 3 and 5. Positions 2 and 6 are orientationally more favorable for substitution, since both are ortho to NH₂ and meta to NO₂ of PNA. It should be noted that the β value of EPNA-6 is larger compared to EPNA-2 and the EPNA. The C-CH₃ is not on the same side as that of N-C₂H₅. Hence the *ortho* effect is not prominent and planarity is retained

Table 2.3: Calculated dipole moment (μ), polarizability (α) and hyperpolarizabilities (β and γ) and the HOMO-LUMO energy gap (ΔE) of MPNA compared with the values of its four methyl substituted derivatives, MPNA-2, MPNA-3, MPNA-5, and MPNA-6. The listed values are in atomic units.

Coefficients	MPNA	MPNA-2	MPNA-3	MPNA-5	MPNA-6
μ_x	2.95	3.097	2.842	2.807	2.941
μ_y	0.272	0.167	0.127	0.391	0.454
μ_z					
μ	2.963	3.101	2.845	2.834	2.976
α_{xx}	172.77	179.84	183.82	184.69	179.64
α_{yy}	110.93	125.45	126.71	126.31	128.07
α_{zz}	60.06	66.8	68.26	68.29	68.24
α	114.59	124.03	126.27	126.43	125.32
β_{xxx}	1343.22	1267.46	1265.4	1270.26	1317.38
β_{xyy}	-44.18	-30.41	-77.33	-69.92	-38.76
β_{xzz}	-21.16	-6.82	-21.08	-0.41	-16.33
β_x	1277.89	1230.23	1166.99	1199.92	1262.29
β_{yxx}	67.32	51.31	72.05	69.15	94.93
β_{yyy}	-3.15	-9.69	-24.94	10.09	2.87
β_{yzz}	13.79	-5.08	-0.59	28.82	23.69
β_y	77.96	36.53	46.52	108.06	121.5
β_{zxx}	0.98	1.66	1.55	-16.69	0.89
β_{zyy}	0.44	1.76	0.6	0.27	1.69
β_{zzz}	1.52	1.84	0.67	0.44	1.78
β_z	2.93	5.27	2.82	-15.97	4.36
β	1280.28	1230.78	1167.93	1204.89	1268.13
γ_{xxxx}	41191	43162	35206	34588	41284
γ_{xxyy}	1995	3635	1489	4385	7320
γ_{zzxx}	4917	5434	7016	5242	838
γ_{yyyy}	6959	7083	6321	7275	5257
γ_{zzyy}	6607	6810	6769	6505	7752
γ_{zzzz}	13676	10129	13153	10380	13727
γ	17773	18426	17046	16902	18417
ΔE	0.3652	0.3585	0.3711	0.3684	0.3598

Table 2.4: Calculated dipole moment (μ), polarizability (α) and hyperpolarizabilities (β and γ) and the HOMO-LUMO energy gap (ΔE) of EPNA and its methyl substituted derivatives. The parent molecule (EPNA) is planar in geometry and the derivatives are obtained by substituting the ring -H atom of the planar EPNA with -CH₃ group. The reported values are in atomic units.

Coefficients	EPNA	EPNA-2	EPNA-3	EPNA-5	EPNA-6
μ_x	3.108	3.196	3.015	2.956	3.069
μ_y	0.481	0.355	0.333	0.585	0.677
μ_z	0.013	0.011	0.012	0.012	0.012
μ	3.145	3.216	3.033	3.013	3.142
α_{xx}	193.99	209.34	204.61	206.77	200.35
α_{yy}	121.47	133.29	137.34	136.13	138.98
α_{zz}	68.45	73.4	76.47	76.64	76.39
α	127.97	138.68	139.48	139.85	138.57
β_{xxx}	1533.96	1420.46	1425.98	1446.22	1494.49
β_{xyy}	-19.54	13.22	-27.31	-37.38	275.76
β_{xzz}	-3.83	-11.06	-10.53	-13.94	-5.45
β_x	1510.58	1422.62	1388.14	1394.9	1764.8
β_{yxx}	-2.77	220.58	246.84	231.64	6.78
β_{yyy}	247.49	-29.27	-49.45	-18.48	-14.96
β_{yzz}	-6.19	-17.55	-16.31	10.46	-0.98
β_y	238.54	173.76	181.08	223.63	-9.16
β_{zxx}	-11.56	-2.64	-3.9	-1.6	-9.64
β_{zyy}	1.4	3.2	4.26	4.15	8.14
β_{zzz}	0.2	1.36	0.55	0.15	-4.54
β_z	-9.95	1.91	0.9	2.7	-6.04
β	1529.34	1433.19	1399.89	1412.70	1764.84
γ_{xxxx}	47657	48274	40116	40494	52887
γ_{xxyy}	4274	5112	2380	3089	5275
γ_{zzxx}	4362	5083	3760	2609	4484
γ_{yyyy}	6403	10729	7927	5271	9210
γ_{zzyy}	4142	6151	5053	3243	5715
γ_{zzzz}	7226	7783	6853	4448	7728
γ	17369	19896	15456	13619	20155
ΔE	0.3611	0.3563	0.3619	0.3605	0.3555

Table 2.5: Calculated dipole moment (μ), polarizability (α), hyperpolarizabilities (β and γ) and the HOMO-LUMO energy gap (ΔE) of PNA compared with the values for MPNA, DPNA and EPNA. The reported values are in atomic units.

Coefficients	PNA	MPNA	DPNA	EPNA
μ_x	2.754	2.95	3.1	3.108
μ_y		0.272	-0.004	0.481
μ_z				0.013
μ	2.754	2.963	3.1	3.145
α_{xx}	148.4	172.77	193.2	193.99
α_{yy}	101.01	110.93	123.57	121.47
α_{zz}	50.95	60.06	69.43	68.45
α	100.12	114.59	128.73	127.97
β_{xxx}	1064.6	1343.22	1587.41	1533.96
β_{xyy}	-34.1	-44.18	-72.82	-19.54
β_{xzz}	-28.47	-21.16	-28.41	-3.83
β_x	1002.02	1277.89	1486.19	1510.58
β_{yxx}	0.03	67.32	-3.5	-2.77
β_{yyy}	0.06	-3.15	-0.02	247.49
β_{yzz}	0.03	13.79	0.59	-6.19
β_y	0.12	77.96	-2.92	238.54
β_{zxx}	-0.02	0.98	0.46	-11.56
β_{zyy}	-0.2	0.44	0.03	1.4
β_{zzz}	-0.04	1.52	-0.14	0.2
β_z	-0.26	2.93	0.35	-9.95
β	1002.03	1280.28	1486.20	1529.34
γ_{xxxx}	30368	41191	47895	47657
γ_{xxyy}	-1480	1995	1523	4274
γ_{zzxx}	5108	4917	5807	4362
γ_{yyyy}	-4252	6959	6822	6403
γ_{zzyy}	-490	6607	2190	4142
γ_{zzzz}	10589	13676	12056	7226
γ	7164	17773	17162	17369
ΔE	0.3717	0.3652	0.3598	0.3611

There can be two possible reasons for this observation. The first one is the magnitude of the optical gap as mentioned earlier. The second possible reason is the

steric effect, created by the crowding of spatially adjacent N-C₂H₅ group and -CH₃ at the 2nd C position of the benzene ring. This means that the p orbitals on nitrogen and the ring carbon atom, to which it is attached, are prevented from becoming parallel to each other, and their overlap is thus inhibited. Electronic interaction with the nucleus is largely prevented, and the transfer of charge does not take place from amino group to nitro group. Since geometry was fixed to a planar one, the reason for the lower β value would be coming from the non-planar excited state geometry of EPNA-2. This non-planar excited state contribution to the β value would not be affecting EPNA-6 molecule as the molecule is free from steric effects. The relative lowering of the β value of the MPNA-2, and DPNA-2 with the parent molecule as compared to PNA-2 can also be explained on the basis of the above mentioned steric effect. PNA-2 molecule is free from steric effect as there is no -CH₃ group in the amino nitrogen.

The electric field response coefficients of PNA and its higher order methyl derivatives obtained by replacing amino hydrogens are given in Table 2.5. As we go from PNA to higher order derivatives, all the NLO coefficients become larger with respect to the number of methyl groups added. The γ value of MPNA is larger than that of its higher order methyl derivatives. The HOMO-LUMO gap becomes smaller as the number of methyl groups increases in the amino nitrogen. The nitrogen becomes more electron rich and favors a large charge transfer to the LUMO. It is interesting to note that the β values of the iso-electronic DPNA and EPNA do not agree with the additive rule of methyl addition. Although the latter one possesses a high HOMO-LUMO gap, it has got a higher β value. This observation can be interpreted using the well-known symmetry effect in nonlinear optics. In line with Neumann's principle, which states that the physical properties of a system are invariant to its symmetry operations, the susceptibility tensors have the symmetry properties of the medium and thus can restrict the combinations of vector components of the various optical fields that could practically be used. For instance, the odd susceptibility terms are always non-zero, while

Table 2.6: Comparison of dipole moment (μ), polarizability (α) hyperpolarizabilities (β and γ) and the HOMO-LUMO energy gap (ΔE) of symmetric molecules (PNA-2,6 and PNA-3,5) with asymmetric molecules (PNA-2 and PNA-3). The reported values are in atomic units.

Coefficients	PNA-2	PNA-2,6	PNA-3	PNA-3,5
μ_x	2.771	2.785	2.63	2.496
μ_y	-0.176	0.000	-0.139	0.000
μ_z		0.000		0.000
μ	2.776	2.785	2.633	2.496
α_{xx}	156.44	164.26	159.71	169.90
α_{yy}	116.89	133.41	116.8	133.14
α_{zz}	59.31	67.55	59.27	67.44
α	110.88	121.74	111.92	123.49
β_{xxx}	1051.4	1038.91	1007.27	940.80
β_{xyy}	-28.64	-17.23	-64.56	-94.80
β_{xzz}	-27.18	-27.19	-27.77	-29.44
β_x	995.58	994.49	914.94	816.56
β_{yxx}	-20.96	0.12	-4.15	0.51
β_{yyy}	-5.14	0.10	-17.84	-0.02
β_{yzz}	-7.64	0.21	-15.49	0.11
β_y	-33.74	0.42	-37.48	0.60
β_{zxx}	0.14	-0.01	-0.88	-0.19
β_{zyy}	0.31	0.15	-0.18	-0.32
β_{zzz}	0.05	0.12	-0.02	0.05
β_z	0.51	0.26	-1.08	-0.46
β	996.15	994.50	915.72	816.57
γ_{xxxx}	30351	29916	25490	22247
γ_{xxyy}	-203	1325	1341	1199
γ_{zzxx}	4072	4356	2886	1016
γ_{yyyy}	4101	5418	3836	3616
γ_{zzyy}	4859	6391	6702	3591
γ_{zzzz}	8978	10071	9125	4146
γ	10148	13910	12061	8325
ΔE	0.3657	0.3621	0.3760	0.3749

Table 2.7: Calculated dipole moment (μ), polarizability (α) and hyperpolarizabilities (β and γ) and the HOMO-LUMO energy gap (ΔE) of EPNA and its methyl substituted derivatives. The parent molecule (EPNA) is non-planar in geometry and the derivatives are obtained by substituting the ring -H atom of this non-planar molecule with -CH₃ group. The reported values are in atomic units.

Coefficients	EPNA	EPNA-2	EPNA-3	EPNA-5	EPNA-6
μ_x	2.387	2.499	2.387	2.387	2.387
μ_y	0.505	0.349	0.344	0.63	0.678
μ_z	-0.055	-0.081	-0.036	-0.035	-0.076
μ	2.44	2.525	2.412	2.469	2.482
α_{xx}	176.01	191.81	176.01	176.01	176.01
α_{yy}	121.32	133.48	137.31	136.68	137.43
α_{zz}	73.6	80.59	81.7	81.85	81.67
α	123.65	135.29	131.67	131.52	131.71
β_{xxx}	912.44	872.25	912.44	912.44	912.44
β_{xyy}	-21.16	3.79	-39.31	-43.63	-8.62
β_{xzz}	-21.9	-18.83	-19.17	-26.11	-24.91
β_x	869.38	857.21	853.95	842.69	878.9
β_{yxx}	123.06	97.04	113.45	126.32	133.17
β_{yyy}	-2.83	-15.79	-36.59	5.85	16.68
β_{yzz}	5.27	-6.98	-8.07	15.73	17.27
β_y	125.51	74.27	68.79	147.9	167.11
β_{zxx}	-169.82	-162.12	-166.13	-166.9	-164.15
β_{zyy}	-5.19	3.79	0.05	-0.75	-4.74
β_{zzz}	-10.15	-7.54	-10.33	-9.75	-1.72
β_z	-185.17	-165.86	-176.41	-177.39	-170.61
β	897.69	876.27	874.68	873.78	910.77
γ_{xxxx}	33509	35650	33509	33509	33509
γ_{xxyy}	2972	5064	4036	5666	4695
γ_{zzxx}	3035	4259	4928	4741	5930
γ_{yyyy}	5309	5472	5669	8345	8033
γ_{zzyy}	2369	2464	3067	3882	3367
γ_{zzzz}	5000	6558	6502	6529	6869
γ	12114	14251	13948	15392	15279
ΔE	0.3740	0.3657	0.3778	0.3775	0.3687

the even terms can be vanishing due to centre of symmetry. Thus, to have effects driven by second order nonlinear susceptibility terms, it is important to have a non-centrosymmetric medium. The even order nonlinear coefficient becomes prominent only if the molecule is less symmetric. Clearly, EPNA is disymmetric, while a DPNA possesses a C_{2v} symmetry. The β value does not grow additively as we move from PNA to its higher order derivatives. This is true due to the fact that the MPNA is disymmetric, while the PNA and DPNA are symmetric in nature.

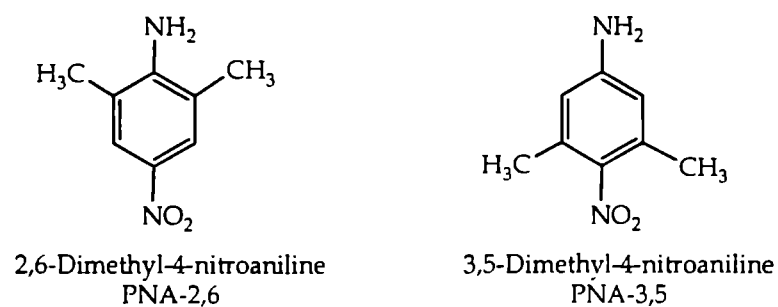


Figure 2.5. Dimethyl derivative of PNA

To put this issue of symmetry factor in further perspective, we focus on the study of the molecules derived by substituting two hydrogen atoms of the phenyl ring of PNA with two methyl groups (Figure 2.5). The coefficients are given in Table 2.6. The HOMO-LUMO gap of PNA-2 is higher than that of its higher methyl derivative, PNA-2,6. But the PNA-2,6 has smaller β value than that of PNA-2, irrespective of the addition of one more electron pushing methyl group at the 6th position of PNA-2. This smaller β value for a PNA-2,6 is due to the fact that a non symmetric PNA-2 becomes C_{2v} symmetric, when a CH₃ group is added to the 6th position of PNA-2. Also, in disubstituted ortho derivatives, the systems become nonplanar due to the *ortho* effect of substituents. The same is true for PNA-3 and PNA-3,5 pair. While studying the geometry effect on the NLO coefficients, planar and non-planar EPNA and its derivatives were compared (Table 2.7). It is observed that the coefficients β and γ are very large in planar system when compared to the non planar ones, α also increases

slightly due to planarity. From the very classical insight about charge transfer, it is very clear that for a continuous charge transfer to occur, systems should be planar. Since β and γ depend more on charge transfer compared to α , those coefficients are much larger in planar geometries. It can also be observed that, the systems with substitution at nitrogen (NH_2 group) give higher values for all the coefficients than the isoelectronic counter part with ring substitution. Comparing dipole moment and optical gap of these systems, it can be explained that the substitution at nitrogen increases the donor strength; hence favoring the charge transfer even though the dipole moment is almost the same for most of the pairs.

2.4. Conclusion

Since charge transfer plays an important role in NLO process, the systems having more favorable features for a charge transfer give higher nonlinear optical coefficients. Hence, strength and number of donors and acceptors, asymmetry and geometry of the systems and positions of the substitutions play important roles in determining NLO responses. Out of the possible structures, many can readily be described on the basis of simple considerations (the sigmatropic effect of the methyl substitutions on NH_2 group, position of substitution in the benzene ring, etc); but more quantitative assessments require direct quantum mechanical calculations of the electric field response. Factors such as structure, primary and secondary, and the resulting electron density distribution turn out to have a great influence on these properties. High electric susceptibilities depend on the nature of the delocalized structures and it is the purpose of molecular design in optoelectronics to find molecular systems that yield the largest possible responses. The larger these linear and nonlinear responses are, the smaller the electric field required to achieve the desired electro-optic effect. As already pointed out, the molecular structure of organic materials can be modified in order to maximize the electric responses.

References

- (1) Prasad, P. N.; Williams, D. J. *Introduction to Nonlinear Optical Effects in Molecules and Polymers*; Wiley: New York, 1991
- (2) (a) Finn, R. S.; Ward, J. F. *Phys. Rev. Lett.* **1971**, *26*, 285. (b) Finn, R. S.; Ward, J. F. *J. Chem. Phys.* **1974**, *60*, 454. (c) Ward, J. F.; New, G. H. C. *Phys. Rev.* **1969**, *185*, 57.
- (3) Buckingham, A. D.; Orr, B. J. *Trans. Faraday Soc.* **1969**, *65*, 673. Brown, J. M.; Buckingham, A. D.; Ramsey, D. A. *Can. J. Phys.* **1969**, *49*, 914.
- (4) Bartlett, R. J.; Purvis, G. D. *Phys. Rev. A* **1979**, *20*, 1313.
- (5) Butcher, P. N.; Cotter, D. *The Elements of Nonlinear Optics*; Night, P. L., Firth, W. J., Eds.; Cambridge University Press: Cambridge, England, 1990.
- (6) Daniel, C.; Dupuis, M. *Chem. Phys. Lett.* **1990**, *171*, 209.
- (7) Perrin, E.; Prasad, P. N.; Mougenot, P.; Dupuis, M. *J. Chem. Phys.* **1989**, *91*, 4728.
- (8) Sim, F.; Chin, S.; Dupuis, M.; Rice, J. E. *J. Phys. Chem.* **1993**, *97*, 1158.
- (9) (a) Sekino, H.; Bartlett, R. J. *J. Chem. Phys.* **1986**, *85*, 976. (b) Liu, S. Y.; Dykstra, C. E. *J. Phys. Chem.* **1987**, *71*, 1749.
- (10) Davydov, B. L.; Derkacheva, L. D.; Dunina, V. V.; Zhabotinski, M. K.; Zolin, V. K.; Kreneva, L. G.; Samokhina, M. A. *JETP Lett.* **1970**, *12*, 16.
- (11) Moylan, C. R. *J. Phys. Chem.* **1994**, *98*, 13513.
- (12) Kanis, D. R.; Ratner, M. A.; Marks, T. J. *Chem. Rev.* **1994**, *94*, 195.
- (13) Albert, I. D. L.; Morley, J. O.; Pugh, D. J. *Chem. Phys.* **1995**, *102*, 237.
- (14) Champagne, B.; Kirtman, B. *Handbook of Advanced Electronic and Photonic Materials*; Nalwa, H. S., Ed.; Academic: San Diego, 2001; Vol. 9, Chapter 2, p 63.
- (15) Morley, J. J. *Chem. Soc., Perkin Trans.* **1995**, *2*, 177; **1994**, *2*, 1211; *J. Phys Chem.* **1994**, *98*, 11818.
- (16) Bishop, D. M. *Adv. Chem. Phys.* **1998**, *104*, 1.
- (17) Ågren, H.; Vahtras, O.; Koch, H.; Jørgensen, P.; Helgaker, T. *J. Chem. Phys.* **1993**, *98*, 6417.
- (18) Mikkelsen, K. V.; Luo, Y.; Ågren, H.; Jørgensen, P. *J. Chem. Phys.* **1994**, *102*, 9362.
- (19) Champagne, B.; Perpete, E. A.; Jacquemin, D.; van Gisbergen, S. J. A.; Baerends, E.-J.; Soubra-Ghaoui, C.; Robins, K. A.; Kirtman, B. *J. Phys. Chem. A* **2000**, *104*, 4755

- (20) Champagne, B. *Chem. Phys. Lett.* **1996**, 261, 57.
- (21) Quineta, O.; Champagne, B.; Kirtmanb, B. *THEOCHEM* **2003**, 633, 199.
- (22) Sykes, P. *A Guide Book to Mechanism in Organic Chemistry*; Orient Longman: New Delhi, 1986.
- (23) Nalwa, H. S.; Miyata, S. *Nonlinear Optics of Organic Molecules and Polymers*; CRC Press: New York, 1997.
- (24) (a) Oudar, J. L.; Chemla, D. S. *J. Chem. Phys.* **1977**, 66, 2664. (b) Oudar, J. L. *Chem. Phys.* **1977**, 67, 446.

EFFECT OF SPACER GROUPS ON THE NONLINEAR OPTICAL PROPERTIES

According to electron donor-electron acceptor concept, structure property relationships of push-pull NLO-phores based on the theoretical and experimental work have led to the definition of molecular engineering rules. These definitions indicate that the hyperpolarizability (β), characterizing the molecular second order NLO efficiency, depends on the strength of the donor and acceptor groups, on the extent of the π -conjugated path and, for conjugating spacers based on aromatic systems, on the resonance stabilization energy of the aromatic system.¹ Intensive studies regarding the NLO efficiencies of molecules containing π -conjugated spacers are seen in the literature.² But the effect of alkyl spacers has not been studied properly.

This chapter is divided in to two parts; in the first part, quantum chemical calculations on the linear and nonlinear electric polarizabilities of dipolar molecules separated by alkyl spacers have been performed on $O_2N-Ph-N=N-Ph-(CH_2)_n-Ph-N=N-Ph-NO_2$, $n = 1-12$. These molecules exhibit a very strong odd-even behavior in the first hyperpolarizabilities (β), with large (small), β for $n=odd$ ($n= even$). Such odd-even oscillations have been reported experimentally on similar systems, but the origin of such phenomena has remained to be unclear. A detailed investigation about the origin of this odd-even oscillations based on conformation of the systems under study is presented in this part.

The second part comprises of the study on polymeric systems, based on *para*-nitroaniline (PNA), in which the alkyl spacers are placed on the two wings (hydrogens of NH_2 group were replaced with alkyl) of PNA. Number of alkyl groups, n , was changed from 1 to 7. Dynamic (ZINDO-SOS) and static (CPHF) theoretical calculations

of polymers and the experimental evaluation of SHG efficiency have also been done, which agreed with the theoretical predictions.

PART-I
ODD-EVEN OSCILLATIONS IN THE FIRST
HYPERPOLARIZABILITY OF DIPOLAR
CHROMOPHORES: ROLE OF CONFORMATIONS OF
SPACERS

3I.1. Introduction

In the field of nonlinear optics (NLO), π -conjugated systems have been a subject of intense study from both experimental and theoretical aspects.³⁻⁵ It is mainly because, the π -electrons are much easier to be excited with the application of laser field than the σ -electrons. Additionally, because of the large energy separation between the σ - and π -electrons in π -conjugated systems, there have been many theories based on purely π -electrons with σ -electrons forming the backbone. Although a more elaborate treatment would be necessary to include the all-electron picture, various effective semiempirical theories developed over the years have been used in a number of cases with reliable estimates of various properties including spectroscopic quantities.⁶ On the other hand, for systems with mainly σ -electrons or metallic clusters with very small π - σ separation, Hamiltonians consisting of all electrons in *ab initio* level⁷ have gained enormous popularity in recent years.^{8,9} However, for large systems, the accurate determination of the excitation characteristics for dynamic spectroscopic applications still rely on semiempirical methods with configuration interactions.

In the present work, NLO properties have been calculated for a few dipolar chromophores that are separated by an alkyl bridge. The size of the alkyl group is varied to obtain an understanding of the orientation of the dipoles together with its effect on NLO properties of the system. The alkyl bridge acts as a harmless stitch, but, since it is flexible, leads to many different orientations in the dipoles. NLO properties of these systems have been calculated with a variation in the number of alkyl groups. The

observation is that for an even number of CH_2 spacers, the hyperpolarizabilities are much smaller than that for an odd number of CH_2 spacers. Thus, there is a manifestation of odd-even oscillation in the optical response functions. Such odd-even oscillations are well-known in the literature for many physical properties like the melting points of organic solids¹⁰ and in the orientation of alkane thiol self-assembled monolayers (SAMs).¹¹ (Figure 3I.1) Also, there have been recent reports of odd-even oscillations in NLO properties of organic molecules similar to those considered in the present work¹² and even in different molecular systems.¹³

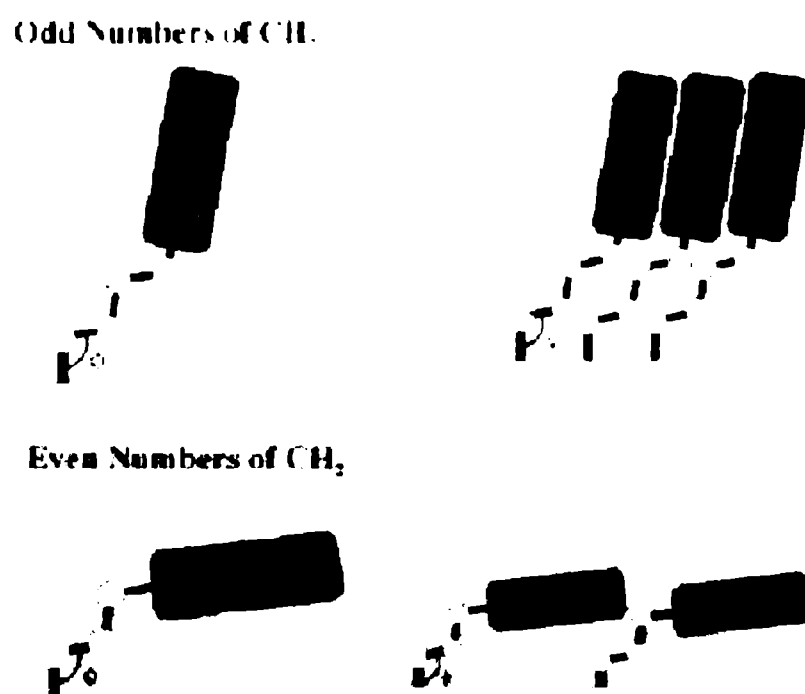


Figure 3I.1. Schematic representation of orientation of SAMs depending on the number of spacers CH_2 (odd -even)

While oscillation in the physical properties such as melting point is generally understood on the basis of packing efficiencies in the van der Waal solids, oscillations in the electrical properties like hyperpolarizabilities are not quite well understood. The present work has been able to clearly show that such oscillations have their origin in the

conformational orientation of the spacers, thereby leading to different packing arrangements in solids or in thin films.

In this chapter, the discussion is about the molecular system considered and the conformational orientations of the spacers for a simple understanding of their energetics, followed by a description about the calculations of the first hyperpolarizability for systems with varying spacer length and explain the odd-even behavior based on the ground state and the excited-state dipole allowed transitions. Lastly, an analytical theory is developed to discuss the exciton splitting in these chromophores for various conformational angles.

3I.2. Conformational flexibility

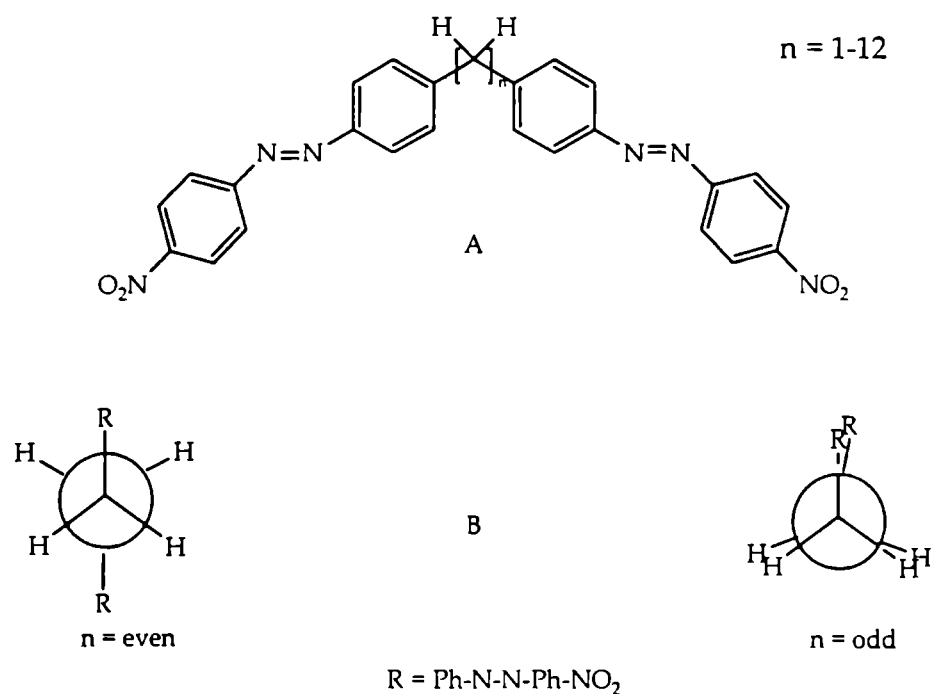


Figure 3I.2. (A) Molecular structure of the system considered. (B) Orientation of the dipoles for odd and even numbered chains

Figure 3I.2 shows the molecular system, bis(4-nitrophenylazo)-diphenylmethane considered for the present study. All the geometries have been

optimized using the AM1 parameterized Hamiltonian available in the Gaussian 03 set of codes.¹⁴ The synthesis and characterization of a similar system, bis(4-hydroxyphenylazo)-2,2'-dinitrodiphenylmethane is described in chapter 4. But a single crystal was not obtained. The geometries obtained by the AM1 calculations have been compared with geometries obtained using the DFT based methods at the B3LYP/6-31G+(d,p) level for the small sized chromophore with $n = 2$. It was found that the geometries obtained by both the methods have similar bond lengths and bond angles.

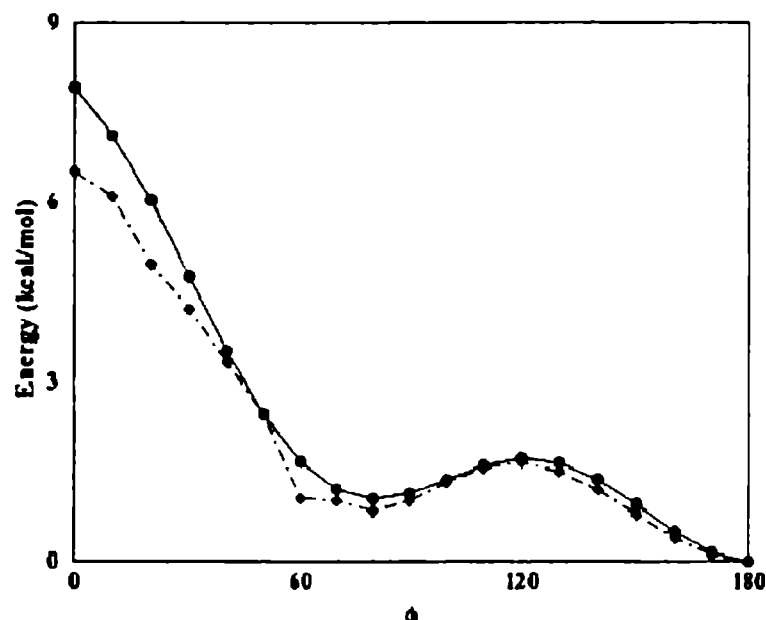


Figure 31.3. Potential energy (in Kcal/mol) with twist along the central C-C single bond for $n=2$, solid line (circles), and $n=12$, dashed line (diamond)

To further verify that the geometries do correspond to the global minima, the geometry for the experimental molecule, bis(4-hydroxyphenylazo)-2,2'-dinitrodiphenylmethane was optimized. For this molecule also, the geometry as well as the interdipolar angle was similar to that considered for this study. Therefore, it is believed that the AM1 Hamiltonian is quite reliable for these systems and thus have proceeded with it for bigger systems with size up to $n = 12$. $R-CH_2-CH_2-R$, $R = Ph-N=N-Ph-NO_2$, is the simplest symmetric case which can be considered to understand the

conformational orientations, as shown in **Figure 3I.2B** Rotation along the central C-C bond produces different geometries. For a torsional angle, $\phi = 0^\circ$, the situation corresponds to an eclipsed geometry while for $\phi = 180^\circ$, the conformation is staggered. In **Figure 3I.3**, the potential energy profile for the system as the torsional angle is increased from 0° to 180° is plotted. The most stable point in the potential energy surface (PES) corresponds to $\phi = 180^\circ$ (staggered orientation in the dipoles) while the most unstable case is for $\phi = 0^\circ$ (the eclipsed form). Also, in the PES, there exists a local minimum between $\phi = 60^\circ$ and 80° and a local maximum at $\phi = 120^\circ$. This is similar to the *gauche* butane interaction well-known in the literature.¹⁵ This arises due to the stronger nonbonding interaction between R and H at an angle of $\phi = 120^\circ$ compared to the weak R, R interaction in the *gauche* form at $\phi \approx 60^\circ$

For $n=2$, the energy difference between the staggered and eclipsed form is 8 kcal/mol and that between the staggered and the *gauche* form is 1.04 kcal/mol. For comparison, the differences are 4.4-6.1 and 0.9 kcal/mol, respectively, for butane.¹⁶ For a longer chain, however, since there are more number of CH₂ groups, the degrees of freedom are much larger, allowing it to be in a state of random relaxed geometry without much constraints. In the same figure (**Figure 3I.3**), the PES for the longest chain considered in the study, $n=12$ is also plotted. It is to be noted that for such a large methylene bridge there is no well-defined unique torsional angle parameter. However, for the sake of comparison, a twist along the central C-C bond, C (6)-C (7) was applied. It comparatively has a lower energy difference between the staggered and eclipsed form (6.5 kcal/mol) and between the staggered and *gauche* form (0.84 kcal/mol). For both $n=2$ and $n=12$, since the energy difference between the eclipsed and the staggered forms are more than the thermal energy at room temperature (0.6 kcal/mol), the staggered form is the most stable orientation for even numbered chain systems. It is also evident from the geometry optimized structures. However, since the *gauche* conformation lies at a local minimum, for longer chains this conformational form becomes thermally accessible. A *gauche* form is interesting because it induces helicity in a linear chain. Such helical chains being chiral exhibits good NLO responses for the even chains.¹⁷⁻¹⁹ It has been reported

for the poled films that the even numbered systems have good NLO responses, particularly for the longer chains.¹² By this study it is believed that the origin of good NLO response functions in such even numbered chain systems is due to the presence of helical chains in a local minimum of the PES.

The odd numbered chains, however, show remarkable contrast. For the odd chains, the favorable arrangement corresponds to an eclipsed orientation for the dipoles, and there exists no local minimum conformation in the PES. This is explicitly shown in **Figure 3I.2B**. One can understand this phenomenon from the simple fact that all the alkyl units being in the sp^3 environment introduces staggered geometry for all central units but eclipsed orientation at the extreme ends where the dipoles are located. So, the odd numbered chains will have an eclipsed orientation for the dipoles. For the even numbered chains, however, there is no such frustration in the dipole orientation, and all the units including the end dipoles remain staggered. Such a remarkable variation between the eclipsed and staggered conformation can be achieved by only changing the number of spacers between the dipoles.

3I.3. Optical response functions: role of spacer length

The geometries (**Figure 3I.2A** with varying n) obtained from the AM1 calculations were used to compute the SCF MO energies and then the spectroscopic properties using Zerner's INDO method.²⁰ The levels of CI calculations have been varied with singles (SCI) to obtain a reliable estimate of the second order optical response functions. The CI approach adopted here has been extensively used in earlier works and was found to provide excitation energies and dipole matrix elements in good agreement with experiment.²¹⁻²³ For the Hartree-Fock determinant, varying number of occupied and unoccupied molecular orbitals were used to construct the CI space. To calculate the second-order NLO properties, correction vector method was used, which implicitly assumes all the excitations to be approximated by a correction vector (CV).²⁴⁻²⁸ The polarizabilities were also computed using the sum-over-states (SOS) formalism, and values similar to those provided by the CV method were obtained.

Table 3I.1: Oscillator Strength (f), Optical Gap (δE) in eV, Ground-State Dipole Moment (μ_g) in debye, Linear Polarizability (α) in units of 10^{-23} esu, and First Hyperpolarizability β , in units of 10^{-30} esu for the Chromophores in Figure 3.I.2A, with Increase in Spacer Length

Spacer	f	δE	μ_g	α	β
n = 1	2.01	4.25	44.4	150.05	537.06
n = 2	2.59	4.42	3.02	156.14	73.03
n = 3	1.78	4.34	46.32	147.50	614.24
n = 4	2.52	4.43	3.36	156.10	50.91
n = 5	1.72	4.43	45.12	153.94	647.88
n = 6	2.50	4.43	3.58	155.66	48.38
n = 7	1.82	4.44	42.34	148.90	813.08
n = 8	2.66	4.46	3.50	149.09	93.31
n = 9	1.56	4.43	47.47	154.08	636.36
n = 10	1.83	4.43	2.35	155.52	70.73
n = 11	1.62	4.43	43.73	161.04	594.89
n = 12	1.84	4.43	3.84	161.86	73.26

Table 3I.1 gives the magnitudes of the ground-state dipole moment (μ_g), oscillator strength (f), the optical gap (δE) [defined as the energy difference between the ground state and the lowest energy dipole allowed state], linear polarizability (α), and first hyperpolarizability (β) for the molecules from $n = 1$ to $n = 12$. It is to be noted that the tumbling average quantities²⁹ for the optical response functions are reported, which may be defined as

$$\bar{\alpha} = \frac{1}{3} \sum_i \alpha_{ii} \quad (31.1)$$

$$\bar{\beta} = \frac{1}{3} \sqrt{\sum_i \beta_i \beta_i^*} \quad ; \quad \beta_i = \sum_j (\beta_{ijj} + \beta_{jji} + \beta_{jij}) \quad (31.2)$$

where, the sums are over the coordinates x, y, z ($i, j = x, y, z$) and β_i^* refers to the conjugate of β_i vector. All the calculations have been performed at a frequency of 1064 nm (1.67 eV) corresponding to the Nd:YAG laser. It is found that while the linear polarizability (α) remains almost constant throughout the series (≈ 155 esu), the ground-state dipole moment as well as the first hyperpolarizability (β) shows strong odd-even oscillations.

Specifically, β , shows an order of magnitude increase for odd numbered chains compared to the even numbered chains. Furthermore, their values remain almost constant with the increase in the number of CH_2 spacers n , albeit for $n = \text{odd}$ and $n = \text{even}$ separately. The even numbered chains have very little dipole moment ($\approx 3D$), while the odd ones have much higher dipole moment ($\approx 45D$). The dipole moment was calculated for the single molecule, Ph-N=N-Ph-NO₂, $\mu_g = 39.20D$. For a perfect parallel arrangement in the dipoles, the classical non interacting picture predicts the total dipole moment as two times single chromophore value for parallel arrangement and zero for a perfect antiparallel arrangement. While, for the even numbered spacers the dipole moments are nearer to zero, the odd numbered spacers show a much smaller value from the classical result of twice the single chromophore value. Such a trend is easy to understand because, for the even numbered chains, the dipoles are staggered and almost perfectly antiparallel (Figure 3I.3).

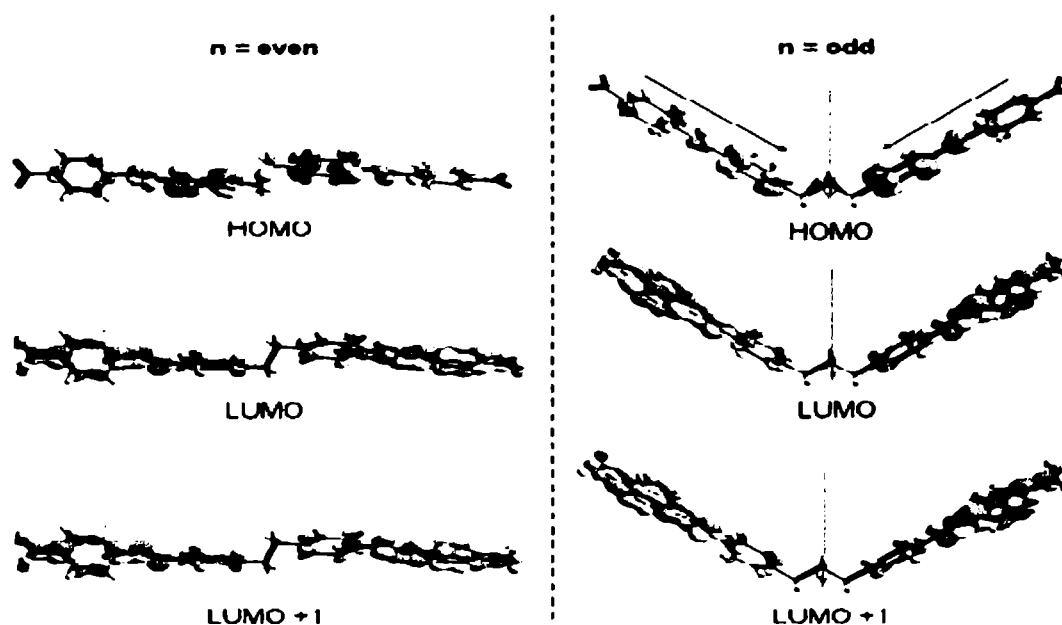


Figure 31.4. Frontier orbital plots for even and odd spacers, While the dipole moments are antiparallel for $n = \text{even}$, $n = \text{odd}$ have a finite angle 110° . The green arrow shows the direction of net dipole moment

But, for the odd numbered chains, even though the orientations are eclipsed, the dipoles are not exactly parallel because of the sp^3 hybridization along the alkyl principal axis. It is straight forward to calculate the angle (ϕ) in which the dipoles are out of phase, using the classical dipole addition formula $\mu_{\text{eff}}^2 = \mu_1^2 + \mu_2^2 + 2\mu_1 \mu_2 \cos \phi$. It is found that ϕ has a magnitude of 110° for the odd chains. It is to be noted that although a classical dipole expression was used for finding the phase angle, it was a very good assumption as the saturated CH_2 groups had very little electronic coupling with the π electrons in the either ends of the bridge. For example, the actual angle for the optimized molecule with $n = 3$ is 112° . The alkyl units basically act as a stitch between the two dipoles. This is illustrated with the frontier wave function plots for the chromophores. The HOMO, LUMO, and LUMO+1 in **Figure 31.4** show no intermixing between the chromophores and thus behave independent of each other. (Within the one-electron picture, HOMO, LUMO, and LUMO+1 represent the ground state, the lowest one-photon state, and the two-photon states, respectively.) For cases as such, even the classical dipole interaction arguments are very accurate.

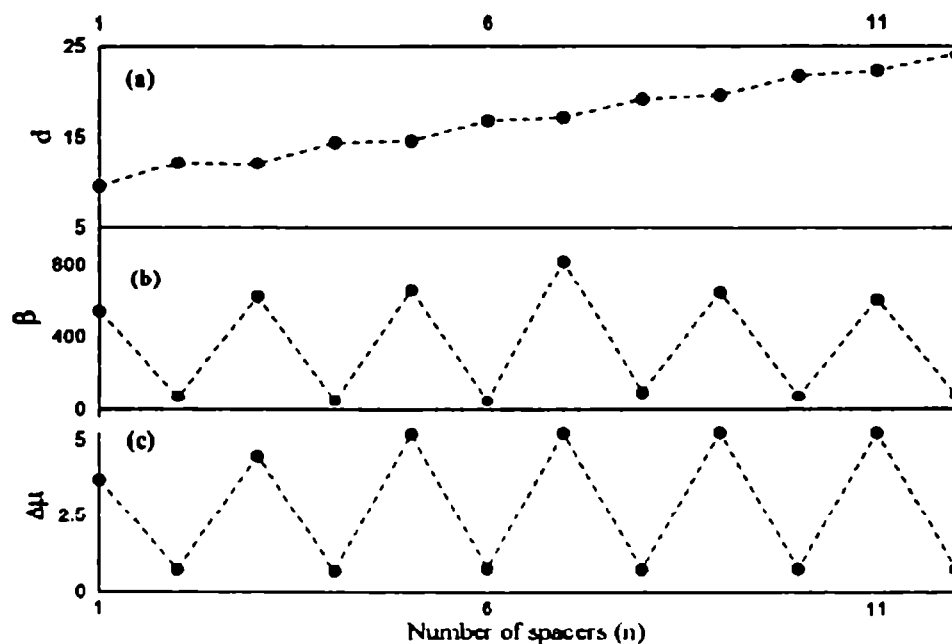


Figure 3I.5. (a) Variation of inter chromophore distance, d (in Å), (b) first hyperpolarizability β (in units of 10^{-30} esu), and (c) difference between the ground-state and the excited-state dipole moment, $\Delta\mu$ (in debye), with increase in the spacer length, n .

With the increase in the number of alkyl units, the distance between the dipoles increases. But, the distance between the even dipoles is more than their odd counterparts as the even ones have a centrosymmetric arrangement which increases their interchromophoric distances. Thus, the distance between the dipoles also exhibit an odd-even effect (Figure 3I.5a). For each even distance, β is small and for each odd distance, β is large. Figure 3I.5b shows the variation in the first hyperpolarizability β with respect to the number of CH_2 units. Very similar to that for the ground-state dipole moment, β also shows a prominent odd-even relation. For odd numbered chain, $\beta \approx 700$ while the even numbered chain have $\beta \approx 80$ (in units of 10^{-30} esu). The calculations are based on a CI basis with its dimension varying until a proper convergence is reached.

With in the framework of the two-state model, the second harmonic generation response (SHG) can be written as ²⁹

$$\beta_{\text{non-level}} = \frac{3e^2}{2\hbar} \frac{\omega_{12} f \Delta\mu}{(\omega_{12}^2 - \omega^2)(\omega_{12}^2 - 4\omega^2)} \quad (3I.3)$$

Where $\hbar\omega_{12}$ is the excitation energy, f the oscillator strength, $\Delta\mu$ the difference between the dipole moments of the ground and the excited state and the ω specifies the excitation frequency of the oscillating electric field. The most important factor in the above expression is that the SHG coefficient is directly proportional to the oscillator strength f , and dipole moment difference, $\Delta\mu$ and is inversely proportional to the optical gap. Thus, any phenomenon that decreases the gap and increases the dipole moment difference between the ground and the excited state will enhance β . But as seen from **Table 3I.1** the optical gap (δE) remains almost constant along the series and shows no such odd-even oscillations. In fact, the oscillator strength for the even numbered chromophores is slightly larger than that for the odd ones. Thus, the only factor that governs such an odd-even oscillation is $\Delta\mu$. **Figure 3I.5c** shows the variation of $\Delta\mu$ with increase with the spacer length. One can clearly see the odd-even variation in $\Delta\mu$ similar to that observed for β . This is to say that the excited state polarization has a strong dependence on the inter chromophoric arrangements.

3I.4. Optical response functions: role of molecular conformations

From the discussion so far, it is evident that, one way to make parallel arrangement of dipoles is to connect the dipoles by an odd number of spacers. The conformation of the methylene itself forces such a parallel orientation. This methodology is elegant because CH_2 units being π -NLO inactive play no electronic role other than fine-tuning the conformational activity. But, at the same time, for even numbered chains, the stable conformers lead to an antiparallel arrangement of dipoles and thus the β is less (in ideal cases, 0). So a proper understanding of the processes associated with this conformational change requires a more detailed analysis.

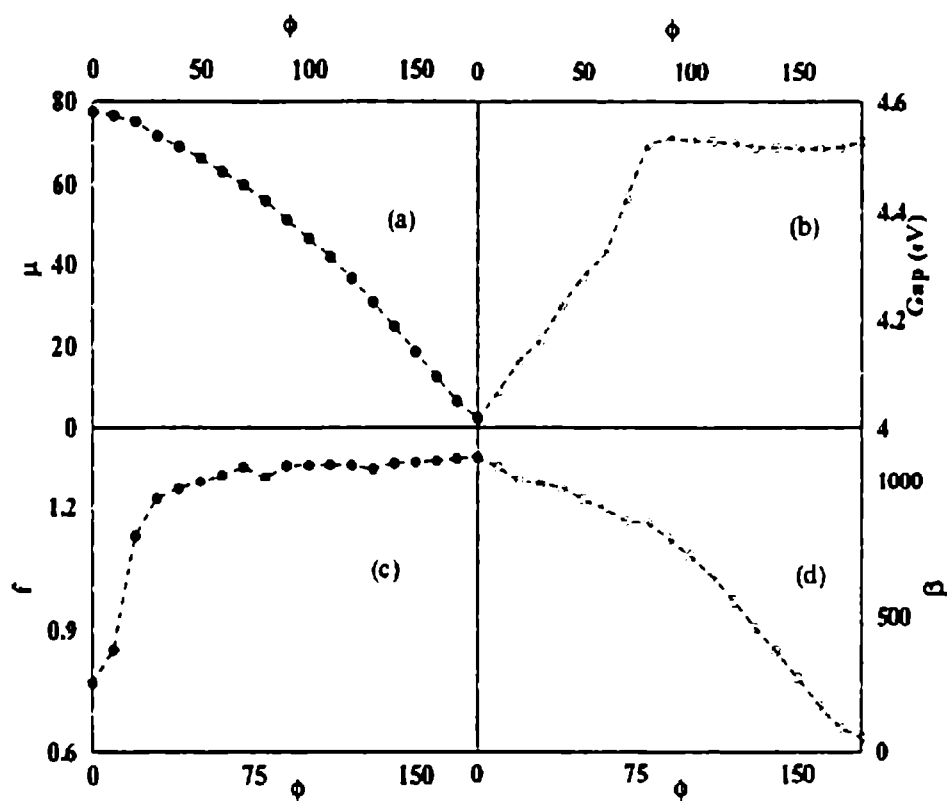


Figure 3I.6 Variation of (a) ground -state dipole moment μ_g (in debye), (b) optical gap (in eV), (c) oscillator strength (f) of the dipole-allowed states, and (d) first hyperpolarizability β (in 10^{-30} esu), with the torsional angle ϕ , from ZINDO calculations.

The simplest even numbered spacer system, $n = 2$, was considered and the variation of the ground-state and the excited-state properties was studied in relation to the variation of the dipolar angle (ϕ). **Figure 3I.6a** shows the variation in the ground-state dipole moment as the torsional angle is increased from $\phi = 0^\circ$ to $\phi = 180^\circ$. μ_g is a monotonically decreasing function and decays to zero at $\phi = 180^\circ$. It is to be noted that, for molecular system selected, the chromophores are not exactly planar, and thus there exists a small but finite dipole moment for staggered orientation. Additionally, ϕ is not 180° for the optimized geometry. However, the antiparallel arrangement is similar in structure to that of the staggered optimized geometry.

For chromophoric aggregates separated by alkyl chains, there is no π -electron coupling between the bridge and the chromophores. This has also been verified from the

studies on oxo-bridged dinitroanilines.³⁰ For such cases one can develop an analytical expression for the extent of exciton splitting due to the dipolar coupling between the organic chromophores. In the present molecular system, D-(CH₂)_n-D, the extent of the dipolar coupling between the two dipoles (named as *m* and *n* in the following equation) can be represented assuming purely electrostatic interaction between the dipoles as

$$H_{mn} = \frac{\vec{M}_{ij} \cdot \vec{M}_{ij}}{r_{mn}^3} - \frac{3(\vec{M}_{ij} \cdot \vec{r}_{mn})(\vec{M}_{ij} \cdot \vec{r}_{mn})}{r_{mn}^5} \quad (31.4)$$

where \vec{M}_{ij} is the transition dipole moment from state *i* to state *j* of a single dipolar unit and r_{mn} is the distance between the two molecular dipole centers, *m* and *n*. It is to be noted that both the transition dipole and the distance (\vec{r}_{mn}) in the numerator are vectorial quantities. Thus, the magnitude of the interaction term will depend crucially on the relative orientations of the dipolar molecules as well as on the axis joining their centers.

For the molecule under study, ϕ is the angle between the planes of the dipolar molecules *m* and $\phi = 0^\circ$ represents the eclipsed dipolar arrangement while $\phi = 180^\circ$ gives rise to a staggered dipolar arrangement. The dot product form of the above equation can be further simplified as

$$H_{mn} = \frac{M_{ij}^2}{r_{mn}^3} (\cos \phi - 3 \cos^2 \theta) \quad (31.5)$$

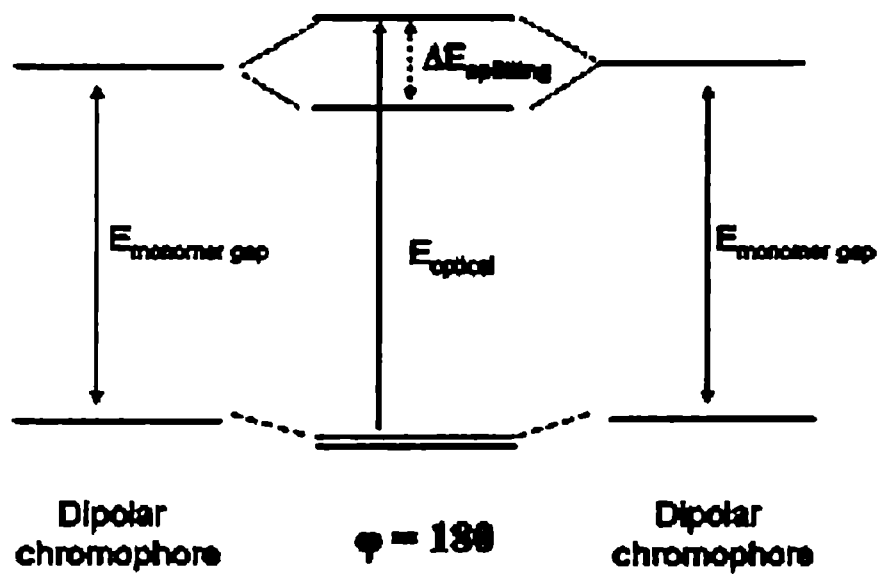
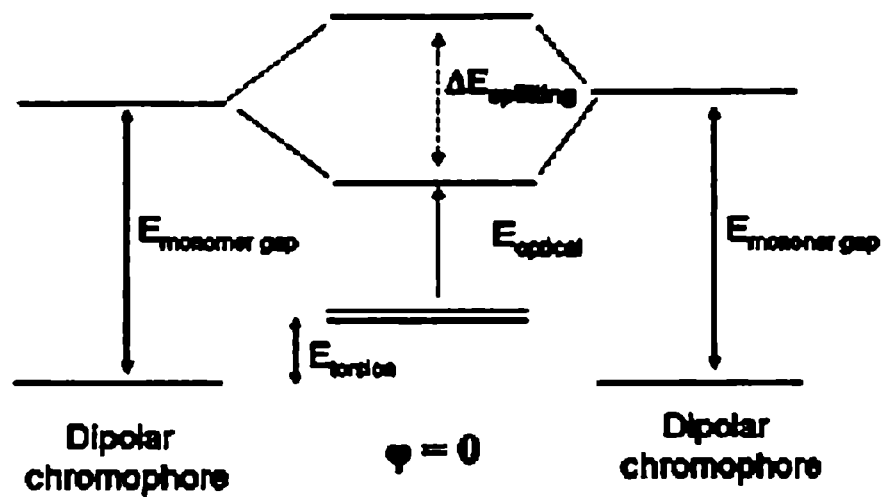


Figure 31.7. Schematic representation of the change in the optical gap due to twist along the C-C bond. Note that the smaller gap in the eclipsed form is due to the stability of the optically excited state together with destabilization of the ground state due to torsion (E_{torsion})

where θ is the angle made by the dipolar axis with the molecular axis. R=Ph-N=N-Ph-NO₂ is a quasi-1-D molecule, and thus the dipolar axis and the long molecular axis

coincides. θ is essentially zero in this case, giving rise to a simplified form for the coupling between the dipoles:

$$H_{mn} = \frac{M_{ij}^2}{r_{mn}^3} (\cos \phi - 3) \quad (3I.6)$$

Note that the θ term has a constant value and does not depend on the orientation of the spacers or the inter chromophoric arrangements. Therefore, even if θ is finite, it will give rise to a constant shift to the energies. From the simple tight binding Hamiltonian (in the limit of nearest-neighbor interactions only), the extent of the excitonic splitting associated with this dipolar coupling between the chromophores can be estimated to be $2H_{m,n}$. Thus, the final expression for the splitting becomes:

$$\Delta E = 2 \frac{M_{ij}^2}{r_{mn}^3} (\cos \phi - 3) \quad (3I.7)$$

The distance r_{mn} was calculated as the distance between the center of masses of the dipolar molecules as ϕ increases from 0° to 180° . From the above analytical expression, it is clear that the extent of Frenkel exciton splitting decreases with increase in ϕ , and thus the optical gap will increase. From the ZINDO calculations, exactly similar behavior was observed. **Figure 3I.6b** shows the variation in the optical gap with increase in the angle ϕ from ZINDO calculations. As ϕ increases, the lowest excited state gets destabilized while the upper excited state becomes more stable, thereby increasing the optical gap. However, the gap saturates after $\phi \approx 80^\circ$. Both the numerator and the denominator (r_{mn}^3) increase with the increase in ϕ as a result of which the gap saturates.

In **Figure 3I.6c**, the variation of the oscillator strength (f) with respect to ϕ is shown. The oscillator strength for the dipole allowed state increases up to $\phi \approx 70^\circ$. However, with further increase in ϕ , the oscillator strength remains constant. **Figure**

3I.6d shows the variation of β with respect to the interdipolar angle. β is a decreasing function of ϕ . However, the decrease is slow up to $\phi \approx 70^\circ$ and then decays rapidly with further increase in ϕ .

Such a variation in β can be well captured by the schematic process of exciton splitting shown in Figure 3I.7. As ϕ increases from 0° to 180° , the extent of excitonic splitting in the dipole allowed excited-state decreases, resulting in the increase in the optical gap (Figure 3I.6b). (For the antiparallel arrangement of the dipoles, the transition occurs to the upper exciton state.) However, at the same time, this process leads to the stabilization of the ground state (from the eclipsed to the staggered form, Figure 3I.3). It is to be noted that the ground-state energy is not a monotonically decreasing function and has a local maximum at 120° . But, the energy scale of the destabilization energy corresponding to the dipole allowed state is much higher (0 - 0.5 eV) than that for the conformational orientation stabilization of the ground state (0-8 kcal/mol), as ϕ is increased. Effectively thus, the optical gap (energy difference between the lowest dipole allowed state and the ground state) would increase with increase in ϕ from 0. Both the two-state model and the full expression for β have the optical gap in the denominator, and thus an increase in gap implies decrease in β . Additionally, with the increase in ϕ , the oscillator strength (f) increases up to $\phi \approx 70^\circ$. Oscillator strength appears in the numerator of the β expression, which explains the initial slow decrease of β (Figure 3I.6c).

3I.5. Conclusions

To conclude, an extensive calculation on the effects of spacer length enhancement on the second-order NLO properties of dipolar molecules connected by CH₂ groups have been performed. β shows a remarkable odd-even variation. For an odd number of spacers, the β value is an order of magnitude higher than that for the even number of spacers. The origin for such oscillation is attributed to the similar oscillations in the dipole moment difference between the ground state and the dipole allowed state and to some extent on the variation in the oscillator strength. This arises due to the change in

the dipolar orientations between the staggered and eclipsed forms for the even and odd numbered chains, respectively.

From the present work, it is clear that this phenomenon of odd-even fluctuation in NLO properties is different from the variation of the physical properties like melting point in organic solids that have their origin in the van der Waals interactions among the solids where crystal packing is the most important parameter. It is also clear that the origin of odd-even oscillations is at the molecular scale. The energy analysis for the potential energy of twisting along the single bond shows that although the staggered form is the most stable conformation for the even numbered chains, but a thermally allowed local minimum exists between $\phi = 60^\circ$ and 80° , corresponding to the *gauche* form that will give rise to helicity in the chain. For example, for every 100 molecules in the staggered form, there are 18 molecules in the *gauche* form (Boltzmann distribution), and even for the $n = 2$ case, the Boltzmann-weighted average first hyperpolarizability, β , has a magnitude of 160.8×10^{-30} esu. In the solid state, because of environment effects, the possibility of existence of such a helical form (local minimum) exists. As a result, for the even numbered chains, although a global minimum form ensures β to be very small, supramolecular effects as in thin films will introduce appreciable β .

References

- (1) (a) Marder, S. R.; Gorman, C. B.; Tiemann, B. G.; Cheng, L. T. *Am. Chem. Soc.* **1993**, *115*, 3006. (b) Marder, S. R.; Cheng, L. T.; Tiemann, B. G. *J. Chem. Soc., Chem. Commun.* **1992**, 672. (c) Cheng, T.; Tam, W.; Marder, S. R.; Steigman, A. E.; Rikken, G.; Spangler, W. *J. Phys. Chem.* **1991**, *95*, 10631-10643 (d) Cheng, T.; Tam, W.; Marder, S. R.; Steigman, A. E.; Rikken, G.; Spangler, W. *J. Phys. Chem.* **1991**, *95*, 10643.
- (2) (a) Marder, S. R.; Cheng, L.-T.; Tiemann, B. G.; Friedli, A. C.; Blanchard-Desce, M.; Perry, J. W.; Skindhøj, J. *Science* **1994**, *263*, 511. Blanchard-Desce, M.; Alain, V.; Bedworth, P. V.; Marder, S. R.; Fort, A.; Runser, C.; Barzoukas, M.; Lebus, M. S.; Wortmann, R. *Chem. Eur. J.* **1997**, *3*, 1091.

- (3) Prasad, P. N.; Williams, D. J. *Introduction to Nonlinear Optical Effects in Molecules and Polymers*; Wiley: New York, 1991.
- (4) Marks, T. J.; Ratner, M. A. *Angew. Chem., Int. Ed. Engl.* 1995, 34, 155.
- (5) Burland, D. M., Ed.; *Chem. Rev.* 1994, 94, 1.
- (6) (a) Mattis, D. C. *The Many-Body Problem*; World Scientific: Singapore, 1993. (b) Heeger, A. J.; Kivelson, S.; Schrieffer, J. R.; Su, W.-P. *Rev. Mod. Phys.* 1988, 60, 781.
- (7) Helgaker, T.; Jorgensen, P.; Olsen, J. *Molecular Electronic-Structure Theory*; John Wiley and Sons: New York, 2000.
- (8) Rao, B. K.; Jena, P. *J. Chem. Phys.* 2000, 113, 1508.
- (9) Maroulis, G.; Pouchan, C. *J. Phys. Chem. B* 2003, 107, 10683.
- (10) Slovokhotov, Y. L.; Neretin, I. S.; Howard, J. A. K. *New J. Chem.* 2004, 28, 967.
- (11) (a) Angelico, V. J.; Mitcell, S. A.; Wysocki, V. H. *Anal. Chem.* 2000, 72, 2603. (b) Alloway, D. M.; et al. *J. Phys. Chem. B* 2003, 107, 11690.
- (12) Asha, S. K.; Kavita, K.; Das, P. K.; Ramakrishnan, S. *Chem. Mater.* 1999, 11, 3352.
- (13) Gangopadhyay, P.; Radhakrishnan, T. P. *Chem. Mater.* 2000, 12, 3362.
- (14) Dewar, M. J. S.; Zoebisch, E. G.; Healy, E. F.; Stewart, J. J. P. *J. Am. Chem. Soc.* 1985, 107, 3902.
- (15) March, J. *Advanced Organic Chemistry: Reactions, Mechanisms and Structure*, 4th ed.; John Wiley and Sons: New York, 1992.
- (16) Eliel, E. L. *Stereochemistry of Carbon Compounds*; McGraw-Hill: New York, 1962.
- (17) Gangopadhyay, P.; Radhakrishnan, T. P. *Angew. Chem., Int. Ed. Engl.* 2001, 40, 2451.
- (18) Botek, E.; Champagne, B.; Turki, M.; Andre, J.-M. *J. Chem. Phys.* 2004, 120, 2042.
- (19) Philip, B.; Sreekumar, K. *J. Polym. Sci., Part A: Polym. Chem.* 2002, 40, 2868.
- (20) Ridley, J.; Zerner, M. C. *Theor. Chim. Acta* 1973, 32, 111. Bacon, A. D.; Zerner, M. C. *Theor. Chim. Acta* 1979, 53, 21.
- (21) Buenker, R. J.; Peyerimhoff, S. D. *Theor. Chim. Acta* 1974, 35, 33.
- (22) Shuai, Z.; Beljonne, D.; Bredas, J. L. *J. Chem. Phys.* 1992, 97, 1132.
- (23) Beljonne, D.; Shuai, Z.; Cornil, J.; dos Santos, D.; Bredas, J. L. *J. Chem. Phys.* 1999, 111, 2829.

-
- (24) Ramasesha, S.; Soos, Z. G. *Chem. Phys. Lett.* **1988**, *153*, 171; Soos, Z. G.; Ramasesha, S. *J. Chem. Phys.* **1989**, *90*, 1067.
- (25) Ramasesha, S.; Shuai, Z.; Bredas, J. L. *Chem. Phys. Lett.* **1995**, *245*, 224.; Albert, I. D. L.; Ramasesha, S. *J. Phys. Chem.* **1990**, *94*, 6540; Ramasesha, S.; Albert, I. D. L. *Phys. Rev. B* **1990**, *42*, 8587.
- (26) Pati, S. K.; Ramasesha, S.; Shuai, Z.; Bredas, J. L. *Phys. Rev. B* **1999**, *59*, 14827.
- (27) Pati, S. K.; Marks, T. J.; Ratner, M. A. *J. Am. Chem. Soc.* **2001**, *123*, 7287.
- (28) Ramasesha, S.; Shuai, Z.; Bredas, J. L. *Chem. Phys. Lett.* **1996**, *250*, 14.
- (29) (a) Oudar, J. L.; Chemla, D. S. *J. Chem. Phys.* **1977**, *66*, 2664. (b) Oudar, J. L. *J. Chem. Phys.* **1977**, *67*, 446.
- (30) Datta, A.; Pati, S. K. *J. Phys. Chem. A* **2004**, *108*, 320.

PART -II
SPACER EFFECT IN SHG OF POLYMERS CONTAINING
AZOMESOGENS

3II.1. Introduction

In this part, a series of polymers were designed based on PNA. The polymers were designed as a condensation product of an azomesogen chromophore and a PNA derivative. The PNA derivative was designed by substituting the two hydrogens of NH_2 groups with alkyl spacers containing varying number of CH_2 from 1 to 7. The hyperpolarizability values, β were calculated by *static* (CPHF) and *dynamic* (ZINDO-SOS) method. Most of the polymeric systems were synthesized and SHG efficiency was measured experimentally.

3II.2. Monomer design

The route of monomer design is shown in Figure 3II.1.

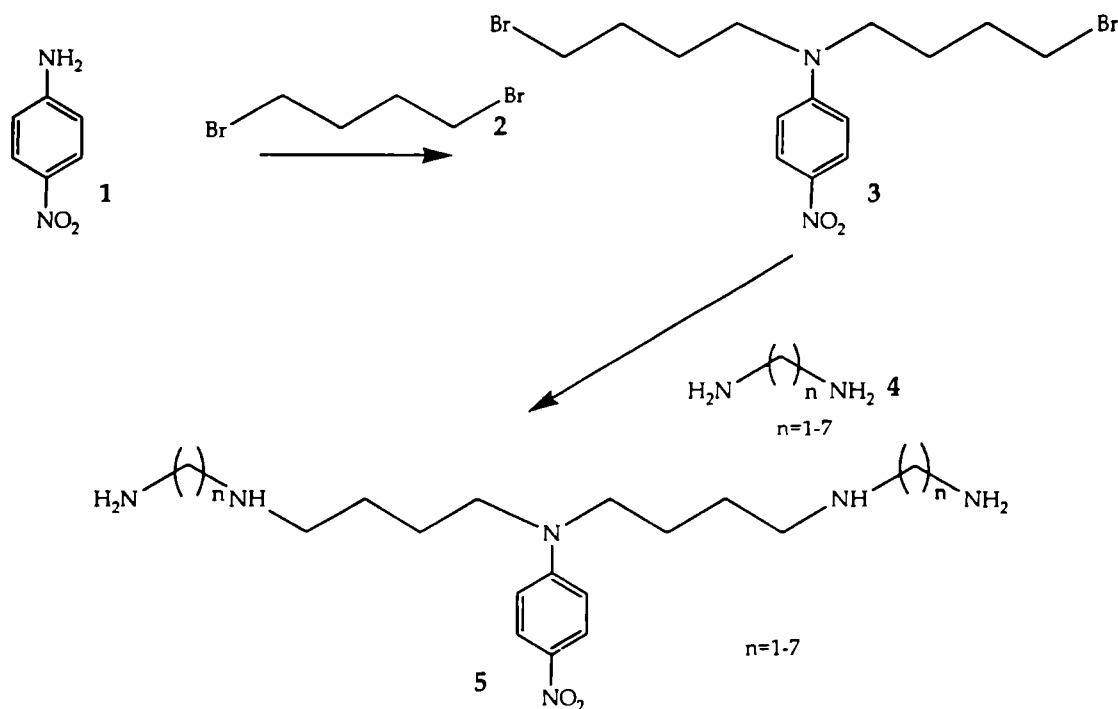


Figure. 3II.1 Route of monomer design

The design starts with PNA. PNA (1) was condensed with dibromobutane (DBB, 2). The condensation product (PNADBB, 3) was reacted with diamines (4) varying from methylene diamine (Meth, $n = 1$) to heptyl diamine (Hept, $n = 7$). The product obtained contained the number of CH_2 groups in the two wings of PNA which varied from 1 to 7 (Meth, Eth, Prop, But, Pent, Hex and Hept) to study the effect of alkyl spacer group in the value of β of the donor-acceptor system. All the monomer systems have been optimized with 6-31G basis sets using restricted Hartree-Fock formalism available in the Gaussian algorithm.¹⁻⁴ The optimized geometries were used to compute the SCF MO energies. The *static* spectroscopic properties of monomers have been calculated using Coupled Perturbed Hartree-Fock (CPHF) method at RHF 6-31++G(d,p) level available in the Gaussian codes.⁵ The *dynamic* spectroscopic properties have been calculated using the Zerner's INDO SOS method with sum over 82 states.⁶⁻⁷

3II.3. Hyperpolarizability β of monomers

The values of *static* Hyperpolarizability, β of monomers are given in Table 3II.1. It is clear that a small odd- even oscillation is observed in the ground state dipole moment μ and Hyperpolarizability, β of these molecules (monomers) while the linear polarizability increases with the number of CH_2 groups. The optimized structures for $n=6$ (Hex) and $n=7$ (Hept) are given in Figure 3II.2. and Figure.II.3. The parallel arrangement of dipoles in odd numbered chains and anti parallel arrangements of dipoles in even numbered chains are clear from the figure. As explained in part I of this chapter the odd- even oscillation in dipole moment, μ and Hyperpolarizability, β is due to the molecular conformation of the chains. But in this case, the oscillations are not so visible and prominent due to the fact that the increment in CH_2 groups has taken place simultaneously in the two wings of the PNA derivatives. Thus two end dipoles are always in parallel (eclipsed) arrangement irrespective of whether the chain is odd or even. This decreases the large change of μ and β between the odd and even numbered chains. Also, in both cases, there was a common butyl unit in both wings of the molecule which contributes a non zero μ and β .

To compare with the results in part I of this chapter, thenonlinear properties of all the optimized structures have been calculated by *dynamic* ZINDO SOS calculations, the results are shown in **Table 3II.2**. The *dynamic* calculation also agrees with the static calculations. Oscillator strength f , and Optical Gap δE , were constant in this case also. The oscillation in $\Delta\mu$ is quite visible in this case. Even though there is a small odd- even oscillations, for μ , and β , it is not visible as in the case of the system studied in part I. **Figure 3II.4** gives a comparative picture.

Table 3II.1: HOMO-LUMO gap (ΔE) in eV, Ground-State Dipole Moment (μ_g) in debye, Linear Polarizability (α) in units of 10^{-23} esu, and First Hyperpolarizability β , in units of 10^{-30} esu for the chromophores (*ab initio* CPHF static property calculations)

Chromophore	ΔE	μ_g	α	β
PNA	0.3507	7.9627	1.35	8.94
DBB	0.4420	0.0005	1.25	1.06
PNADBB	0.4464	4.6995	2.99	1.38
Meth (n-1)	0.3968	8.5079	3.39	3.03
Eth(n=2)	0.3899	5.9852	3.76	2.56
Prop(n=3)	0.3911	8.7202	4.09	3.76
But(n=4)	0.3903	5.1224	4.43	3.40
Pent(n=5)	0.3902	8.7385	4.76	3.81
Hex(n=6)	0.3901	5.1218	5.10	3.41
Hept(n=7)	0.3900	8.1203	5.31	3.90

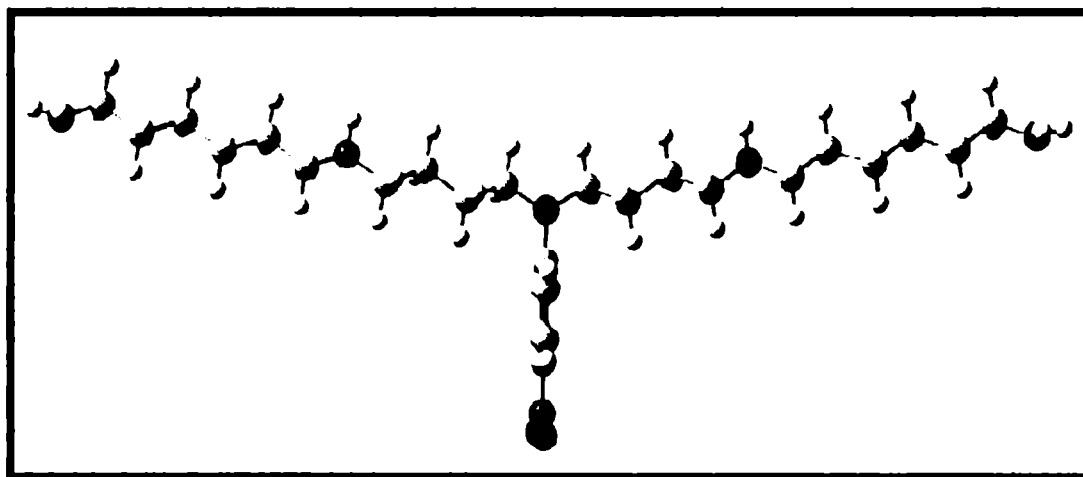


Figure 3II.2. Optimized structure of Hex

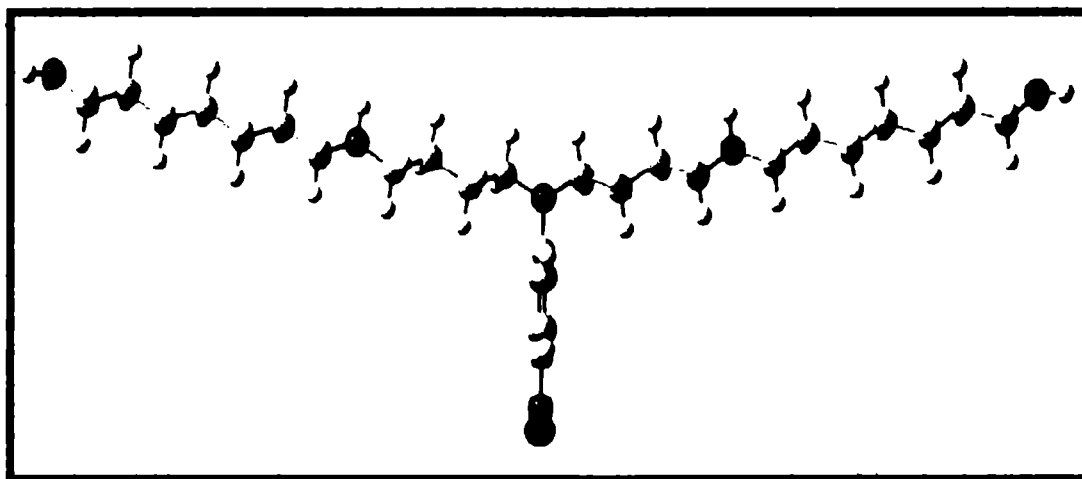


Figure 3.II.3 .Optimized structure of Hept

Table 3II.2: Oscillator strength f , Optical Gap (δE) in eV, Ground-State Dipole Moment (μ_g) in debye, Difference in dipole moment between ground state and excited state ($\Delta\mu$), Linear Polarizability (α) in units of 10^{-23} esu, and First Hyperpolarizability β , in units of 10^{-30} esu for the chromophores (ZINDO SOS dynamic property calculations)

Chromophore	f	δE	$\Delta\mu$	μ_g	α	β_{vec}
PNA	1.0285	7.4823	14.1337	43.6312	2090	220.3553
DBB	0.1920	6.0458	47.6473	40.0614	1920	182.4640
PNADBB	0.2237	5.4948	36.4595	159.8493	7.67	631.5936
Meth(n=1)	0.6690	6.6234	21.9865	53.4916	1560	52.3075
Eth(n=2)	0.2641	4.8258	10.2105	40.9080	1570	51.5850
Prop(n=3)	0.2646	4.8253	21.1804	54.7053	1530	52.2516
But(n=4)	0.2644	4.8243	11.2536	31.7754	1530	52.0509
Pent(n=5)	0.2650	4.8240	21.2518	54.9802	1520	52.4288
Hex(n=6)	0.2654	4.8235	11.2372	31.7022	1500	51.8400
Hept(n=7)	0.2650	4.8233	21.2666	57.6567	1520	52.5469

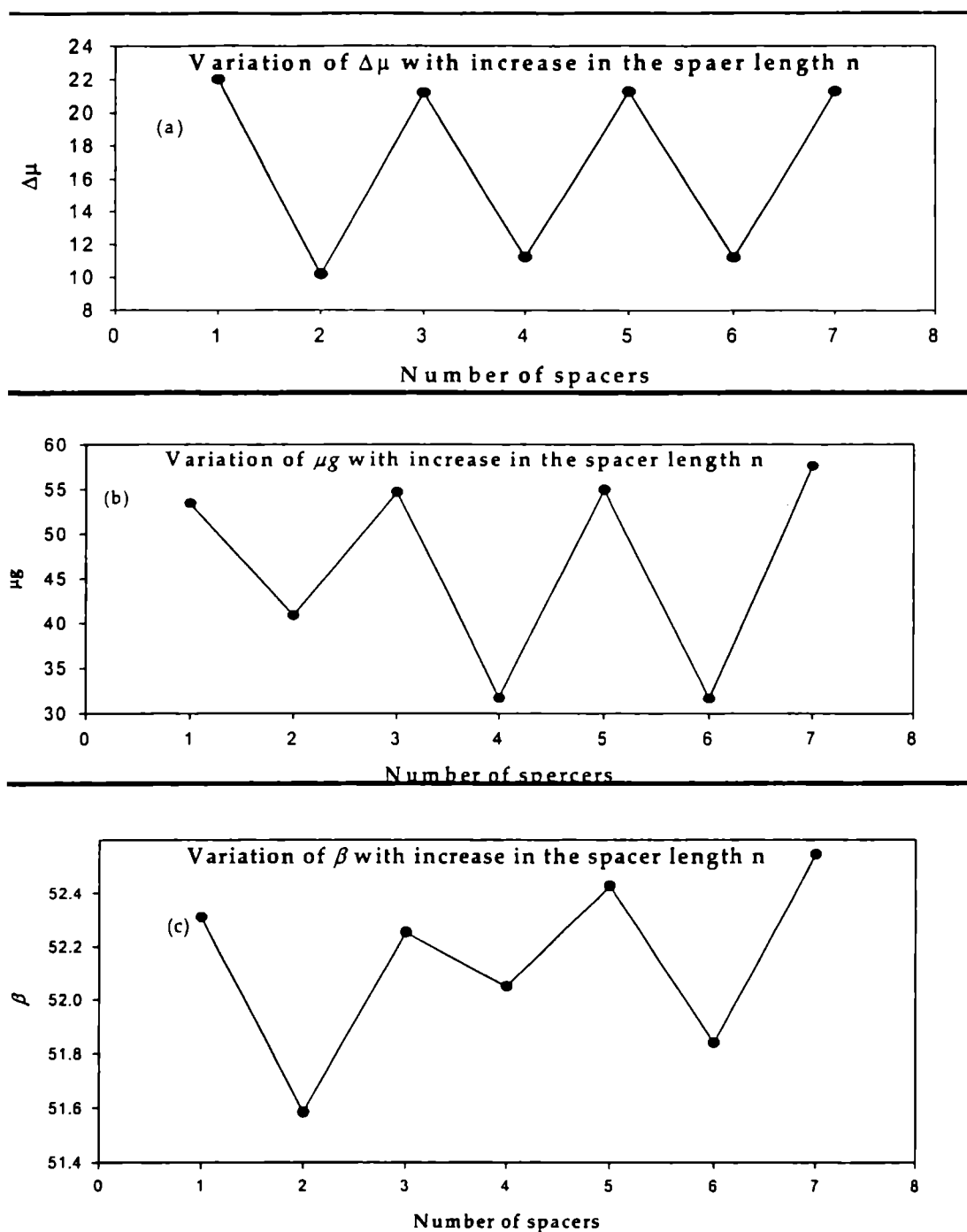


Figure 3II.4. (a) Variation of difference between the ground-state and excited-state dipole moment, $\Delta\mu$ (in debye), (b) ground state dipole moment μ_g (in debye) (c) first hyperpolarizability β , with increase in the spacer length, n.

3II.4. Polymer design

The route of polymer design is shown in Figure 3.II.5. The polymer was designed as a condensation product of previously designed PNA derivatives with

varying number of spacers and an azomesogen chromophore, azobenzene-4, 4'-dicarbonyl chloride (AZCI). Thus a series of polymers with varying number of CH₂ groups from 1-7 in the polymer chain were designed.

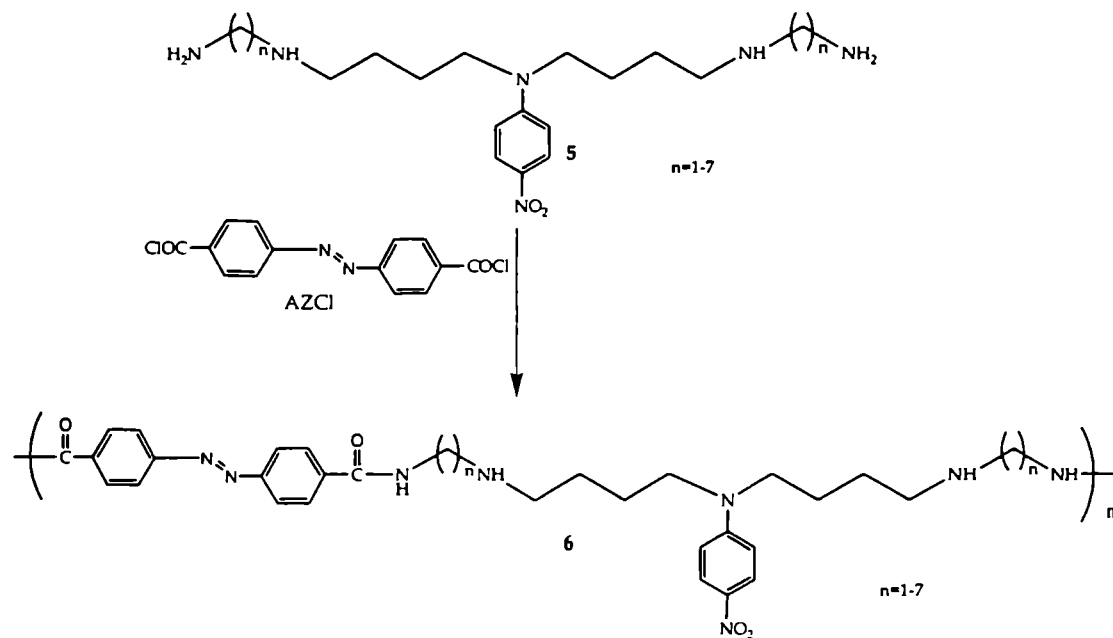


Figure 3II.5 Route of polymer design

All the polymer geometries (two repeating units) have been optimized using the AM1 parameterized Hamiltonian available in the Gaussian 03 set of codes.⁸ *Static* (CPHF) molecular properties of polymers have been calculated with 6-31 G (d) basis sets. The *dynamic* spectroscopic properties have been calculated using the Zerner's INDO SOS method with sum over 82 states. Optimized structure of two repeating unit is given in **Figure 3II.6**.

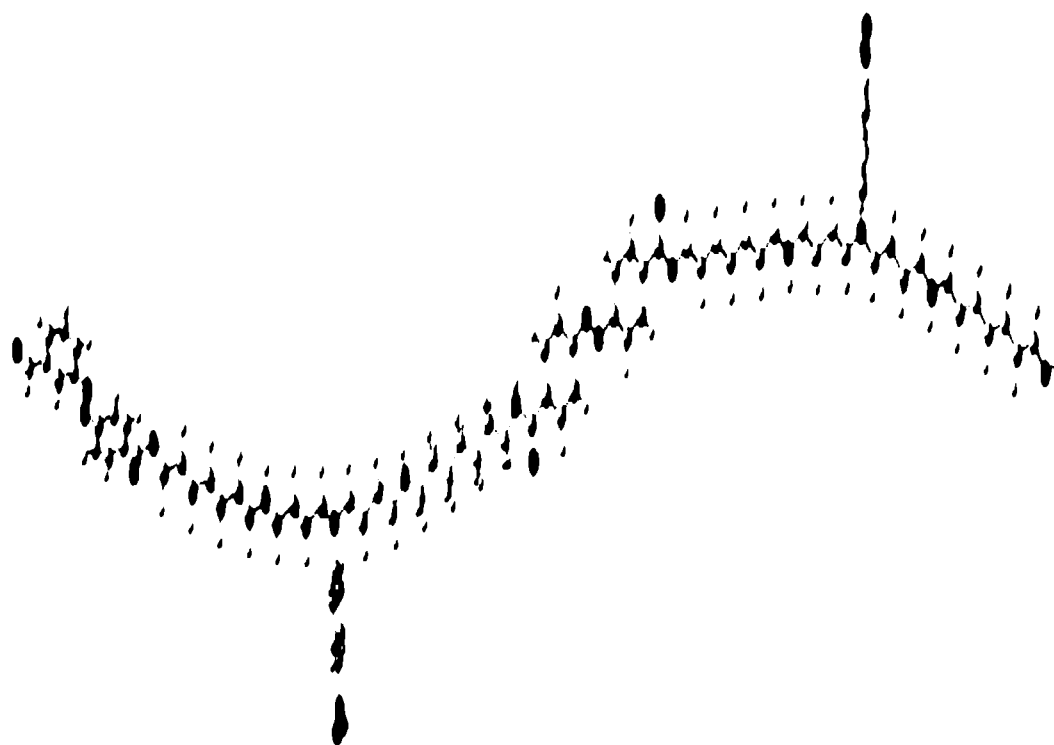


Figure 3II.6 Optimized structure of **Polhept** (Two repeating units)

3II.5. Hyperpolarizability β of polymers

The values of *static* Hyperpolarizability, β of polymers are given in **Table. 3II.3**. In the case of polymers designed from PNA derivatives with varying number of alkyl group, there is no visible odd-even oscillation in the ground state dipole moment and also in the value of first Hyperpolarizability β . While ground state dipole moment decreased randomly from **Polmeth** ($n=1$) to **polhex** ($n=7$), β increased from **Polmeth** to **Polhex**. Closely examining the value of β , it can be seen that for every polymer chain containing even numbered spacer groups there is a slight decrease in the β value. Hence, even though the odd-even oscillation is not much prominent in these types of polymeric systems, with respect to change in conformations of polymeric chains with odd or even numbered spacer groups, there is a small variation in β value by virtue of having odd or even numbered spacer groups. The results from the *dynamic* ZINDO calculation also agree with this observation.

Table 3II.3: HOMO-LUMO (ΔE) in eV, Ground-State Dipole Moment (μ_g) in debye, Linear Polarizability (α) in units of 10^{-23} esu, and First Hyperpolarizability β , in units of 10^{-30} esu for the chromophores (ab initio CPHF static property calculations)

Polymer	ΔE	μ_g	α	β (static)	β (Dynamic)
Polmeth	0.3514	10.8861	8.70	1.40	632.4687
Poleth	0.3540	12.1547	9.01	1.32	493.3536
Polprop	0.3533	10.1751	9.23	5.25	627.5431
Polbut	0.3570	9.0564	9.65	4.77	493.3536
Polpent	0.3575	5.5329	9.98	6.05	627.5431
Polhex	0.3558	8.1486	10.20	5.54	504.6026
Polhept	0.3534	7.0044	10.40	7.30	625.6215

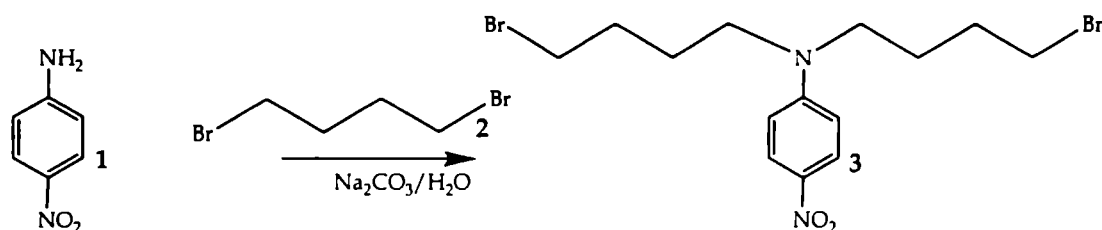
This can be explained as the addition effect of CH₂ spacer group in polymer chains. In spite of showing odd-even oscillations, polymer chains, have shown addition effect due to alkyl spacers in donor portion of the chain. These polymers the number of CH₂ groups were increased in both wings of the chain. Thus instead of an increment of one CH₂ in the polymer chains the increment was for two CH₂ spacer. This increases the push- pull mechanism of electron motion in polymer chain with increase in number of spacer and has shown an additive effect rather than an odd-even effect.

3II.6. Synthesis of monomers

3II.6.1. Synthesis of *N,N*-bis (4-bromobutyl) -4 -nitrobenzenamine⁹

Para-nitroaniline (1g, 0.00724 mol, s.d fine 99% pure) was dissolved in minimum amount of water. Sodium carbonate (1g, 0.00943 mol, s.d fine 98% pure) was added to this solution. The solution was kept under stirring on a magnetic stirrer. The temperature was kept at 98^o C. To this solution dibromobutane (4.23 ml, 0.0362 mol, Lancaster, 98% pure) was added drop wise from a pressure equalizing funnel and refluxed for 4 h under stirring. The reaction mixture was cooled and filtered. A brown solid was obtained. The precipitate was washed with water. Crystallized from ethanol. The crude product was purified by column chromatography using benzene and

benzene: ethyl acetate mixture. Bright yellow crystals of N,N-bis (4-bromobutyl) -4 -nitrobenzenamine was obtained. Reaction scheme is given in **Scheme 3II.1**.



Scheme 3II.1 Synthesis of N,N-bis (4-bromobutyl) -4 -nitrobenzenamine

Characterization

Yield= 85% M.P. =160⁰ C

Elemental analysis: Calculated for C₁₄H₂₀Br₂N₂O₂ - C, 41.20; H, 4.94; N, 6.86. Found - C, 41.10; H, 4.98; N, 6.85

Spectral properties

UVλ_{max} (solid) nm : 415

IR (KBr pellet) cm⁻¹: 1602 (C-N st) (1523 (NO₂ st as), 1476 (CH δ), 1441 (CH δ, of CH₂-Br), 1324 (NO₂ st ay) 1110 (C-Br st)

¹H NMR (300 MHz CDCl₃) δ : 8.10 (d, 2H, aromatic, H1), 6.45 (d, 2H, aromatic, H2), 3.42 (d, 4H, aliphatic H6), 3.40 (d, 4H, aliphatic H3), 2.07 (m, 4H aliphatic H5), 1.57 (m, 4H, aliphatic H4).

¹³C NMR (75 MHz CDCl₃) δ: 152 (aromatic, C1), 139 (C4), 125 (aliphatic C2), 110 (aliphatic C3), 78 (aliphatic C5), 41 (aliphatic C8), 36 (aliphatic C7), 28 (aliphatic C6).

Mass (m/e): 408 (molecular ion peak), 248 (M-2Br), 220 (O₂NC₆H₅N((CH₂)₃)₂).

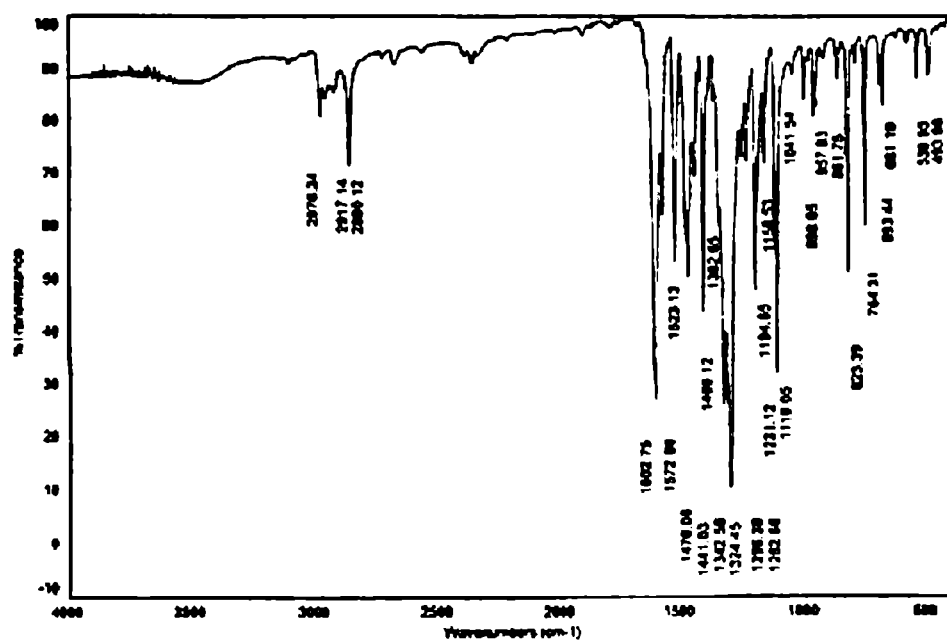


Figure 3II.7. IR spectrum of N,N-bis(4-bromobutyl)-4-nitrobenzenamine

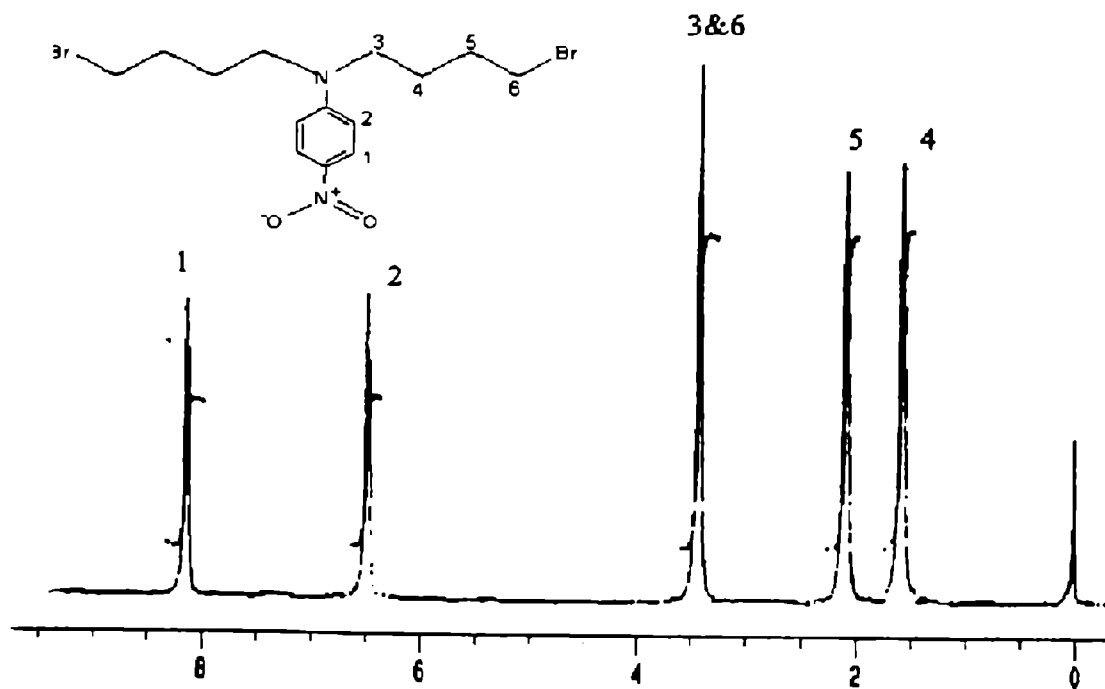


Figure 3II.8. ^1H NMR spectrum of N,N-bis(4-bromobutyl)-4-nitrobenzenamine

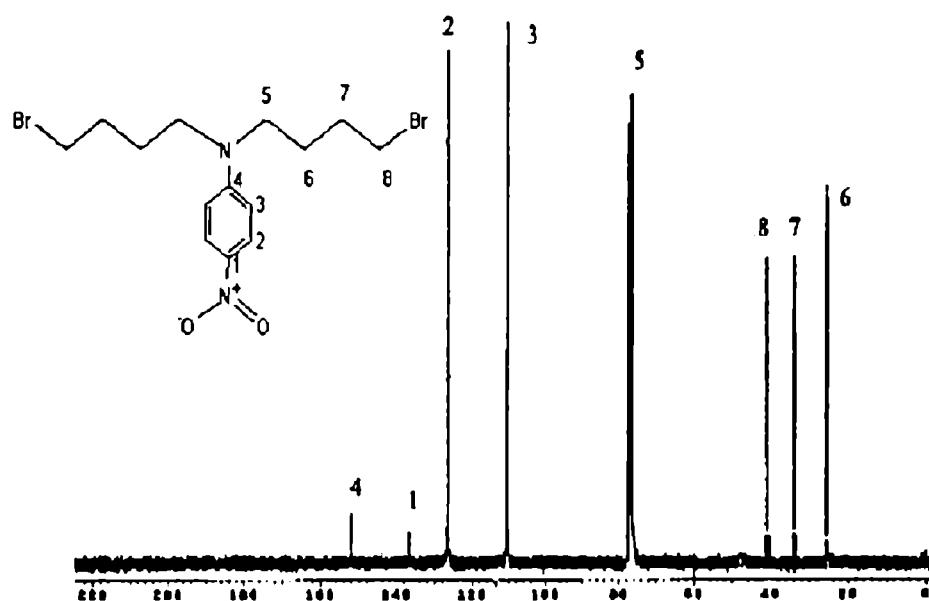


Figure 3II.9 ^{13}C NMR spectrum of N,N-bis (4-bromobutyl) -4 -nitrobenzenamine

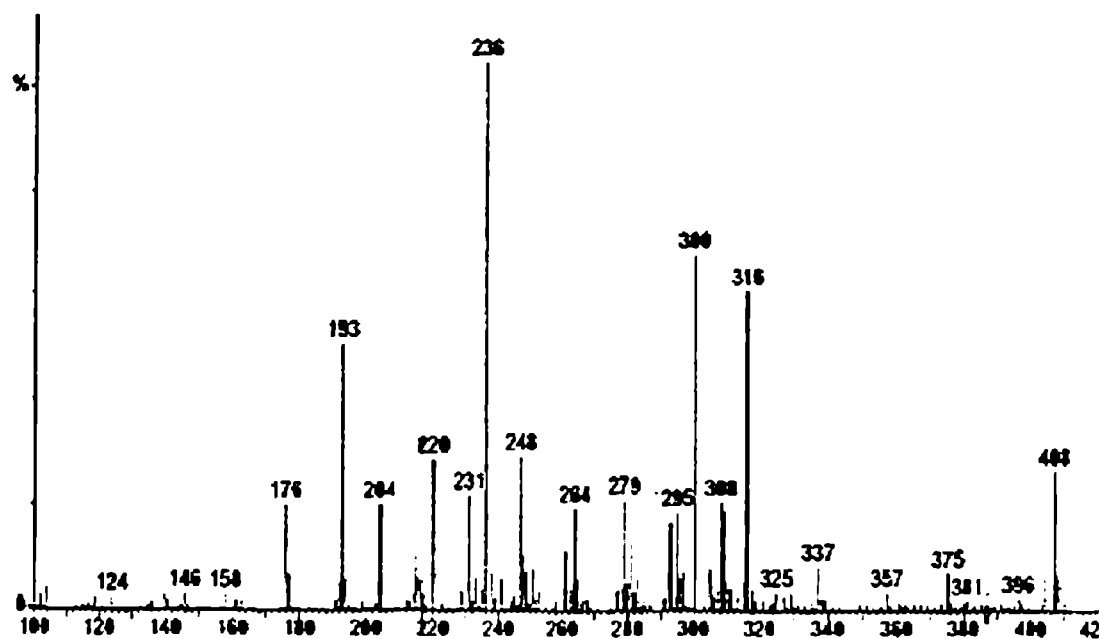


Figure 3II.10 ESI Mass spectrum of N,N-bis (4-bromobutyl) -4 -nitrobenzenamine

It is clear from the ^1H NMR and ^{13}C NMR spectra that disubstitution at NH_2 has occurred. If the product were a monosubstituted one, the aromatic region should have consisted of more number of peaks due to non equivalent protons in the aromatic

region. Also, there would have been a peak above $\delta 4.0$ due to unsubstituted H of NH_2 . 8 different carbons in ^{13}C NMR spectrum confirmed the disubstitution. If it were only monosubstitution, there would have been 10 different carbons in the ^{13}C NMR spectrum.

3II.6.2. Synthesis of *N,N*-bis (4-(2-aminoethylamino)butyl) -4 -nitrobenzenamine (eth)

N,N-bis (4-bromobutyl)-4-nitrobenzenamine (0.2g, 0.000491 mol) was dissolved in THF. To this solution 60% NaH dispersion in paraffin oil (0.0392g, 0.00491 mol, s. d. fine) in THF was added drop wise using a pressure equalizing funnel. The solution was kept at reflux. To this solution, 1, 2-diaminoethane (0.6 mL, 0.0098 mol, s. d. fine) in THF was added drop wise and was refluxed for 6 h. Extraction with ether gave a brown precipitate. The precipitate was washed with dil. HCl and distilled water. Dried and recrystallized from ether. General route of synthesis is given in Scheme 3II.2

Yield 80%. M.P = 160°C . Elemental analysis: Calculated for $\text{C}_{18}\text{H}_{34}\text{N}_6\text{O}_2$ - C, 58.99; H, 9.35; N, 22.93. Found - C, 59.01; H, 9.40; N, 22.81

Spectral properties

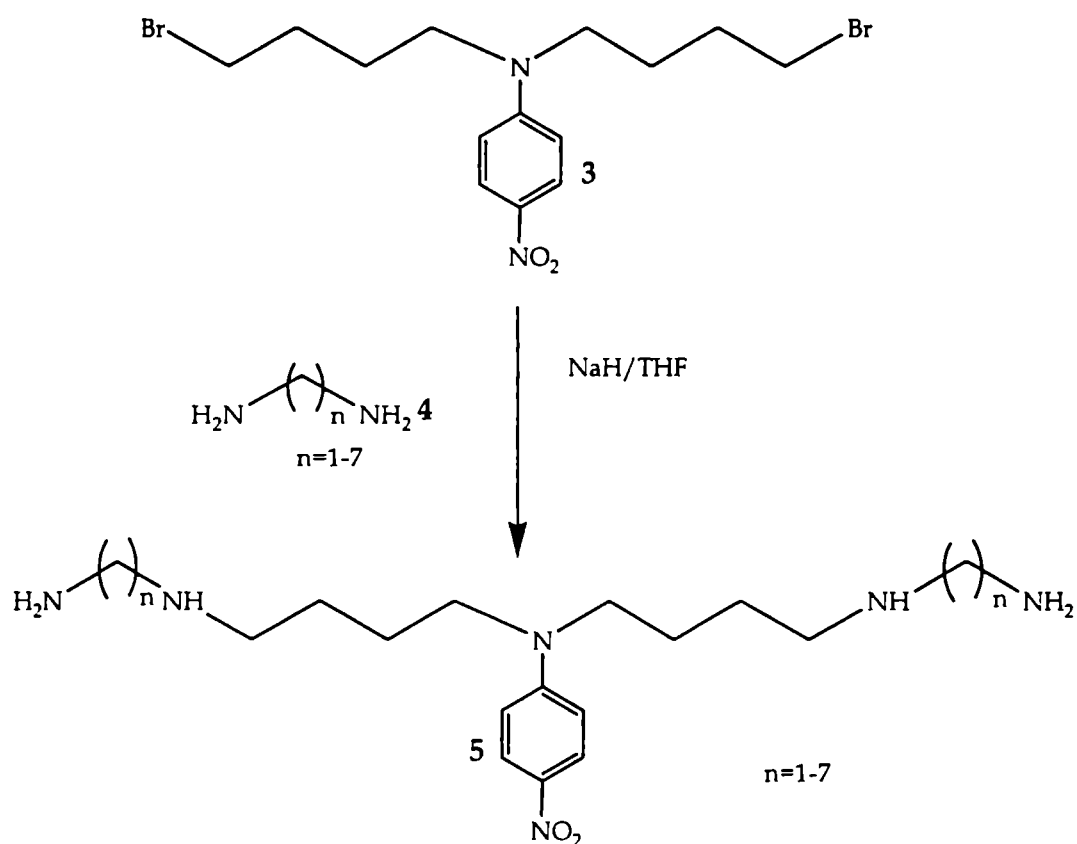
UV λ_{max} (solid) nm : 380

IR(KBr pellet) cm^{-1} : 3500 (NH st), 2900, 2880 (2 sharp hydrogen bonded bands of NH_2 st), 1600 ($\text{NH}_3^+\delta$, $\text{NH}^+\delta$), 1530 (NO_2 st as), 1480 ($\text{NH}_2^+\delta$), 1330 (NO_2 st ay)

^1H NMR (300 MHz CDCl_3) δ : 8.15 (d, 2H, aromatic hydrogen H1), 6.45 (d, 2H, aromatic hydrogen H2), 3.41 (t, 4H aliphatic, H3), 2.95 (m, 8H, aliphatic H8 & H9), 2.62(t, 4H, aliphatic H6), 2.15 (s, 4H, hydrogen of NH_2), 1.75 (s, 2H, hydrogen of NH), 1.25 (m, 8H, aliphatic H4 & H5)

^{13}C NMR (75 MHz CDCl_3) δ : 146.0 (1C, aromatic carbon, C4), 136.5 (aromatic carbon C1), 124.3 (2C, aromatic carbon, C2), 11.5 (2C, aromatic carbon, C3), 78.5, 77.3, 76.4 (1H, aliphatic carbons C5, C8 & C9), 48.5 (1C, aliphatic carbon C10), 31.1 (1C aliphatic carbon C7), 26.3(1C aliphatic, carbon C6)

Mass (m/e): 366 (molecular ion), 251 (M- $(\text{CH}_2)_4\text{NH}(\text{CH})_6\text{NH}_2$), 207 ($\text{O}_2\text{NC}_6\text{H}_5(\text{CH}_2)_4\text{NH}$)



Scheme 3II.2 Synthesis of N,N-bis (4-(2-aminoethylamino)butyl) -4 -nitrobenzenamine

3II.6.3. Synthesis of N,N-bis (4-(3-aminopropylamino) butyl) -4 -nitrobenzenamine (prop)

N,N-bis (4-bromobutyl) -4 -nitrobenzenamine (0.2g, 0.000491 mol) was dissolved in THF. To this solution 60% NaH dispersion in paraffin oil (0.04 g, 0.00491 mol) in THF was added drop wise using a pressure equalizing funnel. The solution was kept at reflux. To this solution 1, 3-diaminopropane (0.7 mL, 0.0098 mol, Lancaster, 98% pure) in THF was added drop wise and was refluxed for 6 h. Extraction with ether gave a brown precipitate. The precipitate was washed with dil. HCl and distilled water, dried and recrystallized from ether.

Yield 84%. M.P = 161.50^o C. Elemental analysis: Calculated for C₂₀H₃₈N₆O₂ - C, 60.88; H, 9.71; N, 21.30. Found - C, 60.40; H, 9.76; N, 21.10

Spectral properties

UVλ_{max} (solid) nm : 385

IR(KBr pellet) cm^{-1} : 3500 (NH st), 2950, 2875 (2 sharp hydrogen bonded bands of NH_2 st), 1625 ($\text{NH}_3^+\delta$, $\text{NH}^+\delta$), 1525 (NO_2 st as), 1450 ($\text{NH}_2^+\delta$), 1320 (NO_2 st ay)

^1H NMR (300 MHz CDCl_3) δ : 8.21 (d, 2H, aromatic hydrogen H1), 6.43 (d, 2H, aromatic hydrogen H2), 3.41 (t, 4H aliphatic, H3), 2.95 (m, 8H, aliphatic H8 & H9), 2.60(t, 4H, aliphatic H6), 2.31 (s, 4H, hydrogen of NH_2), 1.85 (s, 2H, hydrogen of NH), 1.43 (m, 4H, hydrogen between H8 & H9), 1.25 (m, 8H, aliphatic H4 & H5)

^{13}C NMR (75 MHz CDCl_3) δ : 146.1 (1C, aromatic carbon C4), 136.4(aromatic carbon C1), 124.2 (2C, aromatic carbon, C2), 11.3 (2C, aromatic carbon C3), 78.5, 77.3, 76.4 (1H, aliphatic carbons C5, C8 & C9), 48.5 (1C, aliphatic carbon C10), 31.4 (1C aliphatic carbon C7), 30.5 (2C, aliphatic carbon between 9 & 10) 26.3 (1C, aliphatic carbon C6)

Mass (m/e): 394 (molecular ion), 265 ($\text{M}^- (\text{CH}_2)_4 \text{NH}(\text{CH})_6\text{NH}_2$), 207 ($\text{O}_2\text{NC}_6\text{H}_5 (\text{CH}_2)_4 \text{NH}$)

3II.6.4. Synthesis of *N, N-bis (4-(4-aminobutylamino) butyl) -4 -nitrobenzenamine (but*

N,N-bis (4-bromobutyl) -4 -nitrobenzenamine (0.2g, 0.000491 mol) was dissolved in THF. To this solution 60% NaH dispersion in paraffin oil (0.0392g, 0.00491 mol) in THF was added drop wise using a pressure equalizing funnel. The solution was kept at reflux. To this solution, 1,4-diaminobutane (0.8 mL, 0.0098 mol, Lancaster, 98% pure) in THF was added drop wise and was refluxed for 6 h. Extraction with ether gave a brown precipitate. The precipitate was washed with dil. HCl and distilled water, dried and recrystallized from ether.

Yield 80%. M.P. = 159.91 $^\circ$ C. Elemental analysis: Calculated for $\text{C}_{22}\text{H}_{42}\text{N}_6\text{O}_2$ - C, 62.52; H, 10.02; N, 19.89. Found - C, 62.50; H, 10.0; N, 20.0

Spectral properties

UV λ_{max} (solid) nm : 387

IR(KBr pellet) cm^{-1} : 3500 (NH st), 2700 (2 sharp hydrogen bonded bands of NH_2 st), 1600 ($\text{NH}_3^+\delta$, $\text{NH}^+\delta$), 1527 (NO_2 st as), 1480 ($\text{NH}_2^+\delta$), 1330 (NO_2 st ay)

^1H NMR (300 MHz CDCl_3) δ : 8.19 (d, 2H, aromatic hydrogen H1), 6.51 (d, 2H, aromatic hydrogen H2), 3.41 (t, 4H aliphatic, H3), 2.95 (m, 8H, aliphatic H8 & H9), 2.60(t, 4H, aliphatic H6), 2.42 (s, 4H, hydrogen of NH_2), 2.01 (s, 2H, hydrogen of NH), 1.43 (m, 8H, hydrogens between H8 & H9), 1.30 (m, 8H, aliphatic H4 & H5)

^{13}C NMR (75 MHz CDCl_3) δ : 147.2 (1C, aromatic carbon C4), 136.7 (aromatic carbon C1), 1245.1 (2C, aromatic carbon, C2), 11.5 (2C, aromatic carbon C3), 78.5, 77.3, 76.4 (1H, aliphatic carbons C5, C8 & C9), 48.5 (1C, aliphatic carbon C10), 31.4 (1C aliphatic carbon C7), 30.7, 30.5. (2C, aliphatic carbons between 9 & 10) 26.3 (1C, aliphatic carbon C6)
 Mass (m/e): 422 (molecular ion), 278 (M- $(\text{CH}_2)_4 \text{NH}(\text{CH})_6\text{NH}_2$), 207 ($\text{O}_2\text{NC}_6\text{H}_5 (\text{CH}_2)_4 \text{NH}$)

3II.6.5. Synthesis of *N,N*-bis (4-(6-aminohexylamino) butyl) -4 -nitrobenzenamine(hex)

N,N-bis (4-bromobutyl) -4 -nitrobenzenamine (0.2g, 0.000491 mol) was dissolved in THF. To this solution 60% NaH dispersion in paraffin oil (0.0392g, 0.00491 mol) in THF was added drop wise using a pressure equalizing funnel. The solution was kept at reflux. To this solution 1, 6-diaminohexane (1.0 mL, 0.0098 mol, Lancaster, 98% pure) in THF was added drop wise and was refluxed for 6 h. Extraction with ether gave a brown precipitate. Washed with dil. HCl and distilled water. Dried and recrystallized from ether.

Yield 79%. M.P = 160°C . Elemental analysis: Calculated for $\text{C}_{26}\text{H}_{50}\text{N}_6\text{O}_2$ - C, 65.23; H, 10.53; N, 17.56. Found - C, 65.25; H, 10.50; N, 17.50

Spectral properties

UV λ_{max} (solid) nm : 389

IR(KBr pellet) cm^{-1} : 3500 (NH st), 2925, 2850 (2 sharp hydrogen bonded bands of NH_2 st), 1600 ($\text{NH}_3^+\delta$, $\text{NH}^+\delta$), 1525 (NO_2 st as), 1480 ($\text{NH}_2^+\delta$), 1330 (NO_2 st ay)

^1H NMR (300 MHz CDCl_3) δ : 8.20 (d, 2H, aromatic hydrogen H1), 6.45 (d, 2H, aromatic hydrogen H2), 3.41 (t, 4H aliphatic, H3), 2.95 (m, 8H, aliphatic H8 & H9), 2.60(t, 4H, aliphatic H6), 2.30 (s, 4H, hydrogen of NH_2), 1.87 (s, 2H, hydrogen of NH), 1.44 (m, 16H, hydrogen between H8 & H9), 1.28 (m, 8H, aliphatic H4 & H5)

^{13}C NMR (75 MHz CDCl_3) δ : 147.5 (1C, aromatic carbon C4), 136.9 (aromatic carbon C1), 124.1 (2C, aromatic carbon, C2), 11.9 (2C, aromatic carbon C3), 78.6, 77.0, 76.5 (1H, aliphatic carbons C5, C8 & C9), 48.9 (1C, aliphatic carbon C10), 31.2 (1C aliphatic carbon C7), 30.9, 30.3. 29.9 (2C, aliphatic carbons between 9 & 10), 26.3 (1C, aliphatic carbon C6)
 Mass (m/e): 478 (molecular ion), 307 (M- $(\text{CH}_2)_4 \text{NH}(\text{CH})_6\text{NH}_2$), 207 ($\text{O}_2\text{NC}_6\text{H}_5 (\text{CH}_2)_4 \text{NH}$)

3II.6.6. Synthesis of *N,N*-bis (4-(7-aminoheptylamino) butyl) -4 -nitrobenzenamine (hept)

N,N-bis (4-bromobutyl) -4 -nitrobenzenamine (0.2g, 0.000491 mol) was dissolved in THF. To this solution 60% NaH dispersion in paraffin oil (0.0392g, 0.00491 mol) in THF was added drop wise using a pressure equalizing funnel. The solution was kept at reflux. To this solution, 1,7-diaminoheptane (1.2 mL, 0.0098 mol, Lancaster, 98% pure) in THF was added drop wise and was refluxed for 6 h. Extraction with ether gave a brown precipitate. The precipitate was washed with dil. HCl and distilled water, dried and recrystallized from ether.

Yield 80%. M.P 161.24^o C. Elemental analysis: Calculated for C₂₃H₅₄N₆O₂ - C, 66.36; H, 10.74; N, 16.58. Found - C, 66.50; H, 10.60; N, 16.62

Spectral properties

UVλ_{max} (solid) nm : 392

IR(KBr pellet) cm⁻¹: 3500 (NH st), 2900, 2875(2 sharp hydrogen bonded bands of NH₂ st), 1625 (NH₃⁺δ, NH⁺δ), 1527 (NO₂ st as), 1480 (NH₂⁺δ), 1330 (NO₂ st ay)

¹H NMR (300 MHz CDCl₃) δ : 8.25 (d, 2H, aromatic hydrogen H1), 6.50 (d, 2H, aromatic hydrogen H2), 3.23 (t, 4H aliphatic, H3), 2.98 (m, 8H, aliphatic H8 & H9), 2.62(t, 4H, aliphatic H6), 2.51 (s, 4H, hydrogen of NH₂), 1.95 (s, 2H, hydrogen of NH), 1.45 (m, 20H, hydrogen between H8 & H9), 1.31 (m, 8H, aliphatic H4 & H5)

¹³C NMR (75 MHz CDCl₃) δ: 147.3 (1C, aromatic carbon C4), 136.5 (aromatic carbon C1), 124.1 (2C, aromatic carbon, C2), 11.9 (2C, aromatic carbon C3), 78.8, 78.2, 76.5 (1H, aliphatic carbons C5, C8 & C9), 49.1 (1C, aliphatic carbon C10), 31.5 (1C aliphatic carbon C7), 30.8, 30.5, 29.9, 29.5 (2C, aliphatic carbons between 9 & 10) 26.3 (1C, aliphatic carbon C6)

Mass (m/e): 506 (molecular ion peak), 321 M⁻ (CH₂)₄ NH(CH₂)₇NH₂), 207 (O₂NC₆H₅ (CH₂)₄NH)

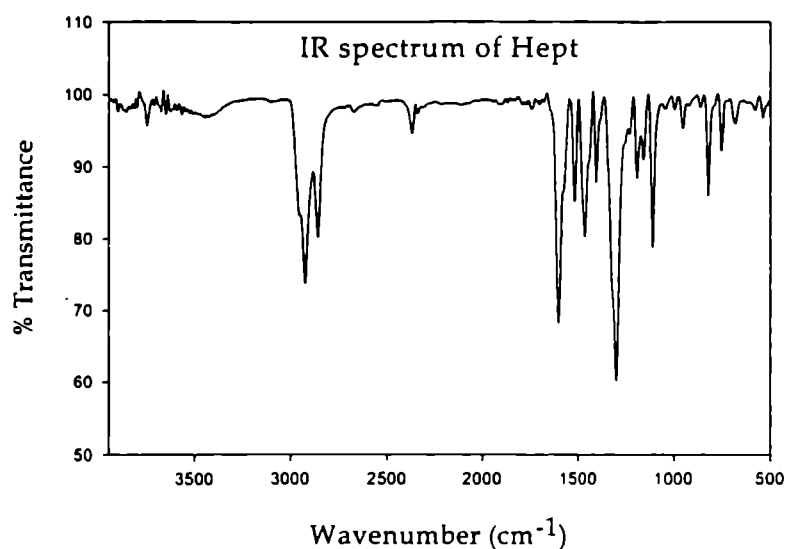
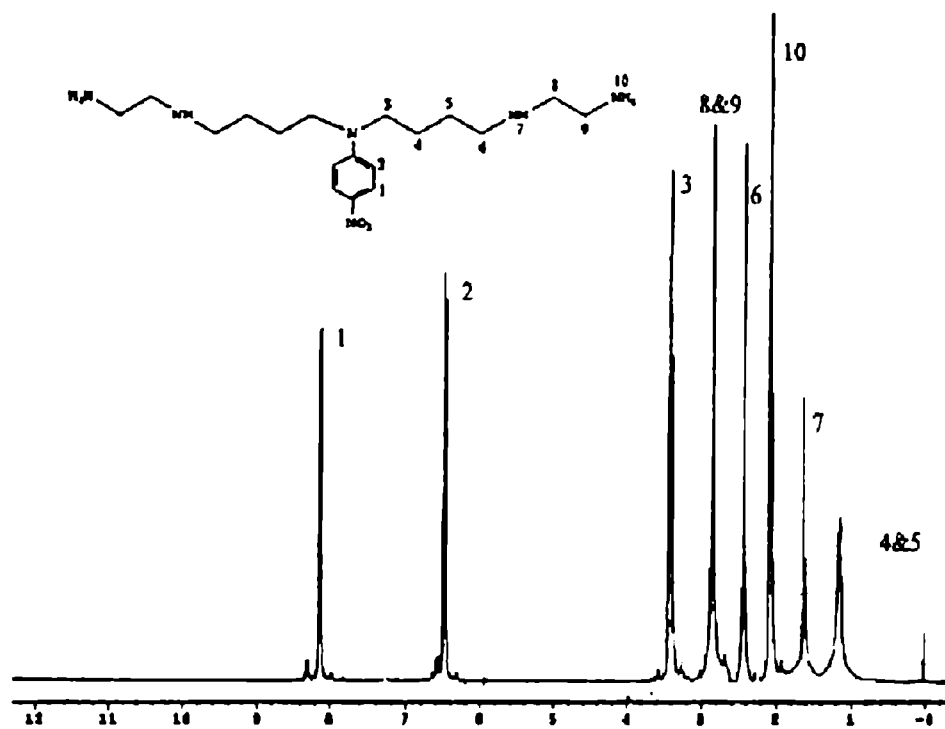
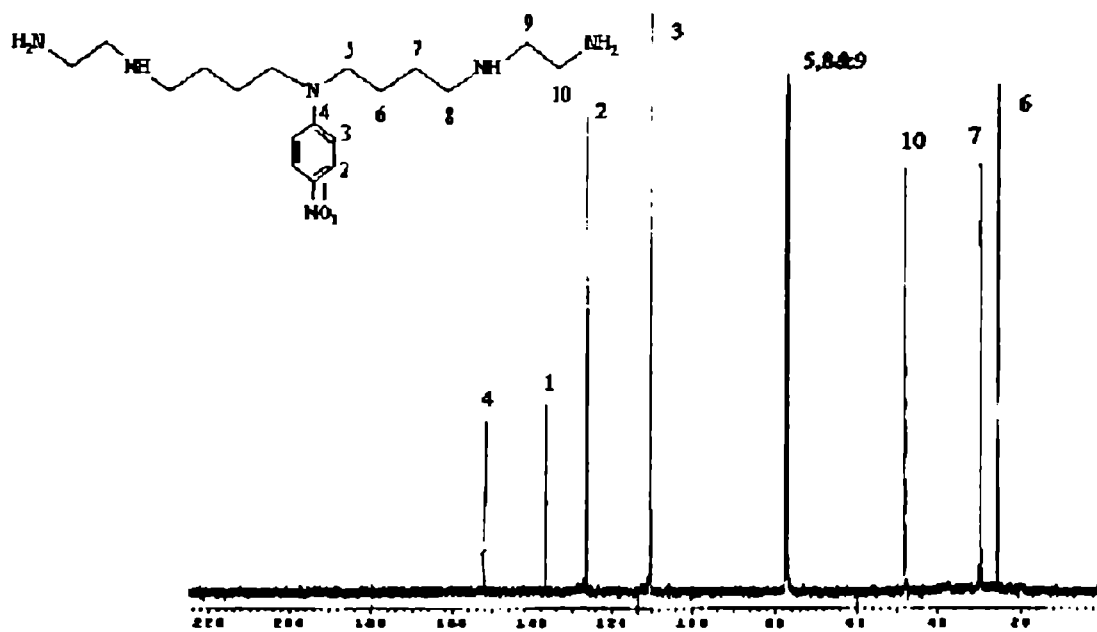


Figure 3II.11. IR spectrum of eth

UV-Vis spectra of these compounds vary with increase in number of CH_2 groups from to 380-392. IR spectra (Figure 3II.11) have shown a sharp distinct doublet at δ 2900-2700 due to primary amine (NH_2 st) usually the doublet appears at δ

3500-3300 cm^{-1} . A lower wave number indicated presence of hydrogen bond.

In ^1H NMR spectra (Figure 3II.12) the aromatic region has only two type of hydrogens. It is because of 1,4-disubstitution which confirmed the disubstitution of Br by diamines. Also the number of hydrogens with aliphatic region is also in good agreement with the disubstitution. ^{13}C NMR spectra (Figure 3II.13) gave additional proof for the proposed disubstituted structure. 4 carbons in the aromatic confirms the disubstitution. Number of aliphatic carbons are also in good agreement with the proposed disubstituted structure. Even numbered molecular ion (Figure 3II.14) confirms the presence of even number of nitrogen atom.

Figure 3II.12 ¹H NMR Spectrum of ethFigure 3II.13. ¹³C NMR Spectrum of eth

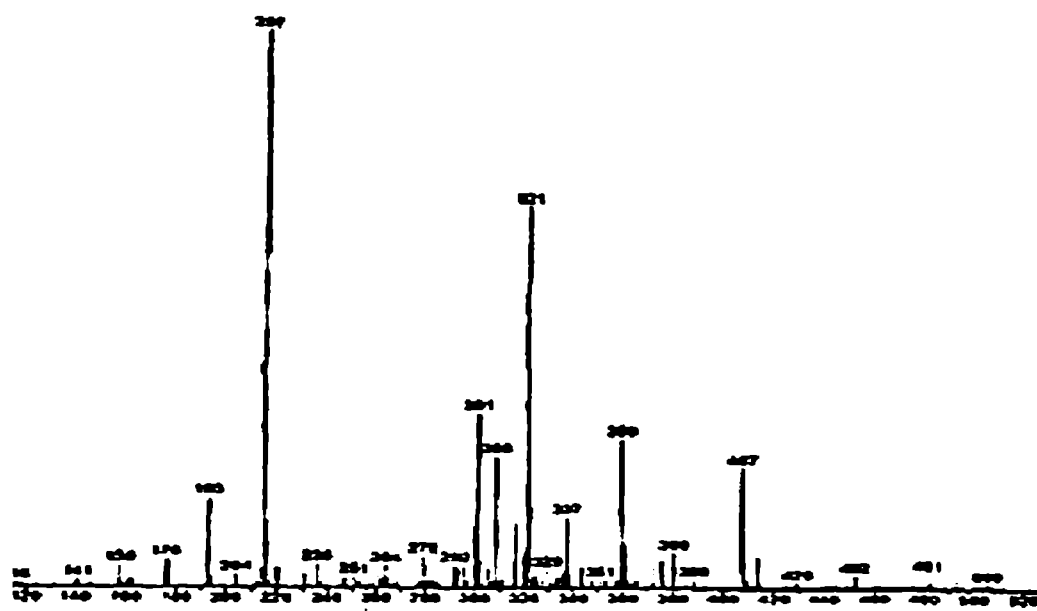
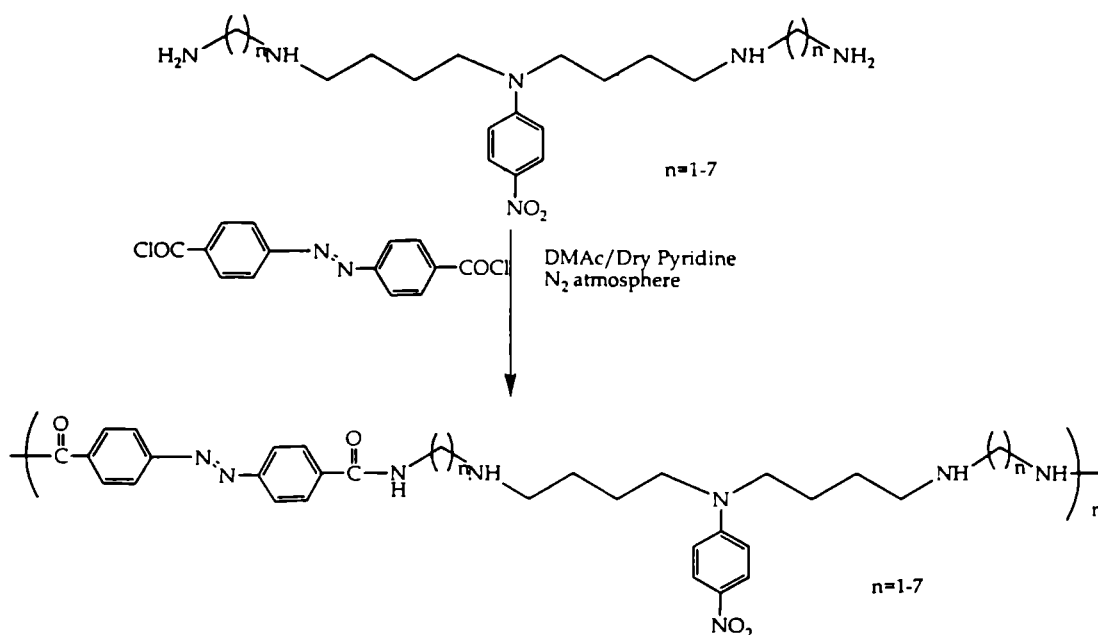


Figure 3II.14. ESI mass Spectrum of Hept

Synthesis of Polymers

All polymer syntheses were done in solution method at high temperatures. Appropriate PNA derivative was dissolved in extremely dry dimethylacetamide (HPLC grade, s.d.fine). To this solution, azobenzene-4, 4'-dicarbonyl chloride (AZCI) dissolved in DMAc was added. Few drops of extremely dry pyridine (99.99%, dry pyridine, reagent grade) were added as acid acceptor. The mixture was refluxed with stirring under nitrogen atmosphere for 24h. The product was precipitated from cold methanol and washed continuously with hot water, methanol and acetone. After filtration and drying in vacuum solid was obtained. Scheme 3II.3 gives the synthetic route of polymers.



Scheme 3II.3 Synthesis of polymers

Poleth: 4,4'-azobenzene dicarbonyl chloride (0.083 g, 0.167 mol) and (N,N-bis (4-(2-aminoethylamino) butyl) -4 -nitrobenzenamine (0.2 g, 0.0005464 mol) were reacted.

Yield: 87 %, $T_g = 110.76^\circ \text{C}$, Initial decomposition temperature (IDT) = 265°C

Polprop: 4,4'-azobenzene dicarbonyl chloride (0.083 g, 0.167 mol) and (N,N-bis (4-(3-aminopropylamino) butyl) -4 -nitrobenzenamine (0.22 g, 0.0005464 mol) were reacted.

Yield: 89 %, $T_g = 93.42^\circ \text{C}$ IDT = 300°C

Polbut: 4,4'-azobenzene dicarbonyl chloride (0.083 g, 0.167 mol) and (N,N-bis (4-(4-aminobutylamino) butyl) -4 -nitrobenzenamine (0.23 g, 0.0005464 mol) were reacted.

Yield: 86 % $T_g = 95.43$, IDT 308°C

Polhex: 4,4'-azobenzene dicarbonyl chloride (0.083 g, 0.167 mol) and (N,N-bis (4-(6-aminoethylamino) butyl) -4 -nitrobenzenamine (0.26 g, 0.0005464 mol) were reacted.

Yield: 84 %, $T_g = 99.35^\circ$, IDT = 320°C

Polhept 4,4'-azobenzene dicarbonyl chloride (0.083 g, 0.167 mol) and (N,N-bis (4-(7-aminoheptylamino) butyl) -4 -nitrobenzenamine (0.28 g, 0.0005464 mol) were reacted.

Yield: 86 % Tg = 121.36^o C, IDT 340^o C

Spectral properties are similar for these polymers.

Spectral properties of polymers

UVλ_{max} (solid) nm : 370-395

IR (KBr pellet) cm⁻¹ : 3426 (N-H st), 1684 (C=O, st, amide I), 1590 (C=O, st sy, amide II), 1522 (NO₂ st as), 1412 (N=N st), 1320 (NO₂ st ay), 1250 (N+N aromatic *trans*)

¹H NMR (300 MHz DMSO d₆)δ : 8.52 (d, aromatic hydrogen H12), 8.35 (d, aromatic hydrogen H11), 8.11 (d, aromatic hydrogen H1), 7.95 (s, hydrogen of NH H10), 6.89 (d, aromatic hydrogen H2), 4.53 (t, aliphatic hydrogen H3 & H9), 2.85 (t, aliphatic hydrogen H8), 2.54 (t, aliphatic hydrogen C6), 1.92 (s, hydrogen of NH H7), 1.34 (m, aliphatic hydrogens 4 & 5)

¹³C NMR (75 MHz DMSO d₆)δ: 167.6 (Carbonyl carbon C11), 156.1 (aromatic carbon C15), 155.7 (aromatic carbon C4), 137.9 (aromatic carbon C1), 136.4 (aromatic carbon C12), 127.8 (aromatic carbon C13), 123.1 (aromatic carbon CC14), 122.0 (aromatic carbon C2), 115.3 (aromatic carbon C3), 51.1 (aliphatic carbon C5), 49.3, 48.9 (aliphatic carbon C8 & C9), 40.2 (aliphatic carbon C10), 28.3 (aliphatic carbon C7), 25.4 (aliphatic carbon C6)

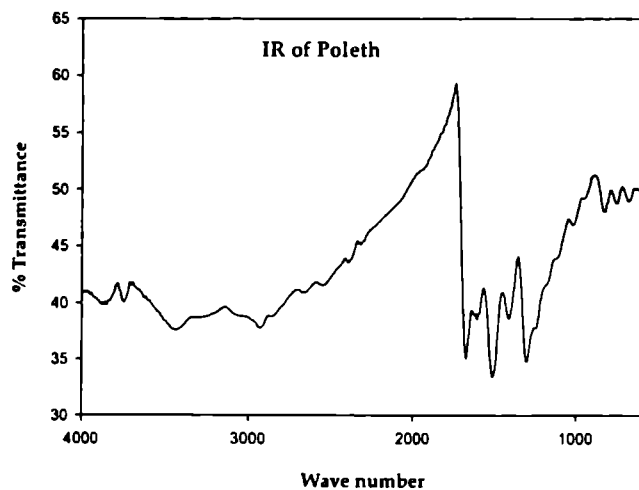
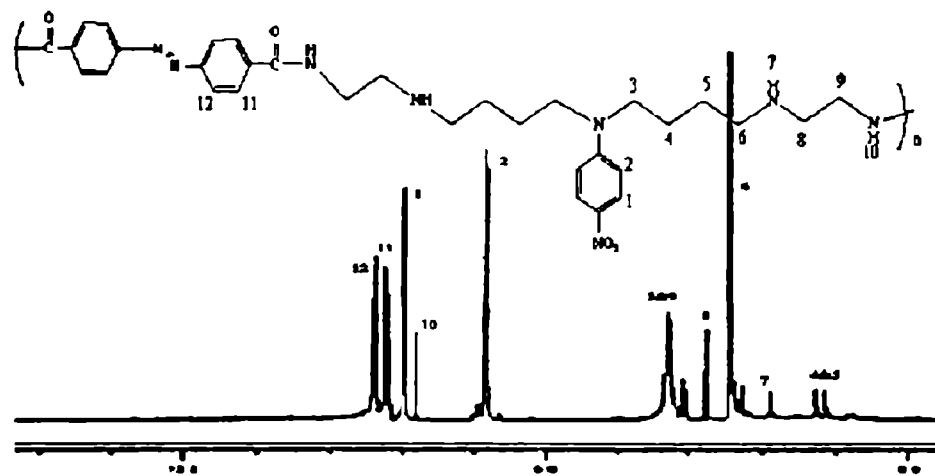
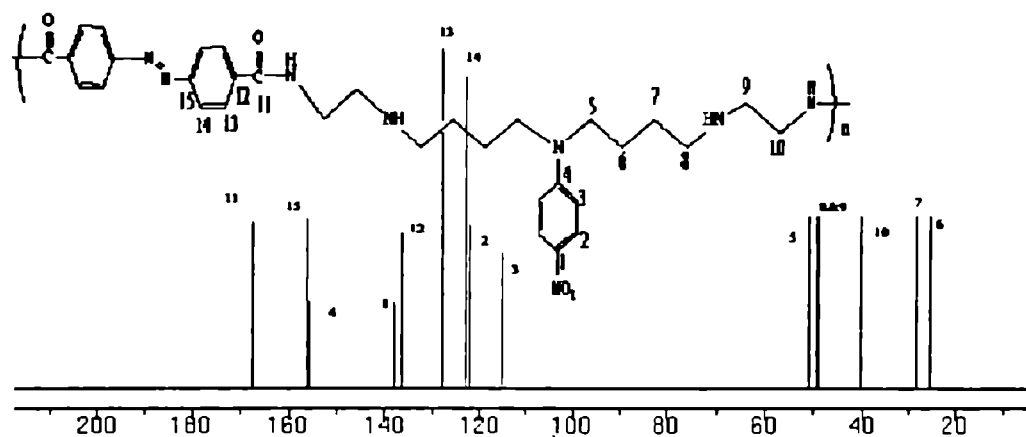


Figure 3II.15. IR of Poeth

From the Tg values and IDT, it can be seen that the polar order and stability increases with the increase in number of alkyl group in the polymer. The carbonyls peaks in IR (Figure 3II.15) spectra at 1684 cm⁻¹ (amide I) and 1590 cm⁻¹ (amide II) indicated the presence of amide formation. In ¹H NMR spectra (Figure 3II.16) four

different types of hydrogen in the aromatic region confirmed the polymerization. The

shift of NH proton to a lower field ($\delta 8$) also confirmed the amide formation during the polymerization. The presence of carbonyl carbon in ^{13}C NMR spectra (Figure 3II.17) confirmed the polymerization. Presence of 8 different carbon atoms in the aromatic region confirmed the proposed structure of polyamide. Mass spectrum of Polhept (Figure 3II.18) (molecular weight of one repeating unit = 771) has shown the molecular ion peak at 6939 confirmed the proposed structure composed of nine repeating units.

Figure 3II.16. ^1H NMR of PolheptFigure 3II.17. ^{13}C NMR of Polhept

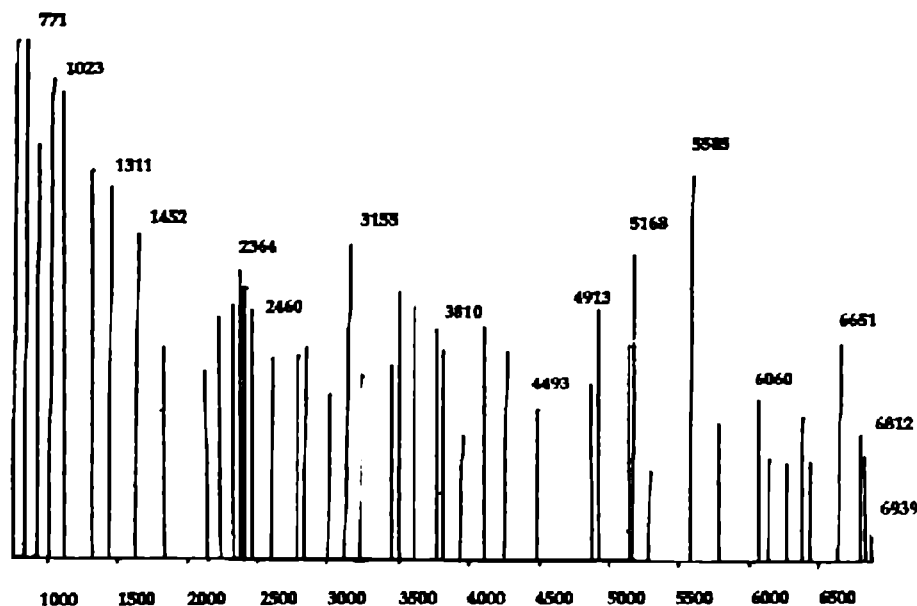


Figure 3II.18 Mass Spectrum of Polhept

3II.8. Evaluation of second harmonic generation efficiency

The NLO efficiencies of the polymers were determined with 2-methyl-4-nitroaniline as the standard using Kurtz and Perry method.¹⁰ Measurements were done by the powder method with a Quanta-Ray Nd-YAG laser from Spectra Physics (1064 nm, 10 ns, 365mJ/S) integrated over 20 pulse and an average of 10 pulse. The samples were ground and graded with standard sieves to the phase matchable size (100-150 μm) and loaded on cuvette with 1mm thickness. MNA samples used as standards were also powdered and sieved (100-150 μm) after drying under high vacuum.

Table 3II.4: SHG efficiency of polymers

Polymer	SHG efficiency*
Poleth	1.2371
Polprop	1.9689
Polbut	1.8091
Polhex	2.2856
Polhept	2.5346

*MAN SHG efficiency = 1

They were also mounted with the same thickness as the polymer samples. The laser beam was directed unfocused onto the sample kept at a 45° angle to the laser beam which provides the phase matchable situation; the emission was collected from the front face of the sample at 90° angle. The SHG signal at 532 nm was detected by Avantes 2048 spectrometer with CCD camera. The results are shown in Table 3II.4.

From experimental measurements of SHG of polymers, it can be seen that the systems have shown increase in SHG efficiency with respect to increase in the number of alkyl spacer groups rather than showing an odd-even oscillation. In the polymer systems, at room temperature the molecules rotate randomly. In such case a restricted rotation about only one single bond is practically impossible. The molecules are rotating with respect to more than one bond. Therefore, the dipolar ends will rotate between the bonds and the population consists of a mixture of eclipsed and staggered conformation of dipolar ends (even though the ground state consists of more stable staggered conformations about a single bond). Under this circumstance, the additive effect of alkyl spacer group play the major role and the SHG efficiency increases with respect to the number of alkyl groups.

3II.9. Conclusion

By this work, it can be concluded that the odd-even oscillation of first Hyperpolarizability, β has molecular origin. The conformation of dipolar ends governs the odd-even oscillations. From theory, it can be seen that in polymers, the odd-even oscillation is not visible due to the presence of more prominent additive effect of alkyl spacer groups. Experimental measurement of SHG of polymeric systems confirms this superiority of additive effect over odd-even oscillation of first Hyperpolarizability in the above explained polymer systems.

References

- (1) Hohenberg, P.; Kohn, W. *Phys. Rev.* **1964**, *136*, B864 .
- (2) W. Kohn and L. J. Sham, *Phys. Rev.* **1965**, *140*, A1133.
- (3) Salahub, D. R.; Zerner, M. C. *The Challenge of d and f Electrons*; ACS: Washington

D.C., 1989.

- (4) Parr, R. G.; Yang, W. *Density-functional theory of atoms and molecules*; Oxford Univ. Press: Oxford, 1989.
- (5) Gerratt, J.; Mills, I. M. *J. Chem. Phys.* **1968**, *49*, 1719.
- (6) Ridley, J.; Zerner, M. C. *Theor. Chim. Acta* **1973**, *32*, 111.
- (7) Bacon, D.; Zerner, M. C. *Theor. Chim. Acta* **1979**, *53*, 21.
- (8) Dewar, M. J. S.; Zoebisch, E. G.; Healy, E. F.; Stewart, J. J. P. *J. Am. Chem. Soc.* **1985**, *107*, 3902
- (9) Gilman & Blatt *Organic Synthesis Collective Volume I*, Second Edn. John Wiley and Sons, Inc: New York, 1980
- (10) Kurtz, S. K.; Perry, T. T. *J. Appl. Phys.* **1968**, *39*, 3798

CHIRAL POLYESTERS CONTAINING AZOMESOGENS FOR NONLINEAR OPTICS: ROLE OF STEREOCHEMISTRY OF CHIRAL MOLECULES

4.1. Introduction

Chiral materials can provide new approaches to second-order nonlinear optics. Chiral molecules possess no reflection symmetry and occur in two enantiomers that are mirror images of each other. Such molecules are essentially noncentrosymmetric with a nonvanishing electric-dipole allowed second-order response. Early research into second-order nonlinear optical materials for applications in frequency conversion and linear electro-optic modulation and conversion has focused mainly on polar molecules due to the requirement for non-centrosymmetric media.¹⁻³ Even in the absence of strong interaction between donor-acceptor groups, chiral medium is showing nonlinear response and persist even in macroscopic samples with high symmetry.^{4,5} In such macroscopic dimensional chiral structures, the poling of chromophores can be achieved through chemical synthesis, and there is no need for external poling.⁶⁻⁸ While nonlinear optical processes at chiral surfaces and in homopolymeric polar, chiral media have received considerable attention,⁹⁻¹³ here, the use of chirality in copolymeric polar bulk media for exploiting practical materials has been considered seriously. This chapter has focused on both molecular and supramolecular aspects.¹⁴⁻¹⁶ The molecular aspects that couple to the macroscopic response depend both on the details of the molecular structure and on the macroscopic symmetry group to which the molecule belongs. It is found that stereochemistry of polar chiral molecules plays a vital role in exploiting large second order nonlinear optical responses.

Azomesogen (azobenzene) polymers are receiving considerable attention because of their potential use in various photonic applications.¹⁷⁻¹⁹ These azomesogen polymers are usually NLO chromophore-functionalized polymer systems which are superior to the guest-host NLO polymer systems in many aspects such as stability,

homogeneity, processing etc. In dye-functionalized polymers, the dye molecules are covalently bonded to the polymer backbone; hence, two chemical entities, which are joined together on a molecular level, offer greater stability than the guest-host polymer system. The NLO dye molecules can be covalently attached to the linear chain of a polymer by simple chemical processes.²

This chapter discusses the development of polyesters having main chain chirality and at the same time with push-pull (donor-acceptor) azobenzene moiety. Due to the prevailing chirality of the main chain and the directional orientation (preferably *trans*) of the azobenzene group, the polyesters are organized with a Λ helical conformation in space. Polymers with such organized geometry are very interesting since they can supplement the directional order of donor-acceptor π electron system and the dipole units are tilted in one direction along the polymer axis which leads to high second harmonic generation efficiency.^{7, 20} This approach helps to satisfy both the essential and necessary conditions for a material to be NLO active (Second harmonic generation); achieving both spatial asymmetry and charge asymmetry without poling. Main chain chirality induces chemical poling. This results in the enhancement of SHG efficiency of the polyesters. Synthetic polymers, which are so far used for NLO applications, are poled with corona discharge at temperatures around their glass transition temperature. During poling, many polymers undergo darkening (loss of optical transparency) and once the external field is removed, they undergo relaxation to the unoriented state, thereby losing the NLO activity. In the present case, since poling is not used, such problems are avoided. The synthesis of chiral main-chain NLO polyesters were carried out by a facile way which involved the polycondensation of chiral units and donor-acceptor π -conjugated azomesogen chromophores.¹⁴⁻¹⁶ The work on this subject, focuses on molecular and supramolecular aspects of material design based on molecular stereochemistry. The approach to this problem parallels that which has been so successful in optimizing copolymeric systems. First consideration was the stereochemistry of the chiral molecules. Along with that the molecular features that might contribute to hyperpolarizability were examined. The focus was on polymer design, synthesis, and characterization. Finally, the supramolecular arrangements of

optimized copolymeric structures that best exploit the molecular response were synthesized. The systematic analysis of the relevant molecular quantities and the experimental measurement described here will result in technologically interesting chiral nonlinear optical materials.

4.2. Computational methods

4.2.1. Monomers

The monomers considered in this study are shown in **Figure 4.1** and **Figure 4.4**. All the monomers, diastereomers of chiral molecules and azomesogen chromophores, have been optimized using restricted B3LYP formalism in density functional theory (DFT) using 6-31+G(d,p) basis set available in the Gaussian algorithm.²¹⁻²⁵ Since DFT methods give more accurate results (with electron correlation) than semiempirical calculations, which are done at extremely minimal (Slater type orbitals) basis set; (electron correlation is only included implicitly by the parameters), and less computationally demanding for geometry optimization compared to *ab initio* methods (with high electron correlation), all the geometry optimizations of monomers have been done by DFT methods. The optimized geometries were used to compute the SCF MO energies. The *static* spectroscopic properties of monomers have been calculated using Coupled Perturbed Hartree-Fock (CPHF) method at RHF 6-31++G(d,p) level available in the Gaussian codes.²⁶ The *dynamic* spectroscopic properties have been calculated using the Zerner's INDO SOS method with sum over 82 states.²⁷ Theoretical value of optical rotation have been calculated using frequency dependent, *ab initio*, Hartree-Fock /6-31G(d) level of theory at a wavelength of 500 nm using Gaussian algorithm.^{28,29}

4.2.2. Polymers

All the polymer geometries (repeating units) were optimized using the AM1 parameterized Hamiltonian available in the Gaussian 03 set of codes.³⁰ The geometries obtained by AM1 calculations have been compared with geometries obtained using DFT based methods at B3LYP/6-31+(d,p) level for one of the polymers. Both the geometries have comparable bond lengths and bond angles. Compared to the small changes in bond length and bond angle, the computational demand for DFT method is much more for

polymers. Hence, geometry calculations are restricted to semiempirical level. The optimized geometries were used to compute the SCF MO energies. Because of the very high cost of computation in calculating the properties of polymers (repeating units) using polarized and diffused basis sets, *static* molecular properties of polymers have been limited to 6-31G(d) basis set level²⁶ The *dynamic* spectroscopic properties have been calculated using the Zerner's INDO-SOS method with sum over 82 states.²⁷

4.3. Designing of molecules

While designing the chiral monomers, the main consideration was about the stereochemistry of the chiral molecules. Stereochemistry is the study of the spatial arrangements of atoms in molecules and complexes. Stereoisomers (stereomers) are molecules with the same atoms and bond structure, but different three-dimensional arrangements of atoms. Stereoisomers can be divided into two categories of enantiomers (mirror images) and diastereomers (non-mirror images). Here 4 pairs of diastereomers are selected for the stereochemical study. The other chromophores were selected on the basis of push-pull donor-acceptor systems and the ability to form polycondensation polymers with the chiral monomers. Design of polymers, which are incorporated with the previously designed monomers, was based on chirality and push pull donor acceptor strength of the whole system, so as to obtain systems with more pronounced NLO activity (higher value of β).

4.3.1. Monomer design

4.3.1.1 Chiral molecules

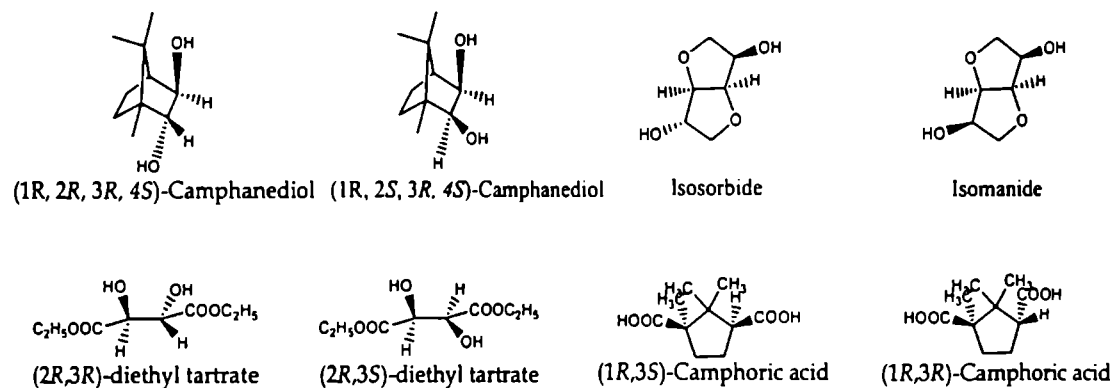


Figure 4.1. Chiral monomers

Four pairs of diastereomers have been selected as chiral monomers. All are dipolar chiral molecules. They are shown in **Figure 4.1**. In these diastereomers (1R, 2R, 3R, 4S) camphanediol [(exo-endo) camphanediol] and (1R, 2S, 3R, 4S) camphanediol [(exo-exo) camphanediol] are bicyclic bridged chiral molecules, 1,4:3,6-Dianhydro-D-sorbitol (isosorbide) and 1,4:3,6-Dianhydro-D-mannitol (isomanide) are bicyclic and heterocyclic chiral molecules. (2R, 3S) diethyl tartrate (*meso*) and (2R, 3R) diethyl tartrate are linear chiral molecules and (1R,3R) camphoric acid (exo-endo) and (1R, 3S) camphoric acid [(D(+)) or (exo -exo)] are monocyclic chiral molecules.

4.3.1.1.1. *Static and dynamic molecular property calculations*

4.3.1.1.1.a. Dipole moment

The values of static and dynamic dipole moments are given in **Table 4.1**.

Table 4.1: Dipole moment of monomers in units of debye

<i>Diastereomers</i>	μ_x	μ_y	μ_z	μ_g <i>Static</i>	μ_g <i>Dynamic</i>
Camphanediol (exo-endo)(I)	1.5521	-0.6410	-0.7251	1.8291	11.2647
Camphanediol (exo-exo)(II)	-1.2250	2.1911	-2.2158	3.3483	12.5664
Isosorbide(III)	-0.3463	1.6845	1.8690	2.5398	15.6456
Isomanide(IV)	-0.6458	1.8237	-0.6505	2.0410	11.7278
(2R,3S)Diethyl tartrate(V)	0	0	0	0	0
(2R,3R) Diethyl tartrate(VI)	-3.3116	-1.1773	-0.2488	3.5234	19.3087
Camphoric acid (exo-endo)(VII)	0.9096	2.2003	0.5283	2.4388	20.0525
Camphoric acid (exo-exo)(VIII)	0.4233	0.6856	1.8312	2.0007	16.6195

From the **Table 4.1** it is clear that one of the diastereomers in each pair has higher dipole moment than the other. This is due to the orientation of the dipolar group. The selection of diastereomers was based on this dipolar orientation. In one of the diastereomers, the dipoles are oriented to the same direction (eg. exo-exo), while in the other isomer the orientation is through opposite directions (eg. exo-endo). The

expectation was that the diastereomers with oppositely oriented dipoles have smaller value of dipole moment. But while analyzing the geometries, after optimization, it could be found that the ground state dipole moment, μ_g of isosorbide (oppositely oriented dipoles) is greater than that of isomanide. In camphoric acid pair, the same has been observed; exo-exo isomer has the higher value than exo-endo pair. This is because in isosorbide, isomanide and camphoric acid diastereomers, the optimized output geometry is more stable (twist and chair forms respectively), than the planar input geometry. In the optimized geometries of camphanediol and diethyl tartrate, diastereomers are not changed much. The blue arrow in **Figure 4.2**, shows the direction of net dipole moment in isosorbide and isomanide. In this twist conformation of isosorbide, the arrangement of oppositely oriented dipoles are in favor of the dipole moment through resultant direction, while in the twist conformation of isomanide, the orientation of dipoles is not in favor of the direction of resultant dipole moment vector (**Figure 4.2**). In the optimized chair conformation of camphoric acid (exo-exo), the same has been true, the orientations of dipoles are not favoring the resultant dipole moment vector. Hence, a decrease in the value of dipole moment for the (exo-exo) isomer of camphoric acid. In the other two pairs, the optimized geometry has not been changed much from the planar input geometry. Thus, for those pairs of diastereomers, the resultant dipole moments are as expected from the input geometry.

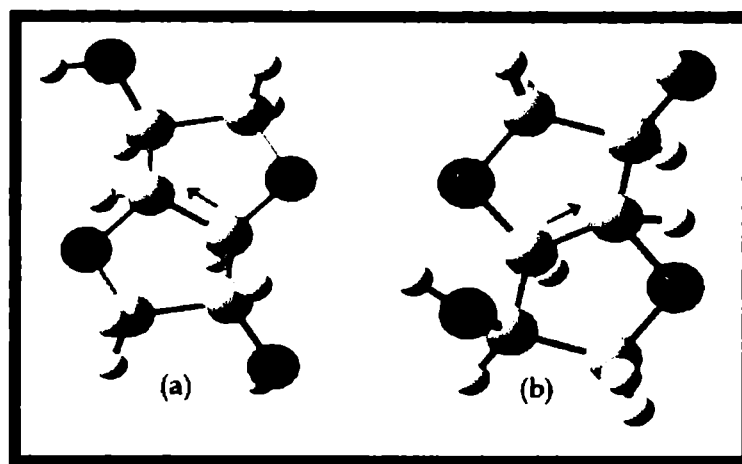


Figure 4.2. Optimized structure of Isosorbide (a) and Isomanide (b)

4.3.1.1.1.b. Polarizability (α)

Table 4.2 gives the polarizability values. For all pairs of diastereomers, the polarizability is almost equal. Thus, it can be concluded that polarizability does not depend much on the dipolar orientation.

Table 4.2: Polarizability α of diastereomers

Diastereomers	α_{xx}	α_{yy}	α_{zz}	α (au)	α_{tot}^* (esu) $\$$ $\times 10^{-23}$	α_{tot}^{**} (esu) $\$$ $\times 10^{-23}$
Camphanediol (exo-endo)	107.2152	112.8685	109.4957	109.8598	1.6279	38.9
Camphanediol (exo-exo)	109.7963	110.0699	109.9183	109.9282	1.6289	38.9
Isosorbide	87.1126	66.6235	71.0871	74.9411	1.1105	38.3
Isomanide	84.8408	68.1332	70.6659	74.5466	1.1046	37.3
(2R,3S)Diethyl tartrate	127.7344	107.5076	85.3803	106.8741	1.5837	97.4
(2R,3R) Diethyl tartrate	98.2089	106.3238	114.7136	106.4155	1.5769	83.3
Camphoric acid(exo-endo)	118.3098	108.8939	114.6224	113.9420	1.6884	94.0
Camphoric acid(exo-exo)	121.6146	107.3292	113.8367	114.2602	1.6931	102.0

$\$ \alpha$ (esu) = $0.148185 \times 10^{-24} \alpha$ (au) *Static values, ** Dynamic values

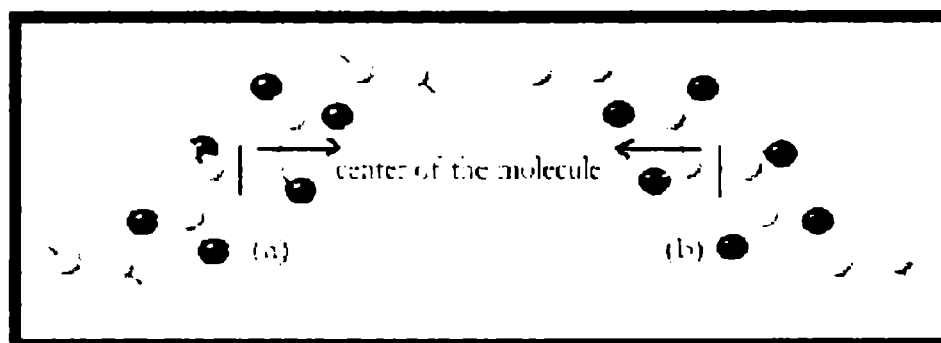
4.3.1.1.1.c. Hyperpolarizability (β)

Figure 4.3. Diastereomers of diethyl tartrate, (2R, 3R) (a) and (2R,3S) (b)

Ab initio calculations using Hartree-Fock CPHF level is used to predict the second order NLO response. From the results of *static* CPHF calculations in Table 4.3, it can be observed that, in spite of the similar values of α obtained for the diastereomers,

the β values have been found to vary considerably according to the stereochemistry of the diastereomer. For (2R, 3S) Diethyl tartrate β value is zero while (2R, 3R) diethyl tartrate has comparatively good β value. This is because of the presence of reflection center (center of symmetry) in the former (Figure 4.3) In the case of isomanide and isosorbide, β value is almost doubled in isomanide compared to isosorbide. The variation in β value with respect to the stereochemistry of camphanediol and camphoric acid diastereomers are not highly pronounced. But in perspective of designing the chiral molecule with good β values, (2S, 3R) -camphanediol (exo-exo) can be selected as a promising candidate.

Table 4.3: HOMO-LUMO Gap (ΔE) in eV, Ground-State Dipole Moment (μ_g) in debye, Linear Polarizability (α) in units of 10^{-23} esu, and First Hyperpolarizability (β) in units of 10^{-30} esu for the diastereomers (ab initio CPHF static property calculations)

Diastereomers	ΔE	μ_g	α	β_{vec}
Camphanediol (exo-endo)	0.4392	1.8291	1.6280	1.0793
Camphanediol (exo-exo)	0.4334	3.3484	1.6290	1.2765
Isosorbide	0.4572	2.5398	1.1105	0.3370
Isomanide	0.4625	2.0411	1.1047	0.6936
(2R,3S)Diethyl tartrate	0.4803	0	1.5837	0
(2R,3R) Diethyl tartrate	0.4741	3.5234	1.5769	0.4938
Camphoric acid (exo-endo)	0.4729	2.4388	1.6885	0.3102
Camphoric acid (exo-exo)	0.4703	2.0007	1.6932	0.3527

According to donor-acceptor concept, the major contribution to β is due to charge transfer. Thus, one will get higher β with the factors that enhance the charge transfer. The HOMO-LUMO gap in the molecular orbital picture plays a vital role in the charge transfer.³⁰ If the gap is small, it is very easy for the charge transfer to occur. Thus the HOMO largely dictates the source of charge transfer and the details of the molecular LUMO govern the acceptor portion of the excitation. One can tailor the asymmetry of the electron density by tuning the energetics (HF-SCF) of the molecule. The HOMO-LUMO gap (ΔE) of the molecules are given in Tables 4.3. There is not much difference in

the HOMO-LUMO gap of each pairs of diastereomers with respect to their stereochemistry. Also, while examining the values of β with respect to corresponding μ values of the respective diastereomer, especially for isosorbide-isomanide pair and camphoric acid pair, it can be seen that the HOMO-LUMO, charge transfer model is inadequate for explaining the difference in β value of chiral molecules in the perspective of stereochemistry.

Dynamic (frequency dependent) Sum Over States (SOS) calculations will give a more transparent idea about the relationship between the first hyperpolarizability and stereochemistry of different diastereomers. Since CPHF method is a frequency independent model, only static fields are considered. But in the SOS method frequency equal to that of Nd:YAG laser (1024 nm, 1.67 eV) has been applied as the field.

Table 4.4: Oscillator strength (f), Optical Gap (δE) in eV, Ground-State Dipole Moment (μ_g) in debye, Difference in dipole moment between ground state and excited state ($\Delta\mu$), Linear Polarizability (α) in units of 10^{-23} esu, and First Hyperpolarizability (β) in units of 10^{-30} esu for the diastereomers (ZINDO-SOS dynamic property calculations)

Diastereomers	f	δE	$\Delta\mu$	μ_g	α	β_{vec}
Camphanediol (exoendo)	0.0173	13.5077	15.2618	11.2648	38.9	1.5634
Camphanediol (exoexo)	0.0292	13.3466	32.7791	12.5664	38.9	2.0995
Isosorbide	0.0343	10.9403	11.1665	15.6456	38.3	0.3135
Isomanide	0.0360	11.0660	23.7540	11.7278	37.3	3.2238
(2R,3S) Diethyltartrate	1.0042	8.7724	0	0	97.4	0
(2R,3R) Diethyltartrate	0.5121	8.6951	5.7691	19.3088	83.3	6.7476
Camphoricacid (exo,endo)	0.4561	8.9083	1.2877	20.0526	94.0	1.4652
Camphoricacid (exo-exo)	0.6857	8.8184	6.7321	16.6195	100.2	5.7858

Table 4.4. reports the two-level parameters such as, magnitude of oscillator strength (f), the optical gap (δE), the difference between the dipole moments of ground-state and the excited state ($\Delta\mu$), the ground-state dipole moment (μ_g), the linear polarizability (α), and the first hyperpolarizability (β) of the *dynamic* SOS calculation.

Even in the presence of applied field ($1.67\text{eV} = 1024\text{nm}$, Nd:YAG frequency), the trend is same as that of *static* calculation. In the case of isosorbide and isomanide, the difference in β value is more prominent, in one order of magnitude. As a chiral molecule *exo-exo*-camphanediol has shown good second order response while applying the frequency dependent experimental conditions also. It can be seen that *exo-exo*-camphoric acid is the best among them under the experimental conditions. Consider the first pair, camphanediol diastereomers. Oscillator strength is low and optical gap is higher for *exo-endo* diastereomer. Both the factors decrease the β value of *exo-endo* isomer. Also, the $\Delta\mu$ value is higher in *exo-exo* isomer (almost doubled). Thus in camphanediol pair, the *exo-exo* isomer has a higher value of β . In diethyl tartrate pair, for the (2R, 3S) diastereomer the β value is zero, i.e. (2R, 3S) diethyl tartrate is not active towards second order NLO properties. This is because of the center of symmetry present in the molecule (center of inversion). The ground state dipole moment and the change in dipole moment are also zero because of this center of inversion. But it has a comparatively high α value compared to all other isomers. Since there is no inversion center in (2R, 3R) diethyl tartrate, and has comparatively large change in dipole moment and oscillator strength, it has got the highest β value. Hence, it can be taken as a potential chiral molecule for second order NLO applications.

While examining the isosorbide-isomanide pair and camphoric acid pair, it can be seen that the β values vary drastically with respect to the stereochemistry of the diastereomer. In isomanide, it is increased in one order of magnitude. Even though the ground state dipole moment μ , is large for isosorbide, and *exo-endo* camphoric acid, the change in dipole moment $\Delta\mu$, is higher for isomanide and *exo-exo* camphoric acid, which mainly determines the value of β . In fact, the optical gap for isomanide is slightly larger than that of isosorbide, but the large difference in $\Delta\mu$ governs β .

To get a clear picture about the dependence of stereochemistry on the β value, all the determining parameters of β , (f , δE , $\Delta\mu$), have been observed thoroughly. It can be seen that for the diastereomer with large $\Delta\mu$ value, the β is also large. According to

Lalama *et al*³¹ the dipole moment difference $\Delta\mu$, between the ground and excited state is the major contributing factor in determining the value of β vector. Also it is stated that, if in $\Delta\mu$, any of the components are absent (eg, y or z component), the contribution to β vector from those directions is also negligible and the major contribution of β is obtained from the charge transfer direction.

Table 4.5: Dipole moment difference between the ground state and excited state in units of debye

Diastereomer	$\Delta\mu_x$	$\Delta\mu_y$	$\Delta\mu_z$	$\Delta\mu$	β_{vec}
Camphanediol (exo-endo)	-0.5175	-12.8195	-8.2654	15.2618	1.5634
Camphanediol (exo-exo)	22.7667	-22.6128	-6.6937	32.7791	2.0995
Isosorbide	-3.9535	-1.5985	12.1870	12.9115	0.3135
Isomanide	22.4625	6.9725	3.3271	23.7540	3.2238
(2R,3S)Diethyl tartrate	0	0	0	0	0
(2R,3R) Diethyl tartrate	-5.3848	-0.5686	-1.9909	5.7691	6.7476
Camphoric acid (exo-endo)	-0.5645	0.7021	-0.9201	1.2877	1.4652
Camphoric acid (exo-exo)	6.5060	0.8467	1.5086	6.7321	5.7858

The value of components of $\Delta\mu$ are summarized in Table 4.5. It is very clear that the major contribution of the $\Delta\mu$ is coming from the z direction and it is the direction of charge transfer in all the optimized geometries. Also, it is well pronounced that the $\Delta\mu$ and $\Delta\mu_x$ values are also higher in the diastereomers with higher value of β . Thus the β has a strong dependence on stereochemistry of the chiral molecule through the dipole moment difference between the ground state and the excited state, $\Delta\mu$ and the direction of its major component (μ_x , μ_y , μ_z). Thus, in designing the chiral molecules the stereochemistry is very important.

4.3.1.1.1.d. Chiral component

Since microscopic first hyperpolarizability, β is a 3rd rank tensor, it has 27 tensor components. But in the general case of a molecule with no symmetry, these 27 elements are reduced to 10 according to Kleinman symmetry for second harmonic generation $\beta(2\omega; \omega, \omega)$. Due to independent interchange of Cartesian coordinates, $\beta_{ijk} = \beta_{ikj}$. These

irreducible 10 tensor components are β_{xxx} , β_{xyx} , β_{xyy} , β_{yyx} , β_{xxz} , β_{xyz} , β_{yyz} , β_{xzz} , β_{yzz} , and β_{zzz} .^{1,32-35} By taking the tensor product of these 10 tensor components, orientationally averaged hyperpolarizabilities can be calculated from the equations given below.³⁶

$$\beta_{\text{vec}}(-2\omega; \omega, \omega) = \sqrt{\beta_x^2 + \beta_y^2 + \beta_z^2} \quad 4.1$$

where

$$\beta_i = \sum_{j=x,y,z} \frac{\beta_{ij} + \beta_{ji} + \beta_{jji}}{3} \quad ; \quad i = x, y, z \quad 4.2$$

In an electric dipole approximation, the tensor component β_{xyz} is the chiral component of the medium and all other nine tensor components are achiral. Because of the property of symmetric tensor product basis set elements, the value of β_{xyz} has become zero in the tensor product. But the chiral component β_{xyz} becomes non-zero and contribute a major portion to the macroscopic (3-D) second order polarizability tensor, χ_{XYZ} .^{8, 11,12, 37,38} Thus while designing the chiral molecule with high β value, the β_{xyz} component becomes important in macroscopic perception. The molecule with large chiral (β_{xyz}) component should give high value for macroscopic second harmonic generation. The molecules which are more symmetric (less chiral) will have small values of the chiral component β_{xyz} .

From Table 4.6, it is very clear that chiral component β_{xyz} is substantially higher for most of the chiral molecules. Also, it is very much dependent on the stereochemistry of the chiral molecule. Exo-exo camphanediol, isomanide, (2R, 3R) diethyl tartrate, exo-exo camphoric acid is the potential chiral candidate in each pair with respect to the chiral component β_{xyz} and stereochemistry. And hence, these four diastereomers will give a major chiral contribution to the macroscopic SHG, χ_{XYZ} . Thus, these are used as promising chiral molecules for constructing chiral media or incorporating in to a polymer chain to get a chiral medium with pronounced SHG

As a crude approximation, the stereochemistry and chirality can be related to each other through the optical rotation $[\alpha]_D$. Optical rotation is a property, by virtue of which the polarized light rotates its plane. Chirality is the necessary and sufficient

condition for optical rotation and the stereochemistry of the molecule determines the amount and the direction of rotation. From Table 4.6, it is clear that, the value of chiral component always agrees with the optical rotation of the diastereomer. The specific rotation of diastereomeric pair, isomanide and isosorbide are available in literature. It is $+45^\circ$ for isosorbide and $+89^\circ$ for isomanide. So there is not much surprise in the large value of chiral component obtained for isomanide compared to isosorbide. Circular dichorism will give a vivid picture about the chirality and chirality parameter, which is beyond the scope of this work due to the non-availability of the CD spectrometer. It can be concluded that, the stereochemistry of the small molecule and the conformation of its macroscopic forms are very important in determining the chiral component and thus macroscopic SHG.

Table 4.6: First hyperpolarizabilities of diastereomers β (Static) in units of au

β Tensors	Camphane diol (exo-endo)	Camphane- diol (exo-exo)	Iso sorbide	Iso manide	Diethyl- tartrate (2R,3S)	Diethyl- tartrate (2R,3R)	Camphoric- acid (exo-endo)	Camphoric- acid (exo-exo)
β_{xxx}	-3.5622	14.6356	-6.423	38.0264	0	39.2226	27.9278	43.9083
β_{xxy}	39.8690	28.6849	6.5766	-20.1099	0	6.8411	-3.8573	9.5022
β_{xyy}	-3.6198	1.3465	-6.4437	-0.2094	0	-11.2329	-21.5895	-32.9704
β_{yyy}	58.5435	38.0116	18.1242	-34.0895	0	4.7007	21.7921	-26.1922
β_{xxz}	11.4376	-15.7655	6.5635	18.9935	0	-25.6202	6.4420	23.4927
β_{xyz}	-1.890	-5.7218	-1.3220	-7.4538	0	1.5503	15.7178	-19.9288
β_{yyz}	-6.7104	-43.1634	2.5726	-4.7536	0	-12.0035	20.1586	-5.2109
β_{zzz}	7.4152	0.0678	2.7583	2.1477	0	18.8723	-13.5133	-23.3222
β_{yzz}	26.2109	8.6866	0.1008	-7.1146	0	13.7831	-9.1267	-20.0598
β_{zzz}	4.0111	-67.1371	19.2154	18.7612	0	16.8920	7.4571	-5.5366
β_x	0.2332	16.0500	-10.108	39.9647	0	46.8620	-7.1751	-12.3844
β_y	124.6233	75.3831	24.8016	-61.314	0	25.3249	8.8082	-36.7498
β_z	8.7384	-126.066	28.3516	33.0011	0	-20.7317	34.0577	12.7453
β_{dec}^*	124.9295	147.7594	39.0015	80.2849	0	57.1594	35.9025	40.8211
β_{rec}^{**}	1.0793	1.2765	0.3369	0.6936	0	0.4938	0.3102	0.3525
$[\alpha]_D^\#$	-35.70	-42.48	+49.31	+80.69	0	+150.97	+46.47	+29.27

* β_{rec} in atomic units, ** $\beta_{dec} \times 10^{-30}$ in esu, β (10^{-32} esu) = 0.863916β (au), # calculated specific rotation

4.3.1.2. Azomesogen chromophores

The azomesogen chromophores have been designed on the basis of donor-acceptor capacity and the ability to form polymers with the previously designed chiral molecules by easy polycondensation method. They are, bis(4-hydroxyphenylazo)-2,2'-dinitrodiphenylmethane (BHDM) and azobenzene-4,4'-dicarbonyl chloride (AZCI) (Figure 4.4.) The former is Λ shaped chromophore with donor-acceptor push-pull groups. The later is a diacid chloride; the most suitable reactant for an -OH group condensation. The results are given in Table 4.7

Table 4.7: Static values of HOMO-LUMO gap (ΔE), dipole moment μ , in debye polarizability (α) in units of $\alpha 10^{-23}$ esu, Chiral component of Hyperpolarizability β_{xyz} in au, total Hyperpolarizability (β_{vec})* in au and β_{vec}^{**} in 10^{-30} esu

Chromophore	ΔE	μ	α	β_{xyz}	β_{vec}^*	β_{vec}^{**}
BHDM	0.3228	2.5498	5.5642	8.7870	935.9275	8.0856
AZCI	0.3308	3.4606	3.4307	-0.0641	116.584	1.0071

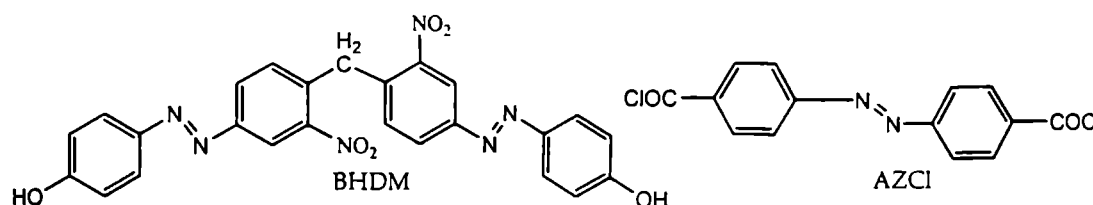


Figure 4.4. Azomesogen chromophores

It is clear that both the molecules, bis(4-hydroxyphenylazo)-2,2'-dinitrodiphenylmethane (BHDM) and azobenzene-4,4'-dicarbonyl chloride (AZCI) are very good NLO active chromophores with high microscopic SHG values. But the value of chiral component is almost negligible in AZCI compared to the total β value (0.075%). The β_{xyz} in BHDM (0.9%) is also negligible compared with the very high β_{xyz} of exo-exo

camphanediol (50%). But the HOMO-LUMO gap is small in these chromophores compared to the chiral molecules. This will help easy charge transfer. When these chromophores form polymers with the early designed chiral molecules, the macroscopic structures should be more chiral than the homopolymer of these chromophores. Hence, these resultant polymers should have high value of β due to the charge transfer and also due to chirality.

From the *Dynamic SOS* calculation also, (Table 4.8) it can be observed that the chromophores have very good beta value with high oscillator strength and low optical gap compared to the chiral molecules and which will form very good NLO active polymers with the chiral molecules.

Table 4.8: Oscillator strength (f), Optical Gap (δE) in eV, Ground-State Dipole Moment (μ_g) in debye, Difference in dipole moments between ground state and excited state ($\Delta\mu$), Linear Polarizability (α) in units of 10^{-23} esu, and First Hyperpolarizability (β), in units of 10^{-30} esu for the chromophores (ZINDO-SOS dynamic property calculations)

Chromophore	f	δE	$\Delta\mu$	μ_g	α	β
BHDM	5.3825	3.6829	19.6174	110.7927	1100	488.9864
AZCI	1.3355	4.1932	3.365	10.6268	927	106.8586

4.3.2 Polymer design

Polymers are designed as the condensation products of chromophores, bis(4-hydroxyphenylazo)-2,2'-dinitrodiphenylmethane (BHDM) and azobenzene-4,4'-dicarbonyl chloride (AZCI) with the previously designed chiral molecules. One repeating unit of each polymer has been considered for the optimization and molecular property calculations. Each repeating unit contains one molecule of bis(4-hydroxyphenylazo)-2,2'-dinitrodiphenylmethane (BHDM), two molecules of azobenzene-4,4'-dicarbonyl chloride (AZCI) and one chiral molecule. SHG properties have been compared with respect to 2-methyl-4-nitroaniline (MNA) as reference. The chiral effect has been studied by designing a repeating unit with out the chiral component. The structures of the polymers are given in Figure 4.5.

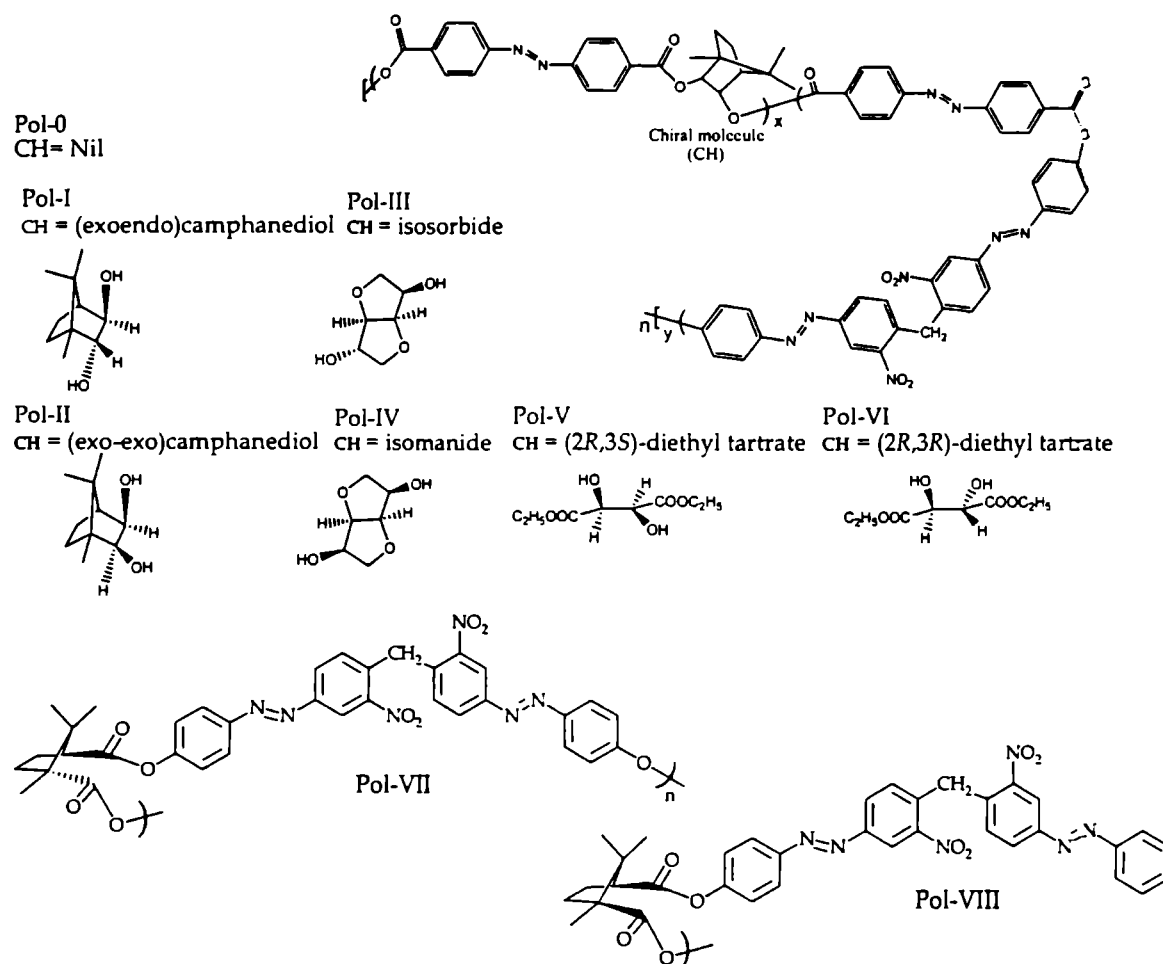


Figure 4.5. Structure of polymers

4.3.2.1 Static and dynamic molecular property calculations

4.3.2.1.a Dipole moment

The *static* and *dynamic* dipole moment values of polymers incorporating chiral molecules (Pol-I to Pol-VIII), the polymer without the chiral molecule (Pol-0) and that of 2-methyl-4-nitroaniline (MNA) are summarized in Table 4.9. It is clear that depending up on the stereochemistry of the chiral molecule; the corresponding polymer has shown variation in dipole moment. The resultant dipole moment of the polyesters is along the helical axis (Figure 4.6). The dipole moment orientation in polyesters matches with the early predicted dipole moment orientation of chiral monomer. (Figure 4.7). The dipole

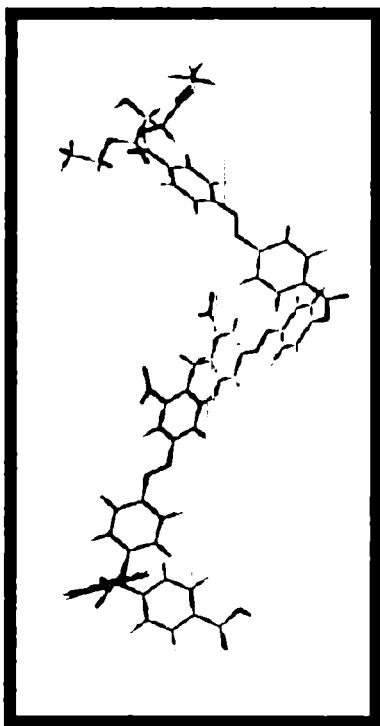


Figure 4.6. Helical structure of polymer Pol-V. Green line indicates the direction of resultant dipole moment

moment values of MNA and the polymer without chiral molecule are close to that of polymers Pol-I to Pol-VIII.

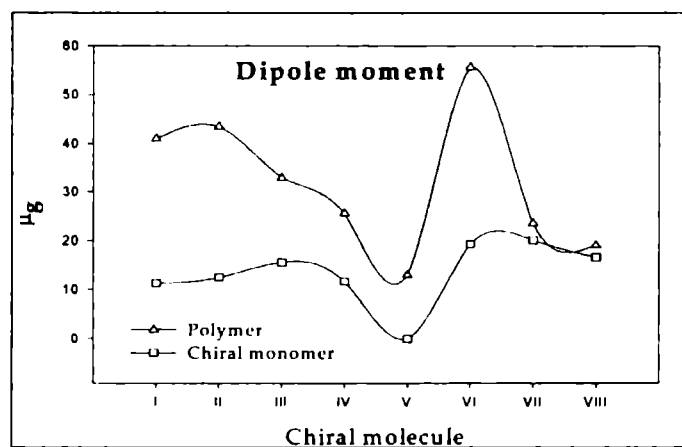


Figure 4.7: Dipole moments (dynamic) of chiral monomers and polymers (Repeating units) in units of debye

Table 4.9: Dipole moment of polymers in units of debye

Polymers	μ_x	μ_y	μ_z	μ_g Static	μ_g Dynamic
Pol-I	2.0609	0.0130	-5.0238	5.4301	41.0062
Pol-II	2.9365	-1.5043	-4.9535	5.9517	43.4733
Pol-III	5.5941	0.3901	-5.1517	7.6149	32.8368
Pol-IV	2.4274	0.4286	-2.8267	3.7505	25.6170
Pol-V	-2.6800	1.6986	1.6649	3.5832	13.1031
Pol-VI	1.8715	-3.5532	-4.0570	5.7085	55.6096
Pol-VII	-2.7721	4.2410	0.0377	5.0667	23.5744
Pol-VIII	-1.9494	4.0845	-0.2992	4.5357	19.0389
Pol-0	2.8049	0.4061	-2.1662	3.5672	33.1546
MNA	-5.9267	-1.3089	1.1946	6.1859	42.4044

4.3.2.1.b Polarizability (α)

In the case of polymers also, α values (Table 4.10.) are not varying much with respect to the stereochemistry. But all the polymers have higher values than MNA.

Table 4.10: Polarizability α of polymers

Polymers	α_{xx}	α_{zz}	α (au)	$\alpha_{tot} \times 10^{-23}$	
				Static*	Dynamic*
Pol-I	825.4632	590.4124	800.9117	11.8683	1170.0
Pol-II	825.2663	588.9055	800.9302	11.8686	1270.0
Pol-III	805.5283	546.0535	769.8875	11.4086	989.0
Pol-IV	790.4255	589.0701	764.6528	11.3310	960.0
Pol-V	815.2945	573.3554	795.8526	11.7934	1190.0
Pol-VI	803.6050	579.6060	477.1678	11.0709	1170.0
Pol-VII	329.2086	415.3341	468.7119	6.9456	1050.0
Pol-VIII	399.3801	415.9719	467.5593	6.9286	1040.0
Pol-0	716.7615	487.7200	702.6447	10.4122	950.0
MNA	118.5149	39.5720	86.22388	1.2777	410.0

$$*\alpha (esu) = 0.148185 \times 10^{-24} \alpha (au)$$

4.3.2.1.c Hyperpolarizability (β)

Static CPHF hyperpolarizability values are summarized in Table 4.11. All the polymers have β values higher than that of the reference material 2-methyl-4-nitroaniline (MNA). Even for the polymer that has not been incorporated with the chiral molecule (Pol-0), the β values are almost double (186%) compared to the reference MNA. From the charge transfer perspective, this can be understood by observing the HOMO-LUMO gap (ΔE). In MNA, ΔE is 0.40 eV and that of polymers are approximately 0.34 eV. Hence, in polymers, charge transfer will occur easily compared to MNA. Thus, HOMO-LUMO gap of monomers plays a vital role in polymer design. The ΔE of chromophores is approximately 0.33 eV and that of chiral molecules is approximately 0.45 eV. The co-polymer of these chromophores and chiral molecules has the ΔE approximately 0.34 eV. The chromophores with good donor-acceptor capacity have

reduced the ΔE of polymers considerably. Thus, the choice of monomers with low HOMO-LUMO gap is important in designing the polymers with high SHG efficiency. All the polymers have helically oriented conformation in the optimized structure.

Table 4.11: HOMO-LUMO gap (ΔE) in eV, Ground-State Dipole Moment (μ_g) in debye, Linear Polarizability (α) in units of 10^{-23} esu, and First Hyperpolarizability (β) in units of 10^{-30} esu for the polymers (ab initio CPHF static property calculations)

Polymers	ΔE	μ_g	α	β_{vec}
Pol-I	0.3490	5.4301	11.8683	9.9628
Pol-II	0.3444	5.9517	11.8686	10.2300
Pol-III	0.3415	7.6149	11.4086	7.8581
Pol-IV	0.3511	3.7505	11.3310	10.2211
Pol-V	0.3482	5.7085	11.0709	8.8682
Pol-VI	0.3505	3.5832	11.7934	10.1684
Pol-VII	0.3433	5.0667	6.9456	12.6699
Pol-VIII	0.3429	4.5357	6.9286	12.6383
Pol-0	0.3441	3.5672	10.4122	7.5995
MNA	0.4047	6.1859	1.2777	4.0778

Figure 4.20 shows the AM1 optimized geometry of the polymer containing three repeating units. The helical structure ensures the macroscopic chirality and thus the asymmetry, basic and essential requirement for second order NLO material. All the polymers have lower ground state dipole moment than MNA. The polymers with low dipole moments could reduce the chromophore-chromophore interaction in the macroscopic assemblies related to more conventional polymeric architecture and therefore be more useful as NLO material.^{39,40} Hence, with all these factors, all the designed polymers are very good materials for second harmonic generation.

While examining the effect of chiral molecule in designing an efficient SHG material, it can be seen that all the polymers (Pol-I to Pol-VIII) with chiral molecules have high β value than the polymer with out the chiral molecule (Pol -0). The HOMO-

LUMO gap is almost same in all the polymers. The chiral effect is clearer from the *dynamic* property calculations (Table 4.12).

Table 4.12: Oscillator strength (f), Optical Gap (δE) in eV, Ground-State Dipole Moment (μ_g) in debye, Difference in dipole moments between ground state and excited state ($\Delta\mu$), Linear Polarizability (α) in units of 10^{-23} esu, and First Hyperpolarizability (β) in units of 10^{-30} esu for the polymers (ZINDO-SOS dynamic property calculations)

Polymer	f	δE	$\Delta\mu$	μ_g	β_{vec}	β_{vec}^*
Pol-I	2.0588	5.1699	20.9684	41.0062	338.9870	9.9628
Pol-II	2.3105	5.2810	20.4410	43.4733	387.4365	10.2300
Pol-III	2.6603	5.4951	35.2631	32.8368	630.2270	7.8581
Pol-IV	2.6388	5.5311	36.1949	25.6171	708.5834	10.2211
Pol-V	2.5280	5.2994	23.8548	13.1032	338.5161	8.8682
Pol-VI	2.4066	5.2728	26.8567	55.6095	364.9942	10.1684
Pol-VII	0.9736	4.7253	34.0544	19.0390	479.0832	12.6699
Pol-VIII	1.0243	4.7356	33.1411	23.5745	478.5394	12.6383
Pol-0	0.2488	13.8755	9.1368	33.1546	4.2718	7.5995
MNA	1.0582	7.2925	13.7011	42.4044	202.3979	4.0778

* *Static values*

It is really surprising that in *dynamic* calculation the value of β_{vec} of the polymer without chiral molecule is very low (in two orders of magnitude) compared to the polymers with chiral molecules. It is not so pronounced in the *static* CPHF calculation due to the limitation of derivative method rather than SOS formalism. In the SOS *dynamic* calculation, contributions from all the excited levels have been taken in to account for getting the total value of β_{vec} .

For **Pol-0**, the polymer without chiral molecule, the oscillator strength (f), which determines the transition probability from the ground state to the excited state, is low compared to the other polymers with chiral building units. Also, the optical gap (δE), which determines the energy gap between the ground state and the lowest dipole allowed state, is large for **Pol-0**. Because of this very small oscillator strength and large

optical gap, charge transfer is difficult in Pol-0 compared to other polymers. Even though, Pol-0 has comparatively good ground state dipole moment, its difference in dipole moment between the ground state and the excited state $\Delta\mu$, is small compared to others. All these factors reduce the value of β_{vec} considerably. Thus all the chiral molecules are effective in making potential chiral NLO polymers. In MNA also, the value of δE is very high and $\Delta\mu$ is very low. But its oscillator strength is much higher than that of Pol-0. Hence, according to SOS calculation, MNA has more β value than Pol-0. It can be concluded that chirality plays a vital role in increasing the microscopic second order response of NLO material.

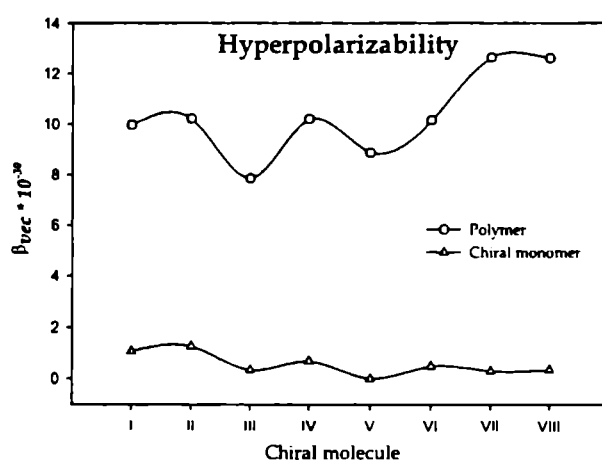


Figure 4.8. Stereochemical effect of chiral monomers and Polymers on β

(incorporated with each member of the diastereomeric pair), all other properties are same except the stereochemistry of the chiral monomer. In all polymers, the stereochemistry of azomesogen chromophores was also kept unaltered. Still, there is visible difference in the microscopic β values with respect to the stereochemistry. In the case of camphanediol pair, the polymer incorporated with exo-exo diastereomer has shown higher β value. In isosorbide-isomanide pair, the effect is more pronounced. (Pol-III and Pol-IV), and the polymer with isomanide has shown high β value. The polymers with (2R, 3S) diethyl tartrate, have also shown a good β value compared to MNA. This is because, while incorporating in to the polymer chain, the center of symmetry of the

The stereochemical effect of the chiral molecule has shown the same trend as predicted for the chiral monomers (Figure 4.8). All polymers are oriented as Λ helix. Even in this highly ordered helical structure, the stereochemistry of the incorporated chiral monomers is an important factor in determining the value of β . For each pair of polymers

chiral monomer has become unimportant and the two chiral centers in the molecule become active in the helical polymer chains. The (2R, 3R) diethyl tartrate has shown higher value of β in that pair. The polymers containing camphoric acid pair have not shown any visible stereochemical effect.

Table 4.13: Dipole moment difference between the ground state and excited state in units of deby and First Hyperpolarizability (β) in units of 10^{-30} esu for the polymers (ZINDO-SOS dynamic property calculations)

Polymer	$\Delta\mu_x$	$\Delta\mu_y$	$\Delta\mu_z$	$\Delta\mu$	β_{vec}
Pol-I	15.7750	-2.2028	12.8114	20.4410	387.4365
Pol-II	19.5195	4.0585	6.4955	20.9684	338.9870
Pol-III	24.8597	18.0235	17.3388	35.2631	630.2270
Pol-IV	26.6185	19.1062	15.3779	36.1949	708.5834
Pol-V	15.2025	7.2909	-16.8753	23.8547	338.5161
Pol-VI	18.0382	-11.1415	16.4855	26.8567	364.9942
Pol-VII	32.9943	-2.5501	-1.7902	33.1411	479.0832
Pol-VIII	33.7235	0.6646	-4.6877	34.0544	478.5394

In the case of polymers also, a clear picture of the effect of stereochemistry in the β_{vec} will be obtained from the $\Delta\mu$ values (Table 4.13). The polymers that showed higher β has also shown high value of $\Delta\mu$ and $\Delta\mu_x$ (x direction is fixed as the charge transfer direction in all optimized geometries). This stereochemical dependence of β of polymers is inherent from the stereochemistry of the incorporated chiral molecules (Figure 4.8). It can be concluded that the stereochemistry of the chiral molecules is very important in designing a good NLO material with high second order nonlinear response.

4.3.2.1.d Chiral component

The values of β tensors are summarized in Table 4.14. The β_{xyz} component of all the polymers is very large compared to MNA. In Pol-0, even if, the value of β_{xyz} is lower than that of other polymers (with chiral molecules), it is not negligible as in the case of MNA. The chirality of the polymers has arrived from 1) the incorporated chiral

molecules and 2) the macroscopic Λ helical structure of the polymers. Even after incorporating in to the polymer matrix, the stereochemistry of the chiral molecule is relevant in predicting the chiral tensor component, χ_{xyz} . The isosorbide system has low χ_{xyz} value than the isomanide system. To conclude, in the macroscopic structure, the contribution to the χ_{xyz} should be very large for these polymers and they will give high macroscopic SHG response.

Table 4.14: First hyperpolarizability tensors of polymers β (static) in atomic units

β Tensors	Pol-I	Pol-II	Pol-III	Pol-IV	PolV	Pol-VI	Pol-VII	Pol-VIII	Pol-0	MNA
β_{xxx}	-891.4448	-859.4220	-269.3773	-907.2016	-1010.94	-745.2186	226.2505	-366.8170	-246.295	562.8668
β_{xyx}	228.8973	243.8666	314.1583	187.0105	176.6139	274.8180	143.2297	138.6167	292.2001	126.1593
β_{yyx}	286.9885	292.1974	257.0262	243.5943	284.7539	273.0921	676.6643	-636.4977	244.0996	-83.3171
β_{yyy}	-385.3391	-335.5022	-350.7704	-430.1264	-429.945	-332.4573	470.9063	-418.7210	-389.542	-95.7037
β_{xxz}	290.6427	316.3345	175.5984	295.4173	269.1672	246.5883	97.4063	80.4576	140.9893	21.55855
β_{xyz}	124.4980	128.0857	103.5382	133.1641	123.8529	194.2914	119.7820	-348.5849	97.96917	-3.36694
β_{yyz}	517.8861	523.6910	469.1134	509.0435	492.3874	489.7958	689.3754	-386.9942	487.883	0.253731
β_{zzz}	187.0674	180.1087	226.9713	181.6496	199.808	188.6180	109.4226	-234.5269	205.7406	-12.592
β_{yzz}	72.2561	85.4088	103.8087	81.8387	106.3873	88.7089	-151.6933	-266.9824	93.39935	30.74238
β_{zzz}	263.2106	278.7315	236.6339	263.9292	280.8862	249.7160	168.2840	-248.9099	226.9094	9.886996
β_x	-417.3889	-387.1160	214.6202	-481.9576	-526.383	-283.5085	1012.3374	-1237.842	203.5457	466.9577
β_y	-84.1857	-6.2268	67.1966	-161.2771	-146.944	31.0695	462.4427	-547.0957	-3.94266	61.19799
β_z	1071.7395	1118.7571	881.3456	1068.3901	1042.441	986.1000	955.0657	-555.4465	855.7817	31.69927
$\beta_{vec}(au)$	1153.2243	1183.8560	909.5863	1183.1107	1177.011	1026.5163	1466.5711	1462.9034	879.664	472.0165
$\beta_{vec}(esu)^*$	9.96289	10.230	7.8581	10.221	10.200	8.8682	12.670	12.638	7.600	4.080

* β (10^{-32} esu) = 0.863916 β (au)

4.4. Synthesis

A series of polymers incorporating chiral molecules are designed with the help of theoretical calculation by optimizing the stereochemical effect of the chiral molecule. The most promising ones have been synthesized and SHG efficiency was measured experimentally. One diastereomer, each from the four diastereomeric pairs, was selected for incorporation in the polymeric structure; except isosorbide-isomanide pair. Polyesters containing both isosorbide and isomanide pair were synthesized to prove the stereochemical effect experimentally. Thus, five polymers were synthesized in the laboratory incorporating chiral monomers, biphenol (5) and diacid chloride (8) by high temperature polycondensation. The chiral molecules selected were (1R, 2S, 3R, 4S)-camphanediol (exo-exo camphanediol), isosorbide, isomanide, (2R, 3R)-diethyl tartrate and (1R, 3S)-camphoric acid (D (+) or exo-exo) (Figure 4.9). The polyester that does not contain any chiral molecule was also synthesized. The synthetic procedures are described in the following section.

4.4.1 Monomer synthesis

4.4.1.1 Synthesis and characterization of chiral molecules

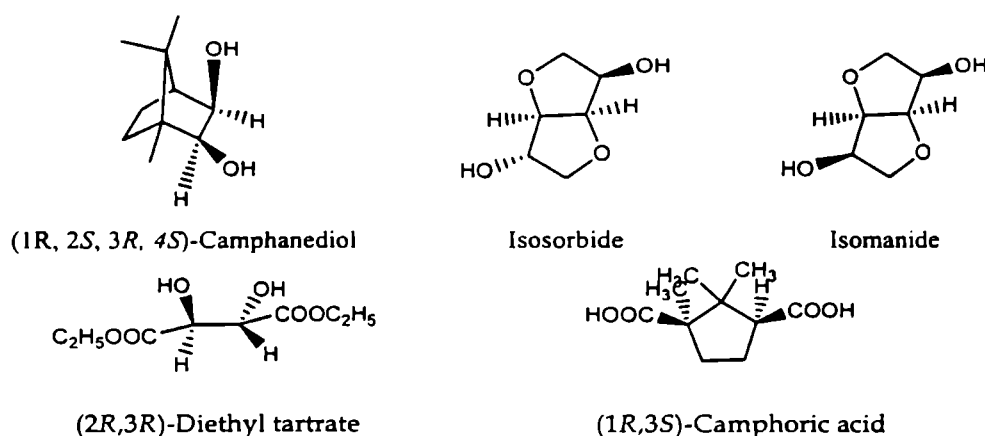


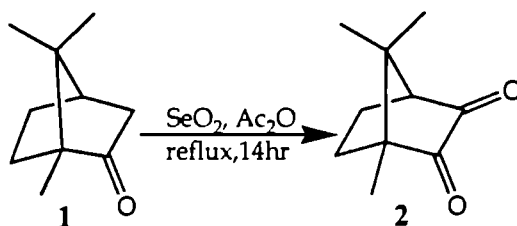
Figure 4.9. Chiral monomers used for polymer synthesis

Theoretical study of eight chiral monomers were done and out of which five chiral molecules (Figure 4.9) were selected for the synthesis of polymeric systems. They

are (1R, 2S, 3R, 4S)-camphanediol (exo-exo camphanediol), isosorbide, isomanide, (2R, 3R)-diethyl tartrate and (1R, 3S)-camphoric acid (D (+) or exo-exo). Isosorbide (Lancaster, 98% pure), isomanide (Fluka, 98% pure), (2R,3R)-diethyl tartrate (Merck - Germany, 97% pure) and (1R,3S)-camphoric acid (D(+)) or exo-exo (Lancaster, 98% pure) were commercially available. (1R, 4S) camphanediol (exo-exo) was synthesized from camphoroquinone.

Synthesis of (1R, 4S)-(-)- camphoroquinone^{41,42}

SeO₂ (s. d. fine 99% pure), D (+) camphor (Lancaster, 97% pure), acetic anhydride (E.Merck, G.R) were used as starting materials for synthesizing camphoroquinone. Unless otherwise specified all other reagents, through out the synthesis, were of analytical grade and all the chemicals were used as obtained.



Scheme 4.1. Synthesis of camphoroquinone

Synthetic procedure: (D) (+) camphor 1 (20.0g 0.13 mol) was taken in a 125mL three necked, round-bottom flask fitted with a reflux condenser with stirring. Selenium dioxide (8.0 g, 0.07 mol) and reagent grade acetic anhydride (14 mL) was added to it. The green solution was stirred at reflux for 1 h, cooled to ambient temperature, and an additional amount of selenium dioxide (8.0 g, 0.07 mol) was added. The mixture was again heated to reflux, and two further batches of selenium dioxide (8.0 g, 0.07 mol) were added at 2.5 h and 6 h intervals. The reaction mixture was heated at reflux for an additional 8 h, during which time, precipitation of selenium metal was observed. It was cooled to ambient temperature and transferred to 125 mL beaker with the aid of 50 mL of ethyl acetate and the solution was filtered by applying vacuum. The filtrate was transferred to a 1-L separating funnel and was washed successively with 10% aqueous sodium hydroxide (200 mL) solution and saturated aqueous sodium chloride (100 mL)

solution. The organic layer was separated and dried over anhydrous magnesium sulphate, filtered and concentrated to get crude (1R,4S) (-) camphoroquinone (2) as yellow crystals. It was recrystallised from a mixture of hexane and 2-propanol. (Scheme 4.1.) This material was used for the synthesis of (1R, 4S) (+) exo-exo 2, 3- camphanediol.

Characterization

Yield 84.5%, $[\alpha]_D = -107.4$ (c=10mg/ml in DMF). M.P 198-199^o C (lit. mp 199^oC) ⁴¹

Elemental analysis: Calculated for C₁₀H₁₄O₂ - C, 72.26; H, 8.49; O, 9.25. Found - C, 72.20; H, 8.55; O,9.30

Spectral properties

UV λ_{max} nm :430

IR(KBr pellet) cm⁻¹: 1767 and 1746 (α diketone ,aliphatic six membered ring), 994 (=CH)

¹H NMR (300 MHz CDCl₃): δ 1.03 (s, 3H, bridge head methyl), 1.11 (s,3H, bridge head CH₃), 1.27 (s, 3H, bridgehead CH₃), 1.88 (m,2H, ring CH₂), 1.75 (m,2H, ring CH₂) 2.35 (m, 1H, bridge head -CH)

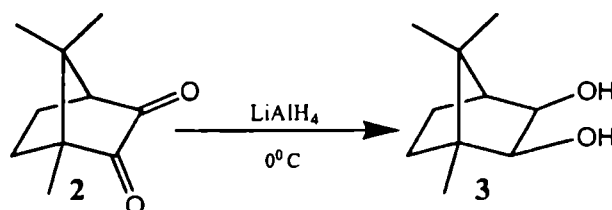
¹³C NMR (75 MHz CDCl₃): δ 15.9 (-CH₃ aliphatic), 22.1 (CH₃, aliphatic) 22.4 (-CH₃ aliphatic), 22.8 (-CH₂, cyclopentane), 31.8 (-CH₂, cyclopentane), 37.7 (-C, cyclopentane) 54.3 (-C, cyclopentane), 55.2 (-CH, cyclopentane), 202(-C, carbonyl), 207.6 (-C, carbonyl)

Mass (m/z) : molecular ion peak at = 166, 28 (-CH₂-CH₂-), 43 (-CH₂-C=O)

IR peaks at 1767 and 1746 cm⁻¹ are characteristic of α diketones in six membered ring system. ¹H NMR peak at δ 2.35 implies the presence of camphor bicyclic ring ketone. Peaks at δ = 22.8, 31.8 ,37.7 in ¹³C NMR are characteristic of camphor bicyclic ring system. δ = 202 and 207.6 are due to six memebered ring carbonyl group.

Synthesis of (1R, 2S, 3R, 4S)-camphanediol

LiAlH₄ (Aldrich, 95% pure) was used for reduction. Extremely dry ether was obtained by benzophenone ketyl procedure.^{43,44}



Scheme 4.2. Synthesis of (1R, 2S, 3R, 4S)-camphanediol

Synthetic procedure: Camphoroquinone (2) (30 g, 0.18 mol) in dry ether (360 mL) was taken in a 500mL beaker kept in an ice bath. LiAlH₄ (98g, 2.5 mol) suspended in dry ether (100 ml) was added to it. After an exothermic reaction, the mixture was kept at 0° C for further 20 min. and refluxed for 1 h. The excess amount of LiAlH₄ was decomposed with 0.5 M sulphuric acid in an ice bath. The reaction mixture was washed several times with dil. sodium hydroxide and dried over anhydrous magnesium sulphate to get crude (1R, 4S)(+) exo-exo 2,3- camphanediol as white solid (3). This solid was recrystallized from dry ether and sublimed at 110° C (**Scheme 4.2.**)

Characterization

Yield 86%, $[\alpha]_D = -12^\circ$ (c=10mg/ml in dry ether).

Elemental analysis: Calculated for C₁₀H₁₈O₂ - C, 70.55; H, 10.66; O, 18.79. Found - C, 70.69; H, 10.51; O, 18.80

Spectral properties

UV λ_{\max} (nm): 315

IR(KBr pellet) cm⁻¹ : 1364, 1390(*gem*-dimethyl group, symmetric and asymmetric C-CH₃ stretching), 3230 (-OH stretching)

¹H NMR (300 MHz CDCl₃): δ 7.25 (-OH), 3.55-4.05 (-CH, 2 & 3), 2.25- 2.65 (-CH, 4), 1.4-1.8 (-CH₂, 5 & 6), 0.85-1.15(-bridge head CH₃ 8 & 9), 0.75-0.84 (bridge head CH₃, 10)

¹³C NMR (75 MHz CDCl₃): δ 79.89, 77.38 (C2), 76.13-77.05 (C3), 48.97, 51.55 (C4), 46.45, 48.76 (C1), 45.12, 46.33 (C7), 38.99, 40.45 (C6), 33.99-24.12 (C8 & C9), 21.86, 21.04 (C5), 20.46, 20.11 (C10)

Mass (m/z) 170 (molecular ion), 169 (M⁺ -H), 152 (M⁺ - H₂O), 141 ([M-1]⁺ -CO), 42(-C(CH₃),

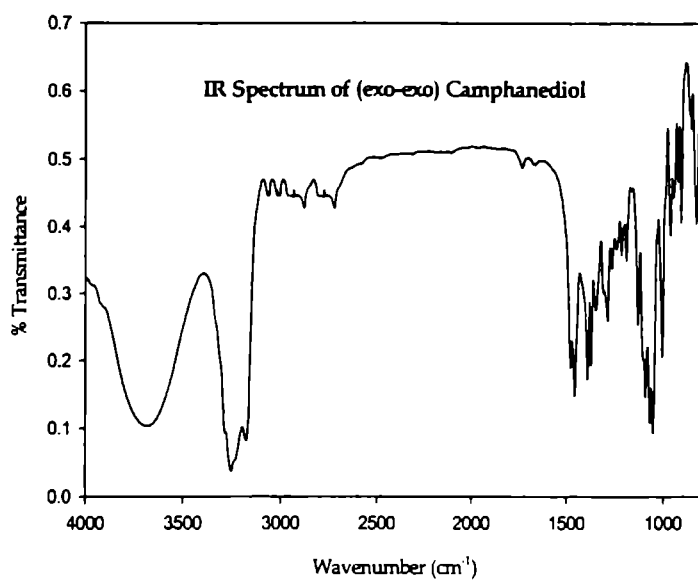
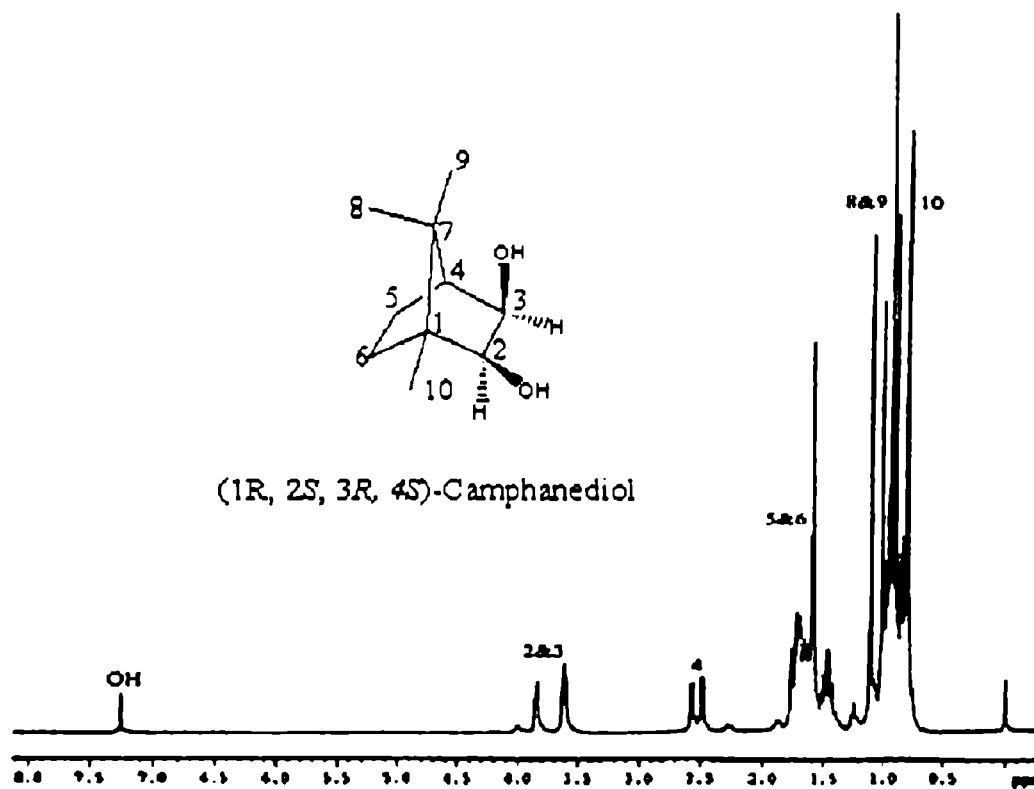


Figure 4.10. IR Spectrum of (exo-exo) Camphanediol

The IR spectrum of exo-exo camphanediol shows a complexity in the 1373-833 cm^{-1} region typical of many stretching and bending vibrations present in organic compounds. Since camphanediol contains a *gem*-dimethyl group $[(\text{CH}_3)_2 \text{C}]$ the spectrum displays a sharp doublet at 1364 and 1390 cm^{-1}

Figure 4.11. ^1H NMR of Camphanediol

The ^1H NMR and ^{13}C NMR spectra of camphanediol are complex spectra due to spin spin coupling. Because the bicyclic bridged system is a strained ring system, coupling exists between all most all the protons and also between the carbons. The $-\text{OH}$ peak at δ 7.5 confirmed the reduction of camphoroquinone into camphanediol. The absence of peaks after δ 100 confirmed that there is no more carbonyl carbon in the compound. $-\text{OH}$ carbons appeared at δ 79.89 and 76.13. The mass spectrum also confirmed the proposed structure.

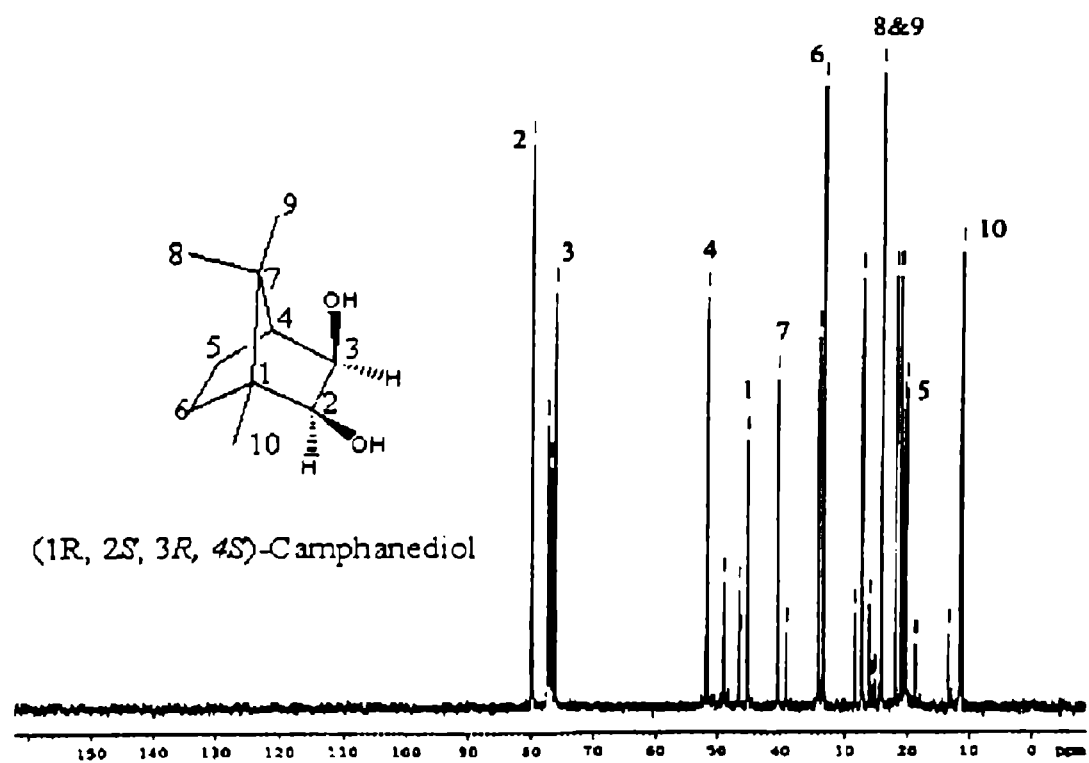


Figure 4.12 ^{13}C NMR of Camphanediol

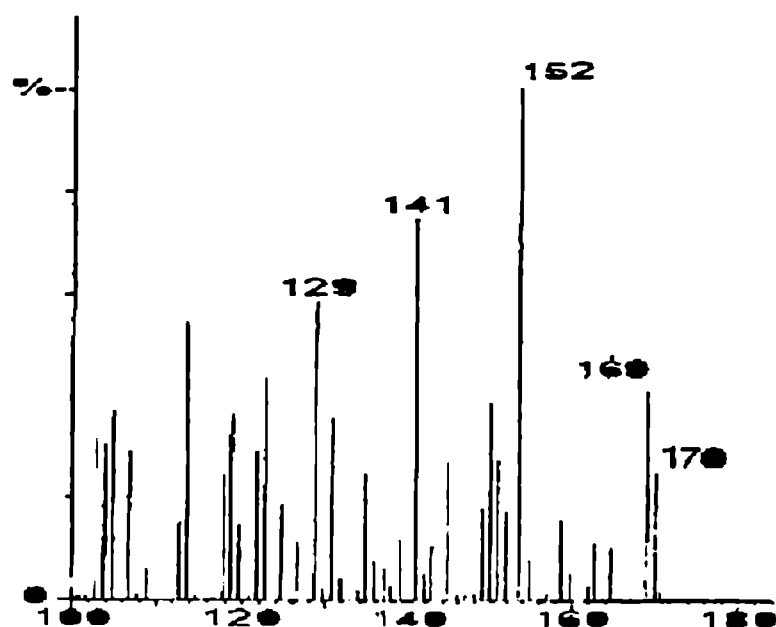


Figure 4.13 ESI mass spectrum of Camphanediol

4.4.1.2 Synthesis and characterization of chromophores

The selected chromophores, bis(4-hydroxyphenylazo)-2,2'-dinitrodiphenyl methane (BHDM) and azobenzene-4,4'-dicarbonyl chloride (AZCl) were synthesized according to the standard procedures. Bis(4-hydroxyphenylazo)-2,2'-dinitrodiphenylmethane (BHDM) was synthesized from 4,4'-diamino-2,2'-dinitrodiphenylmethane.¹⁶ Both are azo benzene compounds. Derivatives of azo benzene compounds containing donor-acceptor groups have been widely exploited as NLO chromophores in polymeric systems.⁴⁵⁻⁴⁸ The synthesis of these compounds can be easily accomplished by a diazo coupling reaction. Diazo coupling reaction is the first reported reaction for the synthesis of azo benzene compounds and it is the single most used reaction for the synthesis of azo dyes till date. This electrophilic substitution reaction leads to regioselectivity and usually a high yield of the product. The reaction involves coupling between a diazotized aromatic amine and a coupling component such as phenol, naphthols, aromatic amines and active compounds.⁴⁹ The regioselectivity of diazo coupling reaction leads to the preferential formation of the *para* isomers. There are

two geometrical isomers known for azo benzene derivatives named *cis* and *trans* (Figure 4.14). Among these the *trans* is more stable but *cis* is naturally occurring.⁵⁰

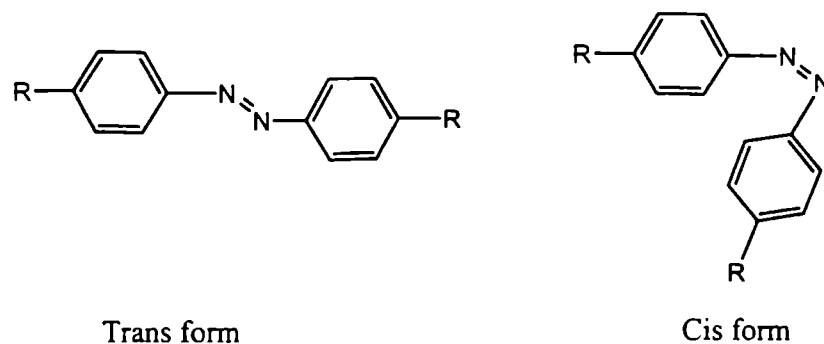
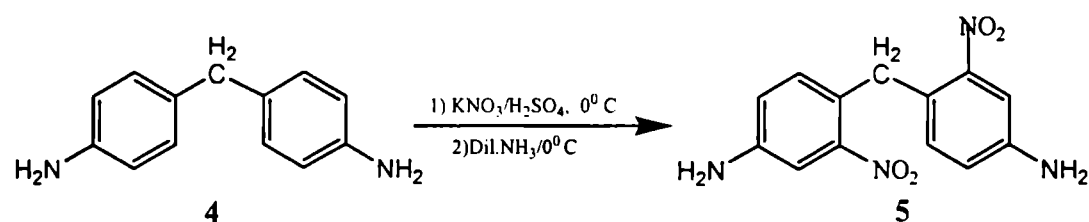


Figure 4.14. Geometrical isomers of azobenzene derivatives

4.4.1.2.1 Synthesis of 4, 4'-diamino-2,2'-dinitrodiphenylmethane

4, 4'-diaminodiphenylmethane (Lancaster 97% pure), Potassium nitrate (s. d. fine. 99% pure) were used for the synthesis of bis(4-hydroxyphenylazo)-2,2'-dinitrodiphenylmethane (BHDM).



Scheme 4.3. Synthesis of 4, 4'-diamino-2,2'-dinitrodiphenylmethane

Synthetic Procedure: 4, 4'-Diaminodiphenylmethane (4) was nitrated using a mixture of anhydrous potassium nitrate and 98% sulphuric acid. 500 mL beaker was placed in a 0°C ice bath with magnetic stirring. It was charged with an ice cold solution of 4,4'-diaminodiphenylmethane (10g, 0.05 mol) in conc. sulphuric acid (40 mL, 18M). To this solution, potassium nitrate solution (10g, 0.1 mol) in conc. sulphuric acid (15 mL, 18 M) was added drop wise during a period of 1h, using a dropping funnel. The stirring was continued for 3 h, keeping the temperature below 5°C. The reaction mixture was poured in to crushed ice and neutralized with ice cold solution of ammonia. The orange-yellow solid was collected by filtration, washed thoroughly with water. Crystallization from a mixture of dioxane-alcohol afforded orange-yellow flakes of 4, 4'-diamino-2,2'-

dinitrodiphenylmethane. This was used for the synthesis of bis(4-hydroxyphenylazo)-2,2'-dinitrodiphenylmethane (BHDM) (5) (Scheme 4.3.)

Characterization

Yield 89.6%. M.P. 205^o C

Elemental analysis: Calculated for C₁₃H₁₂N₄O₄ - C, 54.14; H, 4.16; N, 19.44. O, 22.26

Found - C, 54.11; H, 4.18; N, 18.80; O, 22.91

Spectral properties

UVλ_{max} nm : 308 (NO₂)

IR(KBr pellet) cm⁻¹ : 1540, 1350 (NO₂)

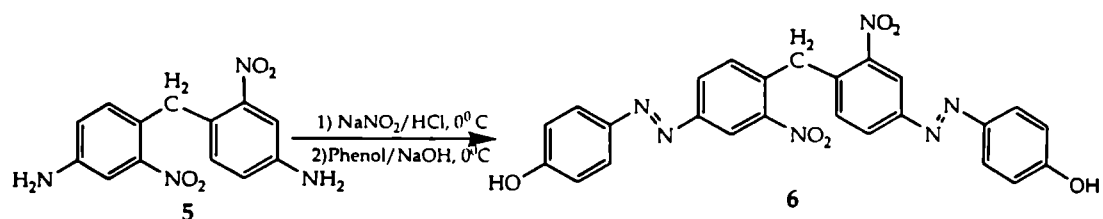
¹H NMR (300 MHz CDCl₃): δ 4.8 (s, 4H, -NH₂), 8.2 (s, 2H,aromatic), 7.6 (d, 2H aromatic), 7.3 (d, 2H, aromatic), 5.0 (s, 2H -CH₂)

¹³C NMR (75 MHz CDCl₃): δ 34 (-CH₂), 118, 124,130, 135, 147, 157 (aromatic)

The 4, 4'-diaminodiphenylmethane (4) was nitrated using potassium nitrate and concentrated sulphuric acid, according to a reported procedure.⁵¹ In 98% sulphuric acid, nitration takes place at the meta position of NH₃⁺ group. The dinitro derivative (5) was reported earlier.⁵¹ Peaks at 1350 and 1540 cm⁻¹ confirmed the nitro substitution. The elemental analysis of the compound confirmed diniration of (4). In ¹³ C NMR spectra of (5) there were only six peaks corresponding to aromatic hydrogens. So the nitro substitution in both the nuclei was symmetrical. Also in ¹H NMR spectra, the absence of singlet peak at or above δ 8.9 showed that there was no aromatic hydrogen *ortho* to nitro groups or the nitro group was substituted in the meta position of the amino group.

4.4.1.2.2 Synthesis of bis(4-hydroxyphenylazo)-2,2'-dinitrodiphenylmethane (BHDM)

Sodium nitrite (s. d. fine 98%), Phenol (E. Merck, 99%) were used for the synthesis of bis(4-hydroxyphenylazo)-2,2'-dinitrodiphenylmethane (BHDM) (5).



Scheme 4.4. Synthesis of bis(4-hydroxyphenylazo)-2,2'-dinitrodiphenylmethane

Synthetic Procedure: An ice cold solution of 4,4'-diamino-2,2'-dinitrodiphenylmethane (5) (10g, 0.035 mol) in hydrochloric acid (20 mL, 6M) was taken in a 500 mL beaker. The solution was kept under magnetic stirring. To this solution, cold aqueous sodium nitrite solution (6 g in 15mL of H₂O) was added drop wise from a dropping funnel. The diazonium salt was obtained as yellow solution. This diazonium salt was added to a cold alkaline solution of phenol (6.58 g, 0.07 mol). The resulting solution on acidification yielded a brown solid (6). It was collected by vacuum filtration, washed with water, dried and purified on a silica gel column using benzene and benzene-ethyl acetate mixture. (Scheme 4.)

Characterization:

Yield : 70%. M.P: 252^o C

Elemental analysis: Calculated for C₂₅H₁₈N₆O₆ - C, 60.24; H, 3.64; N, 16.86. O, 19.26

Found - C, 60.18; H, 3.58; N, 16.76; O, 19.48

Spectral properties

UVλ_{max} nm : 308 (NO₂), 375 (-N=N-)

IR (KBr pellet) cm⁻¹ : 3400 (-OH), 1540, 1345 (NO₂), 1453 (-N=N-)

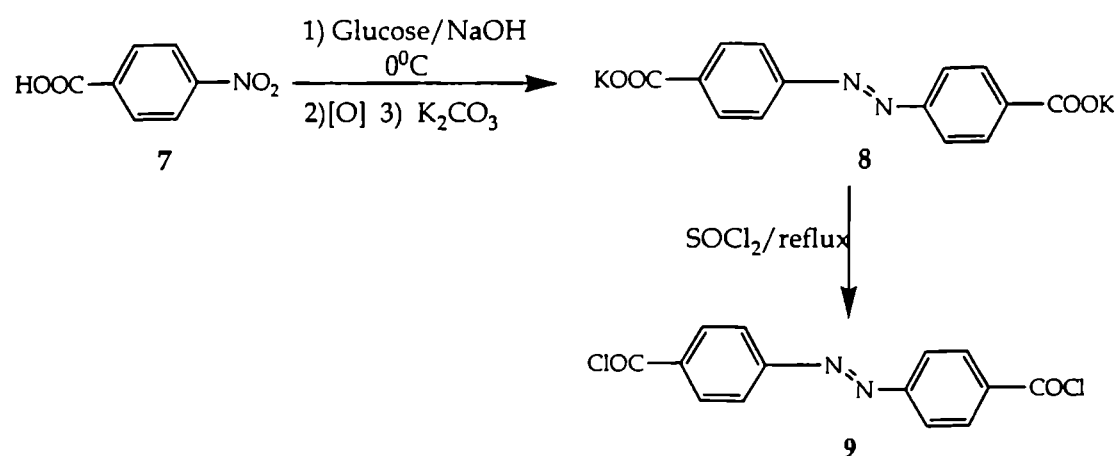
¹H NMR (300 MHz CDCl₃) δ : 5.1 (s, 2H, -CH₂), 7.3 (d, 2H, aromatic), 7.7 (d, 2H, aromatic), 7.8 (d, 2H, aromatic), 8.5 (d, 2H, aromatic), 8.7 (s, 2H, aromatic), 9.9 (s, 2H - OH)

¹³C NMR (75 MHz CDCl₃) δ : 34 (-CH₂) 117, 119, 124, 128, 136, 139, 142, 150, 152 and 154 (aromatic)

The peak at 3400 cm^{-1} in the IR spectrum and a singlet peak at $\delta\ 9.9$ in the ^1H NMR spectrum are due to hydroxyl groups. The peak between 375 and 380 nm in UV-Vis absorption spectrum is due to the azo group ($\pi\rightarrow\pi^*$)

4.4.1.2.3 Synthesis of azobenzene-4,4'-dicarbonyl chloride (AZCl) ⁵²

4-Nitrobenzoic acid (Lancaster, 95% pure), Sodium hydroxide (s d fine, 97%), Glucose (BDH, 99% pure), Potassium carbonate (BDH, 99% pure), thionyl chloride (s. d. fine, 98% pure) were used for the synthesis.



Scheme 4.5. Synthesis of azobenzene-4,4'-dicarbonyl chloride

Synthetic procedure: Azobenzene-4,4'-dicarbonyl chloride was synthesized according to a modified procedure of Tomlinson.⁵² A two necked round bottom flask was equipped with magnetic stirring. The flask was charged with a solution of *p*-nitrobenzoic acid (7) (13 g, 0.0778 mol), sodium hydroxide (50g, 1.25 mol) and water (225 mL). To this magnetically stirred solution at 50°C , was added a solution of glucose (100g, 0.555 mol) in water (150 mL) over a 1 h period using pressure-equalizing funnel. The mixture was warmed on a steam bath until a yellow precipitate was formed. It was then removed and well shaken until the precipitate was dissolved to give a brown solution. A stream of air was drawn through the brown solution for 12 h, using an air blower. The mixture was slowly acidified with glacial acetic acid to pH 6 and a mud like precipitate was collected by filtration. This solid was crystallized from petroleum ether. The product was dissolved in potassium carbonate solution and recrystallisation yielded the potassium

salt of the compound. Bright orange crystals of potassium salt of azobenzene-4, 4'-dicarboxylic acid was obtained (8). This salt was refluxed with freshly distilled thionyl chloride for 24 h. The product was crystallized from petroleum ether to obtain red needles of azobenzene-4,4'-dicarbonyl chloride (9). (Scheme 4.5.)

Characterization

Yield: 80%. M.P: 164^o C

Elemental analysis : Calculated for C₁₄H₈N₂O₂Cl₂ C, 54.75; H,2.63; N, 9.12, Cl, 23.09, O, 10.41. Found- C, 54.72; H, 2.70; N,9.10; Cl, 23.10; O, 10.38.

Spectral analysis

UVλ_{max} nm: 330 (-N=N-)

IR(KBr pellet) cm⁻¹ : 793 (C-Cl), 985 (C-CO), 1780 (C=O), 1450 (-N=N-)

¹H NMR (300 MHz CDCl₃) : δ (d, 7.9 aromatic), 8.1 (d, aromatic)

¹³C NMR (75 MHz CDCl₃) : δ 122,130, 133,151 (aromatic) 168 (carbonyl)

Peak at 793 cm⁻¹ in the IR spectrum indicates the presence of C-Cl bond. Peak at δ 168 in the ¹³C NMR spectrum implies the presence of carbonyl carbon

4.4.2 Polymer synthesis

From the polymer structure designed earlier, Pol-0, Pol-II, Pol-III, Pol-IV, Pol-VI, and Pol-VIII have been synthesized through polycondensation of the chiral molecules and chromophores.

4.4.2.1 Optimization of reaction conditions

Table 4.15: Synthesis of Pol-0 under various conditions

Solvent	Time (h)	Temp(°C)	Yield (%)
DMAc	25	60	45
DMAc	25	120	75
DMAc	25	160	85
DMAc	50	160	88
DMF	50	160	73
DMSO	50	160	68

The optimum conditions for the synthesis of polymers were determined by varying the temperature, time of reaction and solvent. Chiral monomer, (1R, 4S) exo-exo 2,3- camphanediol was taken for optimizing the reaction conditions (Pol-II) Polyesters, Pol-0 Pol-

II, **Pol-II.a**, **Pol-II.b** and **Pol-II.c** were synthesized according to the general procedure shown in Schemes 6 & 8. **Pol-0** was synthesized from bis-(4-hydroxyphenylazo)-2,2'-dinitrodiphenylmethane (6) and 4,4'-azobenzene dicarbonyl chloride (9). **Pol-II**, **Pol-II.a**, **Pol-II.b** were synthesized from (1R, 2S, 3R, 4S)-camphanediol (3), bis-(4-hydroxyphenylazo)-2,2'-dinitrodiphenylmethane (6) and 4,4'-azobenzene dicarbonyl chloride (9) in the presence of extremely dry pyridine (s. d. fine, spectroscopic grade) as an acid acceptor in the solvent dimethyl acetamide. **Pol-II.c** was synthesized from 4,4'-azobenzene dicarbonyl chloride and (1R, 2S, 3R, 4S)-camphanediol (3). The optimum conditions for synthesis of the above polyesters were determined from the synthesis of **Pol-0** and **Pol-II** by a series of experiments by changing temperature, reaction time and solvent. The results are summarized in Table 4.15. and Table 4.16.

Table 4.16: Synthesis of Pol-II under various conditions

<i>Solvent</i>	<i>Time (h)</i>	<i>Temp(°C)</i>	<i>Yield(%)</i>	<i>[α]_D</i>
DMAc	25	60	50	-5.50
DMAc	25	120	72	-7.70
DMAc	25	160	86	-10.30
DMAc	50	160	87	-35.10
DMF	50	160	65	-24.50
DMSO	50	160	70	-30.80

For **Pol-II**, the variation of temperature in DMAc medium showed that the polyester of high specific rotation in good yield was obtained at 160° C. The low value of [α] at low temperatures may be due to

low percentage incorporation of (1R, 2S, 3R, 4S)-camphanediol units. An increase in reaction time from 25 h to 50 h showed only slight increase in [α] and yield. The reaction was also repeated in DMSO and DMF. But the yields and specific rotation were low. So optimum condition for the synthesis of polymers incorporating chiral unit, (1R, 2S, 3R, 4S)-camphanediol was fixed as 25 h stirring of corresponding monomers in DMAc at 160°C. For **Pol-0**, the yield increased with increase in temperature. The experiments were also repeated in DMSO and DMF but the yields were relatively low. The increase of reaction time from 25 h to 50 h showed only a nominal change in yield. So optimum condition for synthesis of **Pol-0** and **Pol-II**, **Pol-II.a**, **Pol-II.b**, **Pol-II.c** was fixed as 25 h stirring of the corresponding monomers in DMAc medium at 160° C.

4.4.2.1. Synthesis and characterization of Pol-0, Pol-II, Pol-II.a, Pol-II.b, Pol-II.c,

4,4'-azobenzene dicarbonyl chloride(9) was dissolved in extremely dry dimethyl acetamide (HPLC grade, s. d. fine). To this solution was added appropriate mole percentage of (exo-exo) camphanediol (3) and bis(4-hydroxyphenylazo)-2,2'-dinitrodiphenylmethane (4). Few drops of extremely dry pyridine (99.99% dry pyridine, s. d. fine) were added as acid acceptor. The mixture was heated under stirring for 25h at 160° C. The product was precipitated from cold methanol and washed continuously with hot water, methanol and acetone. After filtration and drying a brown solid was obtained.

Pol-0: 4,4'-azobenzene dicarbonyl chloride (0.01 mol, 3.06 g) and bis(4-hydroxyphenylazo)-2,2'-dinitrodiphenylmethane (0.01 mole, 4.98 g) were reacted. (Scheme 4.6.)

Characterization

Yield 82 %

Spectral analysis

UV λ_{\max} nm : 362 ($\pi \rightarrow \pi^*$, N=N), 320 ($n \rightarrow \pi^*$, NO₂)

IR(KBr pellet) cm⁻¹ : 1760 (C=O, str, ester) 1345, 1530 (N-O str, NO₂).

¹H NMR (300 MHz DMSO-d₆): δ 8.9-7.3 (d, aromatic), 5.3 (s, methylene)

¹³C NMR (75 MHz DMSO-d₆): δ 172 (ester carbon), 34 (methylene carbon), 124-157 (aromatic ring carbons)

Pol-II.a: 4,4'-azobenzene dicarbonyl chloride (0.01 mole, 3.06g), bis(4-hydroxyphenylazo)-2,2'-dinitrodiphenylmethane (0.0075 mole, 3.74 g) and (exo-exo) camphanediol (0.0025 mole, 0.425 g) were reacted.

Yield: 88 %

Pol-II: 4,4'-azobenzene dicarbonyl chloride (0.01 mole, 3.06g), bis(4-hydroxyphenylazo)-2,2'-dinitrodiphenylmethane (0.0050 mole, 2.49 g) and (exo-exo) camphanediol (0.005 mole, 0.85 g) were reacted.

Yield: 83 %

Pol-II.b: 4,4'-azobenzene dicarbonyl chloride (0.01 mol, 3.06g), bis(4-hydroxyphenylazo)-2,2'-dinitrodiphenylmethane (0.0025 mole, 1.25 g) and (exo-exo) camphanediol (0.0075 mole, 1.275 g) were reacted.

Yield: 79%

Characterization

The spectral patterns of Pol-II.a, Pol-II, Pol-II.b were similar

Spectral analysis

UV λ_{\max} nm : 360 ($\pi \rightarrow \pi^*$, N=N), 322 ($n \rightarrow \pi^*$, NO₂)

IR(KBr pellet) cm⁻¹ : 1760-1750 (C=O str. Ester formed by phenolic unit), 1735-1720 (C=O str. ester formed by camphanediol), 1520-1530 (N-O str., NO₂), 1350-1373 (C-NO₂), 1610-1620 (-N=N-), 1219-1224 (doublet, C(CH₃)₂ of camphanediol), 2900-3000 (C-H stretch in camphanediol)

¹H NMR (300 MHz, DMSO-d₆) : δ 1.25 (s, bridged -C(CH₃)₂ of camphanediol), 2.1 (s, -CH₃ of camphanediol), 2.5 (m, -CH, cyclopentane ring of camphanediol), 3.0 (m, -CH₂ cyclopentane ring of camphanediol), 5.4-5.8 (m, proton near to camphanediol ester group), 6.4 (s, -CH₂), 7.6-8.9 (m, aromatic)

¹³C NMR (75 MHz, DMSO-d₆): δ 170-175 (C of ester formed by phenolic unit), 167-164 (C of ester formed by camphanediol unit), 124-156 (aromatic carbons), 20-25 (bridge head methyl carbons in camphanediol), 40-55 (bridge head C and bridge head -CH), 37 (ethylene carbon), 75 (C adjacent to ester group)

Pol-II.c: 4,4'-azobenzene dicarbonyl chloride (0.01 mol, 3.06 g) and (exo-exo) camphanediol (0.01 mole, 1.7 g) were reacted.

Characterization

Yield: 81 %

Spectral analysis

UV λ_{\max} nm : 365 ($\pi \rightarrow \pi^*$, N=N)

IR (KBr pellet) cm^{-1} : 1720 (C=O, str, ester formed by camphanediol), 1219-1224 (doublet, C(CH₃)₂ of camphanediol), 2900-3000 (C-H stretch in camphanediol)

¹H NMR (300 MHz DMSO-d₆) : δ 7.7, 7.8 (d, aromatic), 1.24 (s, bridged -C(CH₃)₂ of camphanediol), 2.1 (s, -CH₃ of camphanediol), 2.4 (m, -CH, cyclopentane ring of camphanediol), 3.1 (m, -CH₂ cyclopentane ring of camphanediol), 5.6 (m, proton near to camphanediol ester group)

¹³C NMR (75 MHz DMSO-d₆) δ : 166 (ester carbon), 120-128 (aromatic ring carbons), 20,23,25 (bridge head methyl carbons in camphanediol), 41, 42, 45 (bridge head C and bridgehead -CH), 75 (C adjacent to ester group)

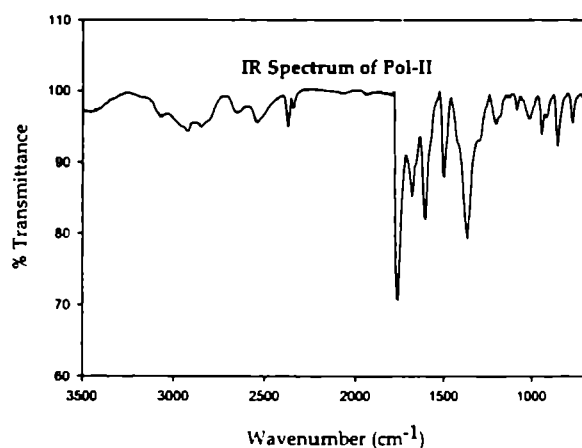


Figure 4.15. IR Spectrum of Pol-II

The polyester, **Pol-0** showed only one ester carbonyl peak between 1755-1760 cm^{-1} due to the ester bonds formed by phenolic units. But polyesters **Pol-II.a**, **Pol-II**, **Pol-II.b** showed additional peak in the region 1720-1730 cm^{-1} . This peak can be attributed due to the ester bonds formed by camphanediol units. **Pol-II.c** showed only one ester peak at 1720 cm^{-1} . In the case of ester

bonds formed by camphanediol unit, there is a benzene ring adjacent to the carbonyl carbon which decreases the C=O bond order by conjugation. This decreases the frequency of C=O str. from the normal value of 1760 cm^{-1} to 1720- 1730 cm^{-1} . In the ester bond formed by a phenolic unit, there is a phenyl group attached to oxygen, which can prevent conjugation and the bond order is retained. So the carbonyl peak appears at the normal position, 1760 cm^{-1} . From the absorbance of the peaks corresponding to the carbonyl vibration between 1750-1755 cm^{-1} and 1720-1730 cm^{-1} , the ratio of chromophore and chiral unit in the polymer was determined. The analysis showed that there is only slight difference between target composition and measured composition. The

incorporation of camphanediol units was also indicated by the peaks in the region 1219-1224 cm^{-1} (doublet, $\text{C}(\text{CH}_3)_2$ of camphanediol), which is characteristic of *gem*-methyl group and 2900-3000 (C-H stretch in camphanediol).

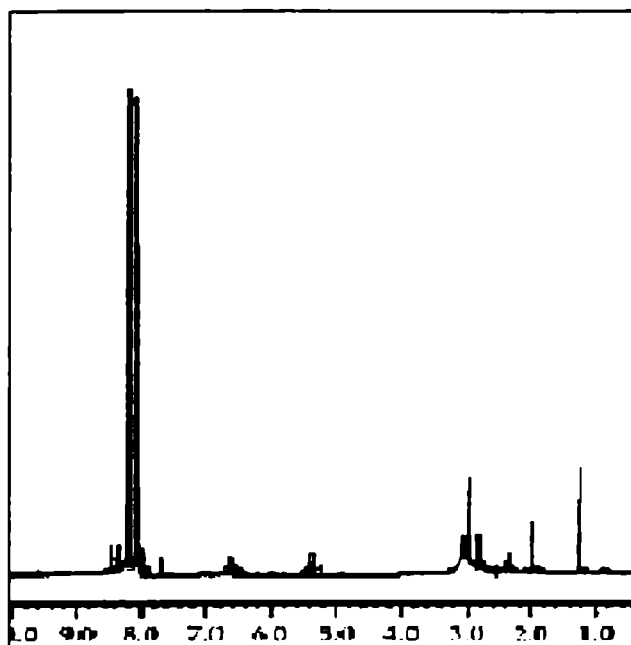


Figure 4.16. ^1H NMR spectrum of Pol-II

The absence of peaks corresponding to $-\text{OH}$ and $-\text{COOH}$ protons can be taken as an indication of high molecular weight. The singlet peak(s) between low field regions between δ 8.7-8.9 was due to the protons in the benzene ring *ortho* to nitro group. The peaks due to all other aromatic protons appeared as doublets between δ 7.6 and 8.4.

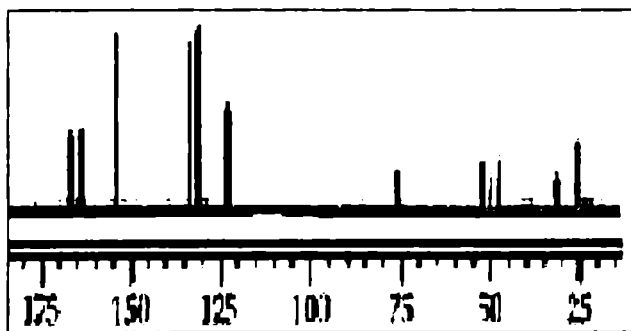


Figure 4.17. ^{13}C NMR Spectrum of Pol-II

49, 54 δ due to cyclohexane $-\text{CH}_2$, 60 δ due to bridge head $-\text{CH}$, and 75 δ due to the carbon atom adjacent to ester group. These six peaks are absent in Pol-0. ^{13}C NMR

The ^1H NMR spectra of polymers showed peaks at δ 1.25 singlet due to bridged- $\text{C}(\text{CH}_3)_2$ of camphanediol, δ 2.1 singlet due to $-\text{CH}_3$ at bridge head of camphanediol, multiplet at δ 2.5 due to cyclohexane ring $-\text{CH}$ of camphanediol and multiplet at δ 3.0 due to cyclohexane ring $-\text{CH}_2$ of camphanediol. The proton adjacent to the ester group gave multiplet between δ 5.4 and 5.8. The CH_2 protons appeared as a singlet at δ 6.4. The absence of

The ^{13}C NMR spectrum of camphanediol containing polyesters showed peaks at δ 25 due to bridge head methyl carbons in camphanediol ($-\text{C}(\text{CH}_3)_2$), peak at δ 30 due to $-\text{CH}_3$ of camphanediol,

spectra of polyesters other than Pol-II.c showed peaks between δ 170-175 due to the carbonyl carbon of ester formed by phenolic units. Polyesters containing camphanediol showed an additional carbonyl carbon peak between δ 167-164. Peaks at δ 124- 156 are due to aromatic carbon

The UV-Vis absorption spectra of the polymers were measured using diffused reflectance method of powder samples. All polymers showed the characteristic azo peak at 360-365 nm and all polymers except Pol-II.c showed characteristic bands due to nitro group at 320 nm. The peak positions in the UV-Vis absorption of polymers were found to be similar to those of corresponding monomers (330 and 375 nm). These results suggest that polar properties of the chromophore part is not much changed by the polymerization process.

The fairly high values for specific rotation show that no extensive racemization has occurred during polymerization stage. The $[\alpha]$ value increased with increase in the percentage of (1R, 2S, 3R, 4S)-camphanediol. The $[\alpha]_D$ values of the polymers were also measured after cooling from high temperature (200°C) below their decomposition temperature. There was only slight change in $[\alpha]$ values. This showed that the polymers even at a high temperature could retain the chiral order. The yield and properties of all polyesters are summarized in Table 4.17.

Table 4.17: Yield and properties of polyesters

<i>Polymer</i>	<i>Yeild (%)</i>	<i>Chiral Composition</i>	$[\alpha]_D$	<i>SHG Efficiency (MNA Reference)</i>
Pol-0	82	0	0	0.50
Pol-II.a	88	25	-25.0	0.88
Pol-II	83	50	-31.4	1.5
Pol-II.b	79	75	-36.8	1.1
Pol-II.c	81	100	-46.0	0.91

SHG efficiency

From Table.4.17, it can be seen that when the chiral loading increases SHG efficiency increases and has the maximum at 50% chiral loading. The SHG efficiency decreases with increase in chiral loading and results in a parabolic curve (Figure 4.18).

The chirality of the polymer systems, synthesized from a polar chiral monomer and a

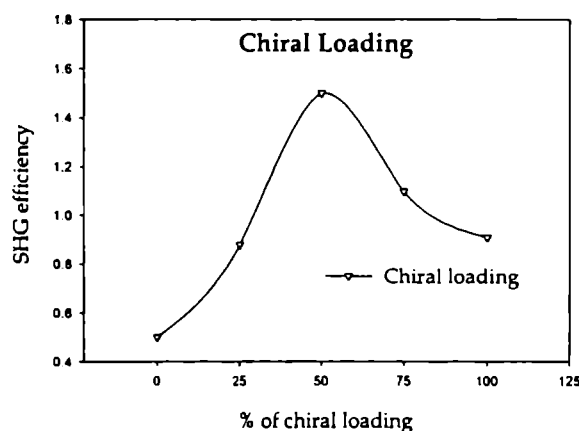


Figure 4.18 Variation of SHG efficiency with chiral loading

dipolar chromophore, enhances the nonlinear optical response in two ways: first by eliminating the dipolar interactions between the chromophores which allows very high chromophore concentration, and second by chiral contributions.⁸ Since both the chiral monomer and the chromophores are dipolar molecules it is necessary to optimize chiral loading according

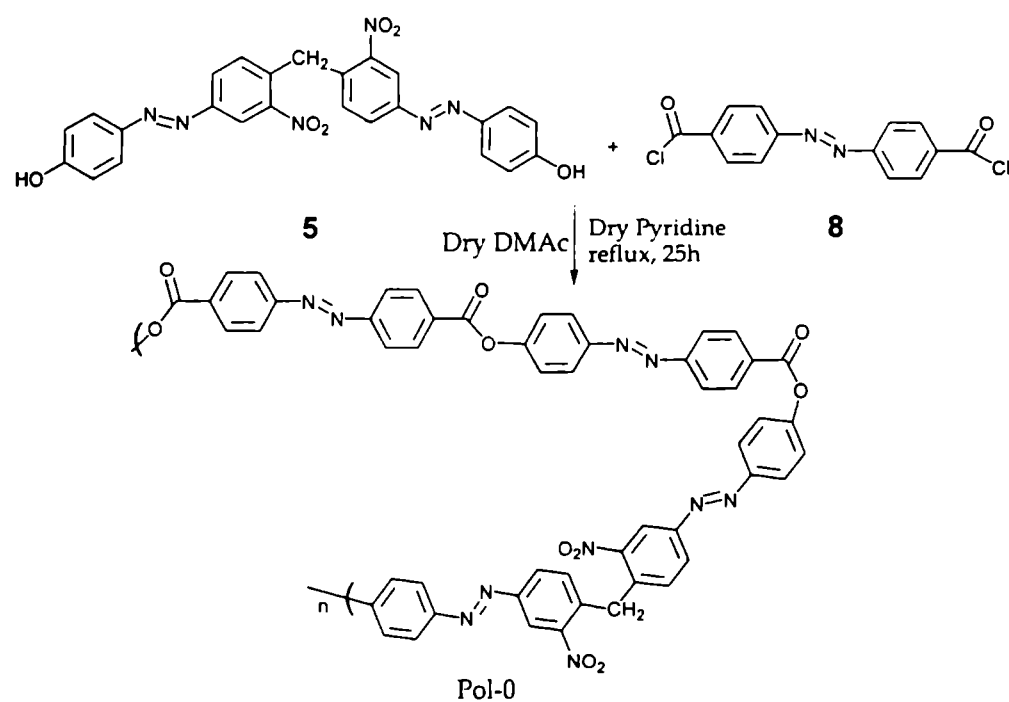
to the polar orientation. More over, the Λ shaped chromophore is the one that gives the Λ helical orientation to the polymer chain; hence, the concentration of Λ chromophore is also important here. Up to 50% chiral loading, the SHG signal increases because of the chiral contribution and decrease in dipolar interaction due to the presence of chiral molecule. After 50%, even though the chiral contribution increases, the SHG efficiency decreases due to the increase in dipolar interaction of the chiral molecules and the decrease in the possibility of attaining charge asymmetry. The decrease in the amount of big Λ shaped chromophore increases the dipolar interaction between the chiral molecules, and reduces the polar order; hence decreases the SHG efficiency. Thus for all further synthesis the chiral loading has been kept at 50%

4.4.2.2. *Synthesis and characterization of polymers with different chiral molecules*

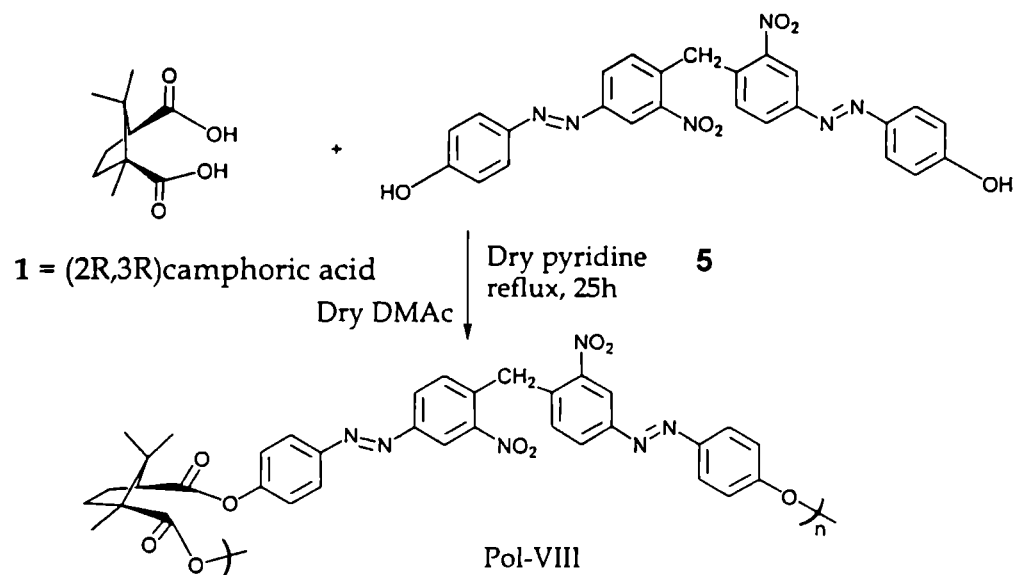
All polymer syntheses were done in solution method at high temperature. 4,4'-azobenzene dicarbonyl chloride (9) was dissolved in extremely dry dimethyl acetamide

(HPLC grade, s. d Fine). To this solution was added chiral molecule and bis(4-hydroxyphenylazo)-2,2'-dinitrodiphenylmethane (4). Few drops of extremely dry pyridine (99.99% dry pyridine, s. d. fine) were added as acid acceptor. The mixture was heated under stirring for 25h at 160° C. The product was precipitated from cold methanol and washed continuously with hot water, methanol and acetone. After filtration and drying a brown solid was obtained.

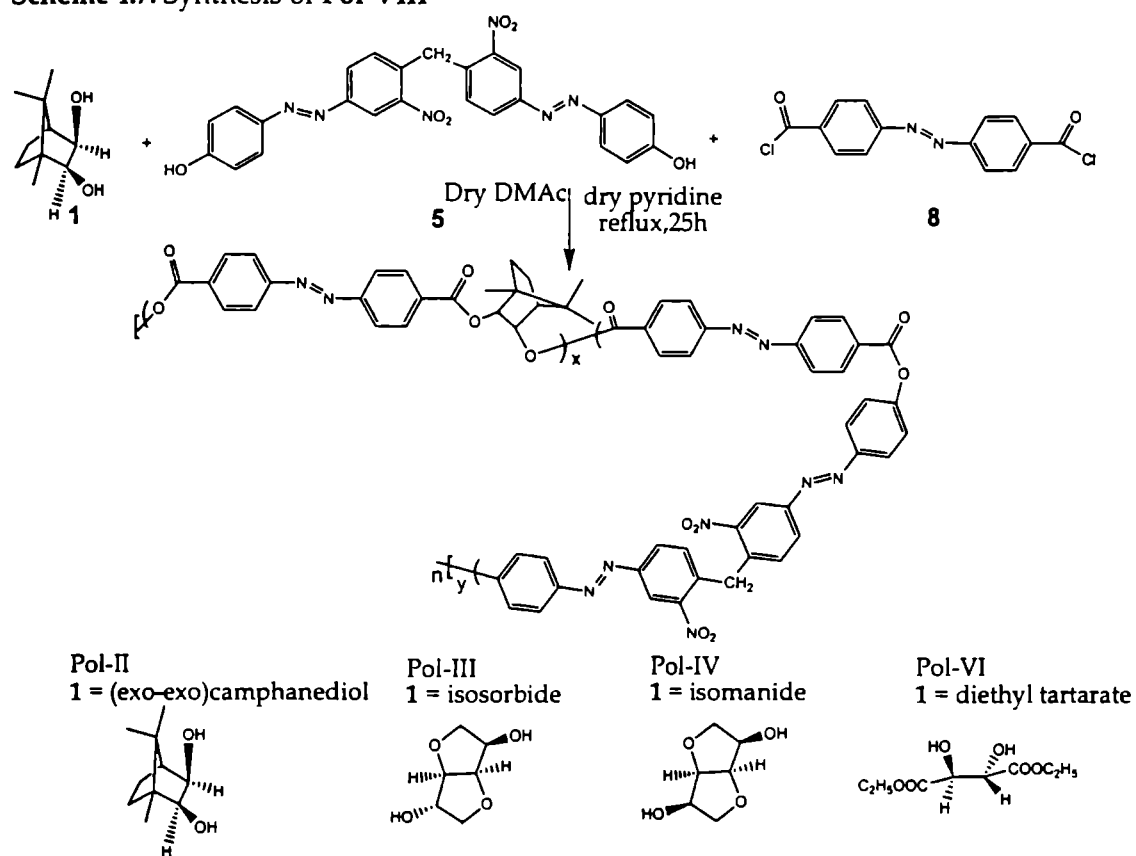
Pol-0: Synthesized according to Scheme 4. 6. **Pol II, Pol-III , Pol-IV and Pol-VI:** Synthesized according to Scheme 4.8



Scheme 4.6. Synthesis of Pol-0



Scheme 4.7. Synthesis of Pol-VIII



Scheme 4.8. Synthesis of Pol-II, Pol-III, Pol-IV, Pol-VI

Characterization was described in section 4.4.2.1

Characterization

Characterization of **Pol-II** was described in section 4.4.2.1

Pol-III (Yield 88%) and **Pol-IV** (Yield 86%) are different only in the stereochemistry of chiral monomers. So their spectral patterns are similar except in ¹H NMR. But in ¹H NMR the -CH protons which have varied stereochemistry in isosorbide and isomanide appeared as multiplets. So a distinction between them is difficult.

Spectral analysis

UVλ_{max} (solid) nm : 360 (π→π*, N=N), 322 (n→π*, NO₂)

IR(KBr pellet) cm⁻¹ : 1760-1750 (C=O str. ester formed by phenolic unit), 1720-1735 (C=O str. ester formed by isosorbide or isomanide unit), 1520-1530 (N-O str.), 1350-1373(C-NO₂), 1610-1620 (-N=N-), 2900-3000 (sp³ -C-H stretch in isosorbide or isomanide unit), 1470-1473 (sp³ C-H bend in isosorbide or isomanide unit), 1235-1240 (C=O str. In isosorbide or isomanide unit)

¹H NMR (300 MHz, DMSO-d₆) : δ 4.4 - 4.8 (m, -CH isosorbide or isomanide unit), 4.2 (q - CH₂ in isosorbide or isomanide unit), 4.0 (t, bridge CH in isosorbide or isomanide unit) 6.4 (s, -CH₂), 7.6-8.9 (m, aromatic).

¹³C NMR (75 MHz, DMSO-d₆) : δ 171 (C in ester formed by phenolic unit), 167-164 (C in ester formed by isosorbide or isomanide unit), 124-156 (aromatic carbons), 74 (-CH₂ in isosorbide or isomanide unit), 75 (-CH in isosorbide or isomanide unit), 92 (-CH bridge in isosorbide or isomanide unit), 37 (methylene carbon).

Pol-VI

Yield -79 %

Spectral analysis

UVλ_{max} nm : 360 (π→π*, N=N), 322 (n→π*, NO₂)

IR(KBr pellet) cm⁻¹ : 3000, 2960, 2900 (sp³ -C-H stretch in tartrate unit), 1760-1750 (C=O str. ester formed by phenolic unit), 1725(C=O str. ester formed by tartrate), 1610-1620 (-N=N-), 1520-1530(N-O str.), 1470 (sp³ C-H bend of CH₂ in tartrate unit), 1380 (C-H bend of CH₃ group), 1350-1373(C-NO₂).

^1H NMR (300 MHz, DMSO- d_6) : δ 1.2 (t, CH_3 in tartrate unit), 4.1-4.3 (q, $-\text{CH}_2$ in tartrate unit), 5.4 (s $-\text{CH}$ tartrate unit), 6.4 (s, $-\text{CH}_2$), 7.8-8.9 (m, aromatic)

^{13}C NMR (75 MHz, DMSO- d_6): δ 174 (ester carbon in tartrate unit), 171 (C in ester formed by phenolic unit), 164 (C in ester formed by tartrate unit), 124-156 (aromatic carbons), 75 ($-\text{CH}$), 63 (CH_2), 37 (methylene carbon), 14 (CH_3)

Pol-VIII: was synthesized according to **Scheme 4.7**.

Characterization

Yield- 85%

Spectral analysis

$\text{UV}\lambda_{\text{max}}$ (solid) nm : 361 ($\pi \rightarrow \pi^*$, $\text{N}=\text{N}$), 320 ($n \rightarrow \pi^*$, NO_2)

IR(KBr pellet) cm^{-1} : 1720 ($\text{C}=\text{O}$ str. ester formed by camphoric acid unit), 1520 ($\text{N}-\text{O}$ str.), 1350($\text{C}-\text{NO}_2$), 1610-1620 ($-\text{N}=\text{N}-$), 1219-1224 (doublet, $\text{C}(\text{CH}_3)_2$ of camphoric acid) 2900-3000 (C-H stretch in camphoric acid)

^1H NMR (300 MHz DMSO- d_6) : δ 1.25 (s, bridged $-\text{C}(\text{CH}_3)_2$ of camphoric acid), 1.3 (s, $-\text{CH}_3$ of camphoric acid), 1.9-2.2 (m, $-\text{CH}_2$ cyclopentane ring of camphoric acid), 2.5(t, $-\text{CH}$ cyclopentane ring of camphoric acid), 5.2 (s, $-\text{CH}_2$), 7.6-8.4 (m, aromatic)

^{13}C NMR (75 MHz DMSO- d_6): δ 179, 178 (C of ester formed by camphoric acid unit) 162, 154 (C, $-\text{CO}$ of phenolic group) 120-156 (aromatic carbons), 53 (carbon from bridge head $\text{C}(\text{CH}_3)_2$), 36 (bridge head $-\text{CH}$), 34, 32 (methylene from cyclopentane of camphoric acid) 30 (methylene carbon), 22 (methyl carbon from $-\text{C}(\text{CH}_3)_2$), 19 (methyl carbon from bridge head $-\text{CH}_3$).

Mass spectrum (**Figure 4.19**) of **Pol-IV** ($m/e = 19686$) equivalent to 17 repeating units (one repeating unit = 1158) is in good agreement with the proposed type of polycondensation as one repeating unit of polyester contains two diacid chloride molecule condensed with one chiral unit and one biphenol unit. The mass spectrum also gives an idea about the degree of polymerization. The high temperature polycondensation method has yielded high molecular weight polyesters

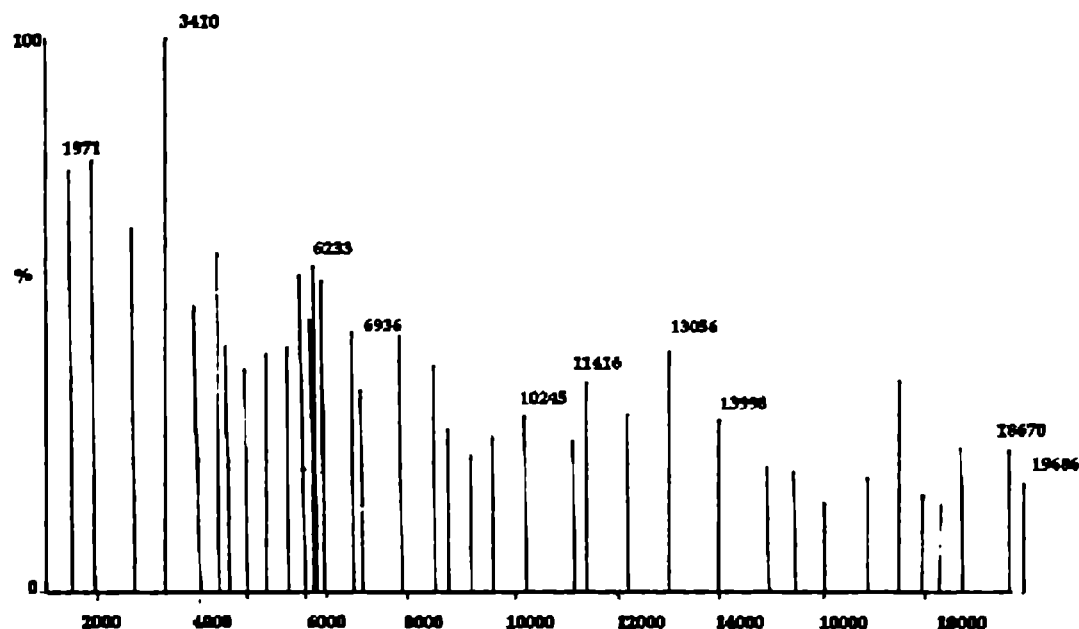


Figure 4.19 Mass spectrum of Pol-V

4.4.2.3. Thermal properties of the polyesters

Glass transition temperature of the polyesters ranges from 30-200^o C (Table 4.18). Since T_g is a measure of long-range order and decrease in segmental motion in polymers, high T_g values indicate the high degree of polar order. It is interesting to note that the polymers with chiral molecules have high T_g values compared to the polymer with out chiral molecule. The introduction of chiral molecule in to the polymer main chain reduced the flexibility of polymers considerably. Also the presence of polar groups increases the T_g of the polymers. The polyesters with isosorbide (152.05^o C), isomanide (197.84^o C), and diethyl tartrate (138.43^o C) have shown high T_g values which indicate that the polar ordering in these systems are really good. The camphoric acid system is also having comparably good T_g value (94.18^o C). Even though camphanediol system has shown the lowest T_g value (52.5^o C), it is higher than the polymer with out chiral molecule (30.3^o C). Thus from T_g , it is very clear that incorporation of chiral molecule increases the polar ordering of the polyesters and increases the SHG efficiency. The polyester with the highest T_g values is the one that contains isosorbide or isomanide. The chiral building unit serves as a part of the chain and decreases the segmental motion considerably; hence introduce high order in the polymer chains. The stereochemical

dependence of these polymers towards polar order can be proved from the Tg values of the polymeric systems. It can be seen that the system with isomanide has shown higher Tg value than the isosorbide system. These two polymers differ each other only in the stereochemistry of isosorbide and isomanide units. The stereochemistry has played a vital role in Tg through polar ordering. Usually the system with *trans* form shows lower Tg value than *gauche* form due to the flexibility of the *trans*. Also the molecule with symmetrically ordered polar groups have low Tg value than the one with unsymmetrically placed polar group.⁵³ In isosorbide, the -OH groups are more symmetrically placed than isomanide. This decreases Tg of polymer containing isosorbide. From the structures of polymers containing isosorbide (Pol-III) and isomanide (Pol-IV), it can be seen that uniform stacking of isomanide polymer is very easy, because the -OH groups are oriented in the same direction; where as in isosorbide polymer, the uniform stacking is difficult due to oppositely oriented -OH groups. Thus the polymer with isomanide has more polar order and has shown higher Tg value compared with the polymers with isosorbide, in which polar ordering is reduced by the presence of oppositely oriented -OH groups. And also, the system with high polar order will show high SHG efficiency.

The initial decomposition temperature (IDT) for all polymers is above 200^o C which indicates that all are thermally stable. The polymer with out chiral molecule has the minimum value of IDT (200^o C) implying that the incorporation of chiral molecule increases the polymer stability also. The isomanide and isosorbide systems have higher thermal stability than other polymers. Thus from the thermal studies, it can be concluded that the polymers incorporated with heterocyclic ring systems are good systems with high Tg and IDT.

4.5. Evaluation of second harmonic generation efficiency

The NLO efficiencies of the polyesters were determined with 2-methyl-4-nitroaniline as the standard using Kurtz and Perry method.⁵⁴ Measurements were done by the powder method with a Quanta-Ray Nd:YAG laser from Spectra Physics (1064 nm, 10 ns, 365mJ/S) integrated over 20 pulse and an average of 10 pulse. The samples

were ground and graded with standard sieves to the phase matching size (100-150 μm) and loaded on cuvette with 1mm thickness. MNA samples used as standards were also powdered and sieved (100-150 μm) after drying under high vacuum. They were also mounted with the same thickness as the polymer sample. The laser beam was directed unfocused onto the sample kept at 45° angle to the laser beam which provided the phase matchable situation; the emission was collected from the front face of the sample at 90° angle. The SHG signal; at 532 nm was detected by Avantes 2048 spectrometer with CCD camera. The results are shown in Table 4.18.

It can be seen that all the polyesters are efficient materials for SHG. The polymer with out the chiral unit also shows SHG efficiency comparable with that of reference MNA (95%). This is because of the Λ helical structure of the polyester, due to the Λ monomer bis(4-hydroxyphenylazo)-2,2'-dinitrodiphenylmethane (BHDM) (5).Figure 4.20.

Table 4.18: Yield and Properties of Polyesters

<i>Polymer</i>	<i>Chiral monomer</i>	<i>Yield</i> (%)	<i>Tg</i> ($^\circ\text{C}$)	<i>IDT</i> ($^\circ\text{C}$)	$[\alpha]_D$	<i>SHG</i> <i>Efficiency*</i>
Pol-II	(exo-exo) Camphanediol	83	52.5	252	-35.6	2.86
Pol-III	Isosorbide	88	152.05	278	+25.0	2.80
Pol-IV	Isomanide	86	197.84	287	+31.4	3.83
Pol-VI	(2R,3R)Diethyl tartrate	79	138.43	231	+36.8	3.07
Pol-VIII	(1R,3S) Camphoric acid	85	94.18	242	+43.9	2.99
Pol-0	With out chiral molecule	82	30.3	200	0.0	0.95

*(MNA Reference), MNA SHG efficiency =1

The polymers with chiral monomers have shown higher SHG efficiency than the reference MNA (three times greater than that of MNA). This is because of increased chirality and increased asymmetry of the polymer chains after incorporating the chiral molecules. Main chain chirality induces chemical poling, i.e., the directional orientation of the dipolar ends with out external poling. The significantly higher nonlinear optical susceptibility of the copolymers discussed in this study indicates considerable

contribution from the chirality of the polymer. Since these polymers are oriented as Λ helix, (Figure 4.20.), it is assumed that the copolymers have broken symmetries along the substrate normal. They therefore, belong to the symmetry group C_a ; even though the monomeric units belong to C_1 point group. For such samples with C_a symmetry, there are four nonvanishing macroscopic susceptibility components; i.e., χ_{zzz} , χ_{xxz} , χ_{zxx} and χ_{xyz} . The first three components have originated from the polar ordering, while the latter can only be present in chiral media. Strong coupling exists between the chiral helical domains and the push-pull azobenzene chromophoric groups. The electron delocalisation due to the π - π^* transition of the azobenzene system induces a displacement of electrons along the helical conjugated backbone. The chance for the existence of a long-range helical order in such polymer systems is rare, because, the arrangement of chiral units and chromophore units is highly random, but helical ordering (short range) is found in the polymers for the segments containing chiral units. This short range polar ordering can be proved from the high T_g values of polymers containing chiral molecules. Thus, the Λ helical structure can supplement the directional order of donor-acceptor π electron system and the dipole units are tilted in one direction along the polymer axis which leads to large values of χ_{zzz} , χ_{xxz} , χ_{zxx} , thus a high second harmonic generation efficiency. At the same time, the over all macroscopic chirality, and the chirality because of the presence of chiral monomers in the polyesters increase the value of chiral tensor χ_{xyz} . Thus chirality of the polymer systems enhances the nonlinear optical response in two ways: first by eliminating the dipolar interactions between the chromophores and second by chiral contributions.

As obtained from the theoretical calculation, to prove the stereochemical effect by molecular design, the polymers with isosorbide and isomanide chiral molecules have been synthesized. The SHG efficiency of these systems was measured with respect to MNA. It has been seen that, as predicted from the theoretical calculation, polyester with the isomanide system showed 175% more SHG efficiency (3.83 times that of MNA) than that of the polymers with the isosorbide system (2.8 times than that of MNA). The theoretical reason was discussed in section 4.3.2.1.c. From a stereochemical point of



Figure 4.20.
AM1 Optimized Structure
of 3 repeating units of Pol-
VI.

view, it can be explained on the basis of the polar ordering and absence of dipolar interaction. Even though the chiral molecule, isosorbide and the polymer with isosorbide have more ground state dipole moment than the isomanide and isomanide polymer, the more ordered and symmetrically packed bipolar ones are in the latter compared to the former. This is by virtue of the dipole orientation in isosorbide and isomanide. In isomanide, both the $-OH$ groups are oriented in the same direction, while in isosorbide, $-OH$ groups are oriented in the opposite direction. Higher T_g value of isomanide system, confirmed this observation. SHG efficiency is directly proportional to polar ordering of the system. Thus isomanide system has more SHG efficiency than isosorbide system even though its microscopic chiral tensor ($\beta_{xyz} = 103.5382$) contribution to macroscopic chiral tensor χ_{xyz} is smaller than isosorbide system ($\beta_{xyz} = 128.0857$). It can be concluded that the stereochemistry of chiral molecules, through the polar ordering of polymers, plays an important role in achieving highly active polymers capable of second harmonic generation.

4.6. Correlation of theoretical and experimental results

The SHG efficiency has shown similar trends in theoretical calculation and experimental measurements (Table 4.19). Polymers with chiral units showed more nonlinear optical susceptibility than MNA in both theory and experiment. Polymer which contains isomanide as the chiral molecule showed maximum second order response in both theoretical calculation and experimental measurements. Polymer which contains isosorbide showed minimum value of β .

Table 4.19: Comparison of theoretical calculation with experimental measurements

<i>Polymer</i>	β (10^{-30}) <i>esu</i> (<i>Static</i>)	β (10^{-30}) <i>esu</i> (<i>Dynamic</i>)	<i>SHG Efficiency</i> *
Pol-II	10.23	338.99	2.86
Pol-III	7.86	630.23	2.80
Pol-IV	10.22	708.58	3.83
Pol-VI	10.17	364.99	3.07
Pol-VIII	12.64	478.54	2.99
Pol-0	7.60	4.27	0.95
MNA	4.08	202.40	1.00

*Experimental β values of polymers compared with that of MNA

Both *ab initio*-CPHF (*Static*) and ZINDO-SOS(*Dynamic*) calculations are in good agreement with the experimental results. Still, the experimental results match more closely with the ZINDO-SOS calculation. As explained earlier, this variation in *static* calculation is because of the derivative formalism rather than the SOS one. In experimental measurements, electrons will go to possible higher energy states; thus higher energy contribution may not be too small to neglect. But *ab initio*-CPHF is numerically more accurate and precise in predicting the trends.

4.7. Conclusion

The influence of chirality can be used to advantage in designing second order nonlinear optical materials. Chiral molecules have no reflection symmetry and occur in two forms that are mirror images of each other. Such molecules are non-centrosymmetric with a nonvanishing electric-dipole allowed second-order response. Theoretical designing of NLO active polymer with high SHG response is in good agreement with the experimental results. Chirality of the polymer systems enhances the nonlinear optical response in two ways: first by increasing the polar order of the polymeric system and second by chiral contributions. In the systems described here, the chirality of Λ helical structure can supplement the directional order of donor-acceptor π

electron system and the dipole units are tilted in one direction along the polymer axis which leads to large values of χ_{zzz} , χ_{xxz} , χ_{zxx} , thus a high second harmonic generation efficiency. At the same time, the over all macroscopic chirality and the presence of chiral monomers in the polyesters increase the value of chiral tensor χ_{xyz} . Since the polar ordering is vital in the case of polymers incorporating polar chiral monomers, the stereochemistry of the chiral monomer plays an important role in designing efficient polymeric SHG materials. The contribution from the chiral component β_{xyz} is also important in designing SHG material, since it determines the macroscopic chiral susceptibility tensor χ_{xyz} which is one of the four major non vanishing susceptibility tensors of a C_α symmetry group such as Λ helix. An easy and facile way to synthesize thermally stable and crystalline polymeric materials for nonlinear optics are studied which have given good SHG response compared to MNA.

References:

- (1) Prasad, P. N.; Williams, D. J. *Introduction to Nonlinear Optical Effects in Molecules and Polymers*; Wiley: New York, 1991.
- (2) Nalwa, H. S.; Miyata S. *Nonlinear Optics of Organic Molecules and Polymers*; CRC Press: New York, 1997.
- (3) Boyd, R. W. *Nonlinear Optics*; Academic Press: San Diego, 1992.
- (4) Giordmaine, J.A. *Phys.Rev.* 1965, 138, A 1599.
- (5) Rentzepis, P.M.; Giordmaine, J. A.; Wecht, K.W. *Phys. Rev. Lett.* 1976, 37, 431.
- (6) Verbiest, T.; Clays, K.; Samyn, C.; Wolff, J.; Reinhoudt, D.; Persoons, A. *J Am Chem Soc* 1994, 116, 9320.
- (7) Verbiest, T.; Elshocht, S. V.; Kauranen, M.; Hellemans, L.; Snauwaert, J.; Nuckolls, C.; Katz, T. J.; Persoons, A. *Science*,1998 282, 913.
- (8) Koeckelberghs, G; Vangheluwe, M; Picard, I; De Groof, L; Verbiest, T; Persoons, A; Samyn, C. *Macromolecules* 2004, 37, 8530.
- (9) Han, S. H.; Belkin, M.A.; Shen, Y. R.; *Phys Rev. B* 2002, 66, 165415.
- (10) Simpson, G. J; Perry, J. M; Ashmore-Good C. L *Phy. Rev.B* 2002, 66, 165437.
- (11) Verbiest, T.; Van Elshocht, S.; Persoons, A.; Nuckolls, C.; Phillips, K. E.; Katz,

- T. J. *Langmuir* **2001**, *17*, 4685.
- (12) Makki, J. J.; Kauranen, M.; Persoons, A.; *Phy. Rev. B.* **1995**, *51*, 1425.
- (13) Walba, D.M.; Xiao, L.; Keller, P.; Shao, R.F.; Link, D.; Clark, N.A. *Pure and Appl. Chem.* **1999**, *71* 2117.
- (14) Bahulayan, D.; Thomas, V.; Sreekumar, K. *Proc SPIE, Smart Mater, Struct. MEMS* **1998**, 3321, 413.
- (15) Maniram, K. A.; Sreekumar, K. *Proc SPIE, Smart Mater, Struct. MEMS* **1998**, 3321, 67.
- (16) Bahulayan, D.; Sreekumar, K. *J. Mater. Chem.* **1999**, *9*, 1425.
- (17) Burland, D. M.; Miller, R. D.; Walsh, C. A. *Chem. Rev.* **1994**, *94*, 31.
- (18) Angiolini, L.; Caretti, D.; Giorgini, E. S. *Polymer* **2001**, *42*, 4005.
- (19) Sandhya, K. Y. Pillai, C.K.S.; Tsutsumi, N. *Prog Polym. Sci.* **2004**, *29*, 45.
- (20) Bouman, M. M.; Haviga, E. E.; Hanseen, R. A. J.; Meijer, E. W. *Mol. Cryst. Liq. Cryst.* **1994**, *256*, 439
- (21) Hohenberg, P.; Kohn, W. *Phys. Rev.* **1964**, *136*, B864.
- (22) Kohn, W.; Sham, L. J. *Phys. Rev.* **1965**, *140*, A1133.
- (23) Salahub, D. R.; Zerner, M. C. *The Challenge of d and f Electrons*; ACS: Washington, D.C., **1989**.
- (24) Parr R. G.; Yang, W. *Density-Functional Theory of Atoms and Molecules*; Oxford Univ. Press: Oxford, **1989**.
- (25) Ridley, J.; Zerner, M. C. *Theor. Chim. Acta* **1973**, *32*, 111.; Bacon, D.; Zerner, M. C. *Theor. Chim. Acta* **1979**, *53*, 21
- (26) Gerratt, J.; Mills, I. M.; *J. Chem. Phys.* **1968** *49*, 1719
- (27) Karna S. P.; Dupuis, M. *J. Comp. Chem.* **1991**, *12*, 487
- (28) Karna S. P.; Dupuis, M. *J. Chem. Phys. Lett.* **2000**, *319*, 595
- (29) Dewar, M. J. S.; Zuebisch, E. G.; Healy, E. F.; Stewart, J. J. P. *J. Am. Chem. Soc.* **1985**, *107*, 3902
- (30) Karis, D. R.; Ratner, M. A.; Marks, T. J. *Chem. Rev.* **1994**, *94*, 195.
- (31) Lalama, S. J.; Garito, A. F. *Phys. Rev. A* **1979**, *20*, 20
- (32) Ouder, J. L.; and Chemla, D. S. *J. Chem. Phys.* **1977**, *66*, 2664

- (33) Ouder, J. L. *J. Chem. Phys.* **1977**, *67*, 446
- (34) Ouder, J. L.; Zyss, J. *Phys. Rev. A* **1982**, *26*, 2016
- (35) Simpson, G. J. *Chem. Phys. Chem.* **2004**, *5*, 1301
- (36) Bishop, D. M. *Adv. Chem. Phys.* **1998**, *104*, 1
- (37) Simpson, G. J. *J. Chem. Phys.* **2002**, *117*, 3398
- (38) Simpson, G. J.; Perry J. M.; Ashmore-Good, C. L. *Phys. Rev. B.* **2002**, *66*, 165437
- (39) Tsunekawa, T.; Yamaguchi, K. *Chem. Phys. Lett.* **1992**, *190*, 533
- (40) Tsunekawa, T.; Yamaguchi, K. *J. Phys. Chem.* **1992**, *96*, 10268
- (41) Organic synthesis, Vol 79, 125
- (42) Fieser, L. F; Fieser, M. *Reagents for organic synthesis*; John Wiley and Sons: New York, **1982**
- (43) Schwartz, *Chem. Eng. News* **1978**, *24*, 88
- (44) Perrin D. D.; Armarego, W. L. F. *Purification of Laboratory Chemicals*; Pergamon press: New York, **1980**
- (45) Heldmann, C.; Warner, M. *Macromolecules* **1998**, *31*, 3519.
- (46) Zhao, Z. Li, Y.; Zhou, J.; Shena, Y. *Eur. Polym. J.* **2000**, *36*, 2417
- (47) Beltrania, T.; Boschb, M.B.; Centorea, R.; Concilio, S.C. *Polymer* **2001**, *42*, 4025
- (48) Zhang, Y.; Wang, T.; Wada, T.; Sasabe, H. *Polym. J.* **1997**, *29*, 685.
- (49) Tedder, J. M.; Venkataraman, K. *The Chemistry of Synthetic Dyes*, Academic Press: New York, **1970**
- (50) Kumar, S; Neckers, D.C *Chem. Rev.* **1989**, *89*, 17
- (51) Joshua, C.P.; Ramadas, P. K. *Synthesis* **1974** 573
- (52) M.L. Tomlinson, *J. Chem. Soc.* **1946**, 756
- (53) Brydson, J. A. *Plastics Materials*; Iliffe Books: London, **1966**
- (54) Kurtz, S. K.; Perry, T. T. *J. Appl. Phys.* **1968**, *39*, 3798

L-TYROSINE BASED CHIRAL POLY (ESTER-AMIDE) S CONTAINING MAIN CHAIN AND SIDE CHAIN AZO GROUP

5.1. Introduction

Amino acids and amino acid derivatives have been demonstrated to function as highly useful chiral auxiliaries for a variety of nitro aromatics and other D-A molecules with large hyperpolarizabilities.¹ Phasematching L-arginine phosphate crystals generates second harmonic signals greater than that of quartz.² Solid state structures of some urea-based peptidomimetics containing β -alanyl unit have shown self-assembly into highly ordered, extended hydrogen-bonded chains and ribbons with modest NLO activity.³ In addition to this function, these molecules are in their own right also of potential for second harmonic generation. Harmonic generation efficiency of single crystals of L-alanine,⁴ and L-threonine⁵ are well studied. Simple derivatives of amino acids have not been adequately examined, and many substances potentially useful for harmonic generation into the UV remain to be found. For example, among the derivatives of amino acids, N-acetyl cystein is highly crystalline, damage resistant, and has a powder efficiency about one-third that of urea.¹ L-tyrosine is an unexplored amino acid in the field of NLO studies. Present study has been focused on the molecular design of highly efficient chiral chromophore based on L-tyrosine.

In general, aromatic ring containing polyamide matrices, which are easily prepared from the corresponding carboxylic acid/anhydride functionalized monomers and the amino-functionalized ones, exhibit relatively high T_g 's. Indeed, the preparation of second-order NLO active main-chain and side-chain type polyamides has been reported.⁶ In our laboratory, poly (ester amide) s based on bismaleamic acid have been investigated as good SHG material.⁷ The primary interest of this study is to design and investigate the NLO properties of L-tyrosine based chiral poly (ester-amide) s

incorporated with different chiral and achiral moieties which increases the NLO response and also with high polymer stability by contributing high T_g values to the polymer.⁸

This chapter includes the design of L-tyrosine based chromophore with high β values. It also includes the design of chiral and achiral diols for polycondensation with the designed chromophore for the purpose of studying the effect of incorporation of additional chiral molecules into an already chiral medium. The synthesis was done after the design of the molecules and theoretical evaluations of the NLO properties was performed. Thus, the *state-of-art* of design and synthesis of highly active NLO materials have been followed in this study.

5.2. Computational methods

5.2.1. Monomers

Since L-tyrosine based chromophores contain more than 400 electrons, geometry optimizations including the polarized and diffused basis sets even with density functional methods are computationally highly demanding. Hence, all the monomers have been optimized to Hartree-Fock common level of theory to avoid the geometry effects in the prediction because of high sensitivity of polarizability to geometry. All the L-tyrosine based chromophores and diol monomers have been optimized with 6-31G basis sets using restricted Hartree-Fock formalism available with the Gaussian algorithm.⁹ The optimized geometries were used to compute the SCF MO energies. The *static* spectroscopic properties of monomers have been calculated using Coupled Perturbed Hartree-Fock (CPHF) method at RHF 6-31++G(d,p) level available in the Gaussian codes.¹⁰ The *dynamic* spectroscopic properties have been calculated using the Zerner's INDO-SOS method with sum over 82 states.¹¹

5.2.2. Polymers

All the polymer geometries (three repeating units) have been optimized using the AM1 parameterized Hamiltonian available in the Gaussian 03 set of codes.¹² The

geometries obtained by AM1 calculations have been compared with geometries obtained using *ab initio* methods at 6-31G level for polymers. Both the geometries have comparable bond lengths and bond angles. Compared to the small difference in bond length and bond angle, the computational demand for *ab initio* method is much more for polymers. Hence, geometry calculations are restricted to this semi-empirical level. Also, because of the very high cost of computation in calculating the properties of polymers (repeating units) using polarized and diffused basis sets, *static* (CPHF) molecular properties of polymers have been limited with 6-31 G(d) basis sets. The *dynamic* spectroscopic properties have been calculated using the Zerner's INDO-SOS method with sum over 82 states.

5.3. Designing of molecules

In this chapter, the main concentration was on the chromophore design based on L-tyrosine. Since L-tyrosine is a potential chiral auxiliary for NLO material, the goal has been targeted to the addition of nitroaromatics and donor-acceptor groups (e.g. *para*-nitroaniline, azo-acid chloride) into the L-tyrosine framework. The diols have been selected on the basis of the coupling ability with the L-tyrosine framework to form polymers with high β value. Both chiral and achiral diols have been selected so as to study the effect on the β value by the incorporation of chiral and achiral molecules in to a chiral medium

5.3.1. Monomer design

5.3.1.1 Chromophore

The route of chromophore design is shown in **Figure 5.1**. The basic chemistry, of organic donor- acceptor NLO materials has been developed on the basis of *para*-nitroaniline (**1**) In this design, *para*-nitroaniline (PNA) was diazotized and coupled with the amino acid, L-tyrosine (Tyr, **2**), to provide the basic chiral framework of (*S*)-2-amino-3-(3-(4-nitrophenylazo)-4-hydroxyphenyl) propanoic acid (PNATY, **3**). By the acylation of PNATY with azobenzene-4, 4'-dicarbonyl chloride (AZCl, **4**), chiral amide framework, bis(*S*)-2-(4-azanyl benzamido)-3-(3-(4-nitrophenylazo)-4-hydroxyphenyl) propanoic

acid (TYAZ, 5) was designed. Chlorination of TYAZ yielded the bis(S)-2-(4-azanyl benzamido)-3-(3-(4-nitrophenylazo)- 4-hydroxyphenyl) propanoic acidchloride (TYAZCl,6).

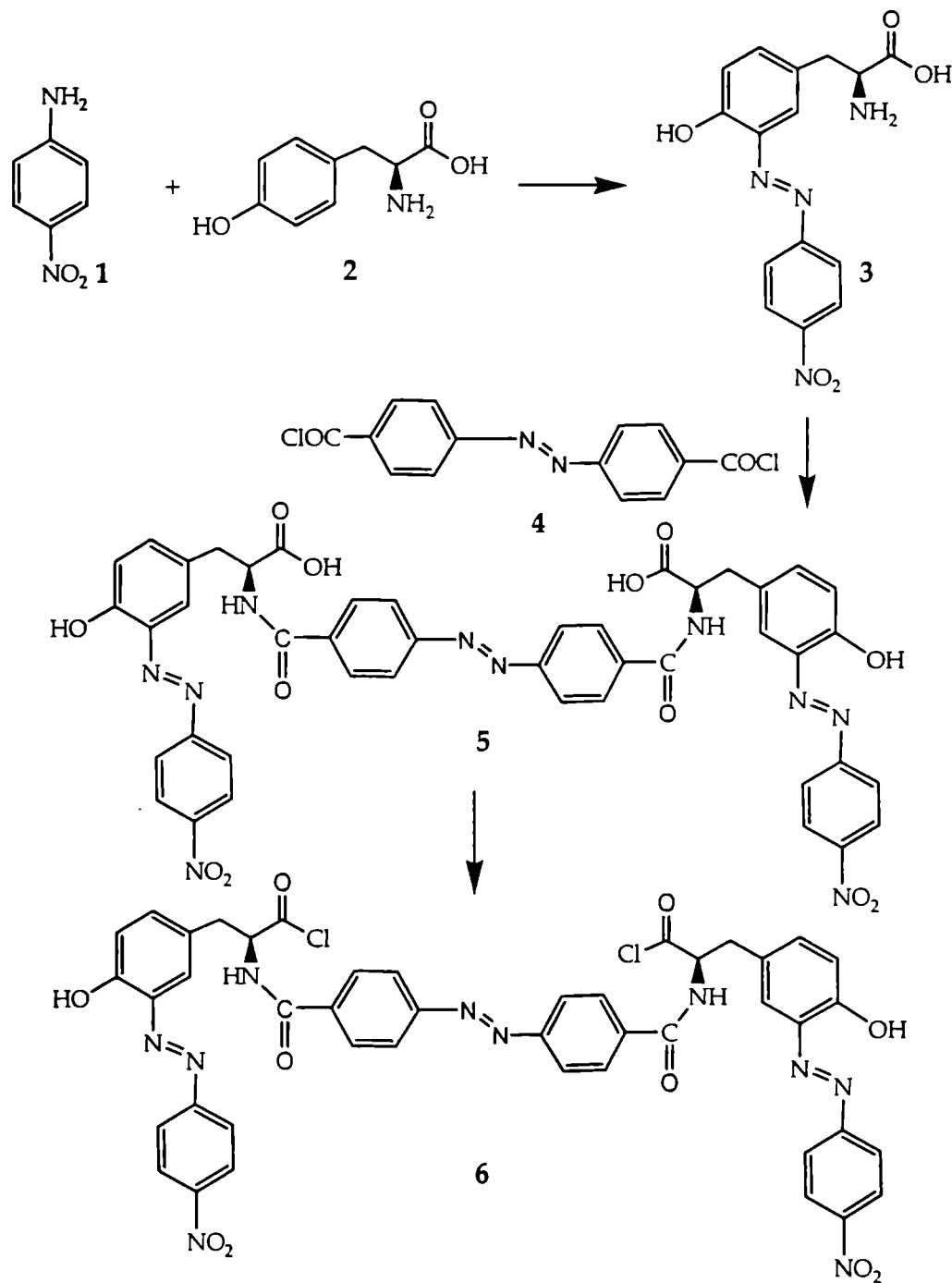


Figure 5.1. Route of chromophore design

5.3.1.1.1. *Static and Dynamic molecular property calculations*

5.3.1.1.1.a. Dipole moment

The values of *static* and *dynamic* dipole moment are given in Table 5.1. Since hyperpolarizability can be calculated as the second derivative of dipole moment, molecular design was concentrated on the molecules with higher dipole moment than the reactant molecule. As an established donor- π -acceptor system, PNA should possess a high dipole moment. From the CPHF-static calculations, the value obtained (7.9627D) is in good agreement with the experimentally determined value (7.2 D).¹³ This also indicates the accuracy of CPHF calculation.

Table 5.1: Dipole moment of chromophores in units of debye

<i>Chromophore</i>	μ_x	μ_y	μ_z	μ_g <i>static</i>	μ_g <i>dynamic</i>
PNA	6.9218	0.0026	-3.9362	7.9627	43.6312
Tyr	1.9130	1.5148	2.0806	3.2068	20.5722
PNATY	2.1497	1.5269	4.7942	5.4715	34.9174
AZCI	1.3614	0.0012	0.0114	1.3615	10.6268
TYAZ	7.6858	3.2330	-0.1818	8.3400	87.0284
TYAZCI	10.1682	4.5984	-0.0456	11.1598	99.5583

L-tyrosine has been used as a chiral auxiliary. It does not possess a high value of dipole moment (3.2068 D). But the coupled product (PNATY) of L-tyrosine with PNA has shown dipole moment (5.4715 D) higher than L-tyrosine and the acylation product (TYAZ) has a dipole moment value (8.3400) higher than that of PNA itself. Chlorination of TYAZ was carried out for the ease of polycondensation with diol molecules. The chlorinated product TYAZCI has high dipole moment. Thus the calculated dipole moment values are in good agreement with the predicted route of design. The ZINDO-SOS *dynamic* calculation follows the same trend as that of the *static* calculation.

5.3.1.1.1.b. Polarizability (α)

The polarizability values are summarized in Table 5.2. It can be seen that the linear polarizability values increase with each forward step in the molecular design. The

coupled product (3.4544 esu) of PNA (1.3474 esu) and L-tyrosine (1.6613 esu) has higher alpha value than that of the reactants. The final acylated (9.6115 esu) and chlorinated (8.5721 esu) products are also showing good alpha values compared with the reactant molecules. This indicates that the designed route is exactly following the goal of designing highly active chromophores for NLO applications.

Table 5.2: Polarizability α of chromophore

Chromophore	α_{xx}	α_{yy}	α_{zz}	α (au)	$\alpha_{tot} \times 10^{-23}$ Static*	$\alpha_{tot}^* \times 10^{-23}$ Dynamic*
PNA	121.6103	48.72226	102.4463	90.9263	1.3474	411.0
Tyr	132.5928	81.87931	121.8485	112.1067	1.6613	294.0
PNATY	221.9997	122.9558	354.3746	233.1100	3.4544	866.0
AZCI	202.9226	102.1023	389.5218	231.5155	3.4307	927.0
TYAZ	545.6926	587.1834	812.9603	648.6121	9.6115	1350.0
TYAZCI	505.0923	528.5364	701.7857	578.4714	8.5721	1430.0

* α (esu) = $0.148185 \times 10^{-24} \alpha$ (au)

5.3.1.1.1.c. Hyperpolarizability (β)

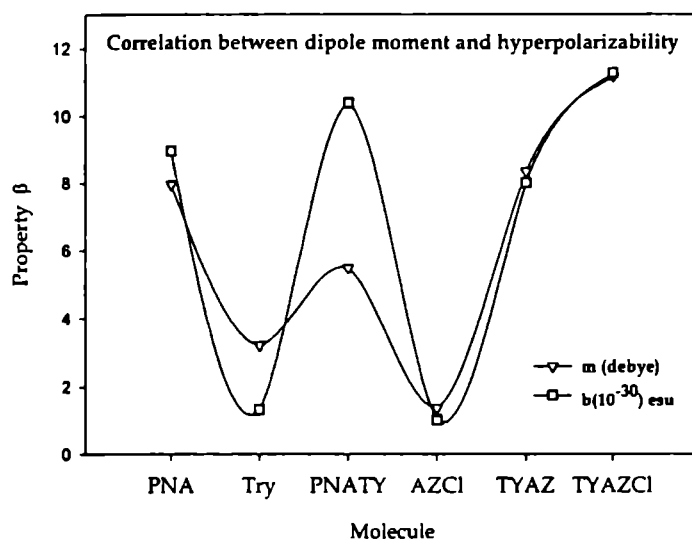


Figure 5.2. Correlation between dipole moment and hyperpolarizability

The static β values of chromophores are summarized in Table. 5.3 Static CPHF calculation of hyperpolarizability values has followed the designed route (based on the dipole moment). (Figure 5.2). Combination of PNA and Tyr produces a very good chromophore

PNATY with a good value of beta (10.374×10^{-30} esu). The static β value of TYAZ is not high as expected. The β value decreases after the acylation. This can be an inadequacy of static method due to the lack of including frequency in the calculation.

Table 5.3: HOMO-LUMO Gap (ΔE) in eV, Ground-State Dipole Moment (μ_g) in debye, Linear Polarizability (α) in units of 10^{-23} esu, and First Hyperpolarizability β , in units of 10^{-30} esu for the chromophores (ab initio CPHF static property calculations)

Chromophore	ΔE	μ_g	α	β
PNA	0.3507	7.9627	1.3474	8.9445
Tyr	0.3461	3.2068	1.6613	1.3165
PNATY	0.3248	5.4715	3.4544	10.374
AZCI	0.3309	1.3615	3.4307	1.0072
TYAZ	0.3264	8.3400	9.6115	8.0164
TYAZCI	0.3320	11.1598	8.5721	11.2620

Table 5.4: Oscillator strength f , Optical Gap (δE) in eV, Ground-State Dipole Moment (μ_g) in debye, Difference in dipole moments between ground state and excited state ($\Delta\mu$), Linear Polarizability (α) in units of 10^{-23} esu, and First Hyperpolarizability, in units of 10^{-30} esu for the chromophores (ZINDO SOS dynamic property calculations)

Chromophore	f	δE	$\Delta\mu$	μ_g	α	β_{vec}
PNA	1.0285	7.4823	14.1337	43.6312	411.0	220.3553
Tyr	1.2761	7.6630	6.6922	20.5722	294.0	51.1458
PNATY	0.9677	4.0466	28.1308	34.9174	866.0	226.5886
AZCI	1.3355	4.1932	3.3658	10.6268	927.0	106.8586
TYAZ	2.6372	4.4560	19.9043	87.0284	135.0	655.9493
TYAZCI	1.7055	4.4863	43.3013	99.5583	143.0	740.2353

In the dynamic ZINDO calculation the values are in good agreement with the proposed route. The acylated product, TYAZ and its chlorinated compound TYAZCI have shown the β values almost 3 times greater than PNATY. The results of dynamic ZINDO calculations are shown in Table 5.4. Even though the oscillator strength, f , of PNATY is small compared to all other molecules, the difference in dipole moment $\Delta\mu$ is

very large in this molecule. On the other hand, in TYAZ $\Delta\mu$ is smaller than PNATY, while the oscillator strength is the highest for this molecule. Thus, even by considering the ground state dipole moments can do prediction of the properties of the chromophore. But the exact picture of accurate and experimentally comparable results will be obtained from the *static* and *dynamic* calculations.

5.3.1.1.1. d. Chiral component

Table 5.5: First hyperpolarizabilities of chromophores β (Static) in units of au

β Tensors	PNA	Tyrosine	PNATyr	AZCl	TYAZ	TYAZCl
β_{xxx}	-713.4750	119.0279	72.9380	35.5150	-139.2570	-315.5060
β_{xxy}	0.0115	-8.1672	-10.9721	0.0007	463.1576	572.7625
β_{xyy}	38.5631	-10.7579	-15.0280	20.2807	-357.8430	-390.9130
β_{yyy}	0.1010	-27.8040	-20.0548	0.0498	-575.2070	-816.2450
β_{xxz}	620.9343	102.4751	281.3565	-1.9033	-368.2410	-515.5590
β_{xyz}	0.0481	21.6840	20.3777	-0.0641	402.8543	476.3268
β_{yyz}	-21.9295	-13.2235	46.7160	-0.0040	350.8687	497.3552
β_{zzz}	-225.082	26.5210	-1.5624	60.3724	-395.2590	-513.6710
β_{yzz}	0.0690	3.5213	-30.5448	0.1063	-126.9660	-210.4860
β_{zxx}	-87.2027	-26.0064	-1525.99	-7.9310	104.5484	86.4357
β_x	-899.9940	134.7910	56.3476	116.168	-892.3590	-1220.09
β_y	0.1816	-32.4499	-61.5717	0.1568	-239.0150	-453.9680
β_z	511.8021	63.2451	-1197.92	-9.8383	87.1761	68.2322
$\beta_{\text{vec}}(\text{au})^*$	1035.3410	152.3862	1200.826	116.584	927.9181	1303.596
$\beta_{\text{vec}}(\text{esu})^*$	8.9400	1.3200	10.4000	1.0100	8.0200	11.3000
%chirality	0.0046	14.4496	1.6969	0.0549	43.4148	36.5394

* β (10^{-32} esu) = 0.863916 β (au)

As explained in chapter 4, chiral component β_{xyz} plays an important role in the total macroscopic second harmonic generation efficiency χ_{xyz} . Since present chapter is mainly on the design of efficient chiral chromophores for the synthesis of polymers so as

to obtain highly efficient chiral polymeric material, it is necessary, to get a good idea about the chiral component β_{xyz} . Values of all the β tensor components of the molecules are summarized in Table 5.5. It can be seen that, the chiral tensor β_{xyz} component of chiral molecules are very large compared to that of the achiral molecules. The β_{xyz} of PNA and AZCI is almost zero while that of TYAZCI is very large (percentage chirality is 43.41%). Thus, from the *static* and *dynamic* calculations, it can be concluded that the molecule TYAZCI, designed based on L-tyrosine framework will give polymers with very high macroscopic NLO response by contributing a major amount from the chiral nature

5.3.1.2 Diol molecules

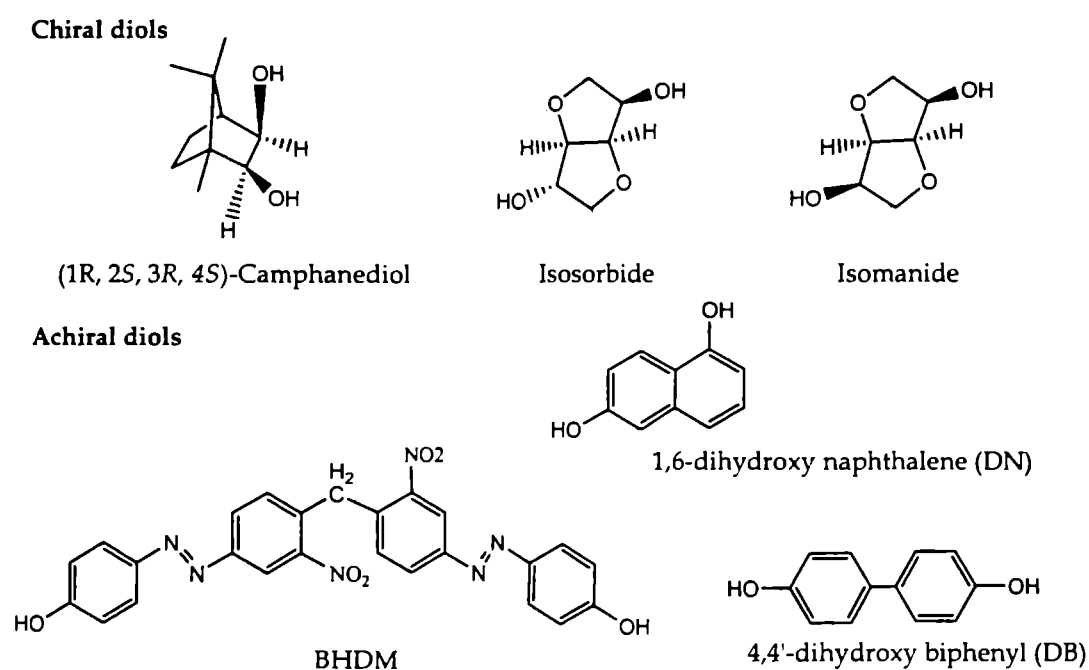


Figure 5.3. Diol molecules

The diol molecules have been designed for the purpose of designing of polymer by easy polycondensation with the previously designed L-tyrosine based chromophore. The effect of chiral and achiral diol incorporation into a chiral medium has also been

studied. Keeping both these aspects, six diol molecules have been selected. Three chiral diols such as (1R, 2S, 3R, 4S) camphanediol (exo-exo-camphanediol), isosorbide and isomanide and three achiral diols such as bis(4-hydroxyphenylazo) 2,2'-dinitrodiphenylmethane (BHDM), 4,4'-dihydroxy biphenyl and 1,6-dihydroxy naphthalene. The structures of the diol molecules are given in Figure 5.3.

5.3.1.2.1. Static and Dynamic molecular property calculations

5.3.1.2.1.a. Dipole moment

The dipole moment values of diol molecules are summarized in Table 5.6. In *static* calculation, the chiral diol molecules have almost the same range of dipole moment values ($\approx 3.5D$). The achiral diols have dipole moments ranging from 1D to 4D. Thus diol molecules with dipole moments ranging from 1D to 4D were selected for designing polymers. Since CPHF *ab initio* calculation is the one which gives the accurate and more precise results, designing was always done based on the CPHF values, while dynamic ZINDO-SOS will give the experimental trend. From the table, it is clear that even though dipole moment values are very different in both calculations (*static* and *dynamic*) the trend is same in both cases. In the diastereomers, isosorbide and isomanide, isosorbide has more dipole moment than isomanide.

Table 5.6: Dipole moment of diols in units of debye

Diols	μ_x	μ_y	μ_z	μ_g <i>static</i>	μ_g <i>dynamic</i>
Camphanediol	-2.5764	1.3194	1.4803	3.2512	18.8980
Isosorbide	1.9131	-1.9957	1.8971	3.6529	20.8563
Isomanide	1.2125	-3.3750	0.3430	3.3025	20.4036
BHDM	-3.4635	-0.2513	-3.1963	4.7197	40.7927
DB	2.4287	-1.0047	0.0164	2.6284	15.7150
DB	1.0882	-0.0012	-1.4253	1.7933	8.8863

5.3.1.2.1.b. Polarizability

In *static* calculation, linear polarizability of diol molecule follows almost the same trend as that of dipole moment. In chiral diol molecules, camphanediol has shown maximum α values. (Comparable with the B3LYP/6-31+G (d,p) *static* and *dynamic* calculation in chapter 4) In *dynamic* calculation, α of 4, 4'-dihydroxy biphenyl is greater than 1,6-dihydroxy naphthalene. The α values of achiral diols are large compare to the chiral ones. The polarizability values are tabulated in Table 5.7.

Table 5.7: Polarizability α of diols

Diol	α_{xx}	α_{yy}	α_{zz}	α (au)	$\alpha_{tot} \times 10^{-23}$	
					Static*	Dynamic*
Camphanediol	107.9886	111.1823	104.4454	107.8721	1.5985	37.00
Isosorbide	78.7438	69.8929	68.9770	72.5379	1.0749	30.30
Isomanide	78.5334	69.5514	68.4718	72.1855	1.0697	31.10
BHDM	277.3586	565.2625	327.4995	390.0402	5.7798	80.00
DB	123.6634	92.0073	201.3266	138.9990	2.0598	82.00
DN	129.3573	63.4897	157.5047	116.7839	1.7306	96.00

5.3.1.2.1.c. Hyperpolarizability

The hyperpolarizability(β) values obtained by *static* calculation of chiral and achiral diols are given in Table. 5.8. In the case of diol molecules, the β values are not in line with the dipole moment values as in the case of chromophore design. The β value of BHDM is very low from the expected value on the basis of dipole moment, where as 1,6-dihydroxy naphthalene has shown maximum value of β irrespective of its low dipole moment. It can be seen from the Table 5.8 that the HOMO-LUMO gap is the smallest in 1,6-dihydroxy naphthalene. Hence, charge transfer is easier in this molecule than any other diol and gives highest β value compared to all other diols concerned. The stereochemical effect explained in chapter 4 is prominent here also. The isomanide molecule is giving β value higher than its diastereomer, isosorbide. There is not much difference in β values with respect to chirality of the diols.

In *dynamic* calculation (Table 5.9) 1,6-dihydroxy naphthalene has shown a large β value compared to all other diols. It is surprising that in spite of a small difference in dipole moment $\Delta\mu$ (0.0011D), its β value is considerably large (115.4206×10^{-30} esu). While observing all other determining two-level parameters of β , it is clear that oscillator strength, which determines the transition probability, is comparatively high (6.6727eV) for this molecule.

Table 5.8: HOMO-LUMO Gap (ΔE) in eV, Ground-State Dipole Moment (μ_g) in debye, Linear Polarizability (α) in Units of 10^{-23} esu, and First Hyperpolarizability β , in Units of 10^{-30} esu for the diols (ab initio CPHF static property calculations)

Diol	ΔE	μ_g	α	β
Camphanediol	0.4316	3.2512	1.5985	1.4982
Isosorbide	0.4463	3.3529	1.0749	0.9714
Isomanide	0.4639	3.6025	1.0697	1.3064
BHDM	0.3350	4.7197	5.7798	1.4805
DB	0.3235	2.6283	2.0598	0.3914
DN	0.3195	1.7933	1.7306	2.3376

Table 5.9: Oscillator strength f , Optical Gap (δE) in eV, Ground-State Dipole Moment (μ_g) in debye, Difference in dipole moment between ground state and excited state ($\Delta\mu$), Linear Polarizability (α) in units of 10^{-23} esu, and First Hyperpolarizability, in units of 10^{-30} esu for the diols (ZINDO-SOS dynamic property calculations)

Diol	f	δE	$\Delta\mu$	μ_g	α	β_{oec}
Camphanediol	0.0421	13.1441	-5.8724	18.8980	37.00	2.1819
Isosorbide	0.0359	11.3503	-0.3471	20.4563	30.30	3.2231
Isomanide	0.0710	11.0648	29.9015	20.8036	31.10	4.7217
BHDM	1.3825	4.6927	19.6174	40.7927	400.0	188.9864
DB	1.4738	7.2836	-0.0003	15.7149	482.0	2.5727
DN	6.6727	1.6507	0.0011	8.8863	496.0	115.4206

Also, the optical gap, δE , which determines the energy gap between the ground state and the lowest dipole allowed excited state, is very small. Thus charge transfer is easier in

this diol and gives rise to high second order response. Here also, the effect of stereochemistry of the molecule on the value of β is observed with the diastereomers, isosorbide and isomanide.

5.3.1.2.1.d. Chiral component

The chiral tensor components β_{xyz} are given in Table 5.10. The β_{xyz} values of the chiral diols are considerably large (3.5 -5 %) compared to achiral diols. In dihydroxy naphthalene it is negligible (0.0071%), while in biphenyl, it is almost comparable with the chiral diols (2.7909 %). This may be ascribed to the prochiral nature of biphenyl ring due to atropisomerism.¹⁴

Table 5.10: First hyperpolarizability of chromophores β (Static) in units of au

β Tensors	Camphanediol	Isosorbide	Isomanide	BHDM	DB	DN
β_{xxx}	-10.6371	73.9567	43.0462	216.3546	18.7792	20.9918
β_{xxy}	43.8721	-9.3928	-37.2348	102.2397	-2.1011	-0.0338
β_{xyy}	1.8530	6.3835	3.9828	835.5654	6.1059	-42.8274
β_{yyy}	94.7726	-56.6015	-96.6737	319.2446	-7.8695	-0.0172
β_{xxx}	22.7889	23.1046	7.8848	60.2572	-19.4143	141.7935
β_{xyz}	-6.9460	5.9513	-5.1115	-10.5550	-1.2643	-0.0194
β_{yyz}	3.8116	5.4817	4.1440	874.8085	19.3518	-30.3861
β_{zzz}	2.8651	1.3445	3.8377	135.5568	16.9497	-77.9663
β_{yzz}	24.1143	4.0012	-7.7733	-174.7390	-7.4174	-0.0252
β_{zzz}	32.9739	17.5415	2.3473	275.6137	0.3694	-362.9200
β_x	-5.9190	81.6848	50.8667	1187.4768	41.8349	-99.8018
β_y	162.7591	-61.9931	-141.6820	246.7453	-17.3880	-0.0761
β_z	59.5744	46.1280	14.3761	1210.6794	0.3069	-251.5130
$\beta_{vec}(au)^*$	173.4205	112.4426	151.2212	1713.6887	45.3056	270.5901
$\beta_{vec}(esu)^*$	1.5000	0.9714	1.3100	1.4805	0.3910	2.3400
%chirality	4.0052	5.2927	3.8014	0.6159	2.7909	0.0071

* β (10^{-32} esu) = 0.863916 β (au)

5.3.2 Polymer design

Design of polymers was based on the polycondensation of TYAZCI with the previously designed chiral and achiral diols. The repeating unit contains one TYAZCI molecule and one diol molecule. All calculations have been performed for three repeating units. The polymers are shown in **Figure 5.4** and **Figure 5.5**. SHG property has been compared with respect to 2-Methyl, 4-nitroaniline (MNA) as the reference material. MNA and polymers were optimized and properties were calculated using common level theory so as to avoid geometry effects in predictions.

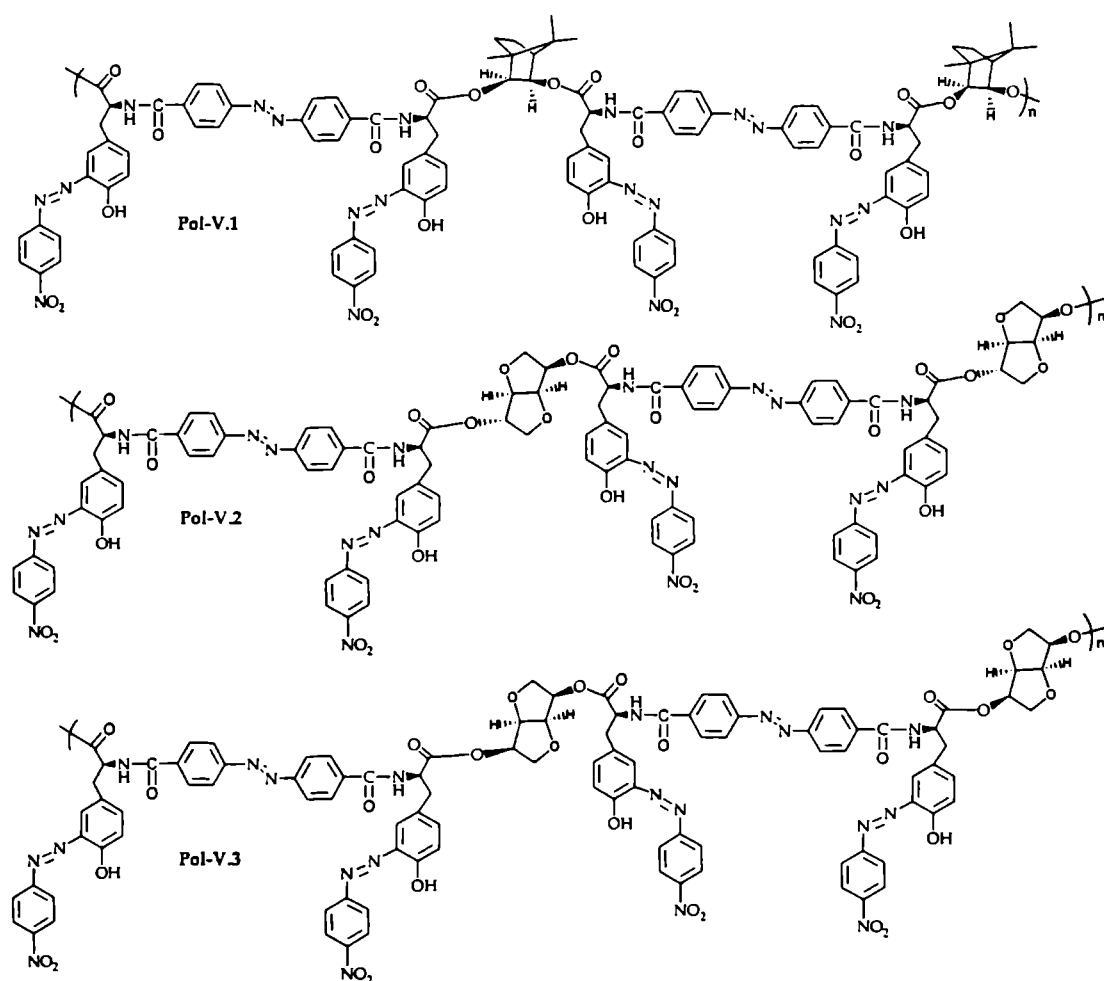


Figure 5.4. Structure of Chiral diol (2 repeating units) incorporated polymers (Pol-V.1, Pol-V.2, Pol-V.3)

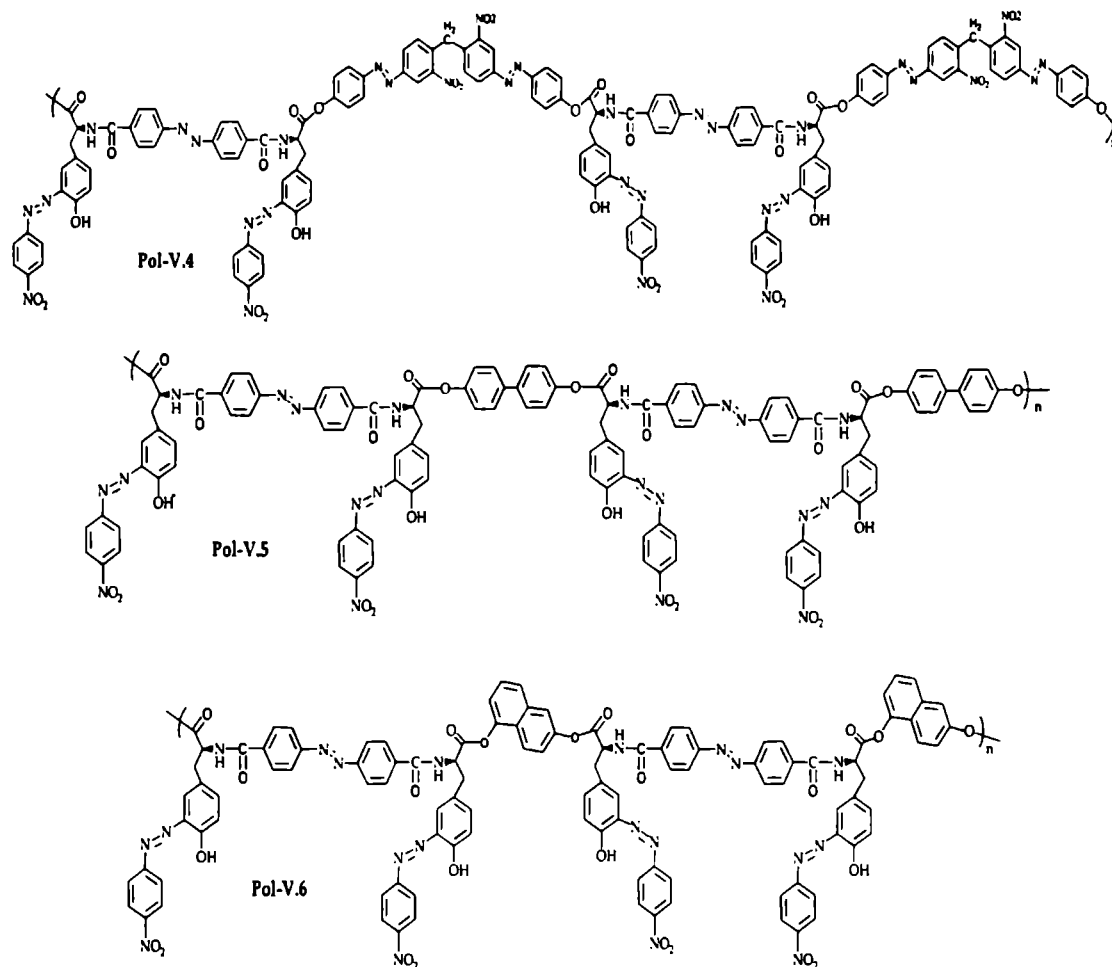


Figure 5.5. Structure of achiral diol (2 repeating units) incorporated polymers (Pol-V.4, Pol-V.5, Pol-V.6)

5.3.2.1 Static and dynamic molecular property calculations

5.3.2.1.a Dipole moment

All the polymers have shown large dipole moments compared to MNA (≈ 5 times). Chirality of chiral diol hasn't affected the dipole moment. Both types of polymers, the one designed from chiral diol and those designed from achiral diol have shown similar values of dipole moment. The dipole moment values of polymers are presented in Table 5.11.

Table 5.11: Dipole moment values of polymers in units of debye

Polymers	μ_x	μ_y	μ_z	μ_g Static	μ_g Dynamic
Pol-V.1	19.7620	8.7396	-0.8627	21.6255	242.1503
Pol-V.2	38.5563	6.7376	0.4145	39.1428	572.2634
Pol-V.3	26.9111	6.0175	-1.2337	27.6033	286.6680
Pol-V.4	8.5608	25.3201	-15.6744	30.9859	423.9742
Pol-V.5	34.1279	15.2220	-0.0963	37.3689	355.5187
Pol-V.6	29.3493	13.4670	-0.2270	32.2923	332.3781
MNA	0.1357	1.3755	-6.8645	7.0023	40.0614

5.3.2.1.b Polarizability (α)

Linear polarizability values are shown in Table 5.12. The chirality of the constituent diols has not affected the polarizability values. The structure of the polymers showed increased polar order by virtue of having greater contribution from the dipolar chromophoric groups (both azo group and amino-nitro group). All the polymers incorporated with chiral or achiral diols have shown the polarizability values in the same range ($\sim 35 \times 10^{-23}$ esu in static calculation). Both the calculations have shown that the present series of polymers have very high α values with respect to MNA. These indicate that these polymers can be used for optical devices.

Table 5.12: Polarizability (α) of polymers

Polymers	α_{xx}	α_{yy}	α_{zz}	α (au)	$\alpha_{tot} \times 10^{-23}$	
					Static*	Dynamic*
Pol-V.1	2022.926	2224.921	2758.197	2335.348	34.606	4056.48
Pol-V.2	1752.230	2303.824	2468.601	2174.885	32.229	152.928
Pol-V.3	1759.414	2276.693	2437.519	2157.875	31.977	3340.80
Pol-V.4	2637.1810	2438.77	2499.221	2525.057	37.410	3250.46
Pol-V.5	1952.120	2572.932	3032.917	2519.323	37.333	3421.44
Pol-V.6	1809.624	2338.003	2943.665	2363.764	35.028	3304.80
MNA	99.4808	38.78715	122.8410	87.036	1.290	400.0012

* α (esu) = $0.148185 \times 10^{-24} \alpha$ (au)

5.3.2.1.c Hyperpolarizability

Static (CPHF) hyperpolarizability values (Table 5.13) of polymers show a different trend compared to that of the dipole moment and polarizability trends. While dipole moment, μ_g and polarizability, α values are in a closer range for polymers the hyperpolarizability values varied from 14×10^{-30} esu to 50×10^{-30} esu. The presence of chiral diols does not have any significant role in increasing the β value. Moreover, isosorbide (Pol-V.2) and isomanide (Pol-V.3) containing polymers have shown the lowest values of β . But in this case also, the stereochemical effect on β is prominent. Isomanide is giving higher β value than isosorbide as in all other cases. All the polymers have shown high value of β . Thus, it can be concluded that the L-tyrosine based chromophore is very efficient in designing good NLO active material with high SHG efficiency. Even though the variation of β can be related to the HOMO-LUMO gap and then to charge transfer, the change in β value is not directly proportional to the difference in energy gap.

Table 5.13: HOMO-LUMO Gap (ΔE) in eV, Ground-State Dipole Moment (μ_g) in debye, Linear Polarizability (α) in units of 10^{-23} esu, and First Hyperpolarizability β , in units of 10^{-30} esu for the polymers (ab-initio CPHF static property calculations)

Polymers	ΔE	μ_g	α	β_{vec}
Pol-V.1	0.3134	21.6255	34.6060	35.9861
Pol-V.2	0.3343	39.1428	32.2290	14.4112
Pol-V.3	0.3374	27.6033	31.9770	18.8488
Pol-V.4	0.3243	30.9859	37.4100	26.9000
Pol-V.5	0.2925	37.3689	37.3330	33.6258
Pol-V.6	0.2836	32.2923	35.0280	34.7583
MNA	0.3970	7.0023	1.2898	5.2684

As described in previous chapters, based on two-level model, the trendsetters in the field of SHG are two-level parameters such as oscillator strength, f , optical gap, δE , and difference in dipole moment between ground state and excited state, $\Delta\mu$. Thus the

variation in β can be explained from the results obtained by *dynamic* ZINDO-SOS calculation.

Table 5.14: Oscillator strength (f), Optical Gap (δE) in eV, Ground-State Dipole Moment (μ_g) in debye, Difference in dipole moments between ground state and excited state ($\Delta\mu$), Linear Polarizability (α) in units of 10^{-23} esu, and First Hyperpolarizability, in units of 10^{-30} esu for the polymers (ZINDO-SOS dynamic property calculations)

Polymer	f	δE	$\Delta\mu$	μ_g	α	β_{vec}
Pol-V.1	5.3562	13.4529	133.6228	242.1503	405.648	2168.197
Pol-V.2	0.4684	17.7927	240.6799	572.2634	15.2928	762.805
Pol-V.3	5.0169	14.3649	142.4032	286.6680	334.080	1536.880
Pol-V.4	3.9045	15.0972	168.9320	423.9742	400.9702	1797.502
Pol-V.5	4.0649	13.8318	185.4564	355.5187	342.144	1966.639
Pol-V.6	4.1477	14.0781	126.1178	332.3781	330.480	1466.959
MNA	0.9502	8.2721	12.0416	39.5013	300.8571	182.464

From Table 5.14, it can be seen that all the polymers have shown high second order NLO response. Pol-V.2 (isosorbide) has the lowest value of β and Pol-V.1 (camphanediol) has the highest value of β . These results are also in agreement with the CPHF predictions. In Pol-V.2 even though the difference in dipole moment $\Delta\mu$ is high, the oscillator strength is minimum compared to all other systems. Also, the optical gap, δE is the maximum in Pol-V.2. Since the charge transfer in molecules is determined by both these factors, low oscillator strength and high optical gap reduces the charge transfer considerably and hence the polymer Pol-V.2 has the lowest SHG response. In Pol-V.1, which has the maximum value of β , the value of $\Delta\mu$ is less compared to Pol-V.2. But f is maximum and δE is the minimum for this polymer compared to all other polymers of this series. This facilitates easy charge transfer and hence high β value for this polymer. The β values of all other polymers are in accordance with the two-level parameters. The chiral diols does not have significant contribution to the trend for predicting the total β_{vec} . Since the medium is already chiral, by virtue of having the tyrosine unit, incorporation of an additional chiral unit does not play any important role in determining molecular second order response β_{vec} . But here also, the effect of

stereochemistry on β value is prominent and follows the same trend as described in chapter 4. The diastereomer, isomanide showed higher β value than its analogue isosorbide. This indicates that polar ordering is vital in any system whether it is chiral or not.

5.3.2.1.d Chiral component

Table 5.15: First hyperpolarizability (β) tensors (static) of Polymers in atomic units

β Tensors	Pol-V.1	Pol-V.2	Pol-V.3	Pol-V.4	Pol-V.5	Pol-V.6	MNA
β_{xxx}	-1048.33	500.3188	219.2635	503.6268	-997.694	-988.283	-24.4201
β_{xxy}	1677.457	921.6536	990.8157	274.3517	1827.039	1731.973	13.5831
β_{xyy}	-1200.67	-1551.85	-1841.85	129.2712	-1282.98	-1200.15	12.7643
β_{yyy}	-2466.73	-399.395	-920.593	239.5554	-2552.55	-2521.87	7.1032
β_{xxz}	-1509.88	-568.978	-611.594	2856.3440	-1525.00	-1474.58	-137.669
β_{xyz}	2389.433	1191.205	1234.665	983.1450	1406.965	1369.30	0.91896
β_{yyz}	1454.972	373.3215	613.6915	-973.1370	1440.737	1437.96	-26.7852
β_{xzz}	-1627.78	-561.931	-537.314	-329.5080	-1380.15	-1565.74	15.0009
β_{yzz}	-717.775	-109.928	-239.676	2485.3480	-577.409	-635.238	-20.2272
β_{zzz}	279.673	98.7310	255.3821	-1103.590	308.7788	286.566	774.273
β_x	-3876.78	-1613.46	-2159.9	303.3897	-3660.82	-3754.17	3.3450
β_y	-1507.05	412.3308	-169.454	2999.2550	-1302.92	-1425.14	0.45917
β_z	224.7625	-96.9257	257.4799	779.6211	224.5186	249.9474	609.819
$\beta_{vec}(au)^*$	4165.467	1668.131	2181.788	3113.7410	3892.251	4023.337	609.8281
$\beta_{vec}(esu)^*$	35.9861	14.4112	18.8488	26.9001	33.6258	34.7583	5.2684
%chirality	57.3629	71.4095	56.5895	31.2534	36.1478	34.0339	0.1506

* $\beta_{vec} \times 10^{-30}$, $\beta (10^{-32} esu) = 0.863916\beta (au)$

In all the polymers, the chiral tensor component β_{xyz} is much large. In Pol-V.2 (Isosorbide) the percentage of chirality is more than 70%, while that of MNA is only 0.15%. This large increase in chiral component β_{xyz} is due to the basic L-tyrosine based framework of the polymers. This framework imparts chirality across the whole polymer

chain and increases the % chirality to a large extent. More over, the possible helical structure of the polymers contributes a considerable amount to the chirality (Figure 5.18). It is obvious that the % chirality and the value of β_{xyz} is more than 50% in polymers with chiral diols. For other diols it is only about 30%. Incorporation of chiral diol unit in to an already chiral medium increases the chiral tensor component. The large β_{xyz} component leads to large macroscopic chiral component χ_{xyz} , which is one of the major components of macroscopic hyperpolarizability. Thus, even though in the microscopic level total β_{rec} values, the contribution due to chiral diol incorporation in the chiral medium is negligible, the chiral incorporation will increase macroscopic second order susceptibility χ through large values of macroscopic chiral component χ_{xyz} .

5.4. Synthesis

A series of polymers based on L-tyrosine framework has been designed and the spectroscopic properties are calculated using *static* and *dynamic* methods. Calculations reveal that all the polymers are good SHG active materials. So these polymeric structures were taken in to the laboratory for synthesis. Six polymers were synthesized having L-tyrosine framework and diols (chiral and achiral) by high temperature polycondensation method. The following section deals with the synthetic procedures.

5.4.1 Monomer synthesis

5.4.1.1 Synthesis and characterization of chiral chromophore

L-Tyrosine based chiral chromophore was synthesized by a two-step process. In the first stage L-tyrosine was coupled with *para* nitroaniline to get PNATY. In the second stage PNATY was acylated with 4'4' azobenzene dicarboxylic acid to get TYAZ. Chlorination of TYAZ yielded TYAZCl.

*Synthesis of (S)-2-amino-3-(3-(4-nitrophenylazo), 4-hydroxyphenyl) propanoic acid (PNATY, 3)*¹⁵

L-Tyrosine (Loba Chemie, 99% pure), *Para* nitroaniline (s. d. fine, 99% pure) Sodium nitrite (s. d. fine, 98% pure), Sodium acetate (s. d. fine 98% pure) were used for

IR(KBr pellet) cm^{-1} : 3076 (NH⁺, NH st), 3115(-OH st), 2065 (distinct side band due to zwitter ion), 1719 (carbonyl), 1589 (COO⁻), 1538 (NO₂ st as), 1510 (NH₃⁺ δ_{sy}), 1429 (N=N- st), 1348 (-NO₂ st ay) 1275 (aromatic trans -N=N-)

¹H NMR (300 MHz DMSO-d₆): δ 11.3 (carboxylic -OH), 9.1 (phenolic -OH), 8.5 (d, 2H, aromatic, near to NO₂, H1), 8.2 (d, 2H, aromatic, near to -N=N-, H2), 7.7 (d, NH₃⁺), 7.4 (d, 1H, amino acid benzene ring near to -N=N-, H3), 7.1 (d, 1H, amino acid benzene ring near to -CH₂, H4) 6.7 (d, 1H, amino acid benzene ring near to -OH, H5), 4.1(t, 1H, -CH), 3.1, 3.2 (d, 2H, -CH₂)

¹³C NMR (75 MHz DMSO-d₆): δ 174.9 (-CO in -COO⁻), 158.8 (aromatic C, -C-N=N-, C4), 150.6 (aromatic C, -C-NO₂, C1), 149.4 (C in amino acid phenyl, -C-OH, C7), 132.4 (C in amino acid phenyl, -C-CH₂, C10), 131.4 (C in amino acid phenyl near to CH₂, C9), 125.1 (C, in amino acid -C-N=N-, C6), 124.7 (C in amino acid phenyl near to CH₂, C5), 123.9 (aromatic carbon near to -N=N-, C3), 121.4 (aromatic C near to -NO₂, C2), 116.1 (C in amino acid phenyl near to -OH, C8), 56.8 (C in -CH), 39.4 (C in -CH₂)

Mass (m/e): 330 (molecular ion), 301 (M-CHO), 285 (M-COOH), 150 (-N=N-C₆H₅NO₂), 122 (base peak, C₆H₅NO₂).

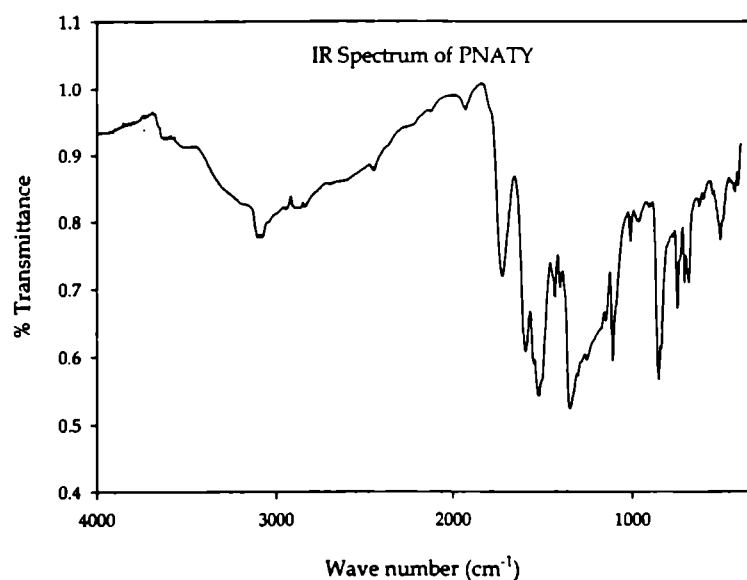


Figure 5.6. IR spectrum of PNATY

A peak between 370 and 379 nm in UV-VIs absorption spectrum is due to the azo group ($\pi \rightarrow \pi^*$). In IR spectrum (Figure 5.6) of PNATY, a distinct side band at 2065 cm^{-1} confirms the zwitter ion form of the amino acid moiety.¹⁶ The NH stretching frequency at 3115 cm^{-1} instead of 3300-3500 cm^{-1} indicates the

presence of NH_3^+ group.¹⁷ The peak at 1719 cm^{-1} confirmed carbonyl absorption and peaks at 1538 and 1348 cm^{-1} confirmed -NO_2 group.

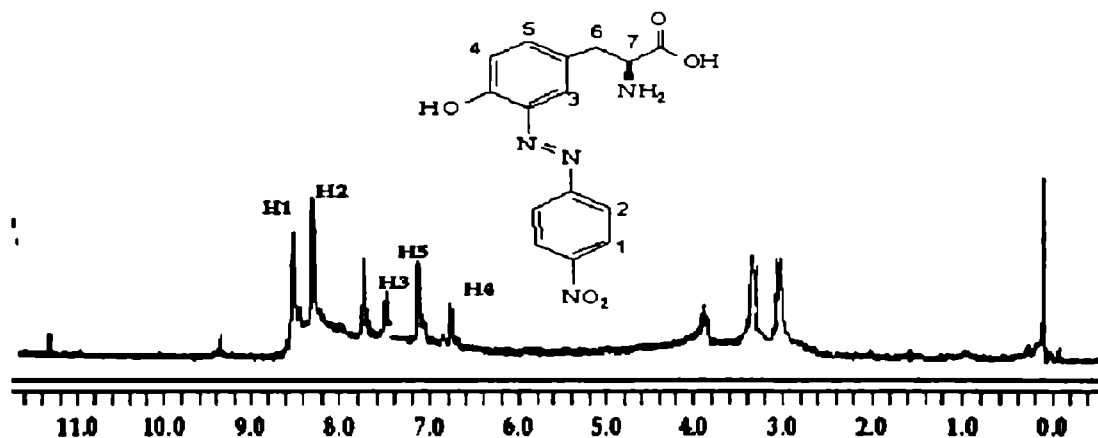


Figure 5.7. ^1H NMR spectrum of PNATY

In ^1H NMR spectrum (Figure 5.7) the doublet at $7.7\ \delta$ confirmed the presence of NH_3^+ . Five doublets in the aromatic region confirm the presence of five different aromatic hydrogen. This confirms monosubstitution of PNA at tyrosine ring. If disubstitution had occurred (at C8 also), aromatic region would have shown only four aromatic peaks. The doublets at $\delta\ 3.1$ and $\delta\ 3.2$ confirms -CH_2 group and -CH proton triplet is seen at $\delta\ 4.1$. Off scale peak at $\delta\ 11.3$ indicates -COOH protons. -OH peak is seen at $\delta\ 9.1$.

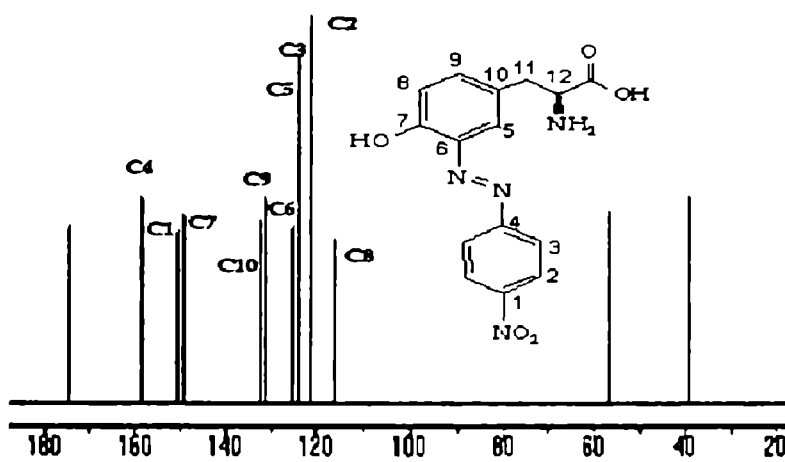


Figure 5.8. ^{13}C NMR of PNATY

Thirteen distinct carbons in ^{13}C NMR spectrum (Figure 5.8)

confirm monosubstitution. If the substitution were at both the *meta* carbon of tyrosine ring, the ^{13}C NMR spectrum would have given only 12

distinct carbons. In the mass spectrum (Figure 5.9), molecular ion peak at $m/e=330$ once again confirms the monosubstitution. Peaks due to $M - \text{COOH}$ at m/e 285, $M - \text{CHO}$ at m/e 301, $\text{C}_6\text{H}_5\text{NO}_2$ at m/e 122 and $-\text{N}=\text{N}-\text{C}_6\text{H}_5\text{NO}_2$ at 150δ confirm the proposed structure for the compound.

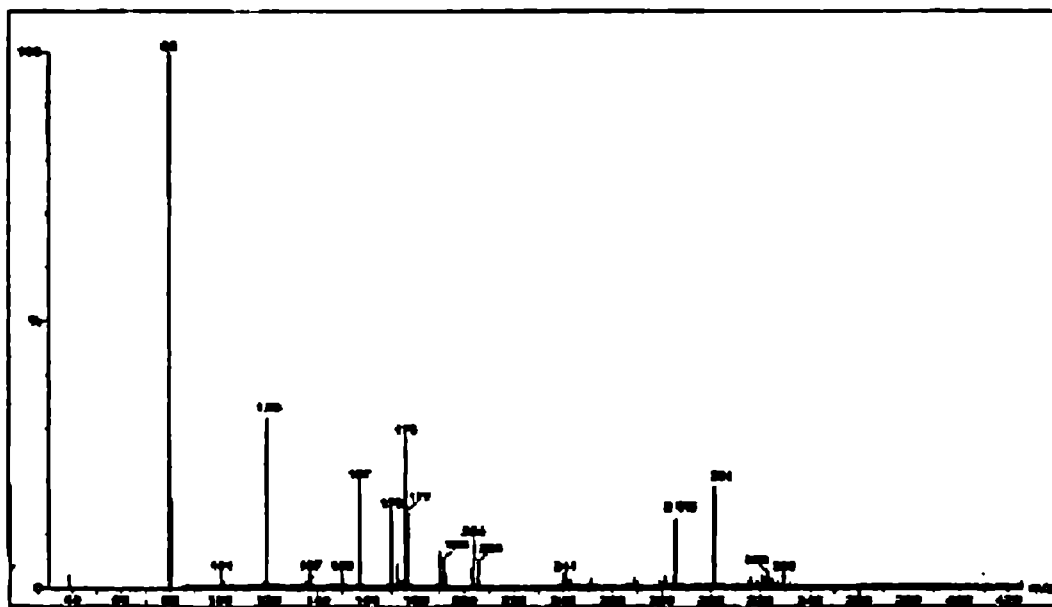


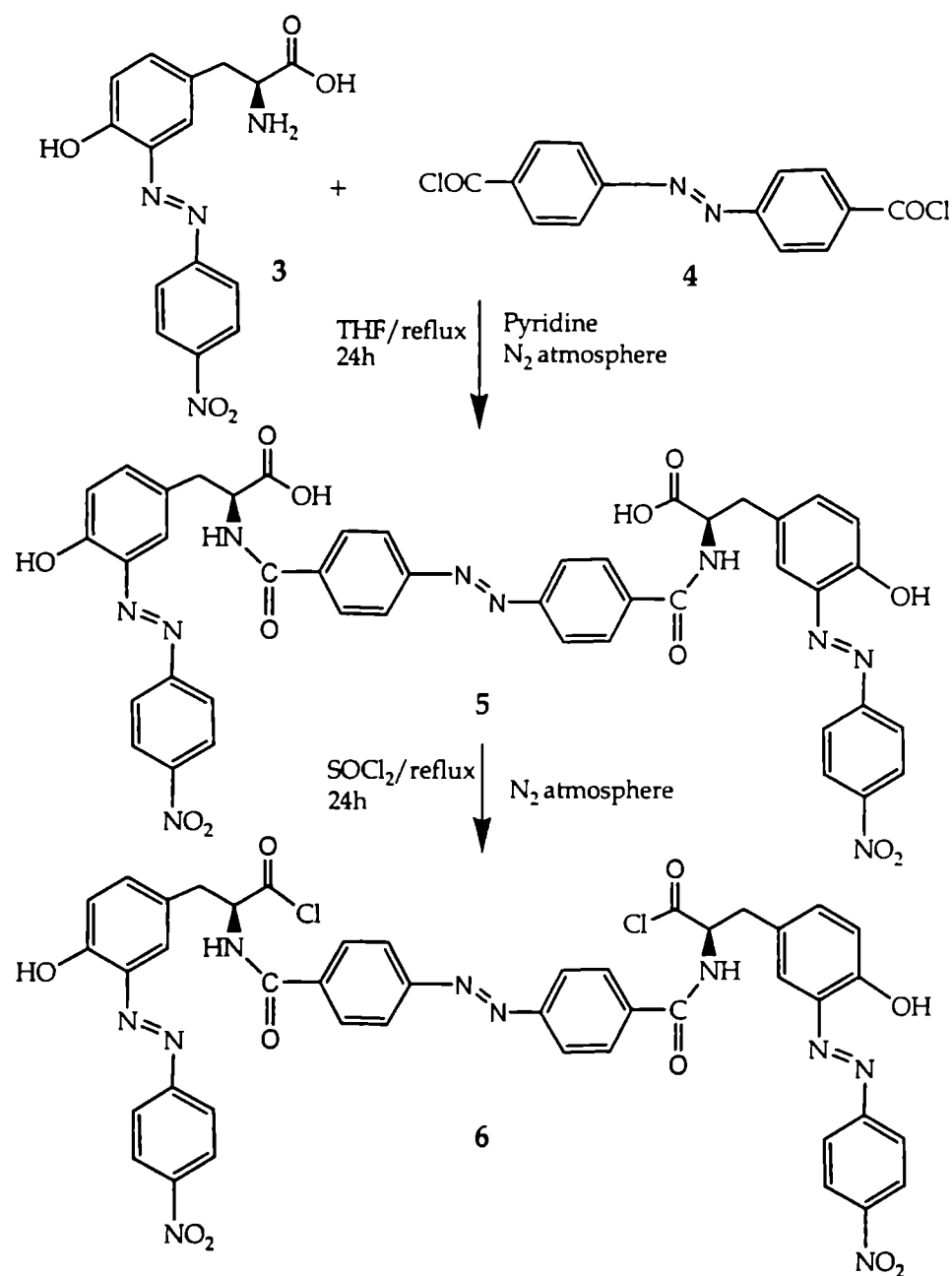
Figure 5.9 Mass spectrum of PNATY

Synthesis of bis((S)-2-(4-azanyl benzamido)-3-(3-(4-nitrophenylazo), 4-hydroxyphenyl) propanoic acid chloride (TYAZCl, 6)

4,4' azobenzene dicarboxylic acid chloride (AZCl, 4) and (S)-2-amino-3-(3-(4-nitrophenylazo)-4-hydroxyphenyl) propanoic acid (PNATY, 3) were used for the synthesis of bis((S)-2-(4-azanyl benzamido)-3-(3-(4-nitrophenylazo)-4-hydroxyphenyl) propanoic acid chloride (TYAZCl, 6). Synthesis of acid chloride has been described in chapter 4

In to a 50 mL three necked round bottom flask equipped with mechanical stirring and heating, PNATY (1 g, .00316 mol) and 4,4'-azobenzene dicarboxylic acid chloride (AZCl, 0.484 g, 0.00158 mol) were added. THF (15 mL) was added as solvent. To this mixture few drops of pyridine were added. The reaction was carried out for 24h at

reflux temperature under nitrogen atmosphere. The reaction mixture was cooled and filtered. Dark brown solid of TYAZ was obtained. It was recrystallized from methanol. (M.P 144^o C). The product TYAZ was refluxed with SOCl₂ for 24h under nitrogen atmosphere to obtain TYAZCl (6). The reaction mixture was cooled, filtered and recrystallized from acetone.



Scheme 5.2. Synthesis of TYAZCl

Characterization

Yield 86%, $[\alpha]_D -11.3^\circ$ Decomposed at 231°C

Elemental analysis: Calculated for $\text{C}_{44}\text{H}_{32}\text{Cl}_2\text{N}_{10}\text{O}_{10}$ - C, 56.72; H, 3.46; N, 15.03. Found - C, 56.53; H, 3.45; N, 15.17

Spectral properties

UV λ_{max} (solid) nm: 300 (NO_2) 379 ($-\text{N}=\text{N}-$)

IR(KBr pellet) cm^{-1} : 3407 (O-Cl st), 3077($-\text{OH}$ st) 1740(carbonyl of acid chloride), 1689 (carbonyl of amide) 1530 (NO_2 st as), 1432 ($-\text{N}=\text{N}-$ st) 1330($-\text{NO}_2$ st ay) 1279 (aromayic trans $-\text{N}=\text{N}-$)

^1H NMR (300 MHz DMSO-d_6): δ 9.2 (2H, phenolic $-\text{OH}$), 8.39 (d, 4H aromatic, near to NO_2 H1), 8.3(4H aromatic, near to $-\text{N}=\text{N}-$,H2)8.17 (4H, aromatic hydrogen from acid chloride near to $-\text{CO}$,H8) 8.03 (4H, aromatic hydrogen from acid chloride near to $-\text{N}=\text{N}$, H9) 7.8 (d, 2H,amide hydrogen), 7.5 (d, 2H, amino acid phenyl ring near to $-\text{N}=\text{N}-$, H3), 7.0 (d, 2H, amino acid phenyl ring near to $-\text{CH}_2$ H5) 6.6 (d, 2H, amino acid benzene ring near to $-\text{OH}$), 4.3(m, 2H, $-\text{CH}$), 3.1, 3.2 (d, 4H; $-\text{CH}_2$)

^{13}C NMR (75 MHz DMSO-d_6): δ 173 ($-\text{CO}$, acid chloride), 167.6 ($-\text{CO}$, amide), 158.8, 156.1, 150.6, 149.4, 136.3, 132.4, 131.2, 127.8, 125.2, 124.7, 123.4, 121.5, 121.1, 116.1 (aromatic), 71.4 ($-\text{CH}$), 37 ($-\text{CH}_2$)

Mass: 930 (molecular ion), 360 ($\text{O}_2\text{N-Ph-N}=\text{N-Ph}(\text{OH})\text{CH}_2\text{-CH}(\text{NH})\text{Cl}$), 312 $\text{O}_2\text{N-Ph-N}=\text{N-Ph}(\text{OH})\text{CH}_2\text{-CH}(\text{NH})$), 236 ($\text{CO-Ph-N}=\text{N-Ph-CO}$)

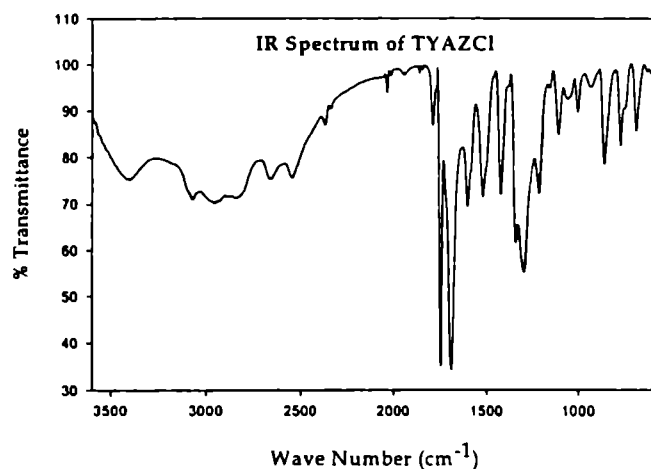


Figure 5.10. IR spectrum of TYAZCl

In the IR spectrum a structured band at 3407 cm^{-1} indicates the presence of O-Cl, hydrochloride of amino acids (confirmed chlorination of TYAZ). Two distinct bands at 1730 cm^{-1} and 1689 cm^{-1} indicate two type of

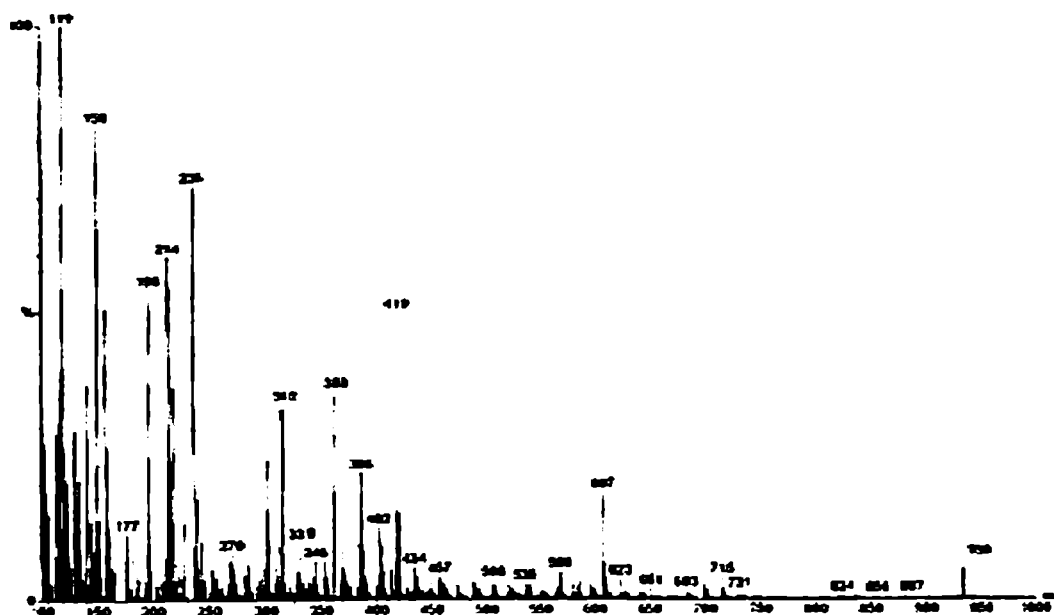
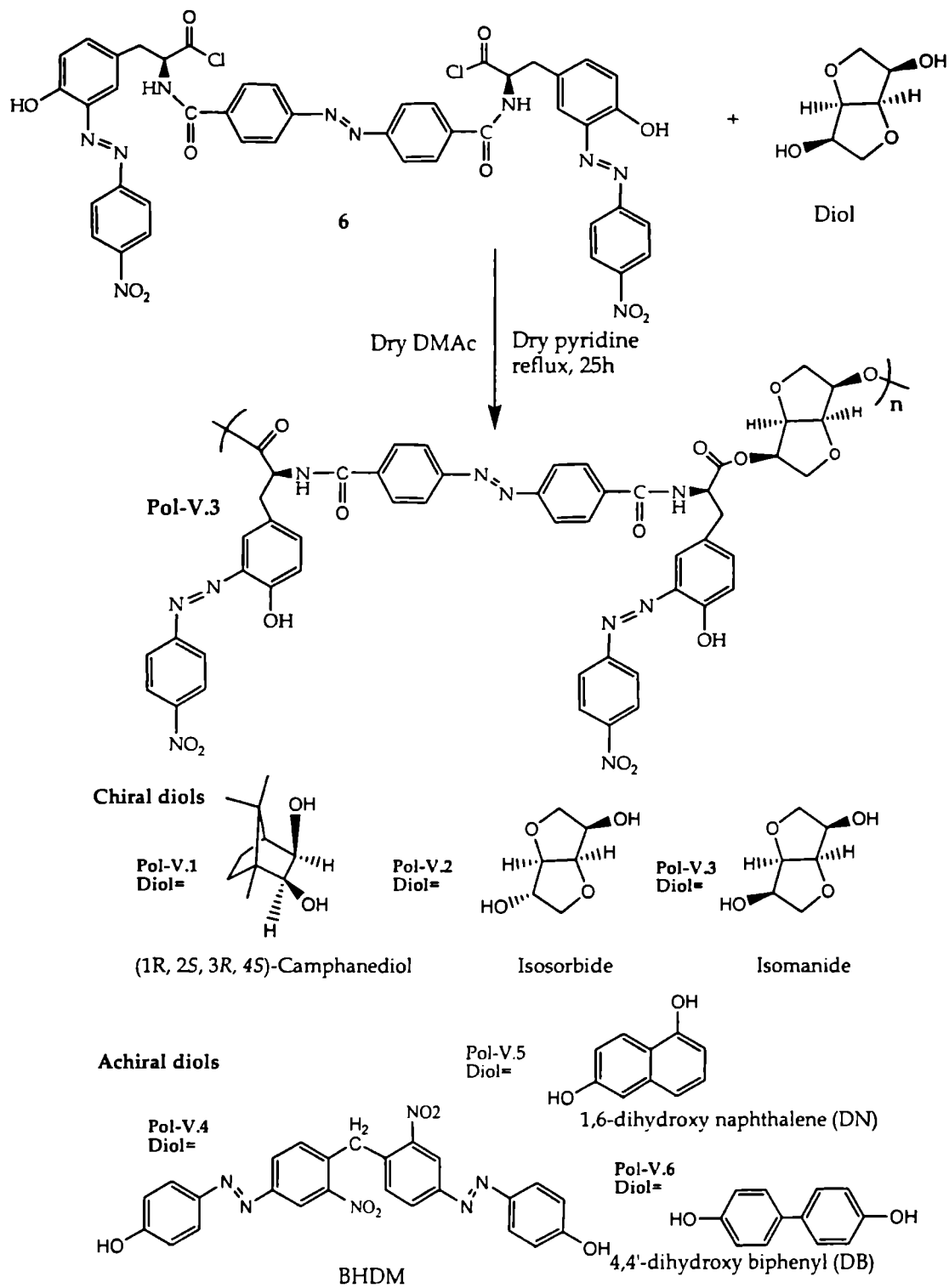


Figure 5.13 Mass spectrum of TYAZCl

5.4.2 Polymer Synthesis

Previously designed polymer structures were synthesized by the polycondensation of L-tyrosine based chromophore with the diols. All polymer syntheses were done by solution method at high temperatures. Appropriate diol molecule was dissolved in extremely dry dimethyl actamide (HPLC grade, s. d. fine). To this solution, bis((S)-2-(4-azanyl benzamido)-3-(3-(4-nitrophenylazo), 4-hydroxyphenyl) propanoic acid chloride (TYAZCl, 6) dissolved in DMAc was added. Few drops of extremely dry pyridine (99.99% dry pyridine, s. d. fine) were added as acid acceptor. The mixture was refluxed under stirring for 25h. The product was precipitated from cold methanol and washed continuously with hot water, methanol and acetone. After filtration and drying a brown solid was obtained. Scheme 5.3 gives the synthetic route of polymers.



Scheme 5.3 Synthesis of poly(ester-amide)s

5.4.2.1. Characterization of polymers

Pol-V.1

Yield: 71%

Spectral properties

UV λ_{\max} (solid): 362 ($\pi \rightarrow \pi^*$, N=N) 323 ($n \rightarrow \pi^*$, NO₂)

IR(KBr pellet) cm⁻¹ : 3393 (NH st, OH st), 2921 (-CH stretch in camphanediol), 1730 (aromatic ester carbonyl), 1685 (amide I carbonyl stretch), 1530 (NO₂ st as, amide II st sy), 1423 (-N=N- st), 1349 (NO₂ st sy)

¹H NMR (300 MHz DMSO-d₆): δ 9.2 (phenolic -OH), 8.4 (aromatic, near to NO₂), 8.1(4H aromatic, near to -N=N-), 7.8 (aromatic hydrogen from ester amide near to -CO), 7.5 (aromatic hydrogen from ester amide near to -N=N-), 7.3 (amino acid phenyl ring near to -N=N-), 7.1 (amino acid phenyl ring near to -CH₂), 6.7 (amino acid phenyl ring near to -OH), 4.8(m, -CH), 4.2, 4.3 (d, -CH₂), 3.1 (m, -CH₂ cyclopentane ring of camphanediol), 2.4 (m, -CH, cyclopentane ring of camphanediol), 2.1 (s, -CH₃ of camphanediol), 1.24 (s, bridged -C(CH₃)₂ of camphanediol).

Pol-V.2 and Pol-V-3

Pol-V.2 (Yield 78%) and Pol-V.3 (yield 75%) are different only in the stereochemistry of the chiral building units. So their spectral patterns are similar except in ¹HNMR. But in ¹H NMR the -CH protons which have the different stereochemistry in isosorbide and isomanide appeared as multiplet. So a distinction between them is difficult.

Spectral properties

UV λ_{\max} (solid): 362 ($\pi \rightarrow \pi^*$, N=N), 323 ($n \rightarrow \pi^*$, NO₂)

IR (KBr pellet) cm⁻¹ : 3393 (NH st, OH st), 2921 (sp³ -C-H stretch in isosorbide or isomanide unit), 1730 (aromatic ester carbonyl), 1685 (amide I carbonyl stretch), 1530 (NO₂ st as, amide II st sy), 1423 (-N=N- st), 1349 (NO₂ st sy), 1235-1240 (C-O st in isosorbide or isomanide unit)

¹H NMR (300 MHz DMSO-d₆): δ 9.2 (phenolic -OH), 8.4 (aromatic, near to NO₂), 8.1(4H aromatic, near to -N=N-), 7.8 (aromatic hydrogen from ester amide near to -CO), 7.5

(aromatic hydrogen from ester amide near to -N=N-), 7.3 (amino acid phenyl ring near to -N=N-), 7.1 (amino acid phenyl ring near to -CH₂) 6.7 (amino acid phenyl ring near to -OH), 4.8(-CH), 4.2, 4.3 (-CH₂), 4.0 (-CH isosorbide or isomanide unit), 3.5 (-CH₂ in isosorbide or isomanide unit), 3.3 (bridge CH in isosorbide or isomanide unit)

Pol-V-4

Yield: 74%

Spectral properties

UVλ_{max} (solid): 274 (-Ph-CH₂-Ph-), 362 (π→π*, N=N), 323 (n→π*, NO₂)

IR(KBr pellet) cm⁻¹ : 3393 (NH st, OH st), 947 (CH₂ in Ph-CH₂-Ph), 1730 (aromatic ester carbonyl), 1685 (amide I carbonyl stretch), 1530 (NO₂ st as, amide II st sy), 1423 (-N=N-st), 1349 (NO₂ st sy)

¹H NMR (300 MHz DMSO-d₆) δ: 9.2 (phenolic -OH), 8.4 (aromatic, near to NO₂), 8.1(4H aromatic, near to -N=N-), 7.8 (aromatic hydrogen from ester amide near to -CO), 7.5 (aromatic hydrogen from ester amide near to -N=N-), 7.3 (amino acid phenyl ring near to -N=N-), 7.1 (amino acid phenyl ring near to -CH₂), 6.7 (amino acid phenyl ring near to -OH), 5.1 (s, 2H, -CH₂ of BHDm), 4.8(-CH), 4.2, 4.3 (-CH₂)

Pol-V.5

Yield: 72%

Spectral properties

UVλ_{max} (solid): 280 (biphenyl), 362 (π→π*, N=N), 323 (n→π*, NO₂)

IR(KBr pellet) cm⁻¹ : 3393 (NH st, OH st), 1730 (aromatic ester carbonyl), 1685 (amide I carbonyl stretch), 1530 (NO₂ st as, amide II st sy), 1423 (-N=N- st), 1349 (NO₂ st sy), 900-750 (ar CH)

¹H NMR (300 MHz DMSO-d₆): δ 9.2 (phenolic -OH), 8.4 (aromatic, near to NO₂), 8.1(4H aromatic, near to -N=N-), 7.8 (aromatic hydrogen from ester amide near to -CO), 7.5 (aromatic hydrogen from ester amide near to -N=N-), 7.4 (aromatic, biphenyl) 7.3 (amino acid phenyl ring near to -N=N-), 7.1 (amino acid phenyl ring near to -CH₂), 6.7 (amino acid phenyl ring near to -OH), 6.5 (aromatic, biphenyl), 4.8(-CH), 4.2, 4.3 (-CH₂).

Pol-V-6

Yield: 73%

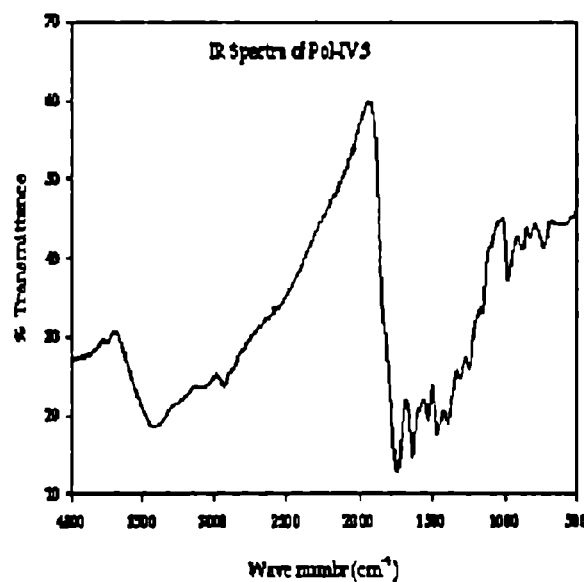
*Spectral properties*UV λ_{\max} (solid): 362 ($\pi \rightarrow \pi^*$, N=N), 323 ($n \rightarrow \pi^*$, NO₂)IR(KBr pellet) cm⁻¹ : 3393 (NH st, OH st), 1730 (aromatic ester carbonyl), 1685 (amide I carbonyl stretch), 1530 (NO₂ st as, amide II st sy), 1423 (-N=N- st), 1349 (NO₂ st sy), 800-760 (characteristic of naphthalene)¹H NMR (300 MHz DMSO-d₆): δ 9.2 (phenolic -OH), 8.4 (aromatic, near to NO₂), 8.1 (4H aromatic, near to -N=N-), 7.8 (aromatic hydrogen from ester amide near to -CO), 7.5 (aromatic hydrogen from ester amide near to -N=N-), 7.1, 7.2 (aromatic, naphthalene 7.3 (amino acid phenyl ring near to -N=N-), 7.1 (amino acid phenyl ring near to -CH₂), 6.9 (aromatic, naphthalene), 6.7 (amino acid phenyl ring near to -OH), 4.8 (-CH), 4.2, 4.3 (CH₂)

Figure 5.14 IR spectrum of Pol-V.3

IR spectrum of polymers (Figure 5.14) has shown two distinct carbonyl peaks at 1730-1715cm⁻¹ and 1680-1700 cm⁻¹. These peaks can be attributed due to aromatic ester carbonyl and due to amide linkage. In the amide linkage, -CO is directly connected to -NH. This decreases the frequency of C=O str. to a lower value than the ester carbonyl. Presence of two distinct carbonyl peaks has confirmed the esterification of TYAZCl with the different diols.

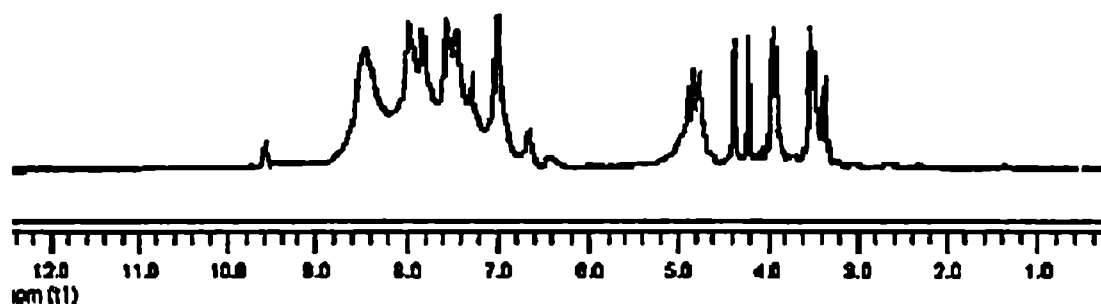


Figure 5.15. ^1H NMR spectrum of Pol-V.3

The multiplet at δ 4.3 in ^1H NMR spectrum (Figure 5.15) of TYAZCl has moved towards δ 4.8 in all polymers, which confirms the esterification. The hydrogens near Cl are more shielded (higher electron density) than the hydrogens near oxygen. So H connected to Cl has appeared at higher field. In Pol-V-1 the aromatic region contains seven distinct peaks in the aromatic region and peaks at lower aliphatic region δ 3.1, δ 2.4, δ 2.1, δ 1.24 which confirmed the presence of camphanediol. Also in Pol-V.2 and Pol-V.3 there are seven distinct peaks in the aromatic region and the lower aliphatic peaks at δ 4.2, 4.3 δ , 4.0, δ 3.5, δ 3.3 which confirmed the presence of isosorbide and isomanide. Pol-V. 4 have more than seven aromatic peaks and the singlet at δ 5.1 due to $-\text{CH}_2$ in BHDM confirmed the esterification of TYAZCl with BHDM. Pol-V.5 and Pol-V. 6 contain the aromatic peaks due to TYAZCl and the diols of biphenyl and naphthalene respectively.

Because of the low solubility of the high molecular weight polymers recording of ^{13}C NMR spectrum in solution was difficult. As representative spectrum, solid-state ^{13}C NMR of polymer Pol-V.3 was taken. It is shown in Figure 5.16. Instead of separate peaks ^{13}C NMR spectrum exhibits broad bands in the aromatic and aliphatic regions. But two different kinds of carbonyl carbon at δ 244 and δ 197 confirmed the presence of ester formation of TYAZCl with the diol, isosorbide. The broad band ranging from δ 160 to δ 110 agrees with the aromatic region of the polymer. The band from δ 80 to δ 20 agrees with the aliphatic region of the polymer.

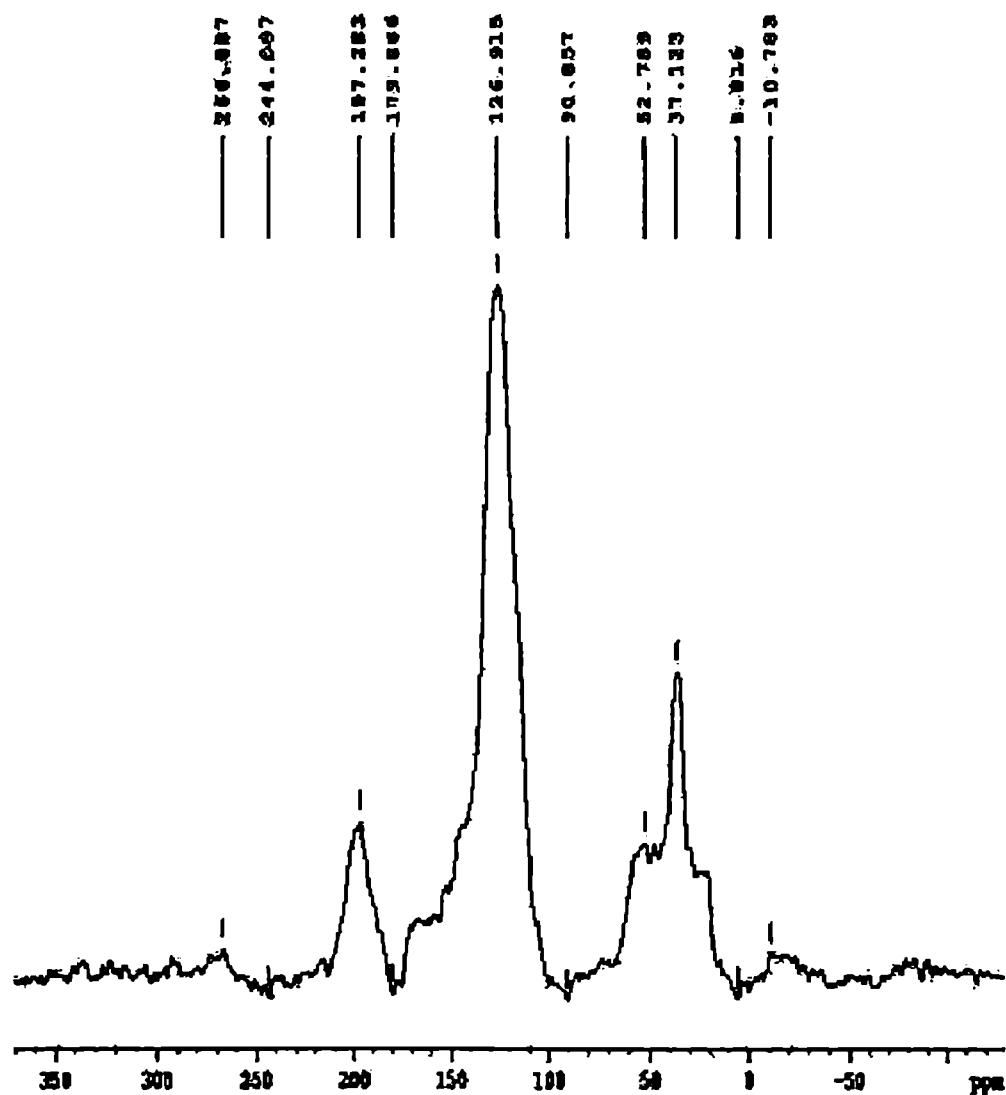


Figure 5.16. Solid State ^{13}C NMR spectrum of Pol-V.3

MALDI TOF Mass spectrum (Figure 5.17): The mass spectrum of Pol-V.4 ($m/e = 20340$) gives an idea about the degree of polymerization. It showed that 15 monomeric units (one monomeric unit = 1356) were involved in the polymerization. The high temperature polycondensation method has yielded comparatively high molecular weight poly (ester -amide) s with a molecular weight up to twenty thousand

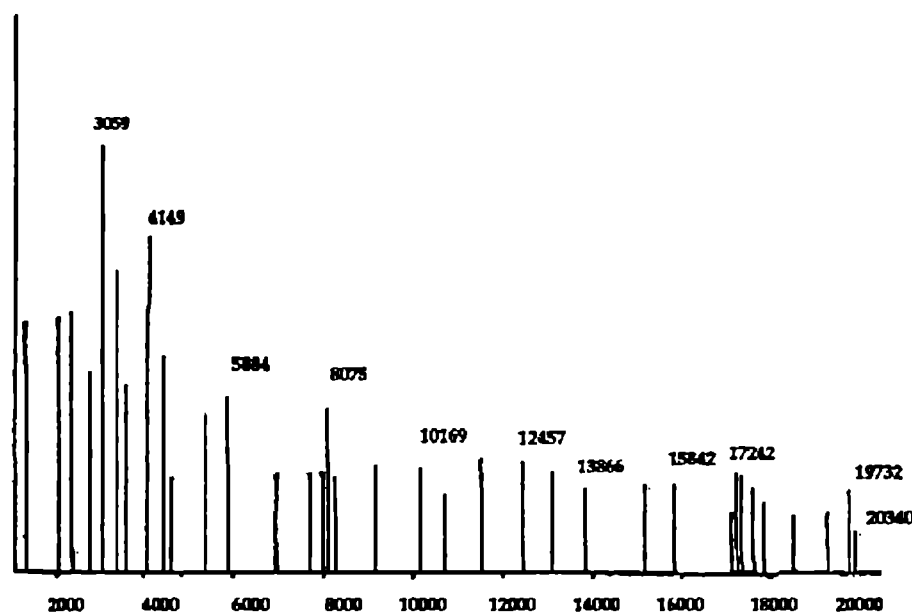


Figure 5.17 Mass spectrum of Pol-V-4

5.4.2.2. Thermal properties of the polymers

Since T_g and polar order in polymers are directly related, high value of T_g indicates high polar order. T_g values are shown in Table.5.16. The polymers with isomanide and camphanediol have high T_g values. This shows the polymer chains exhibit long range order which creates high degree of polar order in these polymers. T_g values reflect in the SHG efficiency. The one with higher T_g has given higher SHG efficiency. This may be explained based on the higher polar order of the polymers. In this series also the stereochemical effect and polar order are prominent. The polymer containing isosorbide has low value of T_g compared to the polymer containing its diastereomer, isomanide and this reflects the polar order in polymer containing isomanide. The low value of T_g for Pol-V.5 may be attributed due the rotational behavior of the biphenyl ring (as a part of long polymer chain). This rotation gives flexibility to the -C-C- bond and gives a low value of T_g

The initial decomposition temperature (IDT) gives an idea about the thermal stability of the polymers. Except for the polymer having dihydroxy biphenyl all the poly

(ester-amide) s have IDT higher than 275^oC. For the polymer with dihydroxy biphenyl it is 236^oC. From the T_g data it can be seen that all the polymers showed higher polar ordering with fairly good thermal stability.

5.5. Evaluation of second harmonic generation efficiency

The NLO efficiencies of poly(ester-amide) s were determined with 2-methyl-4-nitroaniline as the standard using Kurtz and Perry method.¹⁸ Measurements were done by the powder method with a Quanta-Ray Nd-YAG laser from Spectra Physics (1064 nm, 10 ns, 365mJ/S) integrated over 20 pulse and an average of 10 pulse. The samples were ground and graded with standard sieves to the phase matchable size (100-150 μm) and loaded on cuvette with 1mm thickness. MNA samples used as standards were also powdered and sieved (100-150 μm) after drying under high vacuum. They were also mounted with the same thickness as the polymer sample. The laser beam was directed unfocused onto the sample kept at a 45^o angle to the laser beam which provides the phase comparable situation; the emission was collected from the front face of the sample at 90^o angle. The SH signal; at 532 nm was detected by Avantes 2048 spectrometer with CCD camera. The results are shown in Table 5. 16.

Table 5.16: Yield and Properties of Poly(ester-amide) s

Polymer	Diol molecule	Yield (%)	T _g (°C)	IDT (°C)	[α] _D	SHG Efficiency*
Pol-V.1	Camphanediol	71	293.97	291	-24.3	8.53
Pol-V.2	Isosorbide	78	154.27	297	-23.2	7.73
Pol-V.3	Isomanide	75	299.43	287	-20.4	7.93
Pol-V.4	BHDM	74	215.67	275	-16.8	8.02
Pol-V.5	Dihydroxy biphenyl	72	191.89	236	-18.0	7.60
Pol-V.6	Dihydroxy naphthalene	73	197.51	280	-15.9	7.54

*(SHG efficiency of MNA was taken as 1)

Table 5.16 gives the properties of the synthesized poly (ester-amide) s. All the poly (ester-amide) s are efficient materials for SHG with more than seven times SHG response compared to MNA. This is because of the helical structure of the poly (ester-

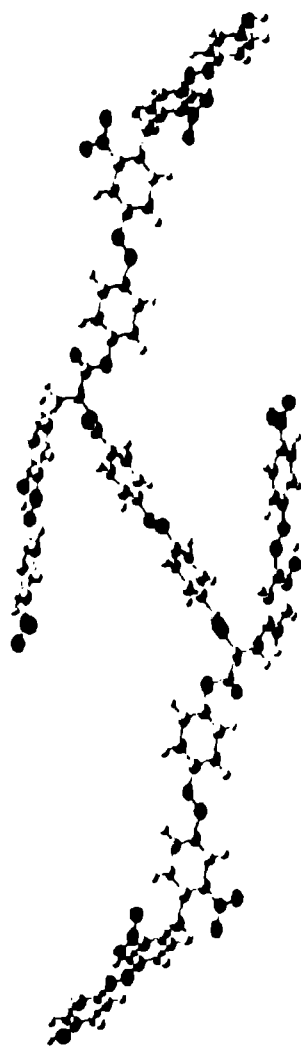


Figure 5.18 Helical structure of Pol-V.4

amide) s due to the L-tyrosine based chiral framework. (**Figure 5.17**). High NLO activity of the poly (ester-amide) s is because of highly extended chiral framework. The main consideration of this chapter was to achieve the chirality through the polymer chain rather than incorporating a chiral molecule as explained in chapter 4. This framework imparts the main chain chirality through out the entire chain, which induces chemical poling with out requirement for the external poling. The chiral framework significantly (up to eight times that of SHG of MNA) enhances the nonlinear optical susceptibility of the copolymers. The data for percentage chirality confirmed the extended chirality of the polymer chains to a long-range order. Since these polymers are oriented as a helix, it is assumed that the copolymers have broken symmetries along the substrate normal. They therefore, belong to the symmetry group C_∞ ; even though the monomeric units belong to C_1 point groups. For such samples with C_∞ symmetry, there are four nonvanishing macroscopic susceptibility components, that is χ_{zzz} , χ_{xxz} , χ_{zxx} and χ_{xyz} . The first three components originate from the polar ordering, while the latter can only be present in chiral media. Out of the four nonvanishing macroscopic susceptibility components, i.e χ_{zzz} , χ_{xxz} , χ_{zxx} and χ_{xyz} , the chiral susceptibility components χ_{xyz} is highly pronounced in this series of polymers due to two reasons: 1) the long range order of chiral frame work 2) the helical orientation of the poly(ester-amide) s (**Figure 5.18**). The long-range order of chiral framework

decreases the dipolar interactions. The Tg data proved that the polar order is also significantly high. These highly ordered structures of the polymers exist as a repeating unit of the chiral framework. This results the large nonchiral susceptibility component, χ_{zzz} , χ_{xxz} , χ_{zxx} . Strong coupling exists between the helical chiral framework and the diols, which resulted in a tightly packed highly ordered polymer framework ideal for high performance NLO active material. The electron delocalisation due to the π - π^* transition of the azobenzene system induces a displacement of electrons along the helical conjugated backbone. Here also, the stereochemical effect as explained and proved in chapter 4 plays its role. Out of the two-diastereomeric diols used for the polycondensation with the chiral framework, the poly (ester-amide) s with isomanide has high SHG value than the isosorbide poly (ester-amide) s. This is because of the more ordered structure, which reduces the dipolar interaction, of the isomanide based poly (ester-amide) s and which was proved from the Tg results. The polymer incorporated with BHDM showed SHG values more than the isosorbide, isomanide systems can be ascribed as the pronounced chiral contribution in the macroscopic level from the Δ helical nature of the poly (ester-amide) s inherited by the BHDM.

5.6. Correlation of theoretical and experimental results

The SHG efficiency has shown almost similar trends in theoretical calculation and experimental measurements (Table 5.17). Experimental measurements showed that all of the polymers have high SHG efficiency than MNA as predicted by theory. Polymers with camphanediol have the maximum susceptibility values in both theoretical calculation and also by experimental measurement. In agreement with the theory, the effect due to incorporation of chiral diol is not prominent in experimental measurements also. In experimental measurement, the least value is for binaphthalene system (Pol-V.6). By both theoretical calculation and experimental measurement, the less efficient one is isosorbide system (Pol-V.2). This may be due to the more scattering tendency of the binaphthalene system occurred during the experimental measurements or higher-level contribution will be more in isosorbide and thus the failure of 82 level ZINDO SOS calculation and derivative level CPHF calculation.

Except for **Pol-V.6** the ZINDO SOS (dynamic) calculation is in good agreement with the experimental results. The variation in *static* calculation is because of the derivative formalism rather than the SOS one. In experimental measurements, electrons will go to possible higher energy states, thus higher energy contribution may not be too small to be neglected. But *ab initio*-CPHF is numerically more accurate and precise in predicting the trends with high-level electron correlation. This defect can be rectified by introducing more electron correlation in frequency dependent CPHF calculation (CPHF *dynamic*). These calculations are computationally high demanding and can be achieved only with supercomputers for the systems with more than 500 electrons.

Table 5.17: Comparison of theoretical calculation with experimental measurements

Polymer	β (10^{-30}) <i>esu</i> (Static)	β (10^{-30}) <i>esu</i> (Dynamic)	SHG Efficiency*
Pol-V.1	35.9861	2168.197	8.53
Pol-V.2	14.4112	762.805	7.73
Pol-V.3	18.8488	1536.880	7.93
Pol-V.4	26.9000	1797.502	8.02
Pol-V.5	33.6258	1966.639	7.60
Pol-V.6	34.7583	1466.959	7.54
MNA	5.2684	198.9601	1.00

*Experimental values of polymers compared with that of MNA

5.7. Conclusion

A series of poly (ester-amide) s based of L-tyrosine chiral framework was designed and the properties were predicted. The goal of obtaining chirality along with the framework was achieved by this design. Theoretical calculation showed that all the polymers were highly efficient NLO materials. Synthesis of these poly (ester-amide) s in high yields could also be achieved. Experimental measurements of SHG were in good agreement with theoretical predictions as all the polymers have shown high SHG efficiency compared to MNA.

References

- (1) Chemla, D. S.; Zyss, J. *Nonlinear Optical Properties of Organic Molecules and Crystals*; Academic Press, Inc: Newyork, 1987
- (2) Monaco, S. B.; Davis, L. E.; Velsko, . S. P.; Wang F. T.; Eimerl D.; Zalkin A. *J. Cryst. Growth* 1987, 85, 252)
- (3) Ranganathan, D.; Kurur, S.; Madhusudanan, K. P.; Karle, I. L. *Tet. Lett.* 1997, 38, 4659
- (4) Razzetti, C.; Ardoino, M.; Zanotti, L.; Zha, M.; Paorici, C. *Cryst. Res. Technol.* 2002, 37, 456.
- (5) Kumar, G. R.; Raj, G. S.; Sankar, R.; Mohan, R.; Pandi, S.; Jayavel, R. *J. Cryst. Growth* 2004, 267, 213
- (6) a) Yu, L. P.; Chan, W.; Bao, Z. *Macromolecules* 1992 25, 5609. (b) Stenger-Smith, J. D.; Henry, R. A.; Hoover, J. M.; Lindsay, G. A.; Nadler, M. P.; Nissan, R. A. *J. Polym. Sci., Part A: Polym. Chem.* 1993, 31, 2899. (c) Weder, C.; Neuenschwander, P.; Suter, U. W.; Pre'tre, P.; Kaatz, P.; Gu'nter, P. *Macromolecules* 1995, 28, 2377
- (7) Philip, B. *Studies on Photostructuring of Synthetic Polymers* PhD thesis, University of Kerala, 2001
- (8) (a) Eckl, M.; Mu'ller, H.; Storiegl, P. *Macromol. Chem. Phys.* 1995, 196, 315. (b) Chern, Y.-T. *J. Polym. Sci., Part A: Polym. Chem.* 1996, 34, 133 (c) Akiyama, E.; Ohtomo, M.; Nagase, Y.; Koide, N. *Macromol. Chem. Phys.* 1995, 196, 3391.)
- (9) (a) Hohenberg, P.; Kohn, W. *Phys. Rev.* 1964, 136, B864. (b) Kohn, W.; Sham , L. *J. Phys. Rev.* 1965, 140, A1133. (c) Salahub, D. R.; Zerner, M. C. *The Challenge of d and f Electrons*; ACS: Washington, D.C., 1989). (d) Parr, R. G.; Yang, W. *Density-Functional Theory of Atoms and Molecules*; Oxford Unv. Press: Oxford, 1989.
- (10) Gerratt , J.; Mills, I. M. *J. Chem. Phys.* 1968, 49, 1719 .
- (11) Ridley, J.; Zerner, M. C. *Theor. Chim. Acta* 1973, 32, 111. Bacon, D.; Zerner, M. C. *Theor. Chim. Acta* 1979, 53, 21.
- (12) Dewar, M. J. S.; Zoebisch, E. G.; Healy, E. F.; Stewart, J. J. P *J. Am.Chem. Soc.* 1985, 107, 3902.

-
- (13) Levin, B. F. *Chem. Phys. Lett.*, 1976, 37, 516.
- (14) Eliel, E. L.; Wilen, S. H. *Stereochemistry of Organic Compounds*; Wiley: New York, 1994
- (15) (a) Vogel, A. I. *A Text Book of Practical Organic Chemistry*; Longman group: London, 1973 (b) Kalsi, P. S. *Organic Reactions and their Mechanisms*; New Age International: New Delhi, 2000
- (16) Pretsch, E.; Buhlmann, P; Affolter, C; *Structure Determination of Organic Compounds Tables of spectral Data*; Springer: Tokyo, 2000.
- (17) Jakubke, H.D.; Jeschkeit, H *Amino acids, peptides and proteins*: Akademik press: Berline, 1977
- (18) Kurtz, S. K.; Perry, T. T. *J. Appl. Phys.* 1968, 39, 3798

L-TYROSINE BASED CHIRAL POLY (ESTER-AMIDE) S CONTAINING AZO GROUP IN THE SIDE CHAIN

6.1. Introduction

Recently, a large number of azobenzene containing side chain and main chain NLO polymers ¹⁻⁵ have been reported. In the case of NLO materials that have to be poled before measuring NLO activity, prevention of relaxation of orientational order is the important goal to be achieved to make polymers useful for applications. Many approaches, for example guest-host system ⁶⁻⁸ and functionalized systems, ⁹ have been introduced for this purpose. Functionalized systems are classified into two; (i) side chain polymers (ii) main chain polymers. Side chain polymers have the chromophores as pendent side groups, with one end of the chromophore attached to the backbone. With main chain NLO active polymers, the chromophores are incorporated into the main chain. Poled order-relaxation may be restricted for chromophores, incorporated into the polymer backbone. The significant difference between this main chain and the side chain ones is that large, segmental motions of the polymer backbone are required for poling and relaxation of the former. The *cis-trans* isomerization of azo group is playing a major role in this orientational ordering. ¹⁰

In a chiral medium, external poling is not necessary, since chemical poling is achieved through the incorporation of chiral molecules or by chiral framework. But in chemical poling, polar ordering of the molecule is quite important so as to achieve high NLO response. In order to reduce the dipolar interaction and increase polar ordering in polymer materials the possibility of introducing main chain and side chain chromophores are to be explored. Very few efforts have been seen in the literature to study the side chain and main chain effects in chiral polymers. The chiral methacrylate polymers bearing side chain azobenzene chromophores has shown dipole-dipole interaction between the side chain azoaromatic chromophores, occurring as a

consequence of their anchorage to the polymer backbone, which favors their aggregation.¹¹

This chapter discusses the effect of side chain azo group in the chiral framework of L-tyrosine. The comparison is made with the polymers containing both the main chain and side chain azo group incorporated within the same L-tyrosine chiral framework. Poly (ester-amide)s with only side chain azo group has been designed and the properties were studied theoretically using *ab initio* and semiempirical methods. Subsequently, the systems were synthesized in the laboratory and SHG efficiencies were measured experimentally using Kurtz and Perry powder method.

6.2. Computational methods

6.2.1. Monomers

Because of the high computational demand in optimizing L-tyrosine based chromophores containing more than 400 electrons, all the monomers have been optimized using restricted Hartree-Fock (RHF) method with 6-31G basis sets available with the Gaussian 03 code. To avoid the geometry effects in the prediction because of high sensitivity of polarizability to geometry, all the geometries were optimized at the same level of theory.¹²⁻¹⁵ The SCF MO energies were computed at these optimized geometries. The *static* spectroscopic properties of monomers have been calculated using Coupled Perturbed Hartree-Fock (CPHF) method at RHF 6-31++G (d, p) level available in the Gaussian codes.¹⁶ The *dynamic* spectroscopic properties have been calculated using the Zerner's INDO-SOS method with sum over 82 states.¹⁷

6.2.2. Polymers

All the polymer geometries (three repeating units) have been optimized using the AM1 parameterized Hamiltonian available in the Gaussian 03 set of codes.¹⁸ For one of the polymer, the geometries obtained by AM1 calculations have been compared with geometries obtained using *ab initio* based methods using the 6-31G basis. Both the geometries have comparable bond lengths and bond angles. Geometry calculations are restricted to this semiempirical level neglecting the small changes in bond length and

bond angle so as to save high computational demand of *ab initio* method. Also, because of the very high cost of computation in calculating the properties of polymers (repeating units) using polarized and diffused basis sets, *static* molecular properties (CPHF) of polymers have been limited with 6-31 G (d) basis sets. The *dynamic* spectroscopic properties have been calculated using the Zerner's INDO-SOS method with sum over 82 states.

6.3. Designing of molecules

In this chapter, the main emphasis was on the chromophore design based on L-tyrosine. Since L-tyrosine is a potential chiral auxiliary for NLO active material, the goal has been pointed on the addition of nitroaromatics and donor-acceptor groups (e.g. *para*-nitroaniline, azo-acid chloride) into the L-tyrosine framework. The diols have been selected on the basis of the coupling ability with the L-tyrosine framework to form polymers with high β value. Both chiral and achiral diols have been selected so as to study the effect on the β value by the incorporation of chiral and achiral molecules in to a chiral medium.

6.3.1. Monomer design

6.3.1.1. Chromophore

The route of chromophore design is shown in Figure 6.1. Since the main aim of this chapter was to study the effect of side chain azo group in NLO response of chiral media, design of the system was done accordingly. The designing of the L-tyrosine chiral framework was explained in chapter 5. Up to (*S*)-2-amino-3-(3-(4-nitrophenylazo), 4-hydroxyphenyl) propanoic acid (PNATY, 3) the design followed the procedure of chapter 5. Then, instead of, azobenzene-4, 4'-dicarbonyl chloride (AZCI), the azo acid chloride, acylation of PNATY was performed with terephthaloyl chloride (TE, 4), a diacid chloride with out azo group. This acylation produced the chiral amide framework of (*S*)-2-terphthalamido- 3-(3-(4-nitrophenylazo)-4-hydroxyphenyl) propanoic acid (TYTE,5). Chlorination of TYTE yielded (*S*)-2-terphthalamido- 3-(3-(4-nitrophenylazo)-4-hydroxyphenyl) propanoic acid chloride (TYTECl, 6).

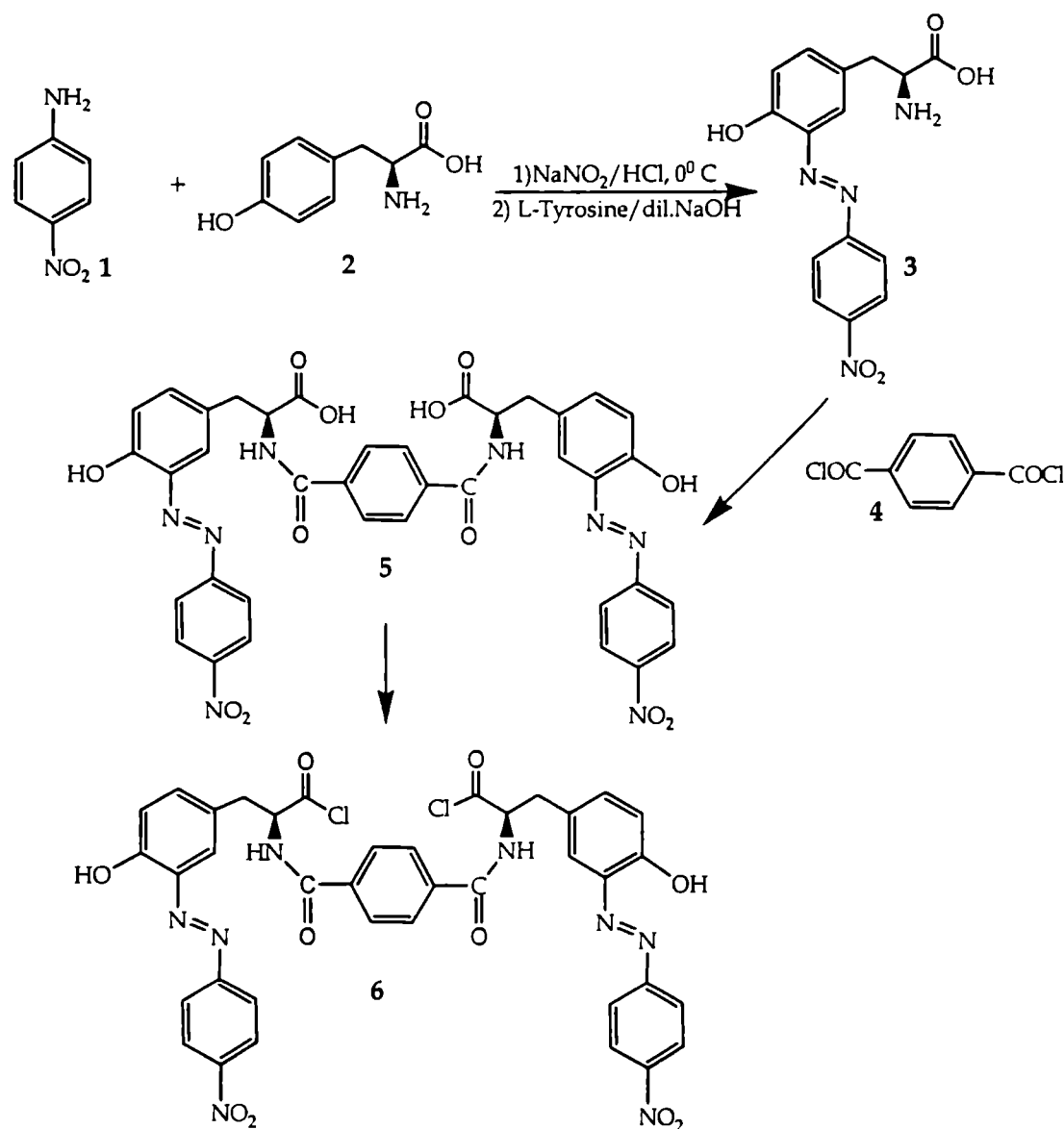


Figure 6.1. Route of chromophore design

6.3.1.1.1. Static and dynamic molecular property calculations

This chapter mainly deals with the comparison of properties of molecules containing side chain azo group with the molecules containing azo group in both the main chain and in the side chain. So, all the properties of this series of monomers and polymers were compared with the results obtained in chapter 5.

6.3.1.1.1. a. Comparison of dipole moment

The dipole moments of chromophores are summarized in **Table 6.1**. In both *static* and *dynamic* calculations, the azo acid chloride, AZCI has more dipole moment than the terephthaloyl chloride, TE, which was used as the diacid chloride with out the azo group in the design of chromophore containing azo group only in side the chain. Followed by TE, the chromophores designed from it, TYTE and TYTECI also have small dipole moments compared with TYAZ and TYAZCI.



Figure 6.2. Electron density in TYTECI

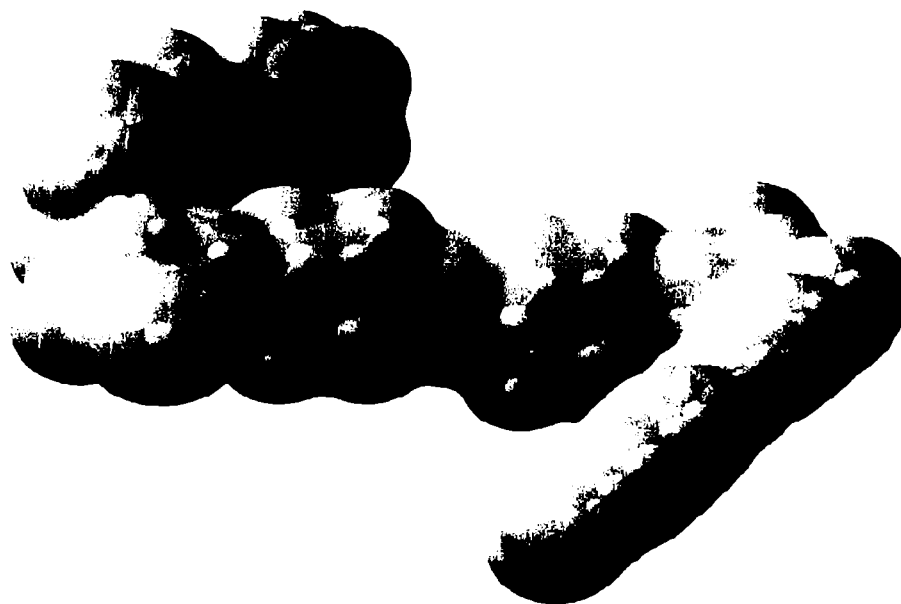


Figure 6.3. Electron density in TYAZCI

This can be attributed to the influence of two amide groups separated only by an aromatic ring. Amide groups are poor electron donors. But azo groups can act as both electron acceptor and electron donor. In the presence of -N=N- (azo) group, the electron density is more shifted towards the NO₂ group (one of the acceptors) and in the absence of azo group the shift of electron density towards the acceptors was reduced in TYTE and TYTECI. (Figure 6.2 and Figure 6.3)

Table 6.1: Comparison of dipole moments (in debye) of chromophores

Chromophore	μ_x	μ_y	μ_z	μ_g static	μ_g dynamic
PNA	6.9218	0.0026	-3.9362	7.9627	43.6312
Tyr	1.9130	1.5148	2.0806	3.2068	20.5722
PNATY	2.1497	1.5269	4.7942	5.4715	34.9174
AZCI	1.3614	0.0012	0.0114	1.3615	10.6268
TE	-1.1503	-0.0007	0.0006	1.1503	0.64485
TYAZ	7.6858	3.2330	-0.1818	8.3400	87.0284
TYTE	7.4275	0.1082	0.0000	7.4285	77.6828
TYAZCI	10.1682	4.5984	-0.0456	11.1598	99.5583
TYTECI	-0.0008	-0.0005	5.3988	5.3988	34.9915

6.3.1.1.1.b. Comparison of polarizability (α)

Table 6.2: Polarizability (α) of chromophores

Chromophore	α_{xx}	α_{yy}	α_{zz}	α (au)	$\alpha_{tot} \times 10^{-23}$ (Static*)	$\alpha_{tot} \times 10^{-23}$ (Dynamic*)
PNA	121.6103	48.7223	102.4463	90.9263	1.3474	411.0
Tyr	132.5928	81.8793	121.8485	112.1067	1.6613	294.0
PNATY	221.9997	122.9558	354.3746	233.1100	3.4544	866.0
AZCI	202.9226	102.1023	389.5218	231.5155	3.4307	927.0
TE	125.6097	61.8341	162.5198	116.6545	1.7287	416.0
TYAZ	545.6926	587.1834	812.9603	648.6121	9.6115	1350.0
TYTE	510.1612	572.2675	550.3932	544.2739	8.0654	1340.0
TYAZCI	505.0923	528.5364	701.7857	578.4714	8.5721	1430.0
TYTECI	521.96281	579.0277	561.6608	554.2171	8.2127	1310.0

* α (esu) = $0.148185 \times 10^{-24} \alpha$ (au)

The polarizability values of TE, TYTE and TYTECI were obtained from *static* method were found to be low when compared with AZCI, TYAZ and TYAZCI. The ZINDO *dynamic* values are also in agreement with *static* values. The polarizability values are summarized in Table 6.2.

6.3.1.1.1.c. Comparison of hyperpolarizability (β)

As in the case of the dipole moment (μ) and the polarizability (α), the hyperpolarizability (β) of TE, TYTE and TYTECI (the molecules without azo group in the main chain) is low as compared with AZCI, TYAZ, and TYAZCI (the molecules have an azo group in the main chain) respectively. This can be explained on the basis of HOMO-LUMO gap (ΔE). Table 6.3 gives the values of β and ΔE . The HOMO-LUMO gap of TE, TYTE and TYTECI is greater than AZCI, TYAZ, and TYAZCI. This helps for the easy charge transfer in the latter group of molecules compared to the former. Since the value of hyperpolarizability of organic molecules depends on the charge transfer from donor to acceptor part of the molecule, molecules with low HOMO-LUMO gap and thus facilitating easy charge transfer, have shown higher value of β .

Table 6.3: HOMO-LUMO gap (ΔE) in eV, Ground-State Dipole Moment (μ_g) in debye, Linear Polarizability (α) in units of 10^{-23} esu, and First Hyperpolarizability (β) in units of 10^{-30} esu for the chromophores (*ab initio* CPHF static property calculations)

Chromophore	ΔE	μ_g	α	β
PNA	0.3507	7.9627	1.3474	8.9445
Tyr	0.3461	3.2068	1.6613	1.3165
PNATY	0.3248	5.4715	3.4544	10.374
AZCI	0.3309	1.3615	3.4307	1.0072
TE	0.3883	1.1503	1.7287	1.0415
TYAZ	0.3264	8.3400	9.6115	8.0164
TYTE	0.3286	7.4285	8.0654	6.7954
TYAZCI	0.3320	11.1598	8.5721	11.2620
TYTECI	0.3284	5.3980	8.2127	5.1018

Dynamic property evaluation (ZINDO) gives exactly the same trend (Table 6.4) as static calculations. While examining TE and AZCI it can be seen that the oscillator strength, f of TE (0.3121 eV), which doesn't possess an azo group, is much lower than that of AZCI (1.3355 eV). Also, the optical gap, δE is higher in TE than in AZCI. Since easy charge transfer is determined by higher value of oscillator strength and lower value of optical gap, charge transfer is not as easy in TE as AZCI. Thus, although TE has higher value of $\Delta\mu$, the difference in dipole moment, its β value was very low compared to AZCI. In TYTE and TYTECI, the change in dipole moment, $\Delta\mu$ is very low compared to the change in dipole moment in TYAZ and TYAZCI. This lowers the value of β in the former compared to the latter azo molecules. It is notable that even the TYTE molecule containing the chiral building unit of tyrosine, its β value is lower than that of PNA (8.9445 esu) because of the low value of change in dipole moment, $\Delta\mu$ (2.5504 D).

Table 6.4: Oscillator strength f , Optical Gap (δE) in eV, Ground-State Dipole Moment (μ_g) in debye, Difference in dipole moments between ground state and excited state ($\Delta\mu$) in debye, Linear Polarizability (α) in units of 10^{-23} esu, and First Hyperpolarizability β , in units of 10^{-30} esu for the chromophores (ZINDO SOS dynamic property calculations)

Chromophore	f	δE	$\Delta\mu$	μ_g	α	β_{vec}
PNA	1.0285	7.4823	14.1337	43.6312	411.0	220.3553
Tyr	1.2761	7.6630	6.6922	20.5722	294.0	51.1458
PNATY	0.9677	4.0466	28.1308	34.9174	866.0	226.5886
AZCI	1.3355	4.1932	3.3658	10.6268	927.0	106.8586
TE	0.3121	5.2411	7.3867	0.64485	416.0	89.6450
TYAZ	2.6372	4.4560	19.9043	87.0284	135.0	655.9493
TYTE	2.6856	4.3285	2.5504	77.6828	1370.0	218.0021
TYAZCI	1.7055	4.4863	43.3013	99.5583	1430.0	740.2353
TYTECL	2.6094	4.3185	10.3396	34.9915	1310.0	367.7223

6.3.1.1.1.d. Comparison of chiral component

It is surprising that the amount of chirality is reduced by more than 50% in TYTE compared to TYAZ. This leads to the assumption that the azo group is playing an

important role not only in charge distribution but also in overall chirality. The *trans* form of the azo group imparts or translates the chirality through out the molecule.

Table 6.5: First hyperpolarizability of chromophores β (Static) in units of au

β Tensors	AZCI	TE	TYAZ	TYTE	TYAZCI	TYTECI
β_{xxx}	35.5150	-36.2513	-139.2570	-392.454	-315.5060	-200.889
β_{xxy}	0.0007	-0.01526	463.1576	9.18604	572.7625	9.4523
β_{xyy}	20.2807	-19.2325	-357.8430	-124.227	-390.9130	-114.725
β_{yyy}	0.0498	-0.02626	-575.2070	-4.2801	-816.2450	-3.9189
β_{xxz}	-1.9033	-0.00611	-368.2410	4.212456	-515.5590	4.3382
β_{xyz}	-0.0641	-0.0222	402.8543	-152.682	476.3268	-157.254
β_{yyz}	-0.0040	0.002373	350.8687	-4.19173	497.3552	-4.3606
β_{zzz}	60.3724	-65.0764	-395.2590	-269.903	-513.6710	-274.927
β_{yzz}	0.1063	-0.04249	-126.9660	-4.15401	-210.4860	-4.2415
β_{zzx}	-7.9310	-0.0247	104.5484	-0.33988	86.4357	-0.3386
β_x	116.168	-120.56	-892.3590	-786.583	-1220.09	-590.542
β_y	0.1568	-0.084	-239.0150	0.751927	-453.9680	1.2919
β_z	-9.8383	-0.02844	87.1761	-0.31915	68.2322	-0.3610
$\beta_{vec}(au)^*$	116.584	120.5603	927.9181	786.5838	1303.596	590.5437
$\beta_{vec}(esu)^*$	1.0100	1.0400	8.0200	6.800	11.3000	5.1018
%chirality	0.0549	0.0184	43.4148	19.4107	36.5394	26.6101

* β (10^{-32} esu) = 0.863916 β (au)

6.3.2. Polymer design

Design of polymers is based on the polycondensation of TYTECI with the previously designed chiral and achiral diols. Properties of diol molecules are explained in chapter 5. The repeating unit contains one TYTECI molecule and one diol molecule. All calculations have been performed for three repeating units. The structures of polymers are shown in Figure 6.4 and Figure 6.5 SHG efficiency has been compared with respect to 2-Methyl-4-nitroaniline (MNA) as the reference material. The structures

of MNA and polymers were optimized and properties were calculated using common level theory so as to avoid geometry effects in predictions.

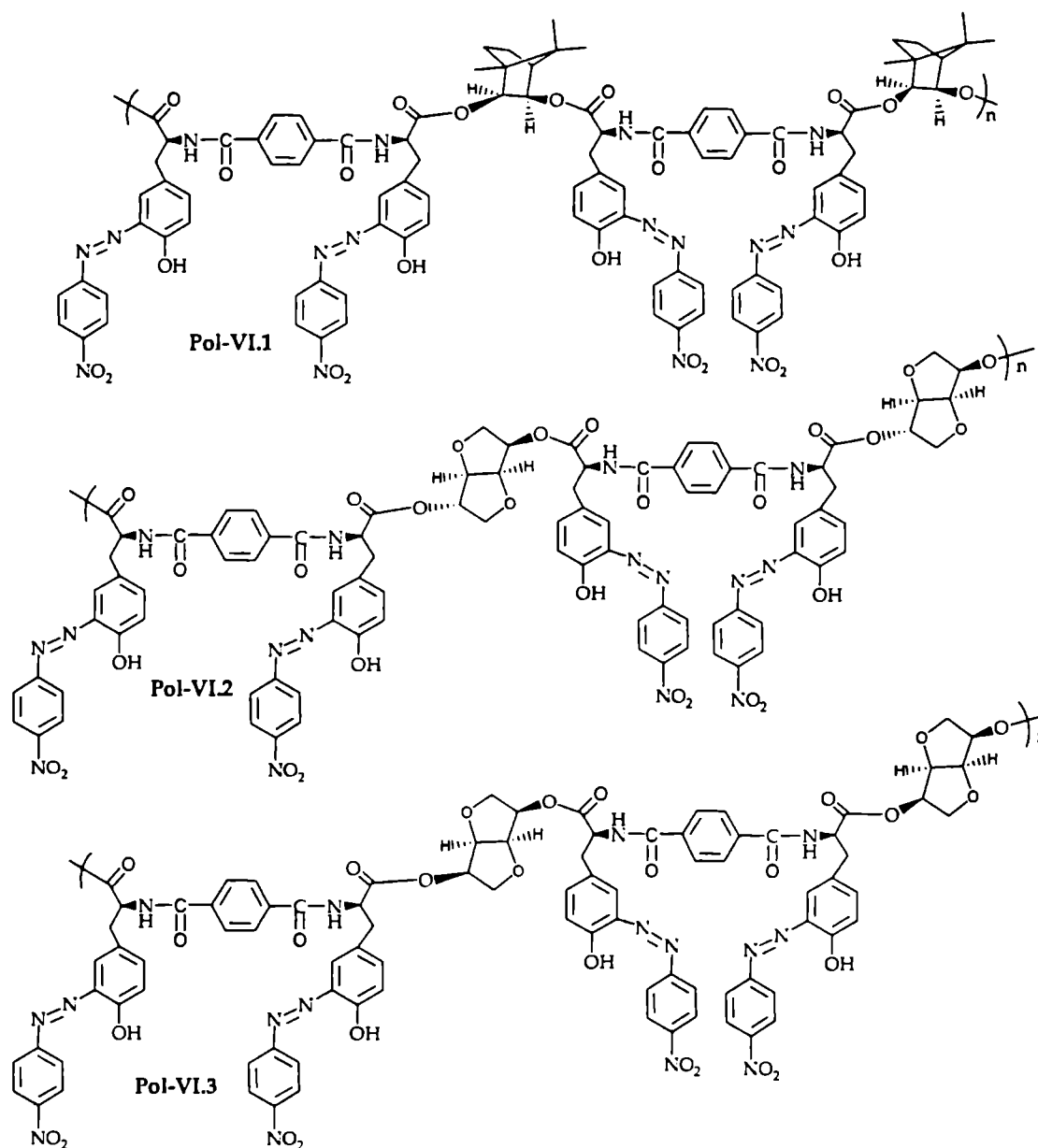


Figure 6.4. Structure of polymers (2 repeating units) incorporated with chiral diols (Pol-VI.1, Pol-VI.2, Pol-VI.3)

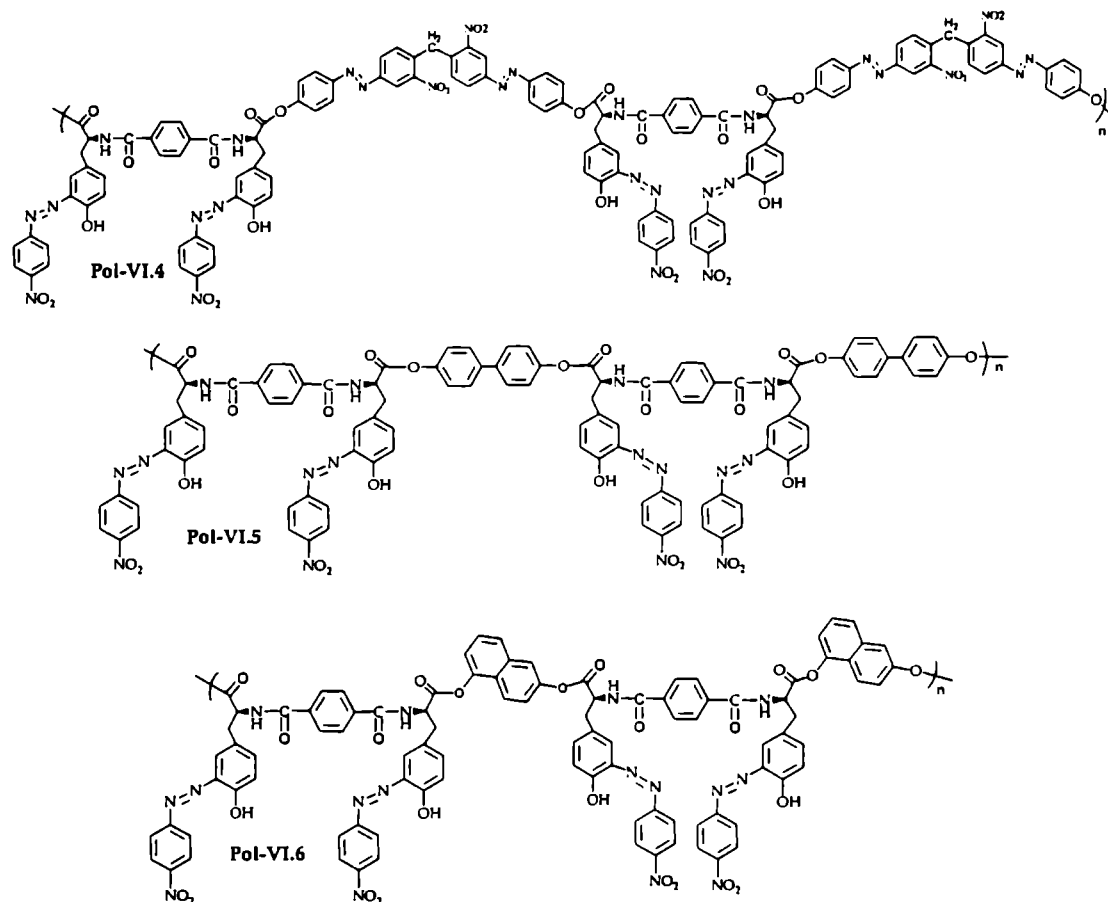


Figure 6.5. Structure of polymer (2 repeating units) incorporated with achiral diols (Pol-VI.4, Pol-VI.5, Pol-VI.6)

6.3.2.1 Static and dynamic molecular property calculations

The properties of the polymers without an azo group in the polymer main chain are compared with the properties of the polymers with an azo group in the polymer main chain. This will give the effect of azo group in determining spectroscopic properties. Even though the polymers with an azo group in the main chain contains an azo group in the side chain also, for convenience, they are named as main chain azo polymers and the polymers with azo group only in the side chain are named as side chain azo polymers. In Pol- VI.4, the achiral diol contains an azo group. Hence, in this polymer, the one repeating unit contains two azo groups whereas its analogue Pol-V.4 contains three azo groups in the main chain.

6.3.2.1.a. Comparison of dipole moment

As in the case of main chain azo polymers, the side chain azo polymers have also shown large dipole moment values compared to MNA. In *static* calculations, the side chain azo polymers incorporated with chiral diols have shown higher values of dipole moments compared to the dipole moments of main chain azo polymers incorporated with chiral diols. But surprisingly the side chain azo polymers with achiral diols have shown smaller values of dipole moment as compared with the main chain azo polymers incorporated with achiral diols. In dynamic calculations there is no such effect due to chiral and achiral diol. The dipole moment is lower in side chain azo polymers compared to main chain azo polymers. It is very much expected. The azo group is a good push-pull group than amide group. It imparts an effective electron push from donor to acceptor more easily than the amide group. The dipole moment values of polymers are summarized in Table 6.6.

Table 6.6: Dipole moment of polymers in units of debye

Polymers	μ_x	μ_y	μ_z	μ_s	μ_d
				Static	Dynamic
Pol-V.1	19.7620	8.7396	-0.8627	21.6255	242.1503
Pol-VI.1	22.6973	8.7306	-3.6824	24.5958	90.46477
Pol-V.2	38.5563	6.7376	0.4145	39.1428	572.2634
Pol-VI.2	33.4160	20.4653	9.5532	40.3326	283.7991
Pol-V.3	26.9111	6.0175	-1.2337	27.6033	286.6680
Pol-VI.3	31.1928	15.6559	16.9468	38.7980	282.1185
Pol-V.4	8.5608	25.3210	-15.6744	30.9859	423.9742
Pol-VI.4	14.9360	0.9432	-1.54860	15.0457	154.1610
Pol-V.5	34.1279	15.2220	-0.0963	37.3689	355.5187
Pol-VI.5	17.5007	0.1477	-0.0066	17.5014	166.0726
Pol-V.6	29.3493	13.4670	-0.2270	32.2923	332.3781
Pol-VI.6	15.8911	15.7878	22.9769	32.0893	284.8405
MNA	0.1357	1.3755	-6.8645	7.0023	40.0614

6.3.2.1.b. Polarizability (α)

Linear polarizability values are shown in Table 6.7. The chirality of the constituent diols didn't affect the polarizability values. All the side chain azo polymers have high α values with respect to MNA as in the case of main chain azo polymers. But from both *static* and *dynamic* calculations the α values of side chain azo polymers are smaller than that of main chain azo polymers. This indicates that the trends in the dipole moment as predicted from *dynamic* calculations have been followed in the prediction of polarizability values.

Table 6.7: Polarizability α of polymers

Polymers	α_{xx}	α_{yy}	α_{zz}	α (au)	$\alpha_{tot} \times 10^{-23}$	
					Static*	Dynamic*
Pol-V.1	2022.926	2224.921	2758.197	2335.3480	34.6060	4056.480
Pol-VI.1	2032.6692	2079.1745	2284.2422	2132.029	31.5936	3348.000
Pol-V.2	1752.230	2303.824	2468.601	2174.8854	32.2290	3091.680
Pol-VI.2	2190.6785	1512.4996	2051.7973	1918.325	28.4268	152.928
Pol-V.3	1759.414	2276.693	2437.519	2157.8752	31.9770	3340.800
Pol-VI.3	2002.3277	1730.1354	1939.0959	1890.52	28.0148	3216.960
Pol-V.4	2637.1810	2438.77	2499.221	2525.0572	37.4100	5732.950
Pol-VI.4	2527.8793	2480.4853	2250.0248	2419.463	35.8529	5677.920
Pol-V.5	1952.120	2572.932	3032.917	2519.3229	37.3330	3421.440
Pol-VI.5	2654.3335	1924.4479	2177.4319	2252.071	33.3724	3057.920
Pol-V.6	1809.624	2338.003	2943.665	2363.7641	35.0280	3304.800
Pol-VI.6	2151.1599	1751.8219	2549.4134	2150.798	31.8717	2728.800
MNA	99.4808	38.78715	122.8410	87.0363	1.2898	400.0012

* α (esu) = $0.148185 \times 10^{-24} \alpha$ (au)

6.4.2.1.c. Comparison of hyperpolarizability

Static (CPHF) hyperpolarizability values (Table 6.8.) of side chain azo polymers diverted from the dipole moment and polarizability trends. The values of β are higher for all the side chain azo polymers when compared to the main chain azo polymers,

while dipole moment, μ_g is higher only for chiral diol containing polymers and polarizability, α values are smaller in all side chain azo polymers irrespective of whether incorporated with chiral or achiral diol. The HOMO-LUMO gaps of side chain azo polymers are not adequate to explain this increase in β . In fact, the gap is higher in side chain azo polymers compared with the main chain azo polymers. This anomaly may be due to the inadequacy of *static* calculation (without much electron correlation)

Table 6.8: HOMO-LUMO Gap (ΔE) in eV, Ground-State Dipole Moment (μ_g) in debye, Linear Polarizability (α) in units of 10^{-23} esu, and First Hyperpolarizability, in units of 10^{-30} esu for the polymers (ab initio CPHF static property calculations)

Polymers	ΔE	μ_g	α	β_{vec}
Pol-V.1	0.3134	21.6255	34.6060	35.9861
Pol-VI.1	0.3398	24.5958	31.5936	66.3681
Pol-V.2	0.3343	39.1428	32.2290	14.4112
Pol-VI.2	0.3344	40.3326	28.4268	68.6399
Pol-V.3	0.3374	27.6033	31.9770	18.8488
Pol-VI.3	0.3366	38.7980	28.0148	87.4436
Pol-V.4	0.3243	30.9859	37.4100	26.9000
Pol-VI.4	0.3178	15.0457	52.1533	65.108
Pol-V.5	0.2925	37.3689	37.3330	33.6258
Pol-VI.5	0.3124	17.5014	33.3724	43.4443
Pol-V.6	0.2836	32.2923	35.0280	34.7583
Pol-VI.6	0.3080	34.1473	31.8717	30.0192
MNA	0.3970	7.0023	1.2898	5.2684

Results of *dynamic* ZINDO-SOS calculation are presented in Table 6.9. It is surprising that, in contrast to *static* calculations, the β values of all side chain azo polymers are lower than that of main chain azo polymers. This can easily be explained on the basis of two-level parameters, oscillator strength (f), optical gap (δE) in eV, and difference in dipole moments between ground state and excited state ($\Delta\mu$). In all the side chain azo polymers either f or $\Delta\mu$ is smaller than that of main chain azo polymers. These parameters decrease the value of β . In a chemical perspective, this can be explained on

Table 6.9: Oscillator strength (f), Optical Gap (δE) in eV, Ground-State Dipole Moment (μ_g) in debye, Difference in dipole moments between ground state and excited state ($\Delta\mu$), Linear Polarizability (α) in units of 10^{-23} esu, and First Hyperpolarizability in units of 10^{-30} esu for the polymers (ZINDO-SOS dynamic property calculations)

Polymer	F	δE	$\Delta\mu$	μ_g	α	β_{vec}
Pol-V.1	5.3562	13.4529	133.6228	242.1503	405.648	2168.197
Pol-VI.1	4.9411	15.0393	135.6050	90.4648	3348.00	1805.727
Pol-V.2	0.4684	17.7927	240.6799	572.2634	15.2928	762.805
Pol-VI.2	4.4928	15.4335	155.7673	283.7991	3091.68	737.973
Pol-V.3	5.0169	14.3649	142.4032	286.6680	334.080	1536.880
Pol-VI.3	4.1369	14.9172	111.1800	292.1185	3216.96	1120.704
Pol-V.4	3.9045	15.0972	168.9320	423.9742	400.9702	1797.502
Pol-VI.4	3.1214	13.6887	237.6463	154.1610	5677.92	1278.510
Pol-V.5	4.0649	13.8318	185.4564	355.5187	342.144	1966.639
Pol-VI.5	7.7026	17.0856	57.4468	166.0726	4057.92	1222.223
Pol-V.6	4.1477	14.0781	126.1178	332.3781	330.480	1466.959
Pol-VI.6	4.2878	15.7644	133.4538	284.8405	2728.80	1078.004
MNA	0.9502	8.2721	12.0416	39.5013	300.8571	182.464

the basis of difference in electron distribution in the presence and absence of azo group. Azo group is a good electron donor (and acceptor also), hence the total charge distribution is uniform through the polymer chain when an azo group is present in the main chain. While in the absence of azo group, this electron distribution breaks at amide group. This is because of the reason that the amide group is not a good donor and in most cases it acts as an acceptor. When an azo group is present in the main chain near to the amide group, it takes the electrons from the main chain azo group and forms weak donor-acceptor system with amide group. This leaves the side chain azo electrons for -NO₂ group. Thus side chain azo -NO₂ system acts as very good donor-acceptor system. Hence, in polymers with main chain azo group, two donor-acceptor systems compliment very well and give good SHG response. While in side chain azo polymers, there is no azo group in the main chain. So the acceptor amide group takes the electron from the side chain azo group and forms a weak donor-acceptor system. So there is a

competition between amide group and the side chain $-\text{NO}_2$ group for the same azo group electrons. This highly reduces the strength of azo $-\text{NO}_2$ donor acceptor system. Hence, in principle, side chain azo polymers occupied with two weak donor-acceptor systems have reduced the SHG response.

6.4.2.1.d Comparison of chiral component

Table 6.10: First hyperpolarizability tensors of Polymers β (Static) in atomic units

#	Pol-V.1	Pol-VI.1	Pol-V.2	Pol-VI.2	Pol-V.3	Pol-VI.3	Pol-V.4	Pol-VI.4	Pol-V.5	Pol-VI.5	Pol-V.6	Pol-VI.6	MNA
β_{xxx}	-1048.33	-3877.8	500.3188	-5353.2	219.2635	-3417.4	503.6268	2747.17	-997.694	-1164.5	-988.283	-2355.26	-24.4201
β_{sxy}	1677.457	579.748	921.6536	-3867.2	990.8157	-1515.3	274.3517	-319.55	1827.039	0.38799	1731.973	-1123.06	13.5831
β_{yyv}	-1200.67	-3243.1	-1551.85	-2781.0	-1841.85	-904.55	129.2712	-3880.2	-1282.98	-593.12	-1200.15	-867.425	12.7643
β_{yyy}	-2466.73	-3793.7	-399.395	-2186.7	-920.593	-3055.6	239.5554	390.385	-2552.55	-16.016	-2521.87	-449.051	7.1032
β_{xiz}	-1509.88	1497.74	-568.978	-1737.0	-611.594	-921.24	2856.3440	285.192	-1525.0	10.7791	-1474.58	-1218.14	-137.669
β_{syz}	2389.433	-1352.4	1191.205	-1190.6	1234.665	-983.50	983.1450	-381.27	1406.965	-652.02	1369.3	-986.331	0.9190
β_{yyz}	1454.972	-36.339	373.3215	-890.71	613.6915	-2362	-973.1370	231.146	1440.737	-10.681	1437.96	-2509.48	-26.7852
β_{szz}	-1627.78	-56.161	-561.931	199.202	-537.314	-217.83	-329.5080	779.452	-1380.15	-956.04	-1565.74	-1191.17	15.0008
β_{yzz}	-717.775	829.839	-109.928	120.494	-239.676	-1137.8	2485.348	-188.86	-577.409	-7.4176	-635.238	-1257.68	-20.2272
β_{zzz}	279.673	-111.56	98.7310	558.592	255.3821	132.547	-1103.590	138.677	308.7788	0.1054	286.566	-830.418	774.2734
β_x	-3876.78	-7177.0	-1613.46	-7935.0	-2159.9	-4539.8	303.3897	-353.55	-3660.82	-2713.6	-3754.17	-4413.86	3.3450
β_y	-1507.05	-2384.1	412.3308	-5933.4	-169.454	-5708.7	2999.255	-118.03	-1302.92	-23.046	-1425.14	-2829.8	0.4592
β_z	224.7625	1349.83	-96.9257	-2069.2	257.4799	-3150.7	779.6211	655.016	224.5186	0.2035	249.9474	-4558.04	609.8187
β_{vec}^a	4165.467	7682.24	1668.131	10121.8	2181.788	7945.20	3113.741	753.641	3892.251	2713.72	4023.337	6947.347	609.8281
β_{vec}^b	36.00	66.40	14.40	87.40	18.80	68.6	26.9001	6.51	33.60	23.40	34.8	30.00	5.27
\$	57.3629	17.6042	71.4095	11.7627	56.5895	12.3785	31.2534	50.5904	36.1478	27.0267	34.0339	14.1972	0.1506

= β Tensors * $\beta_{vec} \times 10^{-30}$, β (10^{-32} esu) = 0.863916β (au), \$ = %chirality a = β_{vec} in au b = β_{vec} in esu

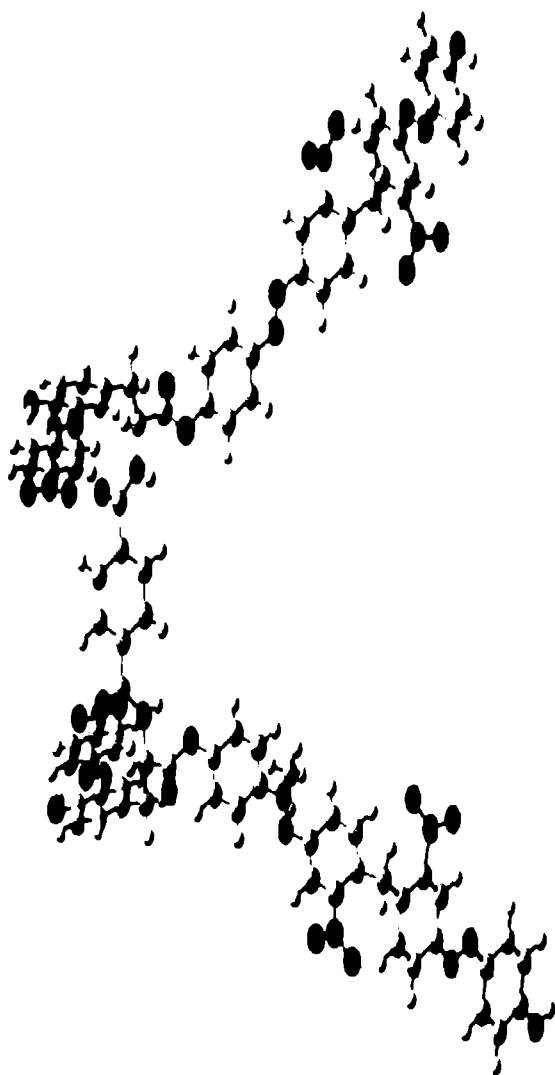


Figure 6.6. Optimized Structure of Pol-VI.4 (One repeating Unit)

polymers with main chain azo polymers, it can be seen that main chain azo polymers have more β_{xyz} values than side chain azo polymers. Due to the absence of azo group in the main chain the polymer chain lacks the helicity. This can be easily understood from the **Figure 6.6**. The presence of main chain azo groups (i.e. the azo group present in the chiral framework) imparts the helicity of the polymer main chain. This increases the overall chirality of the polymer chain and hence the β_{xyz} value. Even though **Pol-VI.4** contains one main chain azo group (from diol), it could not produce a helicity in the

In the first sight of **Table 6.10**, it was very surprising that the percentage chirality is small for chiral diol incorporated side chain azo polymers than that of the achiral diol incorporated side chain azo polymers. But when examining thoroughly, it can be seen that the β_{xyz} values of side chain azo polymers incorporated with chiral diols are larger than those incorporated with achiral ones. The percentage chirality is calculated as a percentage of total hyperpolarizability values, β . Since β is small in the chiral diol incorporated side chain azo polymers, the percentage chirality is also small. But the exact values of β_{xyz} are larger only in chiral diol incorporated side chain azo polymers than the achiral diol incorporated ones. Comparing the values of β_{xyz} of side chain azo

optimized structure. (Figure 6.6.) Hence, from the *dynamic* calculations and from the chiral parameter it can be concluded that the main chain azo polymers are better material for SHG.

6.4. Synthesis

For comparing the influence of incorporating azo group in the main chain and side chain effect of poly (ester-amide) s, a series of side chain azo polymers based on L-tyrosine framework has been designed and the spectroscopic properties were calculated using *static* and *dynamic* methods. *Dynamic* calculations revealed that the side chain azo polymers are poor SHG materials compared to the main chain azo polymers. To study the side chain and main chain effect experimentally, these polymers were synthesized and SHG efficiency was measured using Kurtz and Perry powder method. Six polymers were synthesized from L-tyrosine framework and diols (chiral and achiral) by high temperature polycondensation method. The following section deals with the synthetic procedures

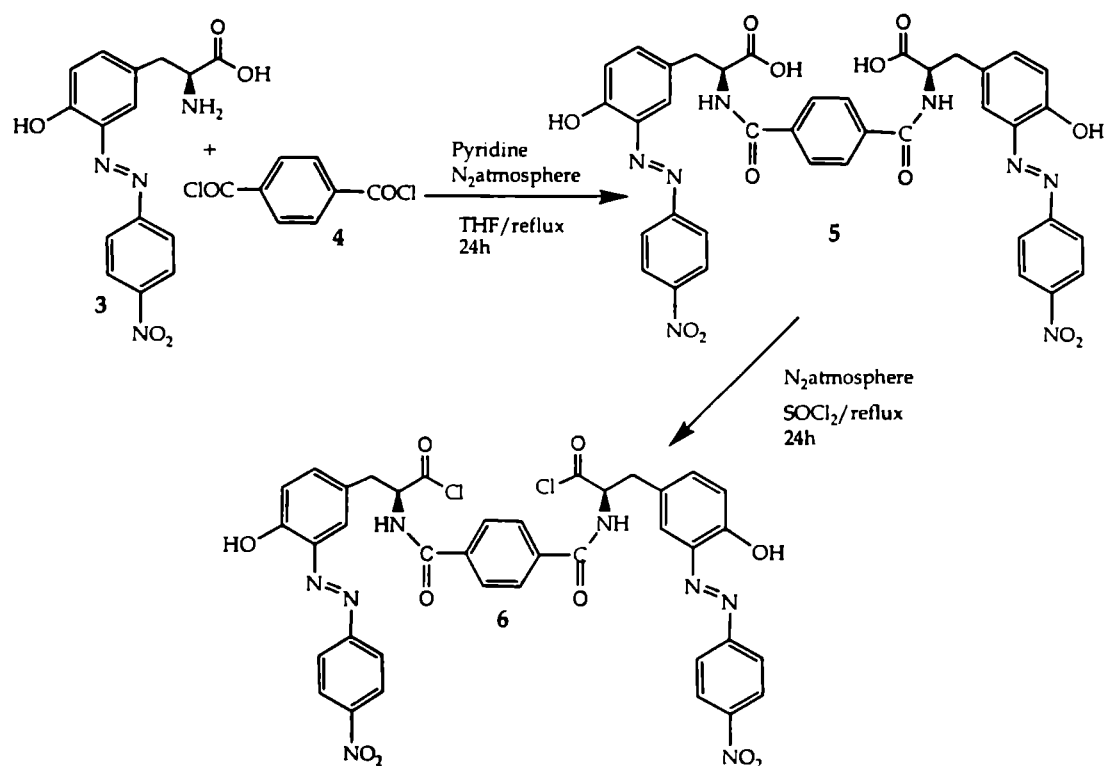
6.4.1 Monomer synthesis

6.4.1.1 Synthesis and characterization of chiral chromophore

L-Tyrosine based chiral chromophore was synthesized by a three-step process. In the first stage L-tyrosine was coupled with *para* nitroaniline to get PNATY. Synthesis of (S)-2-amino-3-(3-(4-nitrophenylazo)-4-hydroxyphenyl) propanoic acid (PNATY) was described in chapter 5. In the second stage, PNATY was acylated with terephthaloyl chloride to get TYTE. Chlorination of TYTE yielded TYTECl.

Synthesis of (S)-2-terephthalamido- 3-(3-(4-nitrophenylazo), 4-hydroxyphenyl) propanoic acid chloride (TYTECl, 6).

Terephthaloyl chloride (TE, 4) and (S)-2-amino-3-(3-(4-nitrophenylazo), 4-hydroxyphenyl) propanoic acid (PNATY, 3) were used for the synthesis of (S)-2-terephthalamido- 3-(3-(4-nitrophenylazo)-4-hydroxyphenyl) propanoic acid chloride (TYTECl, 6).



Scheme 6.1 Synthesis of TYTECI

PNATY (3) (1, g, .00316 mol) and terephthaloyl chloride, 4 (TE, 0.321g, 0.00158 mol) were added to a 50 mL three necked round bottom flask equipped with mechanical stirring and heating. THF (15 mL) was added as solvent. To this mixture, few drops of pyridine was added. The reaction was carried out for 24h at reflux temperature under nitrogen atmosphere. The reaction mixture was cooled and filtered. Dark brown solid of TYTE was obtained. This product was recrystallized from methanol (M.P 244^o C). The recrystallized product TYTE was refluxed with SOCl₂ for 24h under nitrogen atmosphere to obtain TYTECI (6). The reaction mixture was cooled, filtered and recrystallized from acetone.

Characterization

Yield 86%, $[\alpha]_D -11.3^{\circ}$ Decomposed at 209. 31^o C

Elemental analysis: Calculated for C₃₈H₂₈Cl₂N₈O₁₀ - C, 55.15; H, 3.41; N, 13.54. Found - C, 55.10; H, 3.42; N, 13.55

Spectral properties

UVλ_{max} nm: 300 (NO₂), 379 (-N=N-)

IR(KBr pellet) cm^{-1} : 3405 (NH⁺, NH str), 3073(-OH str), 1740(carbonyl of acid chloride), 1689 (carbonyl of amide), 1525 (NO₂ str as) 1438 (-N=N- str, 1332 (-NO₂ str ay) 1279 (aromatic trans -N=N-)

¹H NMR (300 MHz DMSO-d₆): δ 9.4 (2H, phenolic -OH), 8.61 (d, 4H aromatic, near to NO₂), 8.52 (4H aromatic, near to -N=N-), 8.21 (4H, aromatic hydrogen from acid chloride), 7.9 (d, 2H, amide hydrogen), 7.5 (d, 2H, amino acid phenyl ring near to -N=N-), 7.1 (d, 2H, amino acid phenyl ring near to -CH₂) 6.9 (d, 2H, amino acid phenyl ring near to -OH), 4.0 (m, 2H, -CH), 2.8, 2.5 (d, 4H, -CH₂)

¹³C NMR (75 MHz DMSO-d₆): δ 175.6 (-CO, acid chloride), 170.1 (-CO, amide), 161.1, 154.6, 152.6 140.4, 136.3, 132.4, 130.2, 127.8, 126.4, 125.1, 124.7, 118.1 (aromatic), 69.4 (4CH), 34 (-CH₂)

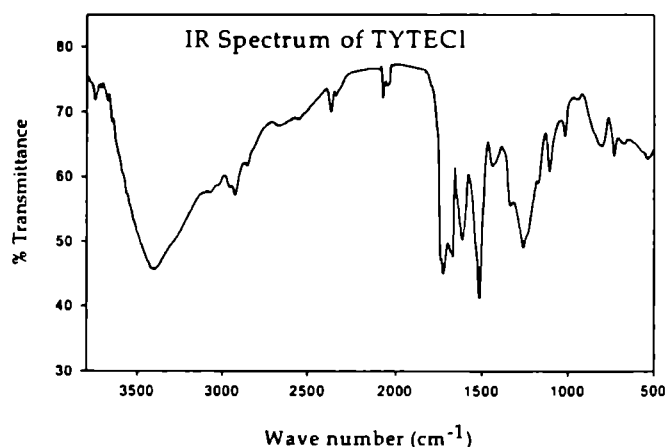


Figure 6.7. IR Spectrum of TYTECI

In the IR spectrum,(Figure 6.7) a structured band at 3405 cm^{-1} indicates the presence of (C=O)-Cl, hydrochloride of amino acids (confirmed chlorination of TYTE). Two distinct bands at 1740 cm^{-1} and 1689 cm^{-1} indicates two types of carbonyl functionality. The band at 17490 cm^{-1} is due to the carbonyl of acid chloride and the latter at

1689 cm^{-1} is due to the amide carbonyl. This confirmed the poly (ester amide) formation. The intensity of -N=N- str. band is less in TYTECI compared to TYAZCI which indicates the decrease in the concentration of azo group.

Six different types of hydrogens in the ¹H NMR spectrum (Figure 6.8) confirmed the disubstitution at terephthaloyl chloride. Monosubstitution would have given eight different hydrogens. Absence of off field peak confirmed the absence of carboxylic -OH hydrogen and thus confirmed chlorination. The peak due to -CH hydrogen was shifted to δ 4.0 which was due to the presence of -COCl near to -CH.

Twelve carbons in aromatic region of ^{13}C NMR spectrum (Figure 6.9) confirmed disubstitution at acid chloride. The peaks at δ 170.1 (due to amide $-\text{CO}$ group) and peak at δ 175.6 (due to carboxylic $-\text{CO}$) also indicated two different carbonyl groups which confirmed the proposed structure.

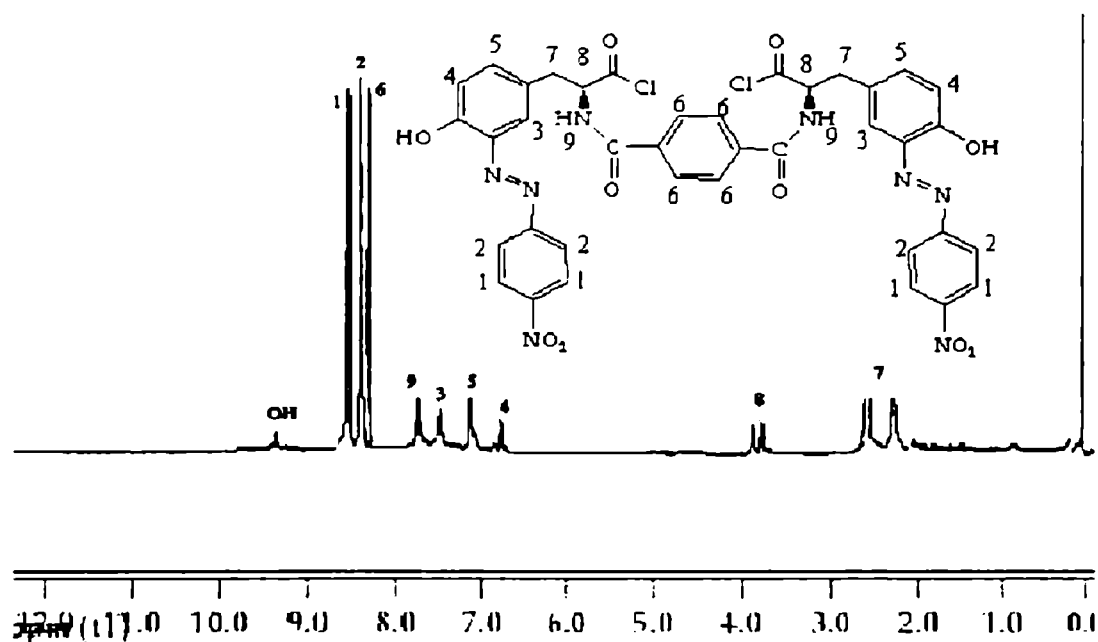


Figure 6.8. ^1H NMR spectrum of TYTECl

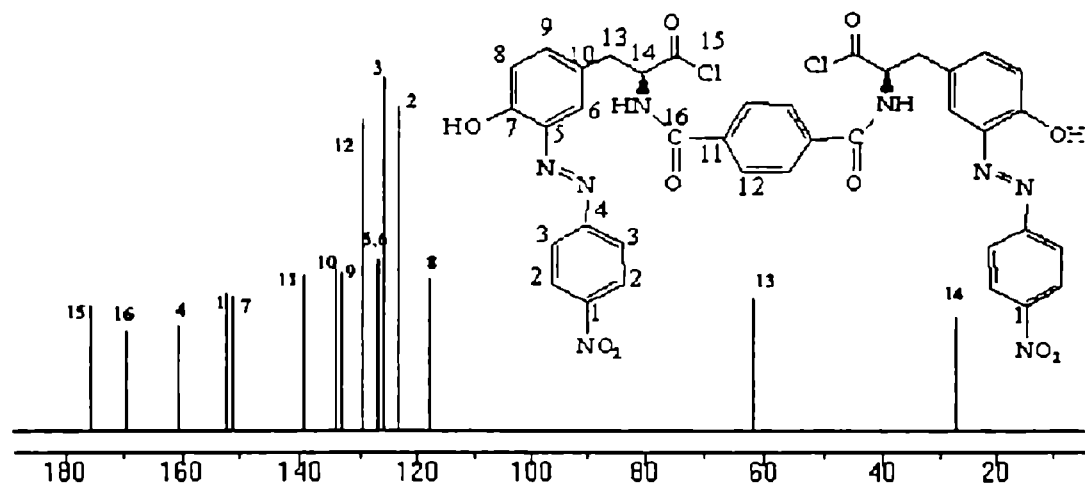
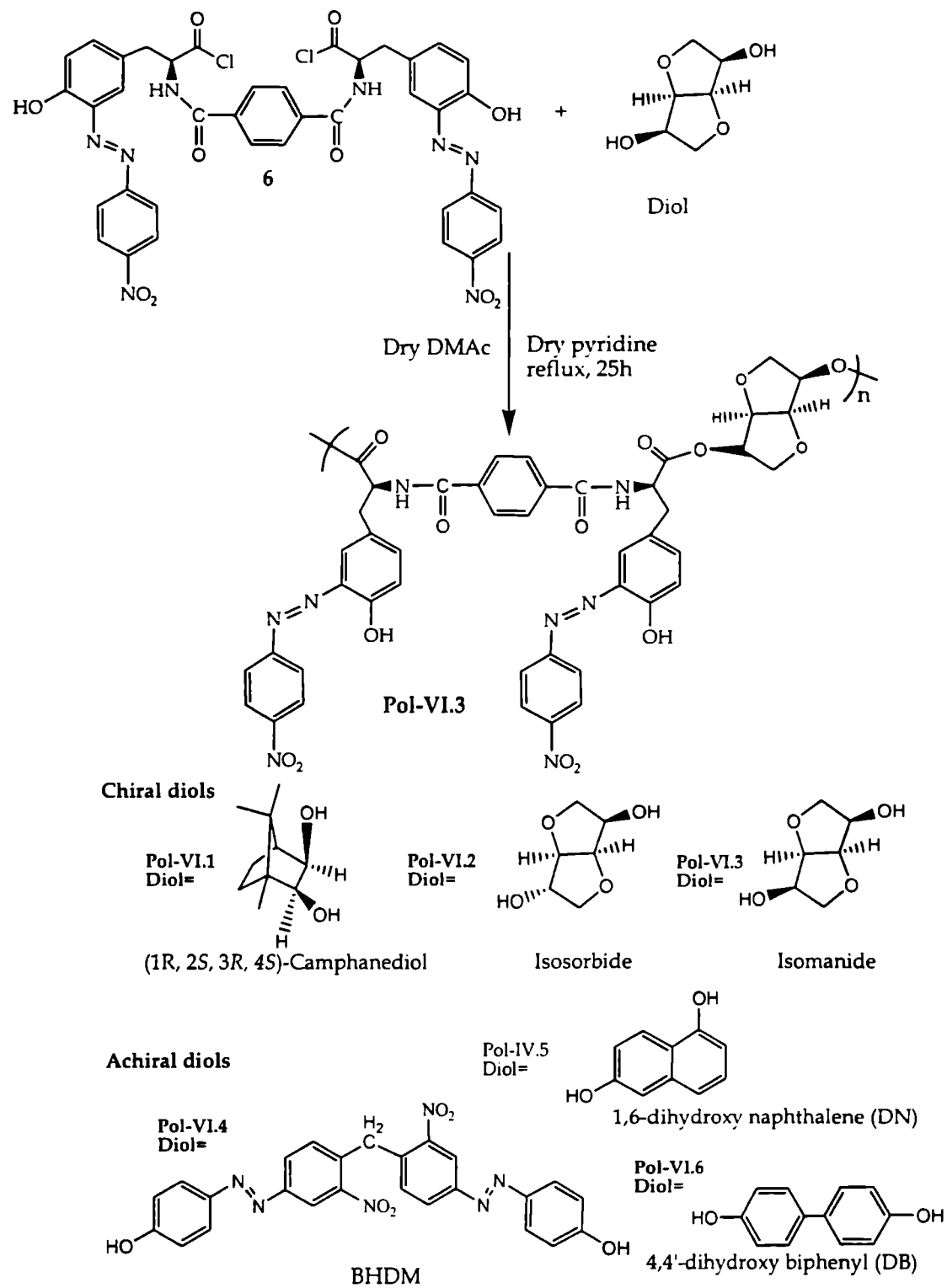


Figure 6.9. ^{13}C NMR spectrum of TYTECl

6.4.2. Synthesis of Poly (ester-amide) s



Scheme 6.2. Synthesis of poly (ester-amide) s

The designed polymer structures were synthesized by the polycondensation of L-tyrosine based chromophore with the diols. All polymer syntheses were done in solution method at high temperatures. Appropriate acid chloride was dissolved in extremely dry dimethyl acetamide (HPLC grade, s. d. fine). To this solution, (S)-2-terephthalamido-3-(3-(4-nitrophenylazo)-4-hydroxyphenyl) propanoic acid chloride (TYTECl, 6) in DMAc was added. Few drops of extremely dry pyridine (99.99% dry pyridine, s.d.fine) were added as acid acceptor. The mixture was refluxed under stirring for 25h. The product was precipitated from cold methanol and washed continuously with hot water, methanol and acetone. After filtration and drying a brown solid was obtained. **Scheme 6.2** gives the synthetic route for polymers.

6.4.2.1. Characterization of polymers

Pol-VI.1

Yield: 70%

Spectral properties

UV λ_{\max} (solid): 362 ($\pi \rightarrow \pi^*$, N=N), 323 ($n \rightarrow \pi^*$, NO₂)

IR(KBr pellet) cm⁻¹ : 3419 (NH st, OH st), 2921 (-CH stretch in camphanediol), 1729 (aromatic ester carbonyl), 1689 (amide I carbonyl stretch), 1532 (NO₂ st as, amide II st sy), 1425 (-N=N- st), 1350 (NO₂ st sy)

¹H NMR (300 MHz DMSO-d₆): δ 9.0 (phenolic -OH), 8.35 (aromatic, near to NO₂), 7.88 (aromatic hydrogen from acid chloride near to -CO), 7.17 (amino acid phenyl ring near to -CH₂), 6.72 (amino acid phenyl ring near to -OH), 4.86 (m, -CH), 4.28, 4.35 (d, -CH₂), 3.13 (m, -CH₂ cyclopentane ring of camphanediol), 2.41 (m, -CH, cyclopentane ring of camphanediol), 2.13 (s, -CH₃ of camphanediol), 1.25 (s, bridged -C(CH₃)₂ of camphanediol).

Pol-VI.2 and Pol-VI.3

Pol-VI.2 (Yield 69%) and **Pol-VI.3** (yield 73%) are different only in the stereochemistry of the chiral building units. So their spectral patterns are similar except in ¹HNMR. But in ¹H NMR the -CH protons which have the different stereochemistry in isosorbide and isomanide appeared as multiplet. So a distinction between them is difficult

Spectral properties

UV λ_{\max} (solid): 362 ($\pi \rightarrow \pi^*$, N=N), 323 ($n \rightarrow \pi^*$, NO₂)

IR (KBr pellet) cm⁻¹ : 3410 (NH st, OH st), 2925 (-CH stretch in isosorbide or isomanide unit), 1731 (aromatic ester carbonyl), 1690 (amide I carbonyl stretch), 1533 (NO₂ st as, amide II st sy), 1424 (-N=N- st), 1345 (NO₂ st sy)

¹H NMR (300 MHz DMSO-d₆): δ 8.9 (phenolic -OH), 8.33 (aromatic, near to NO₂), 8.11(4H aromatic, near to -N=N-), 7.82 (aromatic hydrogen from acid chloride near to -CO), 7.31 (amino acid phenyl ring near to -N=N-), 7.14 (amino acid phenyl ring near to -CH₂) 6.71 (amino acid phenyl ring near to -OH), 4.79(-CH), 4.19, 4.27 (-CH₂), 4.13 (-CH isosorbide or isomanide unit), 3.51 (-CH₂ in isosorbide or isomanide unit), 3.32 (bridge CH in isosorbide or isomanide unit)

Pol-VI-4

Yield: 72%

Spectral properties

UV λ_{\max} (solid): 274 (-Ph-CH₂-Ph-), 362 ($\pi \rightarrow \pi^*$, N=N), 323 ($n \rightarrow \pi^*$, NO₂)

IR (KBr pellet) cm⁻¹ : 3413 (NH st, OH st), 1730 (aromatic ester carbonyl), 1685 (amide I carbonyl stretch), 1530 (NO₂ st as, amide II st sy), 1428 (-N=N- st), 1355 (NO₂ st sy)

¹H NMR (300 MHz DMSO-d₆) δ : 8.88 (phenolic -OH), 8.15 (aromatic, near to NO₂), 7.79 (aromatic hydrogen from acid chloride near to -CO), 7.35 (amino acid phenyl ring near to -N=N-), 7.23 (amino acid benzene ring near to -CH₂) 6.71 (amino acid phenyl ring near to -OH), 5.15 (s, 2H, -CH₂ of BHDM), 4.84(-CH), 4.21, 4.29 (-CH₂)

Pol-VI.5

Yield: 70%

Spectral properties

UV λ_{\max} (solid): 280 (biphenyl), 362 ($\pi \rightarrow \pi^*$, N=N), 323 ($n \rightarrow \pi^*$, NO₂)

IR (KBr pellet) cm⁻¹ : 3390 (NH st, OH st), 1732 (aromatic ester carbonyl), 1687 (amide I carbonyl stretch), 1532 (NO₂ st as, amide II st sy), 1425 (-N=N- st), 1350 (NO₂ st sy)

¹H NMR (300 MHz DMSO-d₆) δ : 8.92 (phenolic -OH), 8.19 (aromatic, near to NO₂), 7.79 (aromatic hydrogen from acid chloride near to -CO), 7.34 (aromatic, biphenyl) 7.29

(amino acid phenyl ring near to $-N=N-$), 7.19 (amino acid phenyl ring near to $-CH_2$), 6.59 (amino acid phenyl ring near to $-OH$), 6.49 (aromatic biphenyl), 4.81($-CH$), 4.26, 4.35 ($-CH_2$).

Pol-VI-6

Yield: 73%

Spectral properties

UV λ_{max} (solid): 362 ($\pi \rightarrow \pi^*$, $N=N$), 323 ($n \rightarrow \pi^*$, NO_2)

IR (KBr pellet) cm^{-1} : 3393 (NH st, OH st), 1730 (aromatic ester carbonyl), 1685 (amide I carbonyl stretch), 1530 (NO_2 st as, amide II st sy), 1423 ($-N=N-$ st), 1349 (NO_2 st sy), 800-760 (characteristic of naphthalene)

1H NMR (300 MHz DMSO- d_6) δ : 8.81 (phenolic $-OH$), 8.22 (aromatic, near to NO_2), 7.73 (aromatic hydrogen from acid chloride near to $-CO$), 7.21, 7.31 (aromatic, naphthalene), 7.45 (amino acid phenyl ring near to $-N=N-$), 7.21 (amino acid benzene ring near to $-CH_2$), 6.80 (aromatic, naphthalene) 6.63 (amino acid phenyl ring near to $-OH$), 4.76($-CH$), 4.19, 4.28 ($-CH_2$)

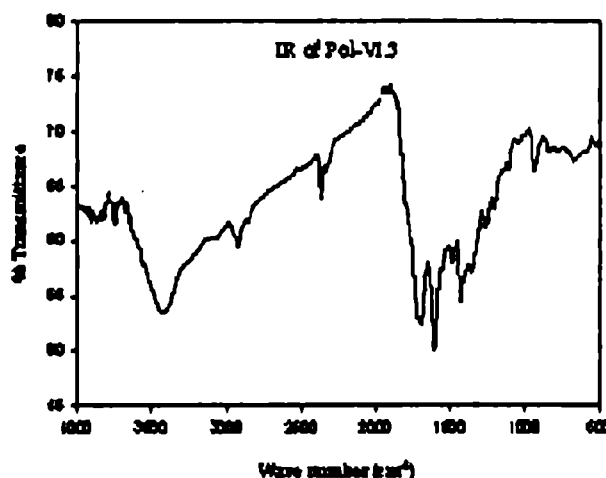


Figure 6.10. IR spectrum of Pol-VI.3

IR spectrum (Figure 6.10) of the polymers have shown two distinct carbonyl peaks at 1730-1715 cm^{-1} and 1680-1700 cm^{-1} . These peaks can be attributed due to aromatic ester carbonyl and due to amide linkage. In the amide linkage $-CO$ is directly connected to $-NH$. This decreases the frequency of $C=O$ st. to a lower value than the ester carbonyl. Presence of two distinct

carbonyl peaks confirmed the esterification of TYTCl with different diols. 1H NMR spectrum is given in Figure 6.11. The poly (ester-amide) s is less soluble in DMSO. So ^{13}C NMR spectra could not able to be recorded. Under the percent level of sophistication a

variable solid state ^{13}C NMR spectra of this series of poly (ester-amide) s could not be recorded

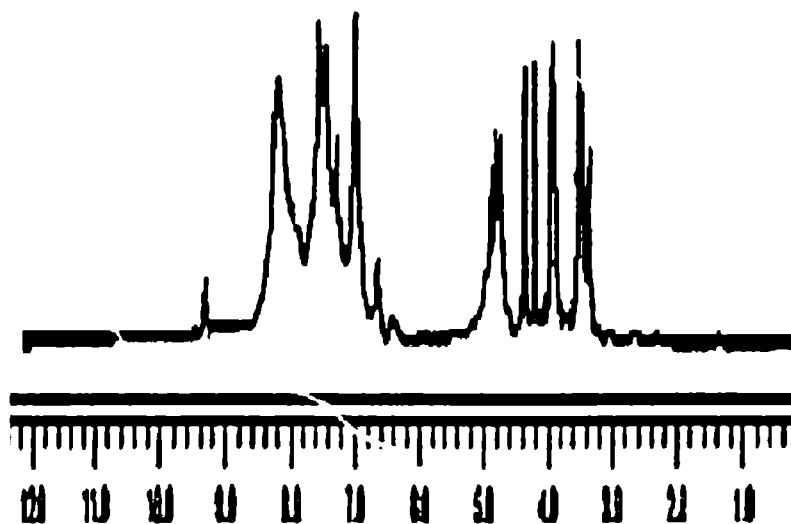


Figure 6.11. ^1H NMR spectrum of Pol-VI.3

Mass spectrum: The mass spectrum (Figure 6.12) of Pol-VI.4 ($m/e = 10016$) gives an idea about the degree of polymerization. It showed that 8 repeating units (one repeating unit = 1252) was involved in the polymerization.

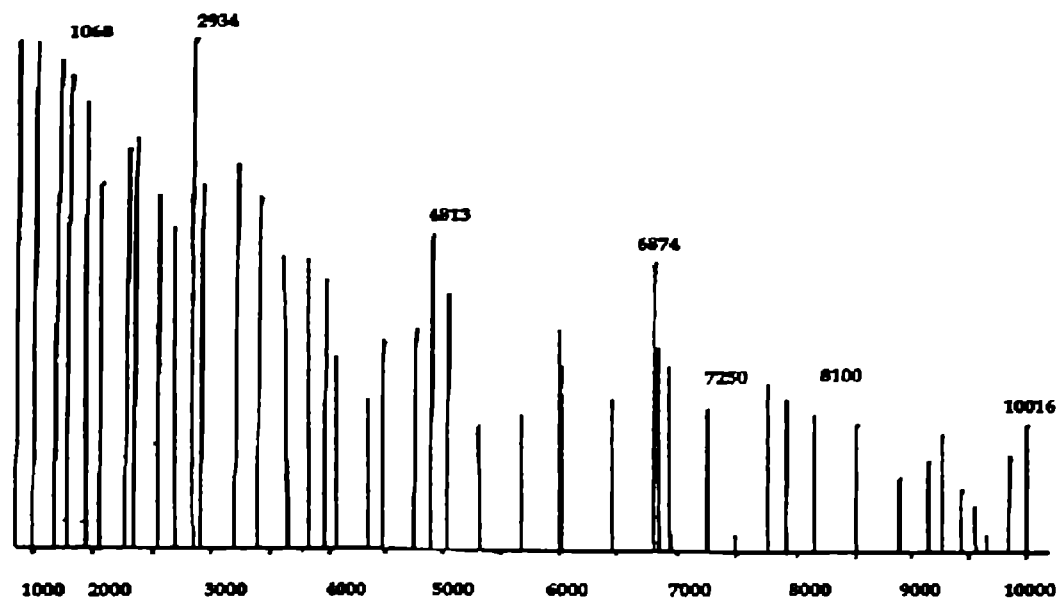


Figure 6.12.. Mass spectrum of Pol-VI.4

6.4.2.2. Thermal properties of the polymers

T_g of side chain azo polymers are low compared to the main chain azo polymers. This may be due to the absence of azo groups in the main chain that decreases the polar order. More over, the efficiency of polymerization of side chain azo compounds is less compared to main chain azo compounds. While the main chain azo polymers contain 15 repeating units in the polymer chain, side chain azo polymers have only 8 repeating units in their chain. Hence main chain azo polymers have shown higher polar order compared to side chain azo polymers. The IDT of side chain azo polymers are slightly higher than that of main chain azo polymers indicating that they are thermally stable. Results are given in Table 6.11

6.5. Evaluation of second harmonic generation efficiency

The NLO efficiencies of poly (ester-amide) s were determined with 2-methyl-4-nitroaniline as the standard using Kurtz and Perry method.¹⁹ Measurements were done by the powder method with a Quanta-Ray Nd-YAG laser from Spectra Physics (1064 nm, 10 ns,365mJ/S) integrated over 20 pulse and an average of 10 pulse. The samples were ground and graded with standard sieves to the phase that match the size (100-150

μm) and loaded on cuvette with 1mm thickness. MNA samples used as standards were also powdered and sieved (100-150 μm) after drying under high vacuum. They were also mounted with the same thickness as the polymer sample. The laser beam was directed unfocused onto the sample kept at a 45° angle to the laser beam which provided the phase that match the situation; the emission was collected from the front face of the sample at 90° angle. The SHG signal at 532 nm was detected by Avantes 2048 spectrometer with CCD camera. The results are shown in Table 6.11.

Table 6.11 gives the properties of the synthesized poly (ester-amide) s containing side chain azo group. The poly (ester-amide) s has SHG efficiency higher than MNA. But compared to main chain azo polymers the efficiency is less. This may be ascribed as due to the low polar order and molecular weight of side chain azo polymers compared to the main chain azo polymers derived from the absence of electron donating azo group in the main chain, which also decreases the donor-acceptor efficiency. Thus, the side chain azo polymers have shown lower value of SHG.

Table 6.11: Yield and Properties of Poly (ester-amide) s

<i>Polymer</i>	<i>Diol molecule</i>	<i>Yield (%)</i>	<i>T_g (°C)</i>	<i>IDT (°C)</i>	<i>[α]_D</i>	<i>*SHG Efficiency</i>
Pol-V.1	Camphanediol	71	293.97	291	-24.3	8.53
Pol-VI.1	Camphanediol	70	220.02	293	-16.3	4.49
Pol-V.2	Isosorbide	78	154.27	297	-23.2	7.73
Pol-VI.2	Isosorbide	69	173.63	326	-12.5	6.33
Pol-V.3	Isomanide	75	299.43	287	-20.4	7.93
Pol-VI.3	Isomanide	73	171.40	325	-12.6	6.38
Pol-V.4	BHDM	74	215.67	275	-16.8	8.02
Pol-VI.4	BHDM	72	176.70	325	-10.1	7.49
Pol-V.5	Dihydroxy biphenyl	72	191.89	236	-18.0	7.60
Pol-VI.5	Dihydroxy biphenyl	70	188.21	328	-13.1	6.53
Pol-V.6	Dihydroxy naphthalene	73	197.51	280	-15.9	7.54
Pol-VI.6	Dihydroxy naphthalene	73	170.21	341	-12.8	6.21

* (MNA Reference, SHG efficiency of MNA was taken as 1)

6.6. Conclusion

From the theoretical and experimental studies of polymers containing azo group in the side chain and in the main chain it was observed that the presence of azo group in the main chain increased the second order NLO efficiency. This can be attributed to the higher polar order for the main chain azo polymer. With an increased donor-acceptor strength (by virtue of having efficient push-pull azo group in the main chain) and higher molecular weight, polar order was found to be higher for the main chain azo polymers, which led to their SHG efficiency

References

- (1) Keum, C. D.; Ikawa, T.; Tsuchimori, M.; Watanabe, O; *Macromolecules*, **2003**, *36*, 4916
- (2) Heldmann, C.; Warner, M. *Macromolecules* **1998**, *31* 3519,
- (3) Xu, Z. S.; Drmoyan, V.; Natansohn, A.; Rochon, P. J. *Polym.Sci. Part A: Polym. Chem.* **2000**, *38*, 2245,
- (4) Lee, T. S.; Kim, D. Y.; Jiang, X. L.; Kumar, J.; Tripathy, S. J. *Polym.Sci. Part A: Polym. Chem.* **1998**, *36*, 283.
- (5) Ikawa, T.; Hasegawa, M.; Tsuchimori, M.; Watsnabe, O.; Kawata,Y.; Egami, C.; Sugihara, O.; Okamoto, N. *Synth. Metal*, **2001**,*124*, 159.
- (6) Meredith, G. R.; Van Dusen, J. G.; Williams D. J.; *Phys. Rev Lett.* **1961**, *7*, 118
- (7) Hampsch, H. L.; Wong, G. K.; Torkelson J. M.; *Macromolecules*, **1988**, *21*, 526
- (8) Singer, K. D.; Sohn, J. E.; Lalama, S. J.; *Appl. Phy. Lett.* **1986**, *49*, 248
- (9) Eich M.; Sen, A.; Lossner, H.; Bjorkund, G. C., Swalen, J. D.; Twieg, R.; Yoon, D. Y.; *J. Appl. Phys.* **1989**, *66*, 2559.
- (10) Yesodha, S. K.; Pillai, C. K. S.; Tsutsumi, N.; *Prog. Polm. Sci.* **2004**, *29*, 45
- (11) Angiolini, L.; Caretti, D.; Giprgini, L.; Slatelli, E.; *Polymer*, **2001**, *42*, 4005
- (12) Hohenberg, P.; Kohn, W. *Phys. Rev.* **1964**, *136*, B864.
- (13) Kohn ,W.; Sham, L. J. *Phys. Rev.* **1965**, *140*, A1133.
- (14) Salahub, D. R.; Zerner, M. C. *The Challenge of d and f Electrons*; ACS: Washington, D.C., 1989
- (15) Parr, R. G.; Yang, W. *Density-functional theory of atoms and molecules*; Oxford

Univ. Press: Oxford, 1989

- (16) Gerratt, J.; Mills, I. M. *J. Chem. Phys.* **1968**, *49*, 1719
- (17) Ridley, J.; Zerner, M. C. *Theor. Chim. Acta* **1973**, *32*, 111. Bacon, D.; Zerner, M. C. *Theor. Chim. Acta* **1979**, *53*, 21.
- (18) Dewar, M. J. S.; Zoebisch, E. G.; Healy, E. F.; Stewart, J. J. P., *J. Am. Chem. Soc.* **1985**, *107*, 3902.
- (19) Kurtz, S. K.; Perry, T. T. *J. Appl. Phys.* **1968**, *39*, 3798

SUMMARY AND CONCLUSIONS

Nonlinear optical (NLO) properties of polymers were studied theoretically and experimentally. The study embodied in this thesis was mainly based on the theoretical design of polymers considering spacer and chiral effects in NLO properties and the syntheses of the designed systems. Nonlinear optical polymers were designed theoretically by *ab initio* and ZINDO calculations. All the polymeric systems were synthesized by condensation polymerization. Second harmonic generation efficiency of the synthesized systems was measured experimentally by Kurtz and Perry powder method. The thesis is divided into six chapters. An overview about the theory of NLO and the importance of polymers as NLO material was given in **Chapter 1**. It also discussed about the use chiral polymers for NLO applications.

Chapter 2 provided a detailed theoretical study of optimization of linear and nonlinear coefficients of *para*-nitroaniline and its derivative systems. Static polarizability and first and second order hyperpolarizability tensors were computed at the correlated level (MP2) using GAMESS-US, Quantum chemical code. Based on the ability to charge transfer, strength and number of donors and acceptors, asymmetry and geometry of the systems and position of the substituents were found to play important roles in determining NLO response. The electron density distribution of the optimized primary and secondary structures turned out to have a great influence on these properties. High value of electric susceptibilities depended on the nature of the delocalized structures and it was repaired for the purpose of molecular design in optoelectronics to find molecular systems that yielded the largest possible responses. The larger these linear and nonlinear responses were, the smaller the electric field required to achieve the desired electro-optic effect.

The effect of spacer groups in SHG efficiency was studied in **Chapter 3**. The first part contained the study of odd-even spacer effect of electric properties of organic molecules (of the type $O_2N-Ph-N=N-Ph-(CH_2)_n-Ph-N=N-Ph-NO_2$) with a change in the

number of spacer methylene groups. The calculations have been performed using sum-over-states (SOS) method on a ZINDO code which used CI and correction vector method. The molecules exhibited a strong odd-even behavior for the 1st hyperpolarizability. By this study it was proved based on the conformational analysis, that the odd-even oscillation of first hyperpolarizability β has molecular origin.

In the second part of Chapter 3 the spacer effect on *para*-Nitroaniline (PNA) derivatives by varying CH₂ groups was studied. The calculations at the Hartree-Fock level (6-31++G** basis set; Gaussian 03 quantum chemical package have been used for the calculation.) and the ZINDO-SOS method agreed with the experimental observations. The polymeric systems incorporating these PNA derivatives were synthesized by the condensation polymerization of the PNA derivatives with azo chromophore. The SHG efficiency was calculated experimentally by Kurtz and Perry powder method. While substituting both the hydrogens of -NH₂ in *para*-nitroaniline, instead of showing odd even oscillation, the SHG efficiency increased with increase in number of CH₂ groups.

Chapter 4 described the influence of chirality in designing second order nonlinear optical materials. It also gave a detailed study of the influence of stereochemistry of the incorporated monomers. Four pairs of diastereomers were selected as monomers. The monomers and polymers were designed using the theoretical calculations at the Hartree-Fock and semiempirical level calculations. The stereochemistry has influenced NLO properties based on the polar order of the diastereomer. The stereochemical effect of monomer was pursued in the polymer design also. The series the polymers were synthesized by condensation polymerization of three monomers (*one* chiral molecule, *one* azo chromophore and *one* acid chloride). Since the chiral molecules were incorporated in the polymer main chain, non-centrosymmetric supramolecular structures could be obtained. In the polymer, such structures extend to macroscopic dimensions and the poling of chromophores could be achieved through chemical synthesis. Hence there is no need of external poling. The permanent dipole moments of the polymeric systems were large because of the coherent addition of dipole moments achieved by a high degree of polar order. The chirality of the material was

associated with the helical supramolecular configuration of the backbone, and strong coupling existed between the backbone and the chromophore. Thus the polymeric systems with chiral molecules showed enhanced SHG efficiency which was double as that of the reference molecule, 2-Methyl, 4-nitroaniline. Theoretical property calculations of polymer were in good agreement with the experimental results. Chirality of the polymer systems enhanced the nonlinear optical response in two ways: first by increasing the polar order of the polymeric system and second by chiral contributions.

In Chapter 5 a series of poly (ester-amide) s based of L-tyrosine chiral framework was designed and the properties were predicted. This design was possible through chiral framework of polymer chains. This chapter included the study of main chain azo groups in the polymeric systems. Theoretical calculation showed that all the polymers were highly efficient NLO materials. This was because of the helicity imparted to the polymer chain due to chirality and main chain azo group. Synthesis of the poly (ester-amide) s in high yields could be achieved. Experimental measurements of SHG were in good agreement with theoretical predictions as all the polymers had shown high SHG efficiency compared to MNA.

A comparison between main chain azo polymers and side chain azo polymers was done in Chapter 6. Theoretical and experimental studies have shown that the polymers containing azo group in the main chain have larger second order NLO efficiency than those containing the side chain azo group. Push pull nature of azo group has played a vital role in this observation. In the absence of azo group in the main chain, the donor-acceptor efficiency of the polymer chain was reduced considerably which in turn decreased the NLO response. Synthesis and characterization of the polymers were done. Experimental measurements of SHG efficiency of polymers was done by Kurtz and Perry method using MNA as reference material.

To conclude, highly efficient second order NLO polymeric materials could be designed theoretically with an understanding of substituent, symmetry, spacer and chiral effects on hyperpolarizabilities. These pre-designed polymeric materials could be

synthesized and characterized in good yield and experimental measurements could show good agreement with the theoretical results.

Due to the high computational demand of higher level electron-correlation methods, the studies were restricted to the common level of theory. This has brought to light the inadequacy of the *static* CPHF methodology in arriving at a reasonable property prediction in the case of polymers. The theory could not substantiate fully the experimental results or vice versa. For more close correlation between theory and experiments, higher level electron correlation methods should be employed. During the present study, at several occasions, it was observed that the results of property predictions arrived at by *static* CPHF methods and *dynamic* methods did not agree mutually. This draw back could also be rectified by using higher electron correlation with large basis sets.